Combinatorial Approach for Development of Optical Gas Sensors

Concept and Application of High-Throughput Experimentation

DISSERTATION ZUR ERLANGUNG DES
DOKTORGRADES DER NATURWISSENSCHAFTEN
(DR. RER. NAT.)

DER FAKULTÄT FÜR CHEMIE UND PHARMAZIE
DER UNIVERSITÄT REGENSBURG

vorgelegt von

Athanasios Apostolidis

aus Regensburg

im Juni 2004

Combinatorial Approach for Development of Optical Gas Sensors

Concept and Application of High-Throughput Experimentation

Doctoral Thesis

by

Athanasios Apostolidis

Für meine Familie

Diese Doktorarbeit entstand in der Zeit von April 2000 bis Mai 2004 am Institut für Analytische Chemie, Chemo- und Biosensorik an der Universität Regensburg.

Die Arbeit wurde angeleitet von Prof. Dr. Otto S. Wolfbeis

Promotionsgesuch eingereicht am: 27.05.2004

Kolloquiumstermin: 21.06.2004

Prüfungsausschuss:	Vorsitzender:	Prof. Dr. Manfred Liefländer
	Erstgutachter:	Prof. Dr. Otto S. Wolfbeis
	Zweitgutachter:	Prof. Dr. Ingo Klimant
	Drittprüfer:	Prof. Dr. Werner Kunz

Acknowledgements

Above all, I would like to thank Prof. Dr. Otto S. Wolfbeis for providing the fascinating subject and for the active support during this thesis.

I also gratefully acknowledge the extensive assistance of Prof. Dr. Ingo Klimant, his helpful ideas, largely contributing to the completion of this thesis, and his open-minded personality during many discussions on or off matters of chemistry.

I gratefully appreciate financial support of the Robert Bosch GmbH and the German Federal Ministry of Education and Research within the “KombiSens” project 03C0305A making this thesis possible.

Furthermore, I would like to thank Gisela Hierlmeier for her technical assistance during our collaboration and the wonderful personal assistance in any adverseness of everyday life.
I gratefully appreciate the extensive help and friendship of Dr. Damian Andrzejewski providing the LabView tools making the accomplishment of this thesis possible.
I want to thank Edeltraud Schmid for her friendly assistance in any official or personal business.

I appreciate the support of Sarina Arain, Claudia Schröder, Bernhard Weidgans, and all other colleagues of our institute.

I would not like to miss the friendship of Dr. Torsten Mayr and Dr. Gregor Liebsch.

Finally, very special thanks to my wife Patricia and my daughter Sophia for their emotional support, and to my parents, Thomai and Georgios Apostolidis, for their emotional and financial support during my whole studies.

Table of Contents

Chapter 1. Introduction

1.1. Combinatorial Chemistry

Combinatorial chemistry (CC) is one of the most impressive technologies developed in the past ten years in chemical and pharmaceutical research. This is illustrated by the increasing number of publications in this field found from a SciFinder search using the phrase "combinatorial chemistry", shown in figure 1.1. The basic principles used in combinatorial chemistry have their origins in the techniques of solid-phase synthesis of peptides according to Merrifield presented in 1963.[1] Progress was achieved with the "multi-pin" technique of Geysen published in 1984 and the "tea-bag method" presented by Houghten in 1985, both addressing the parallel synthesis of peptides.[2-4] In the first multiple polyethylene supports (pins) were dipped into reactant solutions placed in a microtiter plate for reaction. In the second, resin beads sealed in mesh packets (tea bags) were used as support. However, combinatorial synthesis in strict sense was made possible by the "split-pool procedure" from Furka in 1988 and this can be attributed the "birth" of combinatorial chemistry.[4-8]

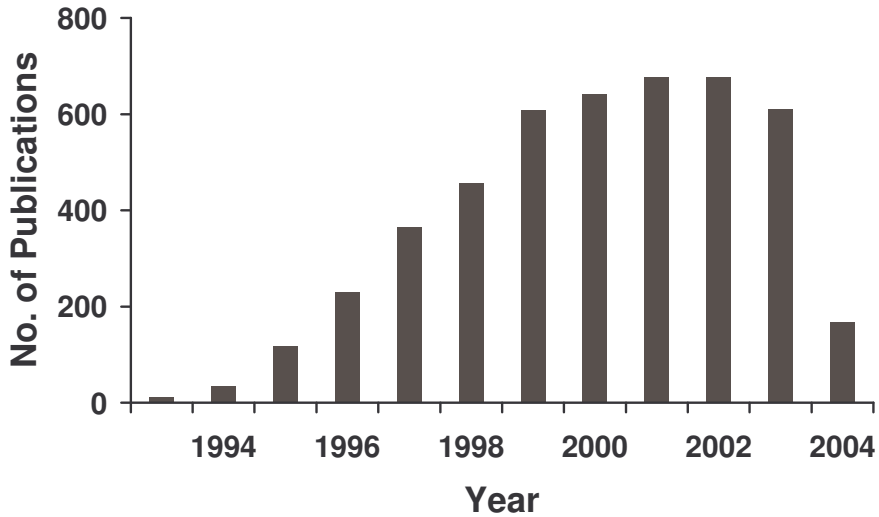

Figure 1.1. Number of publications obtained from a SciFinder search in CAPLUS database using the phrase "combinatorial chemistry". Patents are not included.

In conjunction with the continuous development and improvement of high-throughput instrumentation these techniques have changed the way of drug discovery and optimisation in medical chemistry. Conventionally, this process involves the serial synthesis and testing of

hundreds to thousands of organic compounds as drug candidates attempting to enhance their biological activity, selectivity or bioavailability, while reducing their toxicity to a biological target. The identification of a chemical structure serving these demands comes along with extensive time spent and cost with the synthesis of these compounds being the speed determinant step. Combinatorial high-throughput synthesis enables the rapid production of hundreds to thousands more compounds than conventional organic synthesis methods. Thus, in combination with high-throughput screening methods, CC has attracted attention to pharmaceutical companies cutting down time and cost of the drug discovery process. The position of impact of CC on the key steps of drug discovery is illustrated in figure 1.2. Today, virtually all pharmaceutical companies have at least one division dealing with combinatorial chemistry.

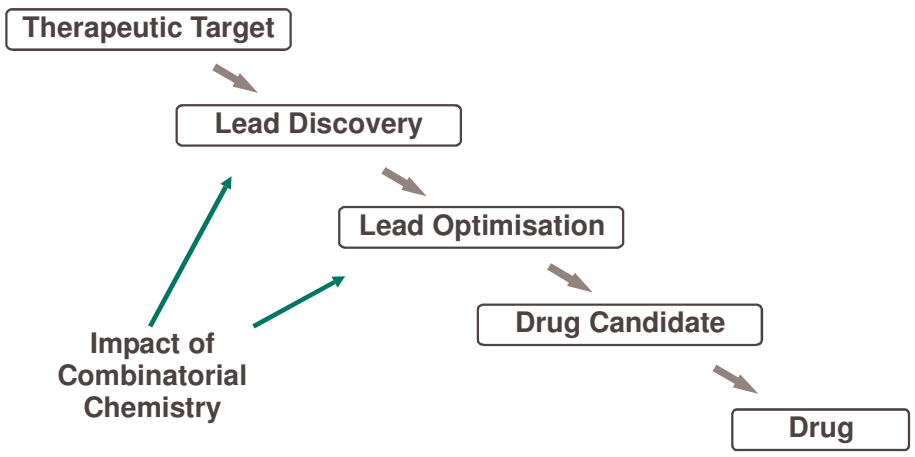

Figure 1.2. Key steps of a drug discovery process and position of impact of combinatorial chemistry. Speeding-up preparation and testing with combinatorial high-throughput methods offers solutions for overcoming the bottlenecks of conventional synthesis. The strategy can be adapted to other research topics by exchanging the target of development (drugs, catalysts, sensors and others).

The potential of this tool is not limited to peptide synthesis only. Considering the research structure in figure 1.2, it is obvious that by changing the target the combinatorial approach can be adapted for other research topics. Thus, the number of applications has extended to a manifold of areas including, more recently, material sciences. CC and high-throughput methods for screening have found numerous applications, for example in life sciences or catalysis. [9-12] Another research topic is the development of molecular receptors for chemosensors.[13,14] The optimisation of material compositions, such as for homogeneous or heterogeneous catalysts, for nanoscale materials, and for the optimisation of process

parameters of materials fabrication are examples of research that involve high-throughput approaches.[15-18]

1.1.1. Concept of Combinatorial Chemistry in Drug Discovery

The combinatorial approach to the discovery and the optimisation of chemical substances bases on the rapid (parallel) production (combinatorial synthesis) and screening (high-throughput experimentation) of a vast number of chemical substances attempting to meet desired physical or chemical properties. In the conventional approach one or only a few samples are prepared at a time and subsequently tested. In contrast to that, here, a substance pool (referred to as library) with high diversity is prepared simultaneously in one preparation procedure under the same reaction conditions cutting down preparation time and, with reducing batch size, cost. The high-throughput experimentation associated provides the fast screening of the samples produced.

The total size of a combinatorial library is determined by the number of building blocks used within a reaction step and the number of reaction steps during the synthesis process. The number of all compounds obtained (N_n) is given by the equation:

$$N_n = \underbrace{a_1 \cdot a_2 \cdot \ldots \cdot a_i}_{n} = \prod_{i=1}^{n} a_i \qquad (1.1)$$

where a_i is the number of building blocks in reaction no. i and n is the total number of reaction steps. Thus, a large compound library can be obtained rapidly starting with a few building blocks only.

1.1.1.1. Combinatorial Synthesis of Organic Libraries

Different concepts are described for the library synthesis supplying either compound mixtures or single substances. The approaches include solution-based synthesis, with the compounds free in solution, or solid-phase synthesis, with the compounds linked to a solid-phase (polymer resin beads), the latter being the most popular method for large combinatorial libraries of organic compounds. Basically two synthesis strategies, as illustrated also in figure 1.3, are pursued:

Split-pool Synthesis

It is based on the work of Furka, as mentioned before. Using only few reaction vessels the combinatorial library is created by repeated performance of this procedure. The polymer beads - starting material in first step, product mixture in following steps - are divided into

equal portions for the separate addition of the building blocks and subsequently recombined (pooled) after reaction. With only few process steps a highly divers library is built up containing all possible combinations of building blocks.

Parallel Synthesis

Here, all components are prepared simultaneously using separate reaction vessels for each product of interest. Since here the number of compounds is limited, to a greater extent, by the number of reaction vessels accessible, the miniaturisation of reactors is mandatory. The microtiter plate is a convenient format for such minireactors. As predominant advantage, assuming complete turn-over for each reaction, the products are obtained with high purity.

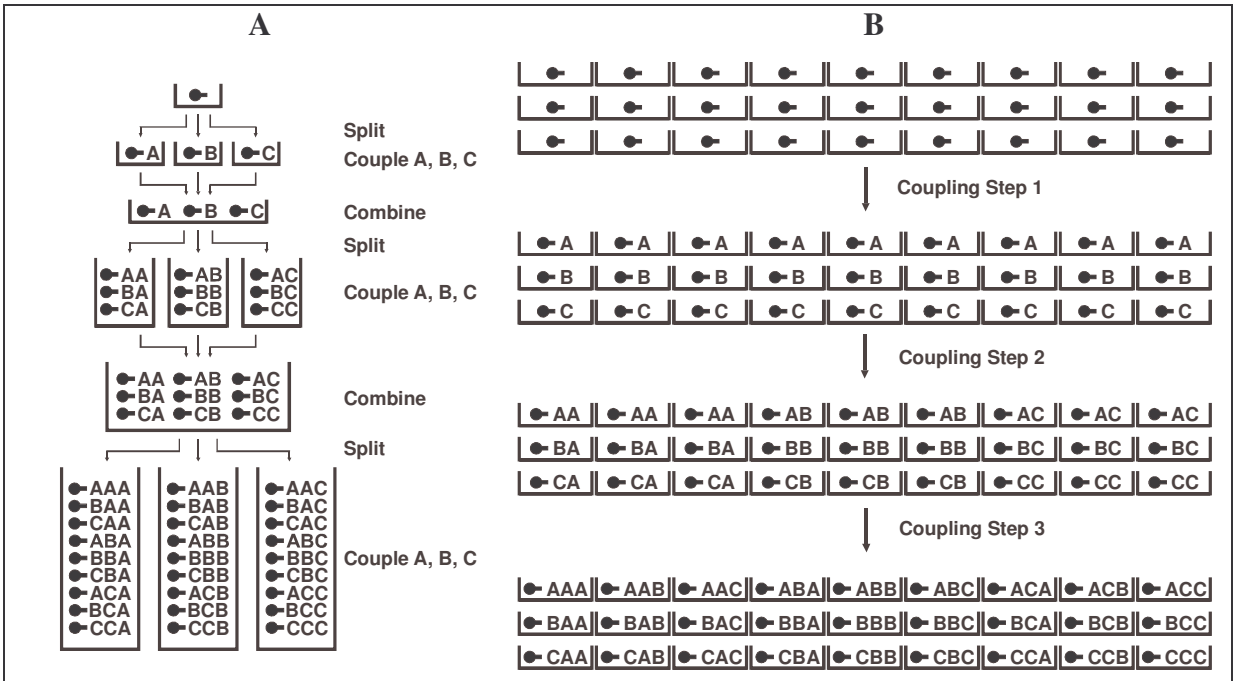

Figure 1.3. Schematic view of split-pool (A) and parallel synthesis (B) of a combinatorial library containing the possible combinations of the three building blocks used.

1.1.1.2. High-Throughput Characterisation of Organic Combinatorial Libraries

Besides the analytical evaluation of compound structure, the characterisation of combinatorial libraries is marked by screening them for the most active compound (hit) interacting with the target of interest. This is achieved by application of high-throughput screening methods with focus on the properties of interest.

For the structure determination, again, it is essential whether the library was prepared by split-pool or parallel synthesis. With compound mixtures present, analytical methods as IR

and NMR spectroscopy or mass spectrometry in combination with HPLC or capillary electrophoresis can be applied, but with big effort. This is complemented by deconvolution methods from high-throughput screening.[4]

The analytical characterisation of single compounds from parallel synthesis is easier, since the structure of a compound can be predicted by the synthesis sequence. Conventional IR and NMR spectroscopy or elementary analysis is possible. Here, the analysis is rather a matter of confirmation than of identification.

For the high-throughput screening of biologically active organic compounds usually well established assays in microtiter plate format (96, 384 or 1546 wells) are performed. Screening compound mixtures results in the determination of lead families. In order to identify a single hit structure iterative deconvolution, deconvolution by positional scanning or deconvolution by orthogonal libraries can be used.[4] These methods involve the repeated preparation and testing of sublibraries with known position of at least one building block. Labelling methods represent an alternative approach. Screening of libraries prepared by parallel synthesis, the most active compound can be identified directly without any additional sublibrary production. The structure of the hit is defined by the preparation protocol, since all compounds are located in separate reaction vessels.

1.1.2. Data Handling and Analysis

It is evident that combinatorial approach to organic chemistry and material science is accompanied by a large amount of experiments. This is tackled with the development of high-throughput synthesis and screening instrumentation. Yet throughout the discovery and optimisation process an even larger amount of data is produced that cannot be handled in conventional manner. Effective data storage, handling and analysis are essential to a successful application of CC. Automation of synthesis and screening comes along with the development of software tools for the preparation and the high-throughput characterisation of combinatorial libraries. These tools provide information on library composition, synthesis and experimental conditions and sample response during testing, and control the instrumentation. Supply on commercially available automated synthesis instrumentation and on software, e.g., databases or laboratory software, is growing and companies have been founded focusing on commercial conversion of high-throughput research.[19,20] For some examples on liquid handling robotics and software solutions see the references.[21-26]

1.1.3. Combinatorial Chemistry in Material Science

Though combinatorial chemistry is commonly associated with organic chemistry, early concepts were first applied to material science. They can be tracked back to the "multi-sample concept" for the development of electronic materials from Hanak published in 1970.[27] Yet the approach suffered from the lack of high-throughput synthesis and screening instrumentation. With the progressive technological development the application of CC in material science is pressed ahead since the middle of the 1990´s.[28] Tremendous advances have been made in the development of combinatorial approaches to the discovery and optimisation of new materials including polymers, materials with potential superconductivity, giant magnetoresistance, phosphorescent materials or catalysts.[28-34]

The development of organic or organometallic catalysts for homogeneous catalysis is closely related to organic chemistry. Thus, the synthesis strategies are similar to those used for drug discovery. The variation of the compounds results from combinatorial synthesis of the organic moieties. The development of inorganic catalysts, for heterogeneous catalysis, and materials development base on a different approach. Instead of "synthesis", here the preparation is referred to as deposition of the inorganic materials onto a substrate by different techniques. These precursors undergo subsequent processing resulting in the combinatorial library to be tested.

Generally, in material development similar challenges arise as in drug discovery with respect to synthesis and screening strategies. In organic chemistry the inversion of reaction sequences will result in distinctly diverse chemical structures. Yet inorganic materials will feature the same stoichiometric composition and structure, although possibly expressing different properties. Mixtures of many partially active substances may outperform those with only one superior compound. Consequently the approaches in combinatorial material development rather pursue the parallel preparation of samples and a parallel or high-throughput serial screening than a split-pool approach.

According to the type of material of interest different deposition methods have been developed.[35,36] These can be divided in (1) thin-film deposition by co-evaporation or sputtering techniques and (2) solution-based technologies, both followed by processing methods for the activation of the materials prepared. The principle of the approaches is illustrated in figure 1.4.

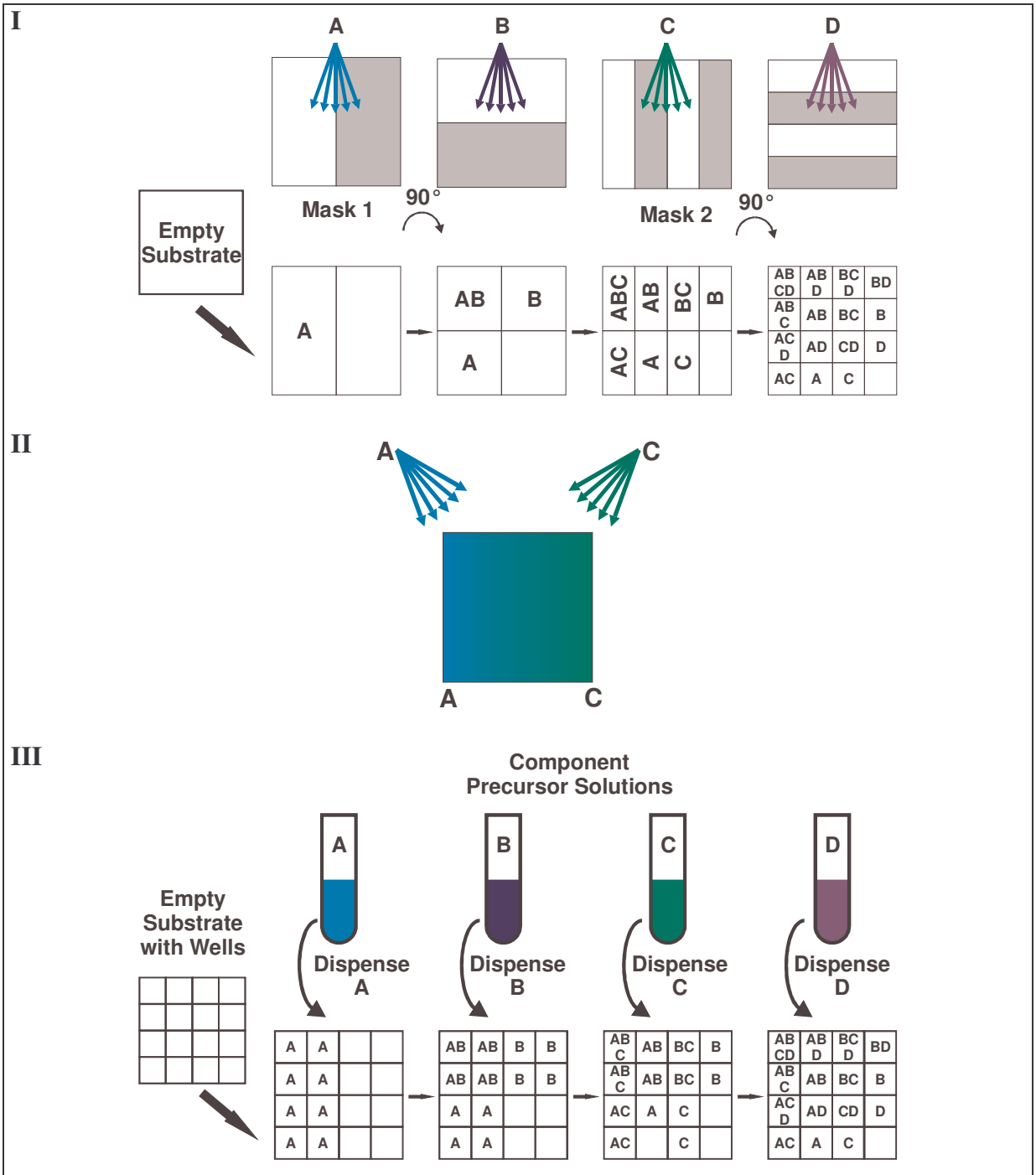

Figure 1.4. Combinatorial approaches for the production of high-diversity libraries in materials science. Thin-film deposition using masking technique (I): The substrate is partially covered via different masks providing the components to be deposited only onto uncovered regions of the substrate. By rotation of masks and use of different mask layouts high compositional diversity is obtained. Co-deposition(II): Two or more components are deposited onto an uncovered substrate simultaneously. The composition of the materials varies because of the spatial arrangement of the component sources referring to the centre of the substrate. Solution-based technology (III): Precursor solutions of each component are dispensed to predefined wells on a substrate. The libraries obtained from method I – III are subject to thermal processing for activation. Thereafter, they are screened for desired properties.

In combination with masking techniques the thin-film deposition, e.g., electron beam evaporation, physical vapour deposition or radio-frequency sputtering, provides discrete compositions, and with co-deposition continuous composition distribution can be achieved.[31,37,38]

Liquid deposition techniques include electrochemical deposition, co-precipitation of the inorganic materials by mixing of precursor solutions or impregnation of a porous carrier with solutions containing the potential catalytic components.[36,38] It is obvious that for a successful application of these methods miniaturisation and automation is necessary. Yet ink-jet technology or automated liquid dispensing systems for the preparation of combinatorial libraries have been developed and applied successfully, though with the need for further progress.

The materials prepared, undergo thermal or electrochemical processing. Potentially, when they are obtained by solution-based methods, processing is preceded by filtration, washing and drying. Finally activated, the combinatorial library is screened towards properties of interest.

Optical imaging, via infra-red (IR) thermography or luminescence imaging, or methods detecting the luminescence of dyes added as indicator, as well as electrical characterisation methods are described approaches towards parallel screening of potential catalysts.[31,39-41] IR thermography has to be used with care for reactions with product mixtures and selective oxidations or hydrogenations since the total heat produced is monitored. High-throughput methods based on the sequential analysis of each library component, like scanning mass spectroscopy, potentially coupled to gas chromatography, can overcome this limitation.[42-44] With the appropriate instrumentation for rapid positional scanning the total product distribution can be evaluated providing additional information on selectivity of active samples.

Beyond the above-mentioned application of CC in material science, it also offers high potential in the development of other materials of interest, i.e., chemical sensors. For example, Dickinson and Walt have shown that substantial sensor diversity can be generated by combinatorial polymer synthesis and testing the resulting materials for sensitivity to organic vapors.[45] This was the first report where CC was mentioned as an approach for the development of optical gas sensors. By continuously varying the monomer batch composition homogeneous gradients in the composition of the resulting polymers were achieved and their performance for the determination of organic vapours was investigated.

Very recently, reports on preparation and characterisation of combinatorial libraries of electrochemical gas sensors have been published.[46-49] This indicates the actual interest on establishing CC in chemical sensor materials research. The automation of material preparation and characterisation along with batch miniaturisation is a major feature of combinatorial approaches for overcoming the bottlenecks of conventional sensor development. Parallel preparation of multiple samples and high-throughput characterisation of high-density combinatorial libraries cut down time required for the realisation of a given sample matrix for a multiple.

In conventional methods - rational design - most of the effort is made in the targeted selection of suitable components for a sensor formulation of desired properties. Strong attention is given on the particular material properties aimed to predict the performance of the sample to be prepared. Unlike that, the main effort of CC in sensor development is in (a) the planning and design of generally applicable preparation routines, (b) the design and automation of test stand, and (c) fast characterisation and evaluation of desired sensor properties. Depending on the target molecule and – given by the mode of detection by the sensor – the analytical method, both devices and methods need to be adjusted according to the physical and chemical properties of the sensor materials under investigation. These are determined by the chemical composition of the samples.

1.2. Optical Chemical Gas Sensors

A chemical sensor can be defined as *"a portable miniaturised analytical device which can deliver real-time on-line information on the presence of specific compounds or ions in complex samples"*.[50] According to the type of transducer they can be divided into electrochemical, optical, mass-sensitive and heat-sensitive sensors.[51]

Usually, optical sensor devices consist of: (a) a light source, (b) a recognition element for identification and interaction with the target, (c) a transducer element converting the recognition into a detectable signal, and, finally, (d) a detector unit detecting and converting the change of optical properties of the sensor - maybe after amplification – into a read-out. The change of optical properties measured can base on absorbance, reflectance, luminescence, light polarisation, Raman and others.[52]

Thereby, demands for an ideal sensor are adequate sensitivity or dynamic range, high selectivity to the targets of interest, fast and reversible response, and excellent long-term stability. Furthermore, it must be robust, simple, reliable, cheap in fabrication, and offer self-

calibrating capabilities. Of course, fulfilling all these demands is hardly possible. Thus, limitations of existing sensors are insufficient long-term stability, interference by species other than the target and – in terms of optical sensors – by background light, and inadequate detection limits. None the less, the field of optical sensing, after many years of constant growth, is still of increasing interest, due to the excellent performance when compared to other analytical methods. This can confirmed by the increasing number of publications and reviews.[51-57]

Optical gas sensors, either intrinsic or extrinsic, have been described for a variety of analytically important gases including – among others – hydrogen[58,59], hydrocarbons[60,61], carbon monoxide[62], carbon dioxide[63-67], oxygen[66-69], nitrogen oxides[70,71], ammonia[72-76], sulfur dioxide[77,78], solvent vapors[79-81] or hydrogen chloride[82,83]. In this thesis focus will be taken on the target gases oxygen, carbon dioxide and ammonia. These, all ahead oxygen sensors, have found many applications in various fields, including biological and environmental monitoring[57,66,84,85], process control[86,87], and medical applications, e.g., in blood gas analysis[88-90], in open-heart surgery[89,91] or in invasive fiber-optic catheters[88,92,93]. Numerous other applications are conceivable.

1.2.1. Sensing Schemes of Optical Gas Sensors

The mode of operation of the optical gas sensor is a consequence of the physical and chemical properties of the target molecule determining the type of interaction with the sensitive chemistry. Thus, various sensing principles for optical determination are conceivable. One is the determination via infrared spectroscopy. Here, the concentration of the target can be investigated directly utilising characteristic absorbance properties of the target molecule as intrinsic sensor in the infrared region of the electromagnetic spectrum. No indicator mediation is needed. For example, carbon dioxide and ammonia can be detected via IR absorption spectroscopy at operational wavelengths of 4.3 µm (CO_2) and 1.5 µm (NH_3), respectively.[94,95] Since instrumentation for this method is bulky and difficult to miniaturise the indicator mediated sensing schemes offer solution for overcoming this drawback.

Other methods utilise indicator dyes (extrinsic sensor) to transduce the concentration of the target gas into an optical measurable signal, when the particular gas has no useful intrinsic optical property. Most frequently used methods include indicator mediated luminescence and absorption spectroscopy.[52,96,97] These are based on the determination of the change of luminescence, mostly intensity or decay time, and the change of absorption properties of the indicator dye when subjected to the target molecule.

1.2.2. Composition of Polymer-Based Optical Chemical Gas Sensors

Depending on the mode of operation of the sensing mechanism and the target molecule the composition of the sensor can range from a simple polymer-indicator combination to highly sophisticated systems including the polymer support, tuning agents (e.g. plasticizers), additional mediators (e.g. lipophilic buffer) and sensitive chemistry (indicator probe). The interactions of all the possible components often are very complex and not coercively predictable. Finally, each component can influence the efficiency of the sensor performance due to particular physical or chemical properties. For example, the efficiency of oxygen quenching of an indicator dye or the concentration of carbon dioxide in a polymer strongly depends on the permeability (P) of the encapsulating medium to the gas. The permeability, again, depends on the solubility (S) and the diffusion coefficient (D) of the gas into the matrix according to the following equation:[98]

$$P = D \times S \tag{1.4}$$

Data for selected polymers to the target gases investigated in this thesis are given in table 1.1.

Table 1.1 Permeability coefficients of selected polymers to gases at 25°C from reference.[98]

Polymer	$P \times 10^{13}$ / (cm^3 (273.15 K; 1013 hPa) × cm/(cm^2 × s × Pa))		
	O_2	CO_2	NH_3
poly(ethylene) (LDPE)	2.2[a]	9.5[a]	21.0[b]
poly(styrene)[b]	2.0	7.9	no data
PVC	0.034	0.12	3.7[c]
PMMA	0.116[d]	2.33[d]	no data
poly(acrylonitrile)	0.00015[a]	0.0006[a]	no data
EC	11.0[c]	84.8	529

[a] 25 °C; [b] biaxially oriented; [c] 20 °C; [d] 35 °C;

As can be seen in table 1.1, the permeability of a polymer to particular gases can differ significantly. Thus, the performance of a sensor for particular gas will, at least, depend on the proper choice of polymer and sensitive chemistry and has to be adjusted to the application of interest. Compatibility of the sensor components and chemical stability of the composition are only two additional demands for the successful development and application of an optical gas sensor. In conclusion a big number of different species of each component have to be tested for their performance in a particular formulation. Remembering the number of possible sensor compositions given by equation 1.1, it is obvious that high-throughput automation of

preparation and characterisation is mandatory for the development of new, and the optimisation of existing sensor materials with increasing numbers of sample compositions to be investigated.

1.3. Aim of the Thesis

The aim of this thesis is to develop a versatile tool for the speed-up of preparation and characterisation of optical gas sensors. The conventional production and testing of optical gas sensors is cost-intensive and, since the target oriented development of sensor materials is still a kind of empirical science, time consuming. The tools developed will be applied to the development of optical gas sensors for oxygen, carbon dioxide and ammonia.

The application of a liquid dispensing automat with purpose-built preparation routines allows the fast production of samples with high diversity according to the target gas of interest. The modular design of the characterisation set-up allows the easy exchange of instrumentation and, therefore, provides versatility of the optical signal to be recorded as analytical information.

In addition, it is expected to gain further understanding on the functionality of optical gas sensors. The tools developed are expected to support future research via speeding up sensor development and, thus, increasing knowledge base for prediction of potential performance of new materials not realised yet.

1.4. References

1 Merrifield R. B., ***Solid Phase Peptide Synthesis. I. The Synthesis of a Tetrapeptide***, J. Am. Chem. Soc. **85**, 2149-2154, (1963).

2 Geysen H. M., Meloen R. H., and Barteling S. J., ***Use of Peptide Synthesis to Probe Viral Antigens for Epitopes to a Resolution of a Single Amino Acid***, Proc. Natl. Acad. Sci. U. S. A. **81**, 3998-4002, (1984).

3 Houghten R. A., ***General Method for the Rapid Solid-Phase Synthesis of Large Numbers of Peptides: Specificity of Antigen-Antibody Interaction at the Level of Individual Amino Acids***, Proc. Natl. Acad. Sci. U. S. A. **82**, 5131-5135, (1985).

4 Jung G., ***Combinatorial Chemistry: Synthesis, Analysis, Screening***, WILEY-VCH, Weinheim (1999).

5 Furka A., Sebestyen F., Asgedom M., and Dibo G., ***Cornucopia of Peptides by Synthesis***, Proceedings of the 14th International Congress of Biochemistry **Vol. 5**, 47, (1988).

6 Furka A., Sebestyen F., Asgedom M., and Dibo G., ***General Method for Rapid Synthesis of Multicomponent Peptide Mixtures***, Int. J. Pept. Protein Res. **37**, 487-493, (1991).

7 http://szerves.chem.elte.hu/Furka/82Eng.htm

8 Terrett N., ***Combinatorial Chemistry***, Oxford University Press, Oxford, UK (1998).

9 Schuth F., Hoffmann C., Wolf A., Schunk S., Stichert W., and Brenner A., ***High-Throughput Experimentation in Catalysis***, Comb. Chem. 463-477, (1999).

10 Scheidtmann J., Weiss P. A., and Maier W. F., ***Hunting for Better Catalysts and Materials - Combinatorial Chemistry and High-Throughput Technology***, Appl. Catal. A **222**, 79-89, (2001).

11 Schunk S. A., Strehlau W., Zech T., and Pietsch J., ***High-Throughput Experimentation - An Additional Tool for Catalysis Research***, PharmaChem **1**, 9-12, (2002).

12 Hagemeyer A., Jandeleit B., Liu Y., Poojary D. M., Turner H. W., Volpe A. F., and Henry Weinberg W., ***Applications of Combinatorial Methods in Catalysis***, Appl. Catal. A **221**, 23-43, (2001).

13 Leipert D., Mack J., Tunnemann R., and Jung G., ***Combinatorial Approaches to Molecular Receptors for Chemosensors***, Comb. Chem. 335-353, (1999).

14 Szurdoki F., Ren D., and Walt D. R., ***A Combinatorial Approach To Discover New Chelators for Optical Metal Ion Sensing***, Anal. Chem. **72**, 5250-5257, (2000).

15 Zhang Y., Gong X., Zhang H., Larock R. C., and Yeung E. S., ***Combinatorial Screening of Homogeneous Catalysis and Reaction Optimisation Based on Multiplexed Capillary Electrophoresis***, J. Comb. Chem. **2**, 450-452, (2000).

16 Thomson S., Hoffmann C., Ruthe S., Schmidt H. W., and Schuth F., ***The Development of a High-Throughput Reactor for the Catalytic Screening of Three Phase Reactions***, Appl. Catal. A **220**, 253-264, (2001).

17 Bosman A. W., Heumann A., Klaerner G., Benoit D., Frechet J. M., and Hawker C. J., ***High-Throughput Synthesis of Nanoscale Materials: Structural Optimisation of Functionalised One-Step Star Polymers***, J. Am. Chem. Soc. **123**, 6461-6462, (2001).

18 Potyrailo R. A., Wroczynski R. J., Lemmon J. P., Flanagan W. P., and Siclovan O. P., ***Fluorescence Spectroscopy and Multivariate Spectral Descriptor Analysis for High-***

Throughput Multiparameter Optimisation of Polymerisation Conditions of Combinatorial 96-Microreactor Arrays, J. Comb. Chem. **5**, 8-17, (2003).

19 www.symyx.com

20 www.hte-company.com

21 www.zinsser-analytic.com

22 www.tecan.com

23 www.hamiltoncomp.com

24 www.accelrys.com

25 www.avantium.com

26 www.spotfire.com

27 Hanak J. J., ***"Multiple-Sample Concept" in Materials Research: Synthesis, Compositional Analysis, and Testing of Entire Multicomponent Systems***, J. Mater. Sci. **5**, 964-971, (1970).

28 Xiang X. D., Sun X., Briceno G., Lou Y., Wang K. A., Chang H., Wallace-Freedman W. G., Chen S. W., and Schultz P. G., ***A Combinatorial Approach to Materials Discovery***, Science **268**, 1738-1740, (1995).

29 Hoogenboom R. and Schubert U. S., ***The Fast and the Curious: High-Throughput Experimentation in Synthetic Polymer Chemistry***, J. Polym. Sci. A **41**, 2425-2434, (2003).

30 Meredith J. C., ***A Current Perspective on High-Throughput Polymer Science***, J. Mater. Sci. **38**, 4427-4437, (2003).

31 Danielson E., Golden J. H., McFarland E. W., Reaves C. M., Weinberg W. H., and Wu X. D., ***A Combinatorial Approach to the Discovery and Optimisation of Luminescent Materials***, Nature **389**, 944-948, (1997).

32 Sun X. D., Wang K. A., Yoo Y., Wallace-Freedman W. G., Gao C., Xiang X. D., and Schultz P. G., ***Solution-Phase Synthesis of Luminescent Materials Libraries***, Adv. Mater. **9**, 1046-1049, (1997).

33 Sun X. D., Gao C., Wang J., and Xiang X. D., ***Identification and Optimisation of Advanced Phosphors using Combinatorial Libraries***, Appl. Phys. Lett. **70**, 3353-3355, (1997).

34 Briceno G., Chang H., Sun X., Schultz P. G., and Xiang X. D., ***A Class of Cobalt Oxide Magnetoresistance Materials Discovered with Combinatorial Synthesis***, Science **270**, 273-275, (1995).

35 Jandeleit B., Schaefer D. J., Powers T. S., Turner H. W., and Weinberg W. H., ***Combinatorial Materials Science and Catalysis***, Angew. Chem. Int. Ed. **38**, 2494-2532, (1999).

36 Senkan S., ***Combinatorial Heterogeneous Catalysis - A New Path in an Old Field***, Angew. Chem. Int. Ed. **40**, 312-329, (2001).

37 Danielson E., Devenney M., Giaquinta D. M., Golden J. H., Haushalter R. C., McFarland E. W., Poojary D. M., Reaves C. M., Weinberg W. H., and Wu X. D., ***A Rare-Earth Phosphor Containing One-Dimensional Chains Identified Through Combinatorial Methods***, Science **279**, 837-839, (1998).

38 McFarland E. W. and Weinberg W. H., ***Combinatorial Approaches to Materials discovery***, Trends Biotechnol. **17**, 107-115, (1999).

39 Holzwarth A., Schmidt H. W., and Maier W. F., ***Detection of Catalytic Activity in Combinatorial Libraries of Heterogeneous Catalysts by IR Thermography***, Angew. Chem. Int. Ed. **37**, 2644-2647, (1998).

40 Reddington E., Sapienza A., Gurau B., Viswanathan R., Sarangapani S., Smotkin E. S., and Mallouk T. E., ***Combinatorial Electrochemistry: A Highly Parallel, Optical Screening Method for Discovery of Better Electrocatalysts***, Science **280**, 1735-1737, (1998).

41 Senkan S. M., ***High-Throughput Screening of Solid-State Catalyst Libraries***, Nature **394**, 350-353, (1998).

42 Cong P., Doolen R. D., Fan Q., Giaquinta D. M., Guan S., McFarland E. W., Poojary D. M., Self K., Turner H. W., and Weinberg W. H., ***High-Throughput Synthesis and Screening of Combinatorial Heterogeneous Catalyst Libraries***, Angew. Chem. Int. Ed. **38**, 484-488, (1999).

43 Reetz M. T., Kuhling K. M., Wilensek S., Husmann H., Hausig U. W., and Hermes M., ***A GC-Based Method for High-Throughput Screening of Enantioselective Catalysts***, Catal. Today **67**, 389-396, (2001).

44 Klein J., Stichert W., Strehlau W., Brenner A., Demuth D., Schunk S. A., Hibst H., and Storck S., ***Accelerating Lead Discovery via Advanced Screening Methodologies***, Catal. Today **81**, 329-335, (2003).

45 Dickinson T. A., Walt D. R., White J., and Kauer J. S., ***Generating Sensor Diversity Through Combinatorial Polymer Synthesis***, Anal. Chem. **69**, 3413-3418, (1997).

46 Aronova M. A., Chang K. S., Takeuchi I., Jabs H., Westerheim D., Gonzalez-Martin A., Kim J., and Lewis B., ***Synthesis and Characterisation of Combinatorial Libraries***

of Semiconductor Gas Sensors, Materials Research Society Symposium Proceedings **804**, 233-239, (2004).

47 Mirsky V. M., Kulikov V., Hao Q., and Wolfbeis O. S., ***Application of Combinatorial Electropolymerisation to the Development of Chemical Sensors***, Materials Research Society Symposium Proceedings **804**, 111-116, (2004).

48 Frantzen A., Scheidtmann J., Frenzer G., Maier w. F., Jockel J., Brinz T., Sanders D., and Simon U., ***High-Throughput Method for the Impedance Spectroscopic Characterisation of Resistive Gas Sensors***, Angew. Chem. Int. Ed. **43**, 752-754, (2004).

49 Mirsky V. M., Kulikov V., Hao Q., and Wolfbeis O. S., ***Multiparameter High-Throughput Characterisation of Combinatorial Chemical Microarrays of Chemosensitive Polymers***, Macromolecular Rapid Communications **25**, 253-258, (2004).

50 Cammann K., Guilbault G., Hall E., Kellner R., Schmidt H. L., and Wolfbeis O. S., ***The Cambridge Definition of Chemical Sensors***, (1996).

51 Cattrall R. W., ***Chemical Sensors***, Oxford University Press Inc., New York (1997).

52 Wolfbeis O. S. (Editor), ***Fiber Optic Chemical Sensors and Biosensors, Vol. 1&2***, CRC, Boca Raton (1991).

53 Lin J., ***Recent Development and Applications of Optical and Fiber-Optic pH Sensors***, TrAC **19**, 541-552, (2000).

54 Klimant I., Huber C., Liebsch G., Neurauter G., Stangelmayer A., and Wolfbeis O. S., ***Dual Lifetime Referencing (DLR) - A New Scheme for Converting Fluorescence Intensity into a Frequency-Domain or Time-Domain Information***, in ***New Trends in Fluorescence Spectroscopy; Application to Chemical and Life Sciences***, Valeur B. and Brochon J. C. (eds.), Springer-Verlag, Berlin (2001).

55 Eggins B. R., ***Chemical Sensors and Biosensors***, John Wiley & Sons, New York (2002).

56 Wolfbeis O. S., ***Fiber-Optic Chemical Sensors and Biosensors***, Anal. Chem. **74**, 2663-2677, (2002).

57 Narayanaswami R. and Wolfbeis O. S. (eds.), ***Optical Sensors; Industrial, Environmental and Diagnostic Applications***, Springer-Verlag, Berlin (2003).

58 Chtanov A. and Gal M., ***Differential Optical Detection of Hydrogen Gas in the Atmosphere***, Sens. Actuators **B79**, 196-199, (2001).

59 Sutapun B., Tabib-Azar M., and Kazemi A., ***Pd-Coated Elastooptic Fiber Optic Bragg Grating Sensors for Multiplexed Hydrogen Sensing***, Sens. Actuators **B60**, 27-34, (1999).

60 Mendoza M., Carrillo A., and Marquez A., ***New Distributed Optical Sensor for Detection and Localisation of Liquid Hydrocarbons Part II: Optimisation of the Elastomer Performance***, Sens. Actuators **A111**, 154-165, (2004).

61 Wark M., Rohlfing Y., Altindag Y., and Wellmann H., ***Optical Gas Sensing by Semiconductor Nanoparticles or Organic Dye Molecules Hosted in the Pores of Mesoporous Siliceous MCM-41***, Physical Chemistry Chemical Physics **5**, 5188-5194, (2003).

62 Schafer K., Jahn C., Sturm P., Lechner B., and Bacher M., ***Aircraft Emission Measurements by Remote Sensing Methodologies at Airports***, Atmos. Environ. **37**, 5261-5271, (2003).

63 von Bueltzingsloewen C., McEvoy A. K., McDonagh C., MacCraith B. D., Klimant I., Krause C., and Wolfbeis O. S., ***Sol-Gel Based Optical Carbon Dioxide Sensor Employing Dual Luminophore Referencing for Application in Food Packaging Technology***, Analyst **127**, 1478-1483, (2002).

64 Mills A. and Eaton K., ***Optical Sensors for Carbon Dioxide: An Overview of Sensing Strategies Past and Present***, Quimica Analitica **19**, 75-86, (2000).

65 McMurray H. N. and Albadran J., ***Colorimetric and Fluorimetric Polymer Membrane Gas-Sensing Materials***, MRS Bulletin **24**, 55-59, (1999).

66 Klimant I., Kuehl M., Glud R. N., and Holst G., ***Optical Measurement of Oxygen and Temperature in Microscale: Strategies and Biological Applications***, Sens. Actuators **B38**, 29-37, (1997).

67 Liebsch G., Klimant I., Frank B., Holst G., and Wolfbeis O. S., ***Luminescence Lifetime Imaging of Oxygen, pH, and Carbon Dioxide Distribution Using Optical Sensors***, Appl. Spectrosc. **54**, 548-559, (2000).

68 Douglas P. and Eaton K., ***Response Characteristics of Thin Film Oxygen Sensors, Pt and Pd Octaethylporphyrins in Polymer Films***, Sens. Actuators **B82**, 200-208, (2002).

69 Amao Y., ***Probes and Polymers for Optical Sensing of Oxygen***, Mikrochim. Acta **143**, 1-12, (2003).

70 Miller L. S., McRoberts A. M., Walton D. J., Peterson I. R., Parry D. A., Sykesud C. G. D., Newton A. L., Powell B. D., and Jasper C. A., ***Optical Gas Sensing Using Thin Organic Films***, Thin Solid Films **284-285**, 927-931, (1996).

71 Freeman M. K. and Bachas L. G., ***Fiber Optic Sensor for NOx Nitrogen Oxides***, Anal. Chim. Acta **256**, 269-275, (1992).

72 Chang Q., Sipior J., Lakowicz J. R., and Rao G., ***A Lifetime-Based Fluorescence Resonance Energy Transfer Sensor for ammonia***, Anal. Biochem. **232**, 92-97, (1995).

73 Werner T., Klimant I., and Wolfbeis O. S., ***Ammonia-Sensitive Polymer Matrix Employing Immobilised Indicator Ion Pairs***, Analyst **120**, 1627-1631, (1995).

74 Mills A., Wild L., and Chang Q., ***Plastic Colorimetric Film Sensors for Gaseous Ammonia***, Mikrochim. Acta **121**, 225-236, (1995).

75 Preininger C. and Mohr G. J., ***Fluorosensors for Ammonia Using Rhodamines Immobilised in Plasticized Poly(vinyl chloride) and in Sol-Gel; A Comparative Study***, Anal. Chim. Acta **342**, 207-213, (1997).

76 Mohr G. J., Draxler S., Trznadel K., Lehmann F., and Lippitsch M. E., ***Synthesis and Characterisation of Fluorophore-Absorber Pairs for Sensing of Ammonia Based on Fluorescence***, Anal. Chim. Acta **360**, 119-128, (1998).

77 Stangelmayer A., Klimant I., and Wolfbeis O. S., ***Optical Sensors for Dissolved Sulfur Dioxide***, Fresenius J. Anal. Chem. **362**, 73-76, (1998).

78 Mohr G. J., ***Chromo- and Fluororeactands: Indicators for Detection of Neutral Analytes by Using Reversible Covalent-Bond Chemistry***, Chemistry **10**, 1082-1090, (2004).

79 Posch H. E., Wolfbeis O. S., and Pusterhofer J., ***Optical and Fiber-Optic Sensors for Vapors of Polar Solvents***, Talanta **35**, 89-94, (1988).

80 Dickert F. L., Schreiner S. K., Mages G. R., and Kimmel H., ***A fiber-Optic Dipping Sensor for Organic Solvents in Wastewater***, Anal. Chem. **61**, 2306-2309, (1989).

81 Reichl D., Krage R., Krummel C., and Gauglitz G., ***Sensing of Volatile Organic Compounds Using a Simplified Reflectometric Interference Spectroscopy Setup***, Appl. Spectrosc. **54**, 583-586, (2000).

82 Supriyatno H., Yamashita M., Nakagawa K., and Sadaoka Y., ***Optochemical Sensor for HCl Gas Based on Tetraphenylporphyrin Dispersed in Styrene-Acrylate Copolymers. Effects of Glass Transition Temperature of Matrix on HCl Detection***, Sens. Actuators **B85**, 197-204, (2002).

83 Morales J. A. and Cassidy J. F., ***Model for the Response of an Optical Sensor Based on Absorbance Measurements to HCl***, Sens. Actuators **B92**, 345-350, (2003).

84 Farrell A. P. and Clutterham S. M., ***On-line Venous Oxygen Tensions in Rainbow Trout During Graded Exercise at Two Acclimation Temperatures***, J. Exp. Biol. **206**, 487-496, (2003).

85 Wolfbeis O. S., Kovacs B., Goswami K., and Klainer S. M., ***Fiber Optic Fluorescence Carbon Dioxide Sensor for Environmental Monitoring***, Mikrochim. Acta **129**, 181-188, (1998).

86 Weigl B. H., Holobar A., Trettnak W., Klimant I., Kraus H., O'Leary P., and Wolfbeis O. S., ***Optical Triple Sensor for Measuring pH, Oxygen and Carbon Dioxide***, J. Biotechnol. **32**, 127-138, (1994).

87 John G. T., Klimant I., Wittmann C., and Heinzle E., ***Integrated Optical Sensing of Dissolved Oxygen in Microtiter Plates: A Novel Tool for Microbial Cultivation***, Biotechnol. Bioeng. **81**, 829-836, (2003).

88 Peterson J., I, Fitzgerald R., V, and Buckhold D. K., ***Fiber-optic Probe for In-Vivo Measurement of Oxygen Partial Pressure***, Anal. Chem. **56**, 62-67, (1984).

89 Miller W. W., Yafuso M., Yan C. F., Hui H. K., and Arick S., ***Performance of an In-Vivo, Continuous Blood-Gas Monitor with Disposable Probe***, Clin. Chem **33**, 1538-1542, (1987).

90 Leiner M. J. P., ***Optical Sensors for In Vitro Blood Gas Analysis***, Sens. Actuators **B29**, 169-173, (1995).

91 Siggaard-Andersen O., Goethgen I. H., Wimberley P. D., Rasmussen J. P., and Fogh-Andersen N., ***Evaluation of the Gas-STAT Fluorescence Sensors for Continuous Measurement of pH, pCO_2 and pO_2 During Cardiopulmonary Bypass and Hypothermia***, Scand. J. Clin. Lab. Invest. Suppl. **48**, 77-84, (1988).

92 Mills A., Lepre A., and Wild L., ***Breath-by-Breath Measurement of Carbon Dioxide Using a Plastic Film Optical Sensor***, Sens. Actuators **B39**, 419-425, (1997).

93 Gehrich J. L., Lubbers D. W., Opitz N., Hansmann D. R., Miller W. W., Tusa J. K., and Yafuso M., ***Optical Fluorescence and its Application to an Intravascular Blood Gas Monitoring System***, IEEE Trans. Biomed. Eng. **33**, 117-132, (1986).

94 Werle P., Muecke R., D'Amato F., and Lancia T., ***Near-Infrared Trace-Gas Sensors Based on Room-Temperature Diode Lasers***, Appl. Phys. **B67**, 307-315, (1998).

95 Bozoki Z., Mohacsi A., Szabo G., Bor Z., Erdelyi M., Chen W., and Tittel F. K., ***Near-Infrared Diode Laser Based Spectroscopic Detection of Ammonia: A***

Comparative Study of Photoacoustic and Direct Optical Absorption Methods, Appl. Spectrosc. **56**, 715-719, (2002).

96 Valeur B. and Brochon J. C. (eds.), ***New Trends in Fluorescence Spectroscopy: Applications to Chemical and Life Sciences***, Springer-Verlag, Berlin (2001).

97 Lakowicz J. R., ***Principles of Fluorescence Spectroscopy 2nd Ed.***, Kluwer Academic/Plenum Press, New York (1999).

98 Pauly S., ***Permeability and Diffusion Data***, in ***Polymer Handbook, Fourth Edition***, Brandrup J. and Immergut E. H. (eds.), Wiley-VCH, New York (1998).

Chapter 2. Combinatorial Approach to the Development of Optical Chemical Gas Sensor Materials

2.1. Background

Optical sensors typically respond to the target species by a change in either their colour or luminescence properties, e.g. by a change in decay time of the efficiency of energy transfer. In case of oxygen sensors, decay time is the preferred parameter since it is intrinsically referenced.[1] For acidic or basic gases, like carbon dioxide or ammonia, the most general characterisation method is the determination of the change of absorbance of a pH-sensitive dye on exposure to the target.

The development of sensor materials is still often a kind of empirical ("trial and error") science. Conventional serial development, rational design, requires intensive research in planning of possible sensor compositions. Assuming a typical optical gas sensor to be composed of a supporting matrix and several target-sensitive components and fine-tuning additives, the number of possible combinations rapidly rises to dimensions that hardly can be handled in conventional laboratories. By using ten different species of each component in a ternary mixture, the number of sensors to be manufactured and tested is 10^3 according to equation (1.1). Varying the concentration of sensitive components and additives 10 times each for the validation of the optimal sensor composition and producing at least three samples per sensor for statistically significant analysis spread up the matrix to $3*10^5$ different sensor materials. Typically, the realisation of the preparation and the characterisation test of each sensor requires 2-4 hours in total. Hence, the analysis of such data matrix would involve up to $12*10^5$ man hours of work.

Preparing 60 samples at a time along with parallel or high-throughput characterisation of sensor samples cuts the time required for the realisation by a factor of 60^2. As a result, combinatorial chemistry coming along with automation of synthesis and high-throughput screening methods promise being a key to overcome the bottle necks of conventional sensor development.

The essence of combinatorial chemistry is the integration of rapid chemical synthesis and the high-throughput screening with large-scale data analysis.[2,3] The approach includes the design, implementation and interlocking of (a) library design, (b) combinatorial synthesis, (c)

high-throughput characterisation of the materials manufactured and (d) database supported library handling and evolution. Sophisticated instrumentation as well as process control and synchronisation by PC is obligatory. The schematic view in figure 2.1 displays the process steps during the development of new sensor materials by combinatorial synthesis and high-throughput characterisation (HTC) and the interlinking of the sections in this approach.

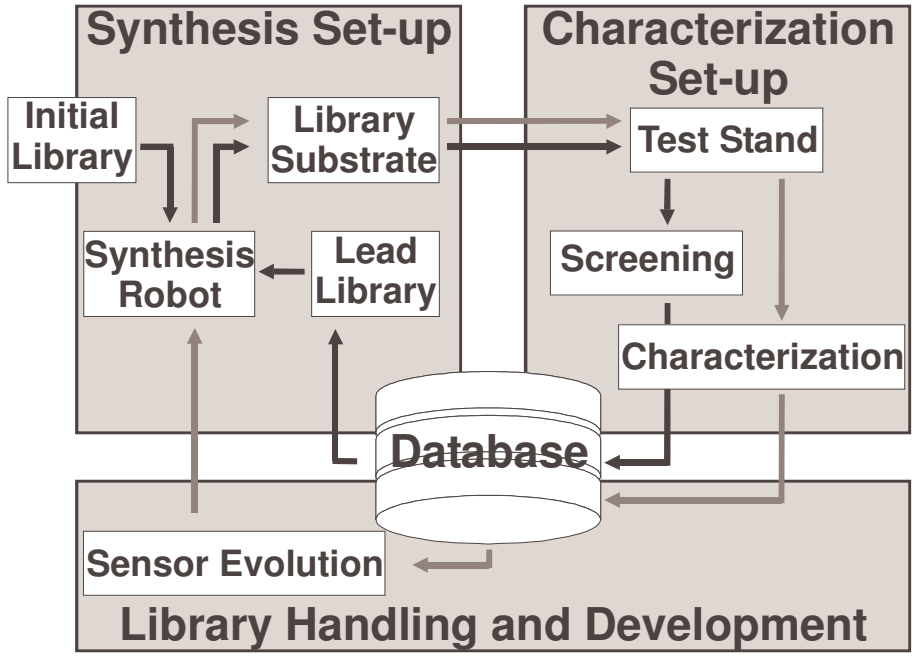

Figure 2.1. Visualisation of the single process steps in the combinatorial development of new sensor materials and the interconnection of the sections of the approach.

2.2. Concept

2.2.1. Library Design

Following a combinatorial approach to the development of new sensor materials, the first step involves the design of a highly diverse library aimed at efficiently exploring large numbers of materials' compositions thought of being of interest. The size of the sensor matrix is spread up by the number of possible combinations of components. It is linked to the complexity of the compositional formulation varying on the requirements imposed to the sensor. Optical gas sensors for the determination of oxygen, carbon dioxide or ammonia are described in literature. They usually consist of

a) a supporting polymer, permeable to the target gas and giving the sensor physical stability,

b) a sensing chemistry, i.e. an indicator dye changing its optical properties on contact with and according to the concentration of the target,
c) a softening agent (plasticizer) for adjustment of physical stability and permeability of the polymer matrix without interfering the detection signal, and
d) in the case of the carbon dioxide sensor, a lipohilic buffer system for adjusting the pH in the micro-environment of the indicator dye.

This composition structure can be extended by any further additive, like a chromoionophore or other chemical substances, according to the target and the analytical characterisation method. Though, not all possible components are coercively present in a sensor formulation. Sensor materials can consist of *m* to *n* ingredients, where *m* is the mandatory and *n* is the overall number of different types of ingredients. Thus, the total N of sensor materials in a combinatorial library is described by the amount of mandatory ingredients, like the polymer and the indicator, complemented by the formulations containing tuning agents in any combination. N can be calculated according to equation 2.1

$$N = a_P \cdot a_D (a_{Pl} \cdot a_{c(Pl)} + 1) \cdot (a_B \cdot a_{c(B)} + 1) \cdot (a_{TA} \cdot a_{c(TA)} + 1) \qquad (2.1)$$

where a_P, a_D, a_{Pl} and a_B represent the number of different species of polymer (P), dye (D), plasticizer (Pl), buffer (B) and any other tuning agent (TA). $a_{c(D)}$, $a_{c(B)}$, $a_{c(Pl)}$ and $a_{c(TA)}$ are the numbers of different concentrations of the particular components used. For each new type of agent a_i the factor $(a_i \cdot a_{c(i)} + 1)$ is added to the equation 2.1.

On basis of the parameters that can be varied, two strategies can be followed for the combinatorial development of optical gas sensor materials. One is the preparation of all possible formulations and the subsequent screening for the desired properties. This approach includes the synthesis of all compositional variations of potentially inactive sensor formulations. Even with appropriate synthesis and testing instrumentation this will result in the attempt of optimising non-sensitive sensor materials. The other combinatorial approach includes the preparation of an initial library containing the mandatory ingredients and its primary testing for exploring the basic parameter space. With the application of filtering rules based on the desired properties a set of hits is selected as lead. This lead library is optimised in several steps by variation of the tuning parameters, i.e. addition of tuning agents and variation of their concentrations. This is illustrated in figure 2.2. The sensor compositions produced are filed in a database containing the ingredients for a specific material and their concentrations within the formulation. These data supply the synthesis automation with the parameters needed for manufacture of the samples to be tested.

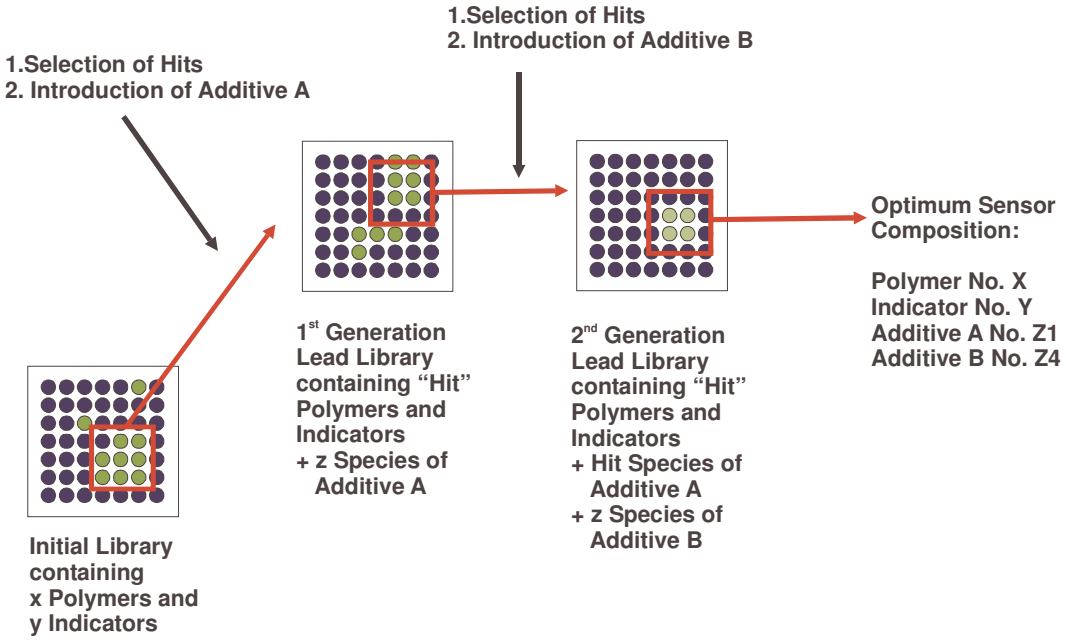

Figure 2.2. Schematic view on the strategy of the combinatorial approach to discovery and optimisation of sensor materials. The "hits" in each library are highlighted by green colour. They are optimised in each next generation of the library introducing new components.

2.2.2. Combinatorial Blending

Optical sensors, as described here, are prepared by immobilisation of the sensing chemistry in a polymer matrix as support. This is achieved either by covalently binding an indicator to the matrix, e.g. via esterification, or physically, e.g. by electrostatic or van der Waals' interactions or dissolution. For an application in gaseous media the sensor materials can be prepared by dissolving the indicator dye and the tuning agents in the organic polymer. The solubility of ionic dyes can be enhanced by ion pairing with lipohilic counter ions.[4,5] Covalent immobilisation is not necessary, since here no bleaching occurs like in sensors applied in liquid media where indicator can be extracted to liquid phase.

In practice the solid indicator dye can be added directly to a solution of polymer dissolved in an organic solvent or stock solutions of each are mixed in the appropriate ratio, both methods forming a homogeneous sensor cocktail. Under the stipulation that all components used are soluble in organic solvents, the automation-assisted synthesis is possible by using a liquid dispensing robot.

Starting from a database containing the compositions of a combinatorial library, including the concentrations of each component, synthesis procedures were programmed with the control software of the liquid handling equipment. The type and amount of ingredients

used for the preparation of a sensor material are given in an EXCEL®-workbook. Via a software interface the control software imports the sensor recipe from the table. The ingredients used for the preparation are provided as stock solutions of known concentration. The transfer of the respective volumes of stock solutions to sample vials is performed by automatic execution of process steps defined in the process algorithm developed. The sensor libraries are prepared by automatic deposition of the sample cocktail onto the substrate and evaporation of the solvent.

2.2.3. High-Throughput Characterisation

High-throughput screening requires the rapid characterisation of the samples' properties under investigation providing the same experimental conditions for all materials. Thus a setup was developed meeting these demands. Generally, it consists of a test chamber for exposing all samples to an atmosphere of defined target concentration simultaneously, a mixing device with gas supply for the creation of the gas mixtures and a detection unit for acquisition of the response signal, i.e. the absorbance spectra or the fluorescence signal. All modules are connected to a PC providing the control of the setup and the data storage.

The modular design enables the configuration of the setup for either the measurement of fluorescence signals or the measurement of absorbance spectra by exchange of the detection instrumentation without interfering the other components. In case of determination of fluorescence properties of the sensor materials, the sensor spots are illuminated with an LED and luminescence is detected by photo-multiplier tubes or photo-diodes. For absorbance measurements the absorbance of the samples is detected via scanning spectrometers or compact spectrometers, (so called multi-channel analysers), covering the visible and near infrared region of the spectrum. The detector is moved to each sample spot to measure the optical properties with two stepper motors arranged rectangularly on an x-y translation stage.

2.2.4. Data Handling

The library preparation delivers a set of data describing the composition of a sample including the species contained in a formulation and the respective content of each component. From screening a set of data is obtained describing the change of the optical properties of the sensors after changing the gas atmosphere the sensor spots are exposed to. These data after processing are transferred to a database containing the information from synthesis. Figure 2.3 shows the connections between the particular tables containing the information on preparation

and characterisation. Examples of such a libraries are given in appendix D-F for the sensor materials investigated in this thesis.

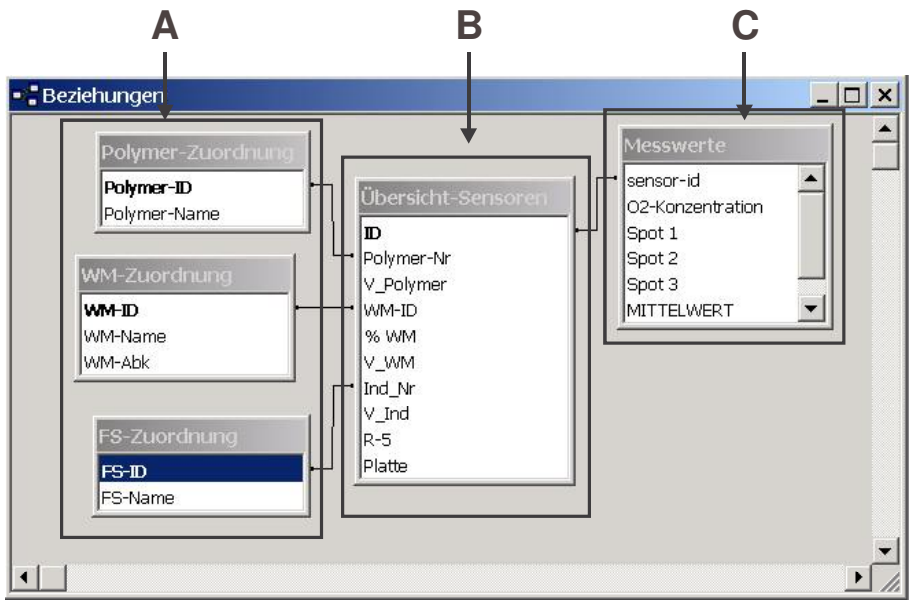

Figure 2.3. Schematic view of the connections of the database tables containing preparation and characterisation data of each sensor under investigation. **A**: Tables containing identifiers for each component used for sensor preparation; **B**: Table indexed via the identifiers of each component, containing preparation data; **C**: Table containing the measurement data linked to the sensor composition via the index in table B.

The application of filtering rules enables the discovery of hit sensors by setting a threshold value for the sensor response and selecting the materials exceeding this value. These hits are combined to a so-called lead library. The materials with the most promising response are extracted and undergo an evolutionary process where the sample composition is fine-tuned in order to obtain spots that display the best performance. This procedure is performed several times until a set of optimal new sensor materials is extracted.

2.3. Experimental Setup for Sensor Preparation and Characterisation

The application of combinatorial chemistry to sensor development involves the implementation of high-throughput instrumentation providing rapid preparation and testing of sample libraries. This system comprises a modified liquid handling device for preparation and a purpose-built optical test rig for screening.

2.3.1. Instrumentation for Library Preparation

For the preparation of the sensor materials of interest in this thesis a device able of handling organic solutions of chemicals including viscous polymer solutions is required. Although the market in liquid handling robots is well populated no commercial system was available at the beginning of the project specially dealing with this demand.[6-8] For reasons of cost and flexibility, a system from Hamilton was purchased that is mostly used for repeated liquid distribution. It was modified to handle viscous polymer solutions and aggressive organic solvents.

The system comprises a MicroLab S® sample handler (Part. No. 172002, Hamilton) and a MicroLab 541C® dual syringe diluter (Part. No. R35892, Hamilton). The sample handler is equipped with an omni-directional XYZ-arm for positioning a stainless steel needle (Part. No. 170460), connected to the dispenser, to any position on a working area (see figure 2.4). The stock solutions were provided in vials arranged in racks on the working space. The sample volumes were aspirated from these and dispensed to mixing vials with the dispenser working with the principle of liquid displacement. This is illustrated in figure 2.5. The handler and the diluter are connected to a PC via serial interface (RS 232) and controlled by MicroLab® Sampler software shown in figure 2.6. With this software tool methods were developed for the execution of preparation processes (see Appendix A - C). Built-in procedures enabled the easy creation of aspiration-dispensation loops and the implementation of washing steps minimising the danger of contaminating sensor cocktails with false components.

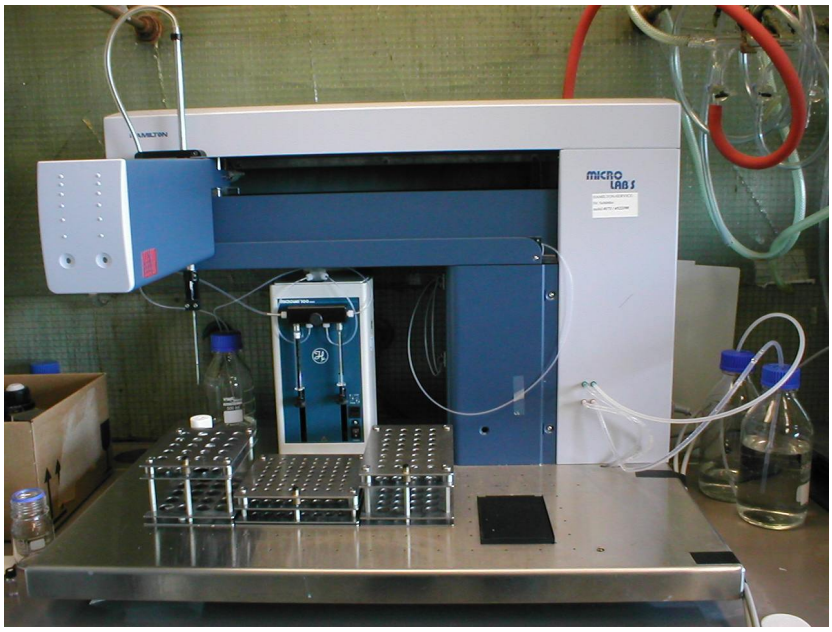

Figure 2.4. Liquid handling system MicroLab® S.

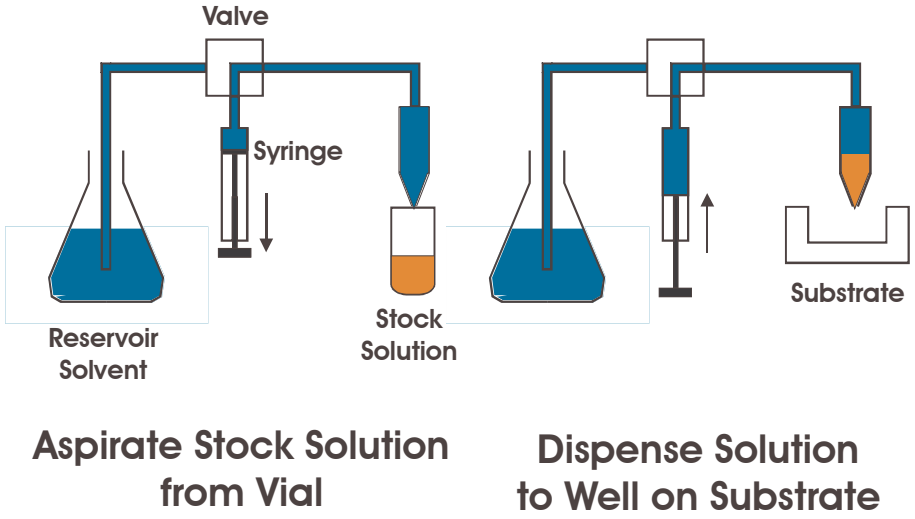

Figure 2.5. Schematic view of the working principle of the dispensing system. The sample solution is aspirated from a stock vial when moving downward the syringe stamp and dispensed to the substrate when moving up the stamp. By changing the position of the valve solvent can be aspirated from reservoir and dispensed to waste for washing the tubing.

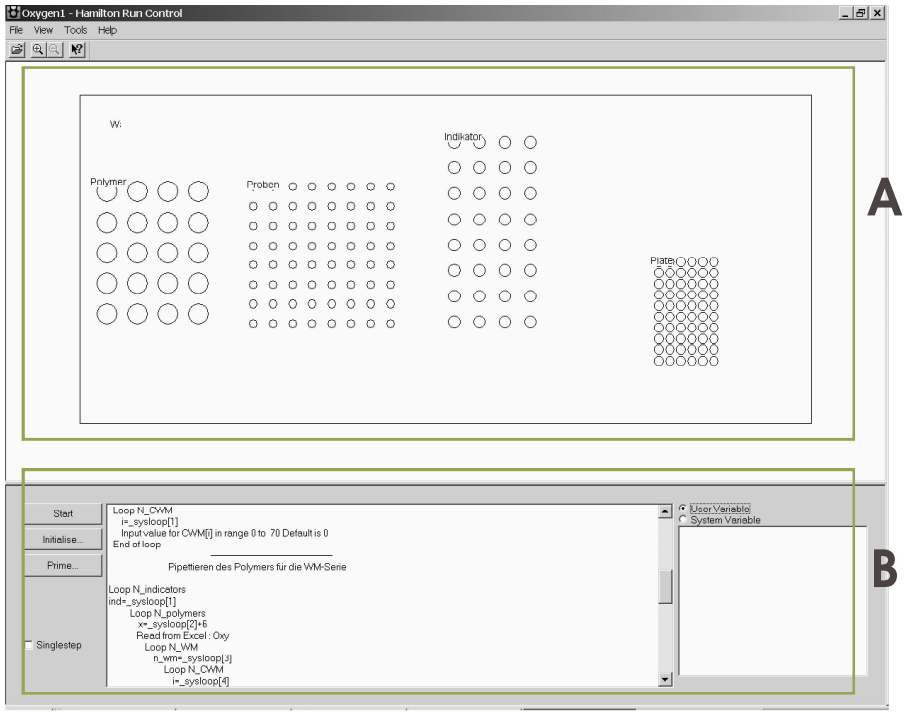

Figure 2.6. Screenshot of the MicroLab® Sampler software with (A) schematic view of the operating area loaded with stock solutions and (B) monitor showing the actual process step of a blending procedure performed.

2.3.2. Setup for Library Characterisation

2.3.2.1. Measurement Setup

Optical gas sensor materials as described here are characterised by detecting the change of optical properties of a sensor spot on changing the gas atmosphere the sample is exposed to. The response of the samples results in a change in either the absorbance of the film or – in case of fluorescence - in a change in decay time of the luminescence.

An apparatus for the characterisation of the libraries was built up comprising (1) a gas chamber, (2) a gas mixing device with mass flow controllers, (3) an x-y table for positioning of the detector head, (4) a PC for synchronisation and control of the modules and (5) a detection unit customised to the method of signal detection. For absorbance measurements the latter module consists of a fiber optic light source for illumination of the samples and a compact CCD-spectrometer (PMA 11, Hamamastu Photonics Deutschland GmbH) equipped with a fiber optic detector head.[9] Absorbance spectra were acquired in the wavelength range from 400 to 800 nm. The detection unit for luminescence measurements features a dual branch glass fiber bundle as light guide for illumination and luminescence determination, a photomultiplier tube (PMT, Hamamatsu Photonics Deutschland GmbH)[9] and a lock-in amplifier (DSP SR830, from Stanford Research Systems)[10] for the acquisition of intensity and phase shift of sensor luminescence. Blue LEDs (product no. NSPB500S, Nichia) and green LEDs (product no. NSPG500S, Nichia) with peak wavelengths of 470 and 530 nm, respectively, were used for fluorescence excitation of the sensor materials.[11] The ruthenium dyes were characterised using the blue LED with a BG12 as an excitation filter and an OG 570 as emission filter, both from Schott (Germany).[12] The modulation frequencies were 90 kHz for $Ru(dphbpy)_3$ and 45 kHz for $Ru(dpp)_3$, respectively. For the Pt(II) complex the green LED with an FITC excitation filter from ITOS (Germany)[13] and an RG 630 emission filter from Schott were used. The LED was modulated at 5 kHz. In figure 2.7 the setup for absorbance and for luminescence measurements is illustrated.

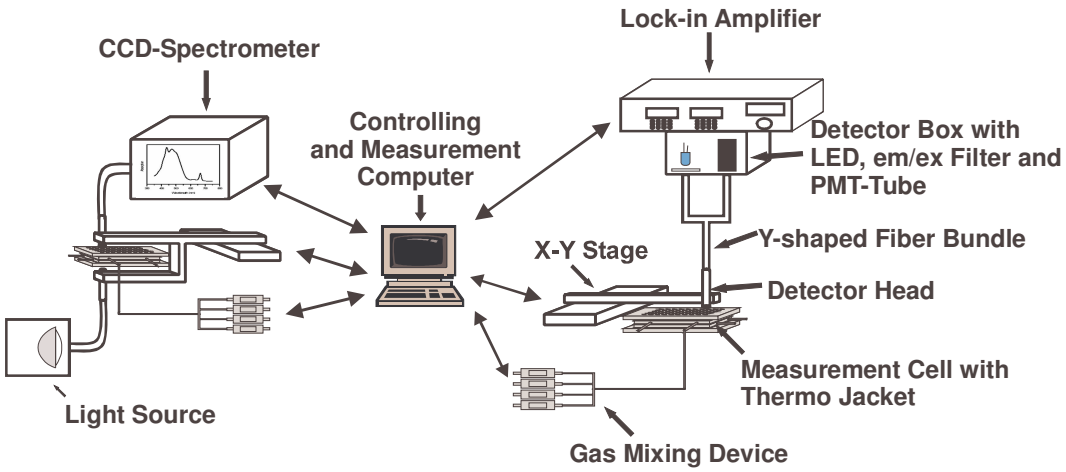

Figure 2.7. Schematic view of the measurement setup for the characterisation of the gas sensor materials. Layout for absorbance (left) and luminescence measurements (right).

The modules are controlled and the data acquired are processed by purpose-built software based on the National Instruments LabView® platform.[14] The software applications for control of the modules and the technical realisation of the characterisation setup were made by a co-worker, Dr. Damian Andrzejewski, according to requirements set in correlation with the experimental parameters of interest.

2.3.2.2. Gas Mixing Device

The characterisation of the sensitivity of the materials under investigation to target gases of interest requires the precise and reproducible supply of gas blends creating atmospheres of defined target gas concentration. This was achieved by blending of an inert carrier gas with target gases. For this purpose mass flow controllers (type 1179) were employed regulating the flow of each component via application of a rated voltage according to the flow rate demanded. They were purchased from MKS Instruments, Germany.[15] The devices used were calibrated correcting differences of rated value and actual voltage measured with a digital voltage meter.

The mass flow controllers were connected to a flute like pipe system leading to the measurement cell as shown in figure 2.8. The controllers for the carrier gas had a minimum flow rate of 100 mL / min and a maximum flow rate of 5000 mL / min. The minimum and maximum flow rate of target gas was 10 and 500 mL / min, respectively. Flow rates of 2000 mL / min should not be exceeded, since due to the dimensions of the gas cell and the tubings connected pressure could be built up in the system. Then the pCO_2 determined does not correspond to ambient barometric pressure.

Blending was performed by injection of target gas into the carrier flow through pipes plugged perpendicularly to the main pipe. The humidity of the test gas was set by blending dry gas with humid carrier. Humidification was achieved bubbling dry carrier gas through two thermostated washing flasks filled with water and subsequent blending of the humid carrier with the other gases used. Humidity in the gas was monitored with a capacitive humidity sensor from E+E Elektronik (Austria) placed in the gas flow.[16]

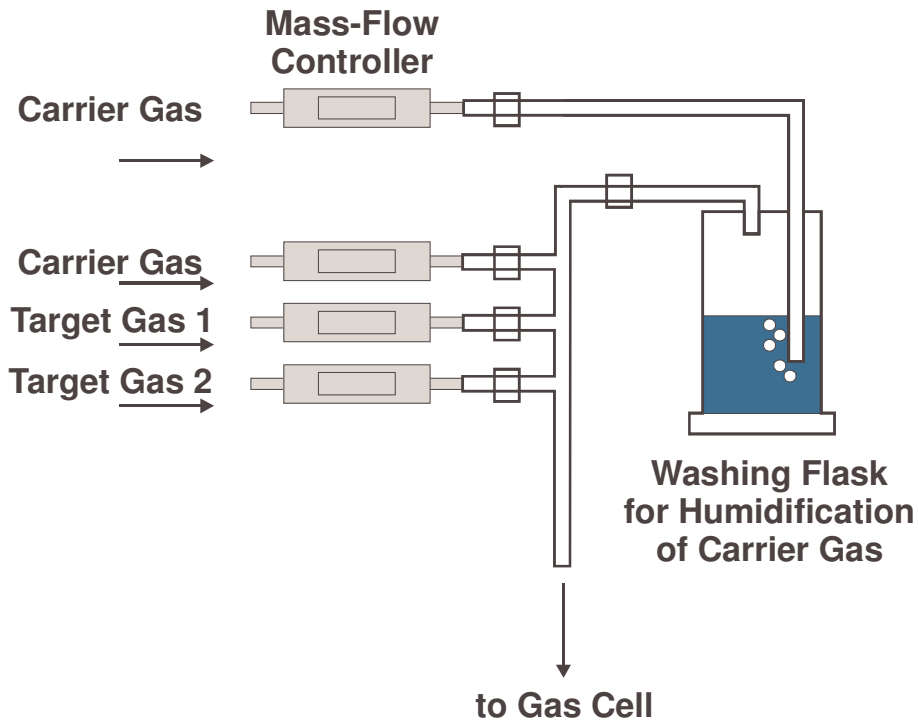

Figure 2.8. Schematic view of the arrangement of the mass-flow controllers for humidification of carrier gas and blending of carrier gas with target gases for production of test atmospheres.

2.3.2.3. Measurement Control

The aim of application of the high-throughput measurement setup was the rapid characterisation of optical properties of gas sensor materials. Thus, the system had to provide control of defined experimental conditions, i.e., the input parameters target gas concentration, constant temperature and humidity and sample identity. The characterisation of the samples required the acquisition of experimental data characterising the optical properties of each sample with automatically allocating the data obtained to the respective sample.

Purpose-built programs developed with Lab View modular programming platform controlled the setup modules fulfilling the requirements given. With these automatic screening of change in luminescence decay time and change in UV/vis-absorption of sensor

materials on changing the gas atmosphere the samples were exposed to was performed. A semi-automatic screening tool was used for the evaluation of response time of absorbance-based sensor materials. See figure 2.9 for screen shots of the screening tools.

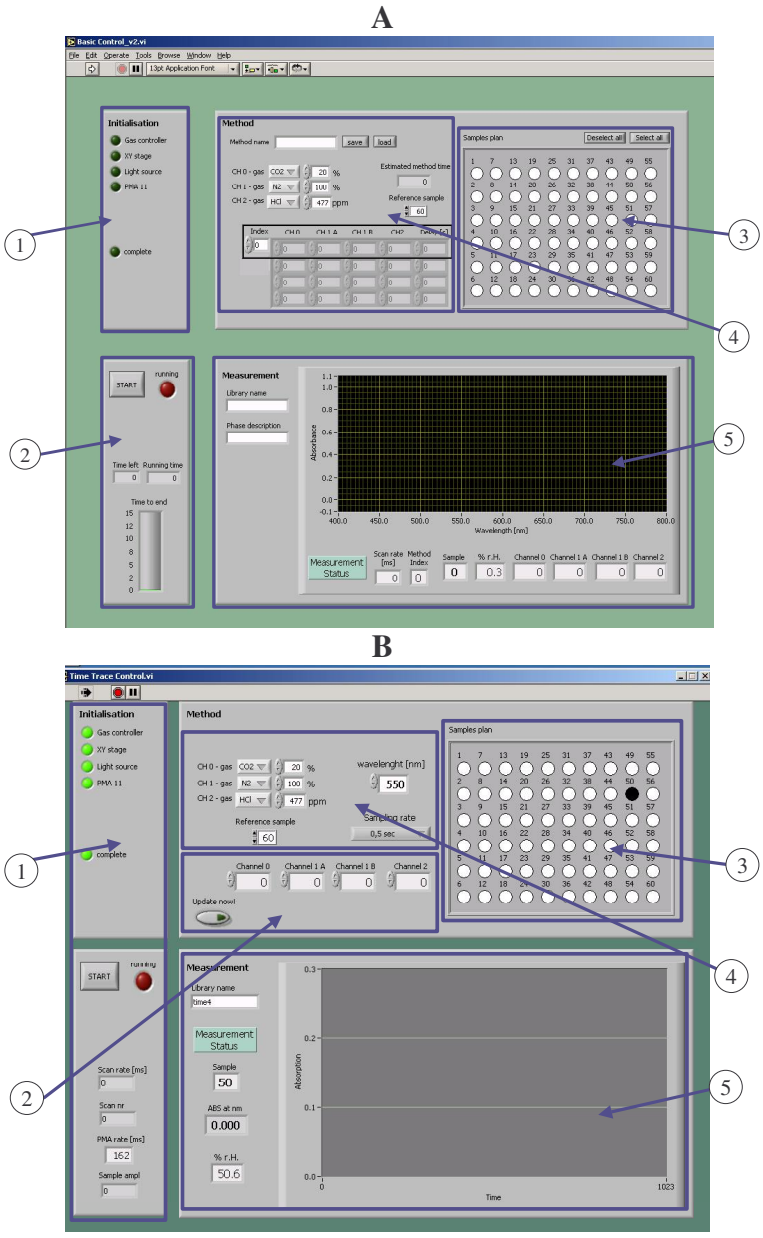

Figure 2.9. Screen shots of the software tools used for screening of optical sensor libraries. **A**: Automatic evaluation of absorbance spectra of samples in defined gas atmosphere with display for instrument status (1), sample selection on plate (3), definition of gas profile (4) and spectrum display (5). **B**: Tool for manual evaluation of sample response with instrument status (1), actual gas composition (2), sample selection (3), display of sampling wavelength and rate (4) and online display of response signal (5).

The software for the determination of luminescence decay time comprised a command window where pre-defined screening procedures were executed. These were built up from operation commands the user set according to the single steps included in the work flow of a screening process. Operation command were defined for moving the x,y-platform from home position to reference position for calibration of the lock-in amplifier or to sample positions for acquisition of luminescence signals of sample spots. The experimental conditions were defined with commands for setting detector parameters as amplitude and modulation frequency of illumination LED, time constant of signal averaging and sensitivity of the detector, as well as with commands for creating the gas atmosphere by controlling flow of gas through each mass flow controller. The signals detected were stored automatically in files given by the user. The combination of the instruction steps to loops enabled the automatic repeated performance of data acquisition for multiple samples under same experimental conditions for screening of properties of interest.

The screening of sensor materials for change of absorbance on exposition to atmospheres of changing target gas concentration was performed using a software tool based on functions similar to the luminescence determination program. Instead of programming a screening sequence manually with operation commands, here the parameters were set in a “drag and drop” mode and via input of values to given menus. The user interface was divided in several areas representing the modules used. The samples under investigation were selected from a facsimile of the substrate on activating respective buttons. The gas sampling sequence was set on manual input of the single channel flow values or on uploading of predefined sampling profiles. Manual input was required for the file name the experimental data was to be stored in. Finally, the user interface provided displays for instrument status, measurement status and graphical display of the absorbance spectrum of the actual sample under investigation for online monitoring of data acquisition. Execution of screening program was automatically without interception by the user.

The tool for online monitoring of sample response provided input of absorbance wavelength of the sample under investigation and real-time setting of gas profile. The signals acquired were stored in respective files with a sampling rate set by the user. A graphical display was used to illustrate the response of the sample to target gas via change of absorbance. Interception by user was possible via dynamic online input of gas flow of each gas used. Once started, data acquisition was performed automatically.

2.4. Results and Discussion

2.4.1. Validation of the MicroLab® S

The preparation of thin-film optical sensor materials requires the reproducible blending of compounds. For the formation of homogeneous films it is necessary to provide adequate viscosity of the polymer solution. Otherwise convection of compounds during drying of the sensor cocktail on the substrate can cause concentration gradients of compounds inside the film resulting in inhomogeneous response to target gases of the sample. The MicroLab S available is designated to perform the blending of stock solutions of compounds including viscous polymer solutions. Thus, the reliability of the aspiration and dispensation steps during preparation has to be validated.

Chemical Compatibility of Parts

Since all aspiration and dispensation steps are performed with one stain-less steel needle on changing from one stock solution to another the needle has to be cleaned inside and outside. This is realised by flushing system solvent through the needle and washing the tip with washing solution (same solvent as system solution) in the washing station mounted on the working space of the robot. On several test with organic solvents THF was selected and employed as solvent for this purpose, since it is the most general solvent for the batches of chemicals applied in this project and clogging of washing pumps by polymer precipitated on change-over of solvents is minimised. During the initial tests it was observed that the tubing of the robot was not compatible to this solvent, though chemical resistance to aggressive organic solvents was demanded to the supplier. The standard tubing was from a thin Teflon core wrapped with a shell tubing from PVC. Mechanical stress caused cracks on junctions of these tubes and fittings of washing pumps or other plastic parts in contact with the solvent. Figure 2.10 shows parts needed to be exchanged. Thus, several modifications were made to provide processibility of aggressive organic solvents with the MicroLab® S. This included the exchange of all standard tubing by more robust tubing from solid PTFE, the exchange of the housing of the washing station and equipping of the washing pumps with robust membranes and covers. Since this improvement no brake-down due to chemical incompatibility occurred.

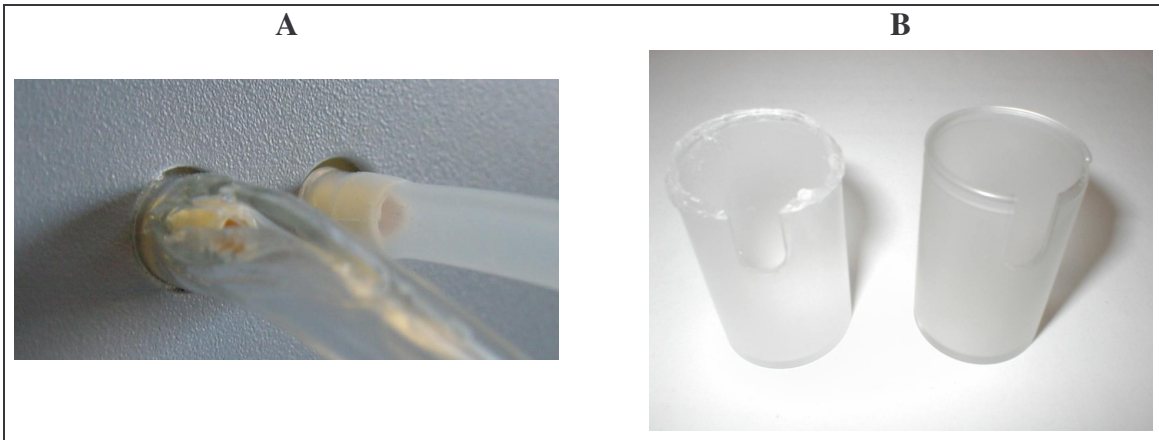

Figure 2.10. Pictures of incompatible system components of MicroLab® S and replacement parts. **A**: Tubing made of PVC in the front destroyed by THF washing solution. It was replaced by a PTFE tubing. **B**: Cover of washing station (left) was dissolved by THF solution used for cleaning the aspiration/dispensation needle.

Accuracy of Dispensation Volume and Viscosity of Solution

After providing the operating efficiency of the liquid handling system the accuracy of dispensing viscous organic polymer solutions was evaluated. The concentration of polymer dissolved in organic solvent was varied in the range of 2 to 10 g per 100 mL stock solution for the polymers of interest. Aliquots of 100, 300 and 500 µL of these solutions, according to 2 to 50 mg of polymer, were dispensed to tared vials and after evaporation of the solvent the amount of polymer transferred was determined. The accuracy of the system was about 99 % with a standard deviation of 0.01 % at aspirating and dispensing 100 µL and 300 µL of stock solution, respectively, and 0.06 % at transferring 500 µL solution. Thus, for each polymer in use the maximum processible polymer concentration and a suitable solvent was evaluated. In table 2.2, the polymers, respective solvents and the maximum concentrations of solid in the solution are listed. On exceeding the processible viscosity of a solution the accuracy of the systems drops dramatically because of false aspiration of air into the hydrostatic system through microscopic spacing between syringe body and stamp.

Table 2.2. List of polymers used for the preparation of optical sensor materials, solvent and concentration of solid in stock solution.

Polymer	Acronym	Solvent	Concentration of Stock Solution / g / 100 mL solution
ethyl cellulose (ethoxyl content 46 %)	EC46	toluene/ethanol (80/20 v/v)	2.5
ethyl cellulose (ethoxyl content 49 %)	EC49	toluene/ethanol (80/20 v/v)	2.5
poly(tetrafluor ethylene-co-vinylidenfluorid-co-propylene)	PFE-VFP	tetrahydrofurane	5.0
poly(styrene-co-acrylonitrile)	PSAN	chloroform	5.0
cellulose acetate	CAc	chloroform	5.0
poly(4-vinyl phenol)	PVPh	tetrahydrofurane	2.5
poly(vinyl methyl ketone)	PVMK	toluene/ethanol (80/20 v/v)	10.0
polysulfone	PSu	chloroform	5.0
poly(vinyl chloride-co-isobutyl vinyl ether)	PVC-iBVE	toluene/ethanol (80/20 v/v)	10.0
poly[(octahydro-5-methoxycarbonyl)-5-methyl-4,7-methano-1H-indene-1,3-diyl)-1,2-ethanediyl]	POMMIE	toluene/ethanol (80/20 v/v)	10.0
poly(bisphenol A carbonate)	PC	chloroform	5.0
poly(4-tert.-butyl styrene)	PTBS	toluene/ethanol (80/20 v/v)	5.0
poly(acrylonitrile)	PAN	dimethylformamide	5.0
poly(vinyl chloride)	PVC	tetrahydrofurane	5.0
polystyrene	PS	toluene/ethanol (80/20 v/v)	10.0
poly(methyl methacrylate)	PMMA	chloroform	5.0

Accuracy of Dispensing Sensor Cocktail to Substrate

After the preparation of sensor cocktails with the robot, the system was used to transfer sample volumes of the solutions made from the mixing vials to a glass substrate fitting into the measurement cell of the optical characterisation setup. The valid characterisation of the

samples required all sample spots to be of homogeneous shape, precisely positioned on the substrate without merging of samples producing cocktail mixtures on the glass. On first tests it was observed that the viscosity of the solutions processed here also is an important factor for the efficient preparation of high quality libraries. When using solutions of low viscosity the merging of sample spots was facilitated because of solvent bleeding over the substrate. Thus, the concentrations of the polymer solutions were set around the highest processible values evaluated and pre-treatment of the substrate was found to be necessary.

Optimisation of the Substrate by Pre-treatment with Hydrofluoric Acid

The design of the substrate was guided by the requirements of (a) accommodation of 60 sample spots to be characterised, (b) fitting into the gas measurement cell of the characterisation setup and (c) impermeability to gas for minimum risk of gas storage in the system. The substrate thus developed was a sheet of borosilicate glass with dimensions of $105 \times 65 \times 1.1$ mm^3 fitting into the measurement cell of the optical setup. Glass was selected as substrate material since it is impermeable to gases and cannot be stained by the indicator dyes used for the particular gas sensors.

The spatial separation of the sample spots was provided by a micro-well plate design. For this purpose the substrate was treated with a ~ 40 % aqueous hydrofluoric acid. In the first step a self-adhesive polypropylene mask with 60 spots cut out was spanned over the surface and the hydrogen fluoride solution was impinged on the cut-outs for 60 minutes creating wells of approx. 100 µm depth and 6 mm diameter. The micro well design and the use of high viscosity solutions provided the precise deposition of individual sensor spots on the substrate without merging of samples. Figure 2.11 shows a library on the substrate before and after treatment with HF. The efficient deposition of sample cocktail was provided by positioning of the robot needle on the surface of the glass substrate granting the contact of solution with the surface on dispensing the cocktail. Due to inescapable convection during the evaporation of the solvent the sample spots appeared to be thicker in the centre. The different shape was a result of varying wetting of the surface by cocktail solution.

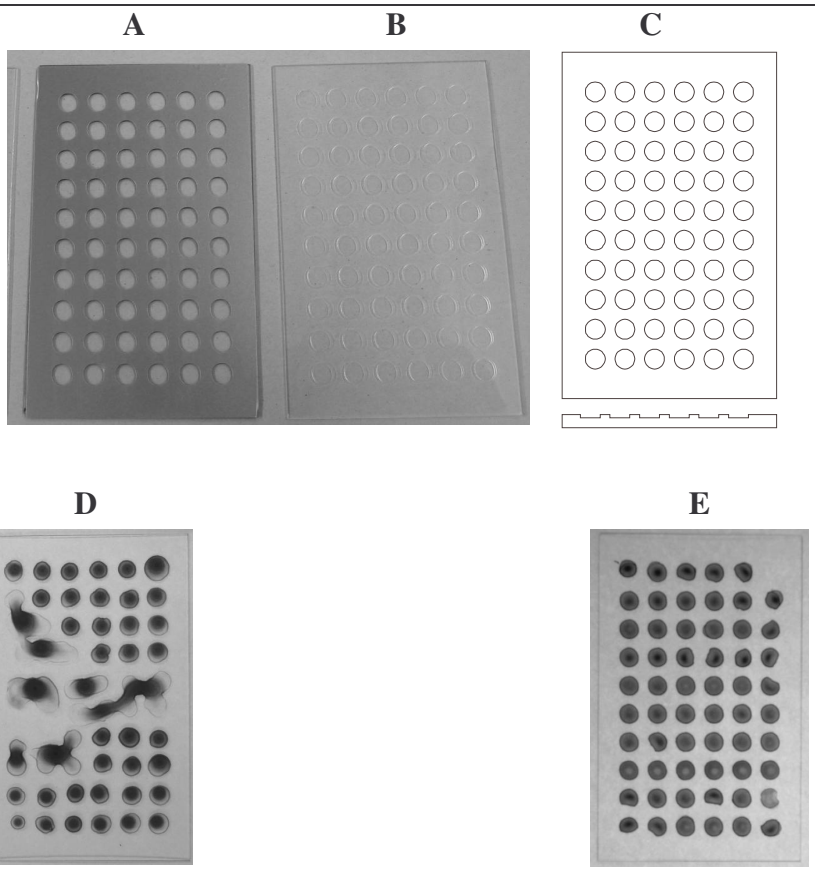

Figure 2.11. **A**: Glass substrate before treatment with etching mask; **B**: Substrate after treatment with 40 % aqueous hydrofluoric acid; C: Schematic view of the etched substrate; **D**: Library deposited on untreated glass plate and **E**: Library on a substrate with micro well design.

Thus, measuring the absorbance spectra of the spots the samples exhibited different extinction values at λ_{max} due to variation of shape and thickness of sensor films. This variation was referenced when the ratio of A_0/A was used for the evaluation of calibration plots of the sensors, where A_0 was the absorbance of the sample in absence of or at a certain minimum concentration of target gas and A was the absorbance of the sample in an atmosphere of defined target gas concentration bigger than in the reference atmosphere the sensor was exposed to. This is illustrated in figure 2.12.

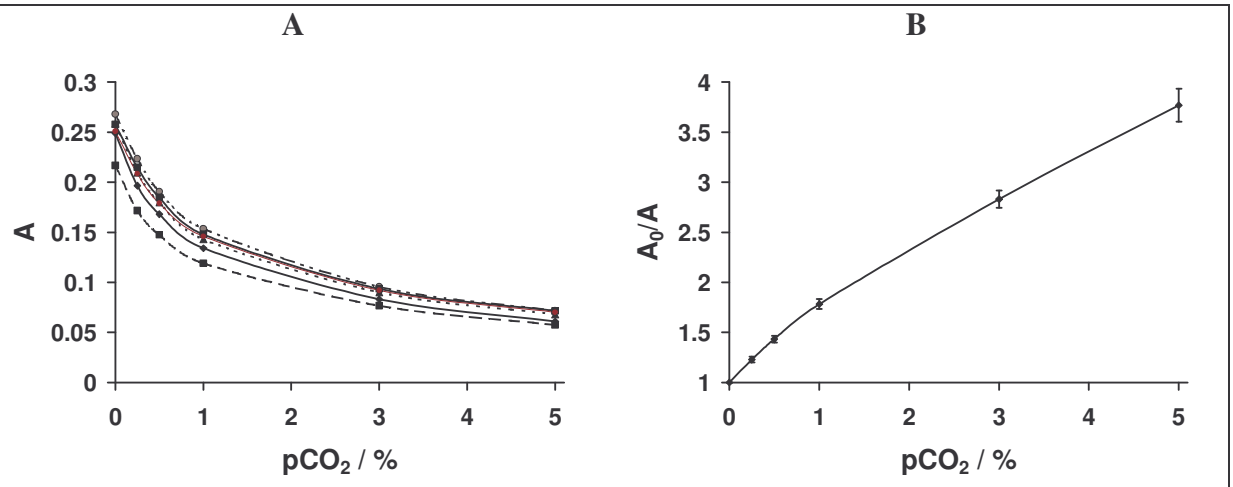

Figure 2.12. A: Absorbance of samples subjected to carbon dioxide at levels between 0 and 5 % (n=6). The plots show significant differences of the particular absorbance values. B: Plot of A_0/A vs. pCO_2 for the same sensor spots, where A_0 is the absorbance of the sample in nitrogen and A is the absorbance at apparent level of CO_2. The relative standard deviation of the ratio A_0/A is > 3 % for each CO_2 level between 0 and 5 %.

2.4.2. Validation of the purpose-built Measurement Setup

After blending of stock solutions and drying off solvent from the sample spots of sensor cocktails transferred onto the glass substrate these libraries were characterised using a purpose-built measurement setup. In order to provide comparability of the data obtained with data from standard measurement instruments the performance of the device was validated.

2.4.2.1. Design of Measurement Cell and Performance of Gas Exchange

The measurement cell was designed to fit the glass substrates with the sample spots deposited in the wells etched into the glass surface for characterisation of the sensory properties of the materials on the solid support. The components were mounted in a sandwich type of construction with screws pressing the components together for sealing the measurement cell from environment. On recommendation of a project partner, Claus Heppel (Robert Bosch GmbH), this locking mechanism was replaced by press locks and as a result simplifying the dismounting and reassembly and speeding up the exchange of substrates.

The design, as shown in figure 2.13, comprised a bottom plate made of aluminium and equipped with guiding angles supporting a coincident stacking of bottom glass plate, water jacket, glass substrate, spacer with drillings for gas in- and outlet and top glass plate. A black coloured cap with 60 windows drilled into the plate made of aluminium was used to seal the

gas cell by pressing the parts together on closing the press lock. These windows built the optical paths for each sensor spot isolating each from the neighbouring spots and provided only parallel light beam to pass the sample to the detector. Interference caused by stray light when measuring absorbance or - in case luminescence measurements – the luminescence of illuminated neighbouring spots was prevented. The gas supporting spacer was made of stainless steel in order to minimise the risk of corrosion when using aggressive gases as hydrogen chloride or ammonia and preventing the storage of gases on diffusive uptake into the spacer material.

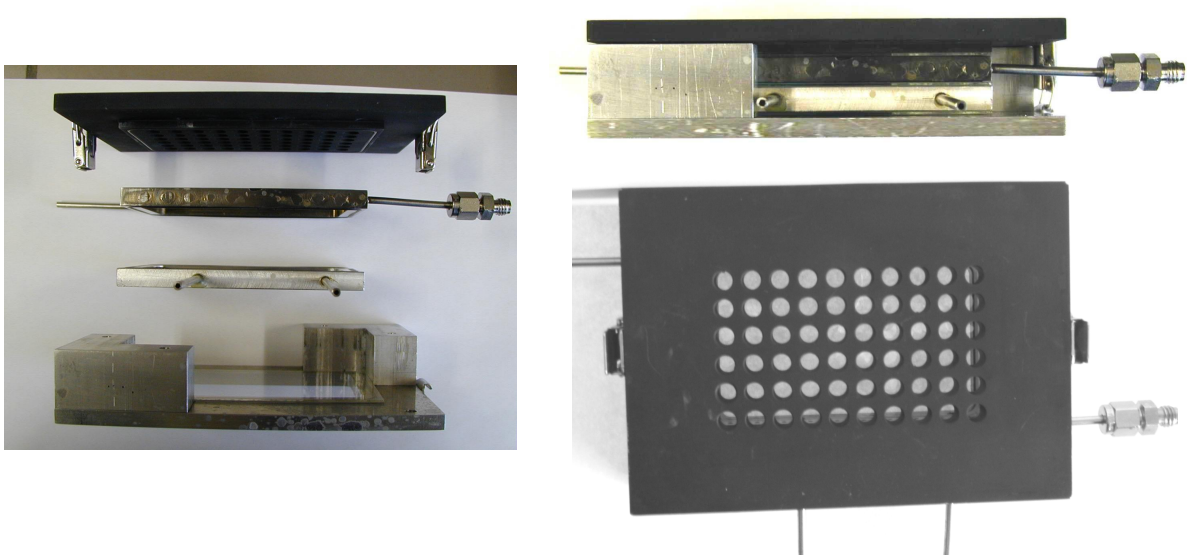

Figure 2.13. Left: View of the dismounted gas measurement cell. From top to bottom: Black coated cover plate with optical paths drilled into the metal body, stainless steel distance ring with drilled holes for gas in- and outlet, water jacket for thermostatisation of the sensor substrate placed between distance ring and water jacket, and solid aluminium support for the alignment of the cell components. **Right**: Front and top view of the mounted cell showing the single optical measurement channels.

The gas flow into and out of the cell was granted though stainless steel pipes connected to channels drilled into perpendicular walls along the spacer ring with openings of this channels towards the inner side of the work piece. The holes were arranged in equal distance placed inline with the positions of the sample spots on the glass substrate.

The gas flow was visualised with a smoke test, where an aerosol was flushed into the mounted cell instead of test gas. The aerosol formed a front moving laminar through the cell to the drillings connected to the outlet pipe. The smoke flowing evenly through the drilled wholes along one side of the test chamber filled the test chamber homogeneously. After this first visual test the distribution of gas flow in the measurement cell was characterised via the

evaluation of the homogeneity of the ratio of luminescence intensity of the oxygen sensitive indicator Ru(dpp) on reducing the oxygen concentration from 10 to 2.5 % v/v in a nitrogen/oxygen atmosphere. Again it was shown that the gas exchange in the cell is homogeneous showing no concentration gradients of oxygen as variations in the ratio would indicate. The measurements were performed with total gas flow between 600 and 1000 mL / min. The gas exchange was lower than 10 s for any of these two flow rates. For pictures from the tests performed see figure 2.14.

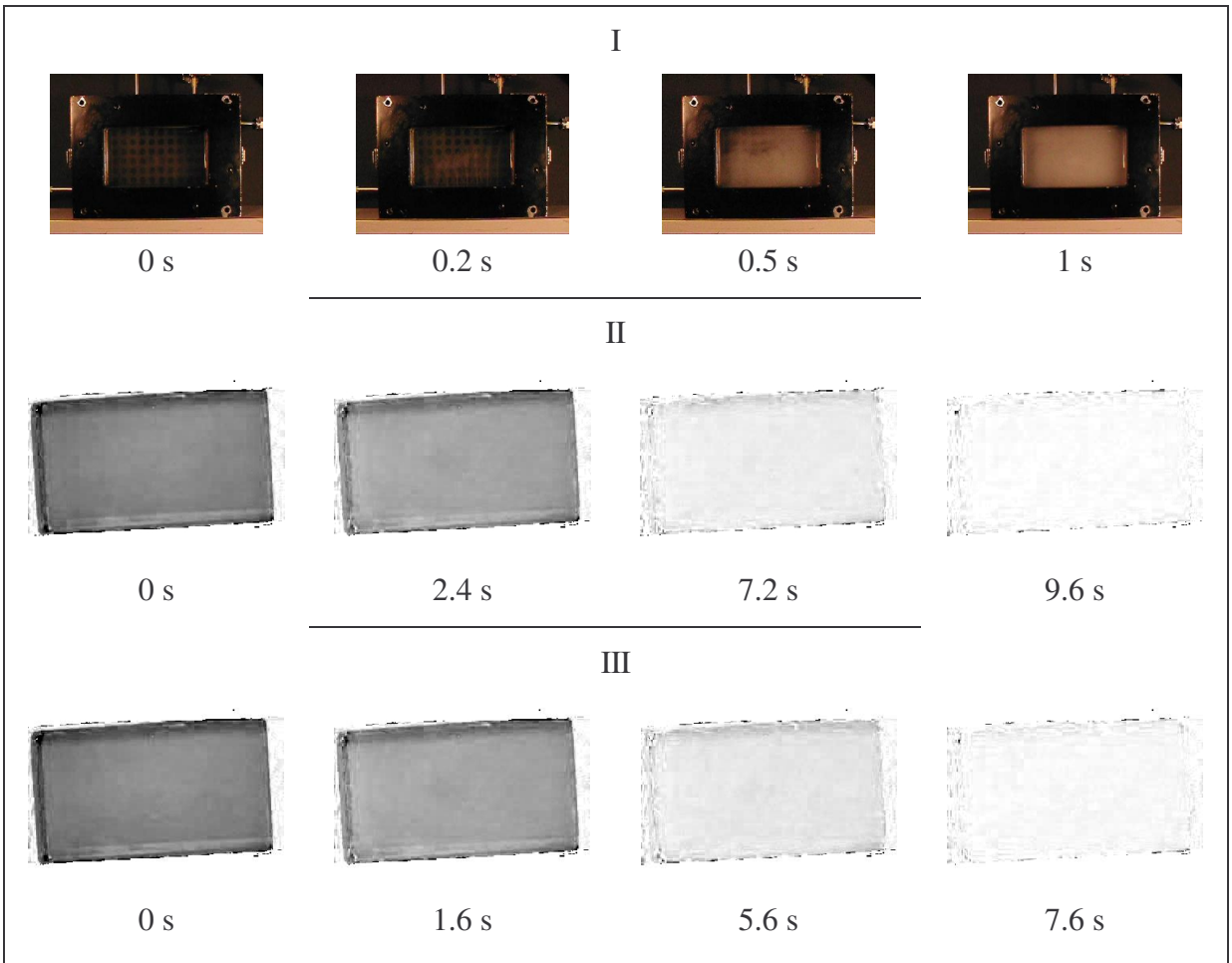

Figure 2.14. Row **I**: Flow of smoke into the test chamber with homogeneous distribution of gas. Rows **II** and **III**: Increase of luminescence ratio of Ru(dpp) on changing oxygen concentration in atmosphere from 10 to 2.5 % v/v at a total gas flow rate of 600 (II) and 1000 mL / min (III), respectively.

2.4.2.2. Performance of the Optical Measurement Setup

Absorbance Measurements

The measurement cell was mounted on a holder at a fixed position. The signal acquisition of each sample was enabled by moving the detector head to the predicted positions of the spots.

For this purpose two linear stages were aligned together perpendicularly building up an x,y translation table. The detector was moved by triggering the stepper motors of the linear stages with voltage pulses. Starting from a reference position the position of the spots were fixed by correlating each with a pair of pulses for the two directions of motion on calibration of the setup. Sample spot no. 60 was left empty for all measurements and used as reference spot for the determination of transmission T = 100 %.

A commercially available optical filter foil (Congo Blue 181, Lee Filters) placed in the measurement cell was used to characterise the performance of the measurement setup and method. The transmission spectra at each sample position were calculated from the light intensities measured with the PMA for each spot using the intensity at the empty spot no. 60 as reference. All spectra, as illustrated in figure 2.15, showed same optical properties with a transmission of 29.9 % at 445 nm with a standard deviation of 0.8 %. This variation was attributed to inhomogeneities of the filter foil and fluctuations of illumination intensity caused by voltage fluctuations in the light source. A spectrum determined with a commercial dual-beam UV/vis spectrometer (Perkin Elmer Lambda 14P) was used for validation of the spectra measured with the high-throughput setup. The difference between the maximum transmissions of both devices was < 2 %. Thus, the optical setup of the detection unit was assumed valid for the characterisation of optical gas sensor materials via absorbance measurement.

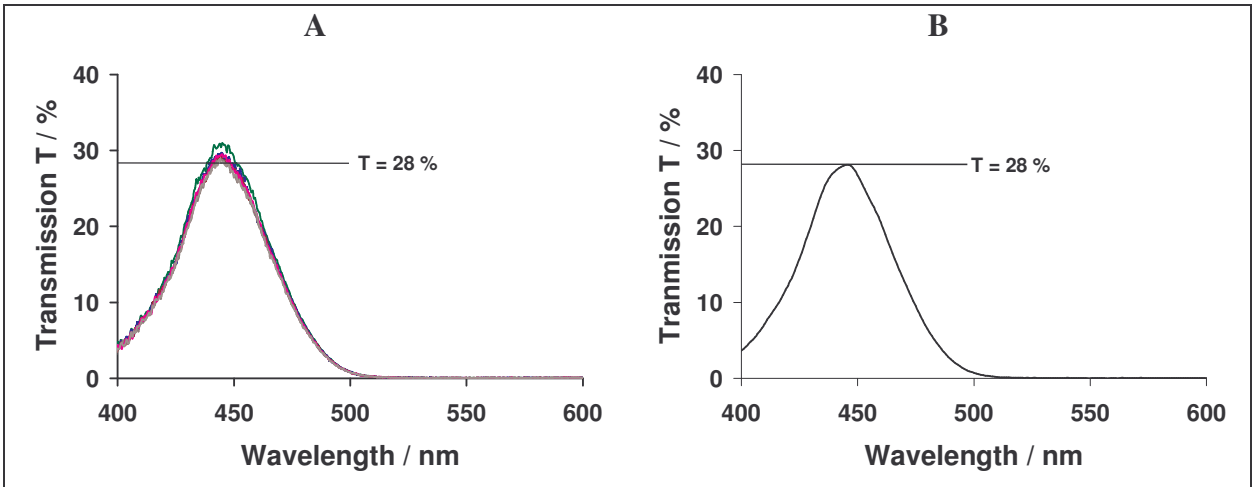

Figure 2.15. Transmission spectra of filter foil Congo Blue 181 from LEE Filters. **A**: Transmission at 6 sample positions measured with setup for high-throughput absorbance measurements using sample position 60 on the substrate as reference. The spectra are reproducible with relative standard deviation < 1 %. **B**: Transmission measured with commercial UV/vis spectrometer (Perkin Elmer Lambda 14P). The difference between the transmission measured with high-throughput setup and commercial spectrometer ΔT is < 2 %.

Luminescence Measurements

The arrangement of the detection unit and method of determination for fluorescence measurements was similar to standard arrangements used at our institute. It only differed in the positioning of the detector head. The detector head of the dual branch optical fiber was mounted to the same holder as the detector head of the fiber-optic CCD-spectrometer. The setup was assumed feasible and valid for fluorescence measurements also, since the precision of movement was validated earlier. This was accomplished by placing a reference luminescent foil in the test chamber and measurement of the luminescence intensity at particular sample spots.

2.5. Conclusion

The combinatorial approach to the development of new materials is characterised by the rapid production of a big number of samples of different composition. It is obvious that the successful implementation of this method to the development of optical gas sensor materials is aligned with instrumentation sufficiently speeding up preparation and screening of materials under investigation. The basic components of optical gas sensor materials have been identified as supporting matrix, sensitive chemistry and additive agents tuning performance of sensor materials. The instrumentation developed for the realisation of the approach has been validated. It was shown that the robotic system is capable of handling organic components dissolved in even aggressive organic solvents. This included viscous organic polymer solutions enabling the preparation of sensor cocktails by blending of different stock solutions and transfer to optical substrates for measurement. The measurement setup developed was validated proving functionality of components. It was possible to detect luminescence signals from substrates containing multiple sensor materials. The software control proved the reproducible and precise acquisition and storage of absorbance spectra of multiple sensor samples on a glass substrate. Furthermore, the modular setup of the devise grants feasibility of changing the method of detection from luminescence decay time to absorbance measurements by simply exchanging the detection unit depending on the signal to be detected.

2.6. References

1 Lippitsch M. E., Pusterhofer J., Leiner M. J. P., and Wolfbeis O. S., ***Fiber-Optic Oxygen Sensor with the Fluorescence Decay Time as the Information Carrier***, Anal. Chim. Acta **205**, 1-6, (1988).

2 McFarland E. W. and Weinberg W. H., ***Combinatorial Approaches to Materials Discovery***, Trends Biotechnol. **17**, 107-115, (1999).

3 Senkan S., ***Combinatorial Heterogeneous Catalysis - A New Path in an Old Field***, Angew. Chem. Int. Ed. **40**, 312-329, (2001).

4 Weigl B. H. and Wolfbeis O. S., ***New Hydrophobic Materials for Optical Carbon Dioxide Sensors Based on Ion Pairing***, Anal. Chim. Acta **302**, 249-254, (1995).

5 Mohr G. J., Werner T., Oehme I., Preininger C., Klimant I., Kovacs B., and Wolfbeis O. S., ***Novel Optical Sensor Materials Based on Solubilisation of Polar Dyes in Apolar Polymers***, Adv. Mater. **9**, 1108-1113, (1997).

6 www.tecan.com

7 www.zinsser-analytic.com

8 www.hamiltoncomp.com

9 www.hamamatsu.de

10 www.srsys.com

11 www.nichia.com

12 www.schott.de

13 www.itos.de

14 www.ni.com

15 www.mksinst.com

16 www.epluse.at

Chapter 3. Application of High-Throughput Screening in a Study on Optical Oxygen Sensors

3.1. Introduction

Oxygen is an essential parameter in many biological systems and a basic requirement for respiration of aerobic organisms.[1] Oxygen analysis is important for understanding and regulation of biological processes.[2,3] Optical (fiber) sensors display excellent performance when compared to the well-established oxygen electrodes (Clark electrode). Their big advantage is no consumption of oxygen during measurement and the possibility of non-invasive determination of the gas due to information guiding via light. Thus, oxygen optodes have successfully introduced into (commercial) sensors for blood oxygen analysis, to bacterial detection, in open-heart surgery, in invasive fiber optic catheters and in bioreactor monitoring.[4-11] They are also used for oxygen determination in environmental research as in deap-sea monitoring and numerous other application areas are conceivable.

The most common type of oxygen sensors are based on the quenching of luminescence of a suitable indicator. The luminescence decay time is the preferred parameter for determination of oxygen concentration with this method, since it is intrinsically referenced.

The wide range of application has encouraged intensive research for well described optical oxygen sensor materials. Yet the development lacks in time consumption and cost of conventional laboratory research. Combinatorial methods for the preparation of new sensor compositions comprise a speed-up and with miniaturisation of batches reduction of cost in the development of new materials and in optimisation of existing formulations. Thus, the high-throughput approach described in chapter 2 was applied to a study on optical oxygen sensors aimed to illustrate the feasibility of this method and the setup developed for sensor material evaluation. The development of oxygen sensors represents an excellent model system for the application of the combinatorial approach, since optical oxygen sensors display a rather simple sample composition and the knowledge base on oxygen sensors is widespread. Intensive research on the development in this field is performed.

3.2. Theoretical Background – Luminescence Quenching-Based Sensing

The luminescence decay time τ_0 of a luminophor is defined by the average time the molecule spends in the excited state prior to return to the ground state.[12] For monoexponential decay the luminescence intensity I at a certain time t is given by the equation

$$I(t) = I_0 \times e^{-\frac{t}{\tau_0}} \tag{3.1}$$

where I_0 is the maximum luminescence intensity during excitation and t is the time after switching off the excitation light source. Thus, the decay time τ_0 can be defined also as the time where $I = \frac{I_0}{e}$.

Two methods for time-resolved measurements are used for the determination of luminescence decay times, namely time-domain and frequency-domain lifetime measurements.[12] For use in oxygen sensors the latter is the method of choice. In the frequency domain method the sample is excited by sinusoidally modulated light and the lifetime of the luminophor causes a time lag between absorbance and emission (phase modulation method). This is expressed by the phase shift θ between excitation and emission phases, and the decreased emission intensity relative to the incident light, called demodulation m (see figure 3.1).

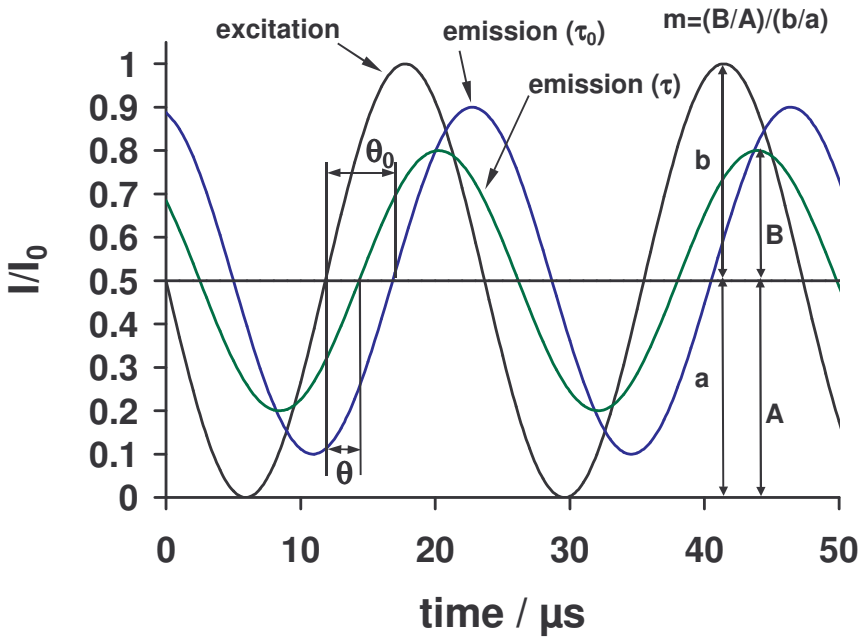

Figure 3.1. Scheme for determination of decay times via phase-modulation method. The blue line represents the measurement signal with a phase shift θ_0 between reference and sample signal in absence of quencher. The green line shows the signal with a phase shift $\theta < \theta_0$ at apparent level of quencher.

The luminescence decay time τ of the luminescent probe in atmospheres of defined oxygen concentration can be calculated from the equation

$$\tau = \frac{\tan\theta}{2\pi f_{mod}} \tag{3.2}$$

where θ is the luminescence phase shift between excitation and emission and f_{mod} is the modulation frequency of the illuminating LED.

Luminescence quenching is referred to any process decreasing the luminescence intensity of a probe (signal transducer) including collisional quenching or energy transfer. Oxygen is known to act as quencher of luminescence of many fluorophors.[12] Thus, an important class of O_2-sensors is based on the decrease of the luminescence signal (intensity or lifetime) of an oxygen-sensitive material, i.e. the indicator dye, as a function of oxygen partial pressure pO_2.[13-15] Usually, the quenching of luminescence is described by the Stern-Volmer equation,

$$\frac{I_0}{I} = 1 + k_q \tau_0 [Q] = 1 + K_{SV}[Q] \tag{3.3}$$

where I_0 and I are the luminescence intensities of the indicator in absence and presence of a quencher Q at a concentration of [Q], k_q is the bimolecular quenching constant, and τ_0 is the lifetime of the non-quenched indicator luminescence. In term of collisional (dynamic) quenching the ratio I_0/I in equation 3.3 can be substituted by τ_0/τ resulting in the lifetime form of the Stern-Volmer equation,

$$\frac{\tau_0}{\tau} = 1 + k_q \tau_0 [Q] = 1 + K_{SV}[Q] \tag{3.4}$$

where τ is the luminescence lifetime in presence of the quencher.

3.2. Materials and Methods

3.2.1. Chemicals

3.2.1.1. Indicator Dyes

Indicator dyes were selected from oxygen-sensitive luminescent metal organic complexes with diimine and porphyrin ligands shown in table 3.1 and figure 3.2. Ruthenium(II)-tris(4,7-diphenyl phenanthroline) di(trimethylsilyl propanesulfonate) (**$Ru(dpp)_3TMS_2$**) (Ru(dpp)) and ruthenium(II)-tris(4,4´-diphenyl bipyridyl)di(trimethylpropanesulfonate) (**$Ru(dpbpy)_3TMS_2$**) (Ru(dphbpy)) used were synthesised according to an adapted protocol as described by

Klimant et al.[15] 5,10,15,20-tetrakis-(2,3,4,5,6-pentafluorophenyl)-porphyrin-Pt(II) (**Pt(PFPP)**) and 5,10,15,20-tetrakis-(2,3,4,5,6-pentafluorophenyl)-porphyrin-Pd(II) (**Pd(PFPP)**) were purchased from Porphyrin Systems (Germany).[16] Indicator stock solutions for processing with the MicroLab® S were prepared dissolving 20 mg of dye in 5 mL of chloroform.

Table 3.1. Excitation wavelength of illuminating LED, emission wavelengths and room temperature decay times of oxygen-sensitive luminescent indicators used in this study.

Indicator	τ_0^*	λ_{ex} / nm	λ_{em} / nm
Ru(dpbpy)	0.4 µs	470	600
Ru(dpp)	4 µs	470	615
Pt(PFPP)	59 µs	530	650
Pd(PFPP)	650 µs	530	670

* in polystyrene when exposed to nitrogen atmosphere

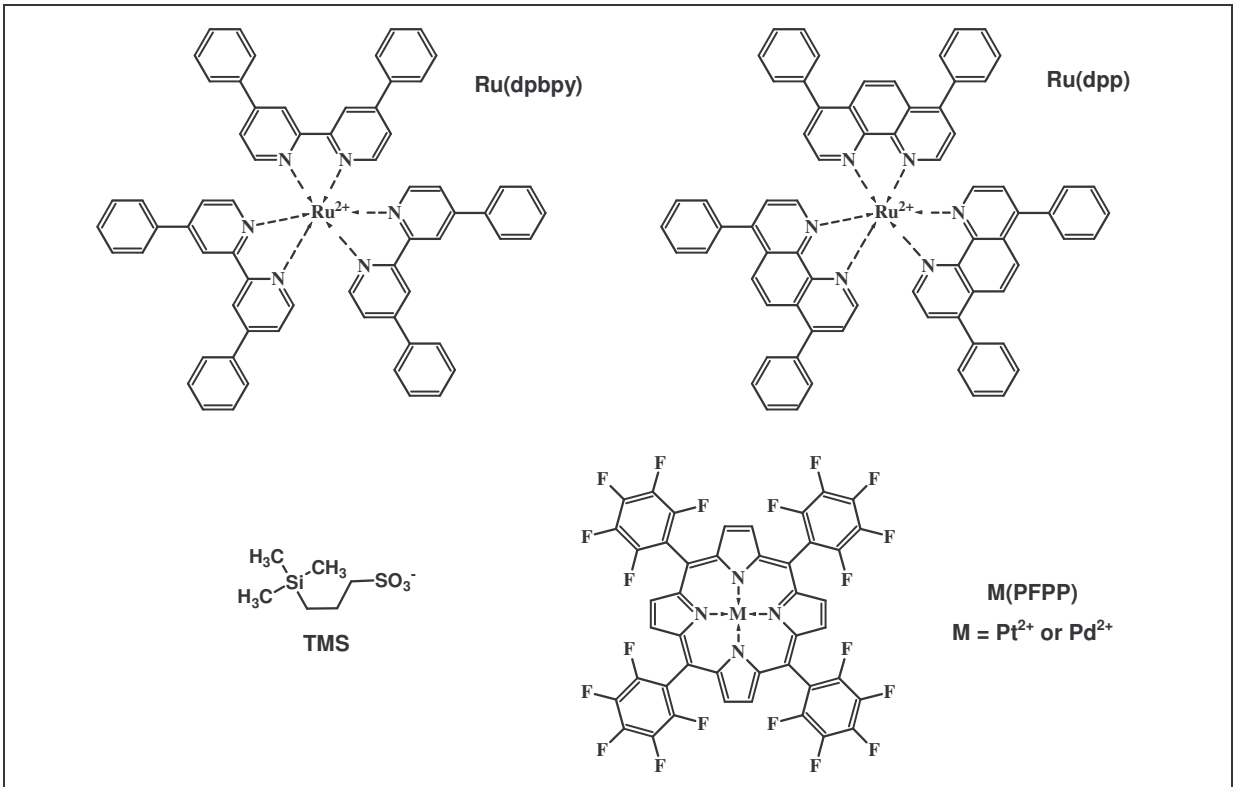

Figure 3.2. Chemical structures of the oxygen probes used in this study and the TMS counter ion of the ruthenium complexes.

3.2.1.2. Solvents

Ethanol, toluene, chloroform, N,N-dimethylformamide and tetrahydrofurane were purchased from Merck.[17] All solvents were of analytical grade and used without further purification.

3.2.1.3. Polymers

All polymers used are listed in table 3.2. They were purchased from Aldrich[18], with exception of PMMA being from Goodfellow.[19] The chemical structures of the components are shown in figure 3.3. Stock solutions of the polymers were prepared dissolving each polymer in the respective organic solvent for processing with the MicroLab® S liquid handler.

Table 3.2. List of polymers used for preparation of oxygen sensor films and concentration of stock solutions processed with MicroLab® S.

Polymer (Prod. No.)	Acronym	Solvent	Conc. of Solution / g / 100 mL
ethyl cellulose (20067-0)	EC46	toluene/ethanol (80/20 v/v)	2.5
ethyl cellulose (20066-2)	EC49	toluene/ethanol (80/20 v/v)	2.5
poly(tetrafluor ethylene-co-vinylidenfluorid-co-propylene) (45458-3)	PFE-VFP	tetrahydrofurane	5.0
poly(styrene-co-acrylonitrile) (18286-9)	PSAN	chloroform	5.0
cellulose acetate (18095-5)	CAc	chloroform	5.0
poly(4-vinyl phenol) (43621-6)	PVPh	tetrahydrofurane	2.5
poly(vinyl methyl ketone) (18274-5)	PVMK	toluene/ethanol (80/20 v/v)	10.0
polysulfone (37429-6)	PSu	chloroform	5.0
poly(vinyl chloride-co-isobutyl vinyl ether) (46829-0)	PVC-iBVE	toluene/ethanol (80/20 v/v)	10.0
poly[(octahydro-5-methoxycarbonyl)-5-methyl-4,7methano-1H-indene-1,3-diyl)-1,2ethanediyl] (46710-3)	POMMIE	toluene/ethanol (80/20 v/v)	10.0

poly(bisphenol A carbonate) (18162-5)	PC	chloroform	5.0
poly(4-tert.-butyl styrene) (36970-5)	PTBS	toluene/ethanol (80/20 v/v)	5.0
poly(acrylonitrile) (18131-5)	PAN	dimethylformamide	5.0
poly(vinyl chloride) (34676-4)	PVC	tetrahydrofurane	5.0
polystyrene (18242-7)	PS	toluene/ethanol (80/20 v/v)	10.0
poly(methyl methacrylate) (ME306010)	PMMA	chloroform	5.0

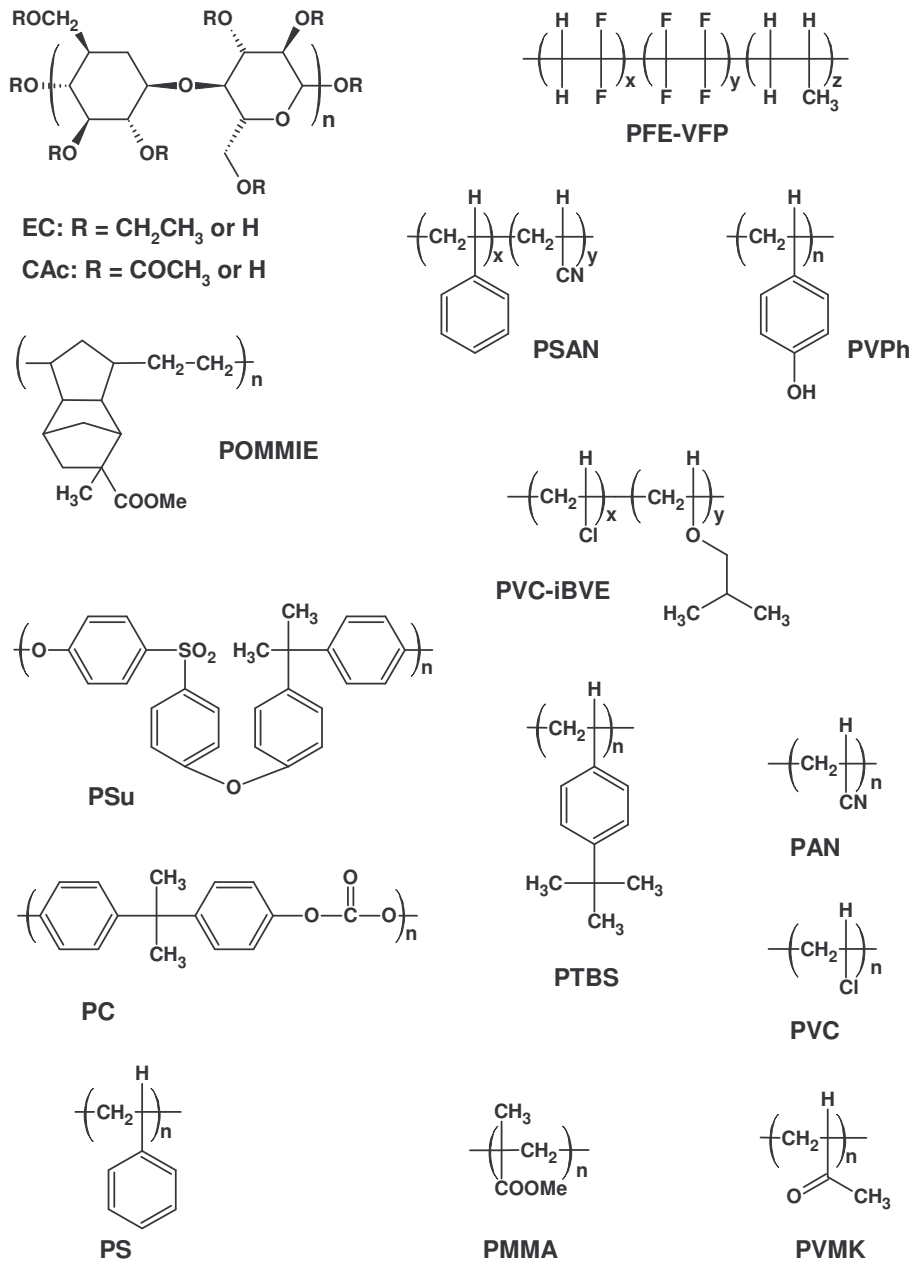

Figure 3.3. Chemical structures of the polymers used in the study on optical oxygen sensors

3.2.1.4. Plasticizers

The plasticizers tributyl phosphate (**TBP,** prod. no. 90820), tris(2-ethylhexyl)phosphate (**TOP,** prod. no. 93301), 2-(octyloxy)benzonitrile (**OBN,** prod. no 75069) and 2-nitrophenyl octyl ether (**NPOE,** prod. no. 73732) were used to plasticize the above mentioned polymers. All plasticizers shown in figure 3.4 were purchased from Fluka.[18] Stock solutions processed with MicroLab® S were made diluting 1 mL plasticizer with chloroform to form 10 mL solution.

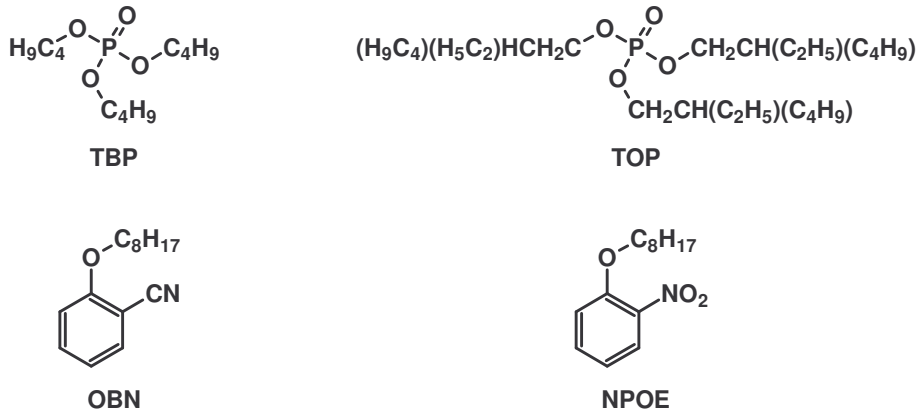

Figure 3.4. Chemical structures of the plasticizers used in this study.

3.2.1.5. Gases

Oxygen (purity 99.999 %), synthetic air (20.9 % v/v oxygen in nitrogen) and nitrogen (purity 99.999 %) were purchased from Linde GmbH.[20] Test atmospheres of defined oxygen concentration were produced using computer controlled mass flow controllers (type 1179A; from MKS Instruments) for blending nitrogen with target gas in respective flow ratios.[21]

3.2.2. Preparation of Sensor Materials

Thin-film oxygen sensor materials are typically composed of a polymer, a fluorescent (quenchable) indicator and – in some cases – a plasticizer. The stock solutions of polymer, indicator dye and, when used, plasticizer, as described above, were mixed by the robot to create the sample cocktails of predetermined composition. A blending algorithm developed with the MicroLab® sampler software (MSS) controlled all steps of the production of the cocktails. The volumes of each component needed to create these formulations were

calculated by the blending algorithm from data given in an EXCEL® spread sheet. The standard sample composition was fixed to 15 mg of supporting matrix. The dye concentration of all sensors prepared was 0.5 % w/w referring to the weight of matrix. The concentration of plasticizer used for a given polymer indicator pair was varied from 0 to 50 % w/w plasticizer referring to the total weight of support. Thus, libraries of oxygen sensor materials were prepared with plasticizer contents of 0, 10, 33 and 50 % w/w.

After preparation, aliquots of 8 to 10 µL of each cocktail were transferred to the glass substrates with the MicroLab® S robot (according to a transfer protocol written with the MSS), and the solvent was then evaporated. The resulting thin films with an average thickness of 5 – 10 µm were mounted in the measurement setup for the characterisation.

3.2.3. Instrumentation and Measurement

3.2.3.1. Instrumentation for Blending

The blending procedures were performed by the liquid handling system. A preparation protocol was developed controlling the operation of the robot during all process steps. The source code included combinations of aspiration / dispensation steps for each component stock solution and washing steps for cleaning the needle (see Appendix A). The volumes of stock solutions to be blended given in the composition spreadsheet were imported via an integrated EXCEL® interface providing syringe drives with the respective trigger signal for aspiration and dispensation. The robot was supplied with the respective solutions to be processed placing them in racks on the working area of the device.

3.2.3.2. Luminescence Decay Time Measurements

Phase shift measurements were performed using the characterisation setup described in chapter 2. All measurements were performed at 22°C, unless otherwise stated. The dual-phase lock-in amplifier (DSP SR830, Stanford Research Inc.) was used for sine-wave modulation of the LED and for determination of phase shift of sensor luminescence. The optical setup consisted of an excitation LED equipped with and excitation filter, a dual branch glass fiber bundle of 2 mm in diameter and a red-sensitive PMT module, equipped with a long-pass filter, supplying the lock-in with the sensor signal. Modulation frequencies, excitation LEDs with appropriate peak wavelengths, excitation filters and long-pass filters were selected with respect to the indicator dyes under investigation. The details are listed in table 3.3.

Table 3.3. Experimental parameters of the optical setup according to the fluorescent indicator under investigation.

Oxygen Probe	LED used (λ_{max})	Modulation Frequency / Hz	Excitation Filter	Long-pass Filter
Ru(dphbpy)	blue (470 nm)	90000	BG12	OG 570
Ru(dpp)	blue[a] (470 nm)	45000	BG12[b]	OG 570[b]
Pt(PFPP)	green[c] (530 nm)	5000	FITCE[d]	RG 630[b]
Pd(PFPP)	green (530 nm)	537	FITCE[d] / BG39[b]	RG 630

[a] Prod.no. NSPB500S, Nichia; [b] Schott Germany; [c] Prod.no. NSPG500S, Nichia;
[d] ITOS Germany

3.3. Results and Discussion

3.3.1. Choice of Materials

The most common type of optical oxygen sensors are those based on the quenching of the luminescence of suitable indicators.[22] Ruthenium organic compounds and metallo porphyrins are well described in literature as oxygen-sensitive indicators with excellent performance in a predetermined operation range.[14,15,23-26] For application in sensors these probes need to meet the following criteria: (a) a sufficient sensitivity to oxygen with respect to the range of application, (b) compatibility of the luminescence excitation of the probe with solid state light sources as LEDs or diode lasers for excitation, (c) sufficient- commercial- availability or accessibility, (d) high photostability, (e) solubility in organic media and (f) ease of immobilisation. The indicator dyes selected for use in this study are known to fulfil most of these requirements. Ruthenium diimine complexes are easily accessed via the synthesis described by Klimant and Wolfbeis[15] and some of them are commercially available. Platinum- and palladium porphyrines can easily be accessed from suppliers with a wide range of ligands.[16]

The quenching efficiency has been found to be strongly dependent on the type of polymer used and thus can be fine tuned by proper choice of the polymer matrix.[22,27,28]. For use in this study the polymer matrices need to meet the requirements of (a) commercial availability, (b) stability, (c) solubility in organic solvents and (d) gas permeability (most data available from handbooks[29]). The polymers used here fulfil most of these requirements. Selection of plasticizers was made according to compatibility to the polymer matrices.

3.3.2. Library Design

The combination of different polymers, plasticizers and indicator dyes in various ratios defines a set of sensor materials (the library). For statistically significant analysis of the sample properties usually 3 to 6 spots of each sensor material have to be tested. Thus, the number of samples under investigation can easily rise to several hundreds to thousands test candidates. In practice, the number of samples tested in one calibration cycle is limited by the number of available sampling positions (spots) within the sample substrates. The characterisation setup used is designed for handling a plate with 60 sensor spots that can be placed on the glass substrates used as support. Preparing at least 3 spots of each sample material maximum 20 different sensor compositions can be calibrated in one cycle. Thus, the complete library has to be split up into compartments, referred to as plates (i.e. the glass substrates), containing these up to 20 different formulations.

With the characterisation setup the luminescence intensities and the phase shifts between excitation and emission phases of the luminescent dyes are acquired automatically as "sensor information". Optical filters adjusted to the emission wavelength of the probes are used to separate the luminescence detected with the PMT from background fluorescence. Also, optical filters and light sources for excitation and modulation frequency need to be adjusted to the optical properties of the respective sample probe under investigation. Each time switching from one type of luminescent indicator dye to another these parameters need to be altered. Thus, under practical considerations the library design was adjusted to this requirement. The sensor materials prepared were arranged on the glass substrates as a series of probes with identical indicator dye to be tested. Only polymer type and, when used, plasticizer type and content in a formulation were varied. This minimised the number of setup modifications performed manually.

In this study, indicator dyes known to display sensitivity to oxygen were used to show the feasibility of the approach to optical gas sensor development. Thus, the development process was entered at the stage of selection of hits (see figure 2.2 in chapter 2, *section 2.2.1. Library Design*). The materials prepared (composed of polymer and indicator) all displayed various sensitivity to oxygen and were referred to as lead library. Introduction of plasticizers to the basic composition was referred to as fine-tuning of the sensory properties of the materials.

The libraries under investigation were characterised by recording the phase shift of the dye luminescence incorporated in polymer matrix, either plasticized or non plasticized, with

varying the oxygen concentration from 0 – 100 % air saturation. The number of information obtained from sensor preparation and characterisation was hardly to be managed manually. Thus, a data base tool was developed based on Microsoft Access® for storing information from blending (sensor composition) and from characterisation (decay time ratios at respective oxygen partial pressure). Each sensor material prepared was marked with a unique identifier (ID) and the complete data set for the respective material was linked to this identifier for analysis. Mandatory parameters for identification of a sensor material prepared were found to be pointers for (a) polymer type, (b) plasticizer type, (c) plasticizer concentration and (d) indicator species used in the recipe for the respective sensor film. The software built-in queries enabled a clustering of materials according to filtering rules applied to the respective records in a data set. This enabled visualisation of characterisation data of the respective sensor fitting the search parameters.

3.3.3. Characterisation of the Sensor Materials

The variance of luminescence phase shifts between excitation and emission phases of the sensor materials were recorded as a function of oxygen partial pressure. The calibration plots were covering the range from 0 – 100 % air saturation when using the indicator dyes Ru(dphbpy), Ru(dpp) and Pt(PFPP), and the range from 0 – 10 % air saturation when using Pd(PFPP), respectively.

Apparently, the luminescence of the probes was quenched by oxygen. Increasing the oxygen partial pressure in the test atmosphere resulted in a decrease of the phase shifts between excitation and emission phases observed. Using equation (3.2) for calculation of the decay times the ratios τ_0/τ were plotted as a function of oxygen partial pressure for characterisation of the sensor materials, where τ_0 was the decay time of the luminescence of a probe in absence of oxygen and τ was the decay time on exposure to the respective oxygen partial pressure.

3.3.3.1. Effect of Polymer on Sensitivity of Oxygen Probes

Ideally the quenching of luminescence of probes, exhibiting mono exponential decay, encapsulated uniformly in a homogeneous matrix fits the simple Stern-Volmer-equation (3.4). In practice, the calibration plots for most materials used as oxygen sensors showed a downward curvature. This is illustrated in the figures 3.6 to 3.9 showing the calibration plots of $Ru(dphby)_3$, $Ru(dpp)_3$, Pt(PFPP) and Pd(PFPP), respectively, encapsulated in the polymers

under investigation. This observation was in good agreement with many literature.[15,30-33] Thus, the well accepted two-site quenching model was applied for fitting the experimental data to describe the calibration plots of the materials.[34,35] In this model the linear equation (3.4) is modified to

$$\frac{\tau_0}{\tau} = \frac{1}{\frac{f_1}{1 + Ksv_1 \bullet pO_2} + \frac{(1 - f_1)}{1 + Ksv_2 \bullet pO_2}} \qquad (3.5)$$

where f_1 is the fraction of encapsulated probe with the Stern-Volmer constant Ksv_1 in one domain and Ksv_2 in another domain of the matrix. This can be attributed to heterogeneous micro structure of the polymer with different permeability to oxygen and, thus, varying availability of probe for luminescence being quenched by oxygen.[31,34-36] The data obtained for f_1, Ksv_1 and Ksv_2 are shown in the table insets in the figure 3.5 - 3.8 for $Ru(dphby)_3$, $Ru(dpp)_3$, Pt(PFPP) and Pd(PFPP), respectively.

The calibration plots of $Ru(dphbpy)_3$ encapsulated in the polymers PFE-VFP, PSAN, PVPh, PVMK, POMMIE, PC, and PVC showed a factor f_1 of 1, indicating a uniform distribution of probe in the respective homogeneous polymer. This was also observed for $Ru(dpp)_3$ in PVMK and PVC, and Pt(PFPP) in PAN. As a result the response of these materials was described with a linear Stern-Volmer equation. The fit functions obtained for the calibration plots of the remaining polymers showed a fraction f_1 lower than 1 indicating a reduction of the availability of probe to quenching with the value f_1 decreasing. It is remarkable that for most of the compositions Ksv_2 was fitted to zero. The ratios Ksv_1/Ksv_2 – for those Ksv_2´s obtained from the fit as significantly different from zero – were in the range from ~ 16 – 62 for the respective polymers. Together with the low fraction of the second quenching constant the resulting downward curvature of the calibration plots were thus attributed to a fraction of luminescence being insensitive to oxygen quenching. This can be explained by shielding of the indicator from contact with oxygen.

Due to the high sensitivity of Pd(PFPP) to oxygen and poor luminescence intensity the maximum oxygen partial pressure used was lower than 22 hPa for the various polymers. At higher oxygen levels no luminescence signal was detected because of the efficient quenching by oxygen. The calibration plots obtained showed similar behaviour as those for the other indicator dyes. The fraction of luminescence being quenched by oxygen was in the range of 0.9 – 1. Thus, the downward curvature of the plots was not that distinct in comparison to the ruthenium complexes and Pt(PFPP) in the respective polymers. A linear slope can be assumed in the measured oxygen concentration range for Pd(PFPP) dissolved in EC49, PFE-VFP, PSAN, PVPh, PVMK, PAN and PVC. A Ksv_2 significantly different from zero was observed

when Pd(PFPP) was encapsulated in PTBS. A fraction of 0.1 was quenched with a $Ksv_2 \approx 1/28\ Ksv_1$. Compared to this, Pt(PFPP) encapsulated in PTBS exhibited a fraction of 0.2 with a Ksv_2 ($1.65 * 10^{-3}\ hPa^{-1}$) of ~ $1/62\ Ksv_1$, respectively.

Comparing PTBS with PS as encapsulation medium for the dyes $Ru(dpp)_3$, Pt(PFPP) and Pd(PFPP), sensor materials with the latter polymer were always less sensitive. The ratio of Ksv_1 between the two polymers (Ksv_{1PTBS}/Ksv_{1PS}) was 4.7, 3.7 and 3.9 using Ru(dpp), Pt(PFPP) and Pd(PFPP), respectively. The fractions f_1 were almost equal for a selected dye in the two polymers assuming a comparable curvature of the calibration plots. As a result, PTBS was found to be a better matrix than PS with enhanced sensitivity of the probes to oxygen. This was a novel observation and correlated with expectations, since the *tert.*-butyl residue was expected to distort the close packing of polymer chains in comparison with poly styrene.
Highlighting the probe Pt(PFPP) in various polymer matrices, best performance of materials characterised was obtained when EC46, EC49, PFE-VFP and CAc were used as encapsulation medium. The Ksv_1 calculated were 0.14, 0.11, 0.04 and $0.6\ hPa^{-1}$, respectively. Whereas EC49, EC46 and CAc showed downward curvature of the calibration plots with f_1 of 0.89, 0.90 and 0.89, the fit for PFE-VFP showed an almost linear correlation of τ_0/τ versus pO_2, illustrated by an f_1 of 0.98.

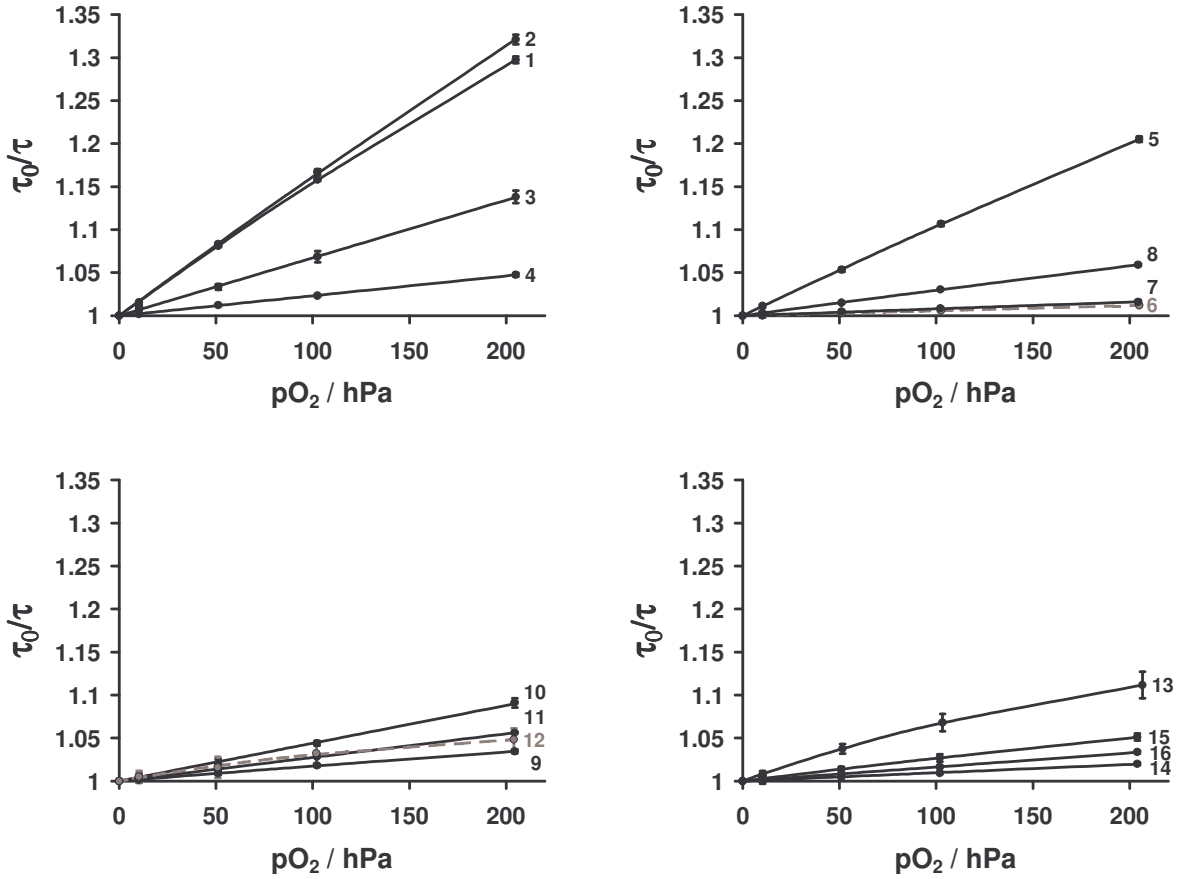

	Polymer	f_1	$Ksv_1 \times 10^3$ / hPa^{-1}	$Ksv_2 \times 10^3$ / hPa^{-1}	χ^2
1	EC46	0.72	2.3	0	7×10^{-7}
2	EC49	0.85	1.9	0	2×10^{-5}
3	PFE-VFP	1	0.7	0	7×10^{-7}
4	PSAN	1	0.2	0	3×10^{-7}
5	CAc	0.75	1.4	0	4×10^{-7}
6	PVPh	1	0.1	0	3×10^{-8}
7	PVMK	1	0.1	0	6×10^{-7}
8	PSu	0.58	0.5	0	9×10^{-8}
9	PVC-iBVE	0.35	0.5	0	2×10^{-7}
10	POMMIE	1	0.4	0	3×10^{-6}
11	PC	1	0.3	0	5×10^{-7}
12	PTBS	0.10	4.0	0	3×10^{-6}
13	PAN	0.24	3.4	0	4×10^{-7}
14	PVC	1	0.1	0	1×10^{-6}
15	PS	0.32	0.9	0	1×10^{-6}
16	PMMA	1	0.2	0	9×10^{-7}

Figure 3.5. Calibration plots and data of Ru(dpbpy) in various non plasticized polymers.

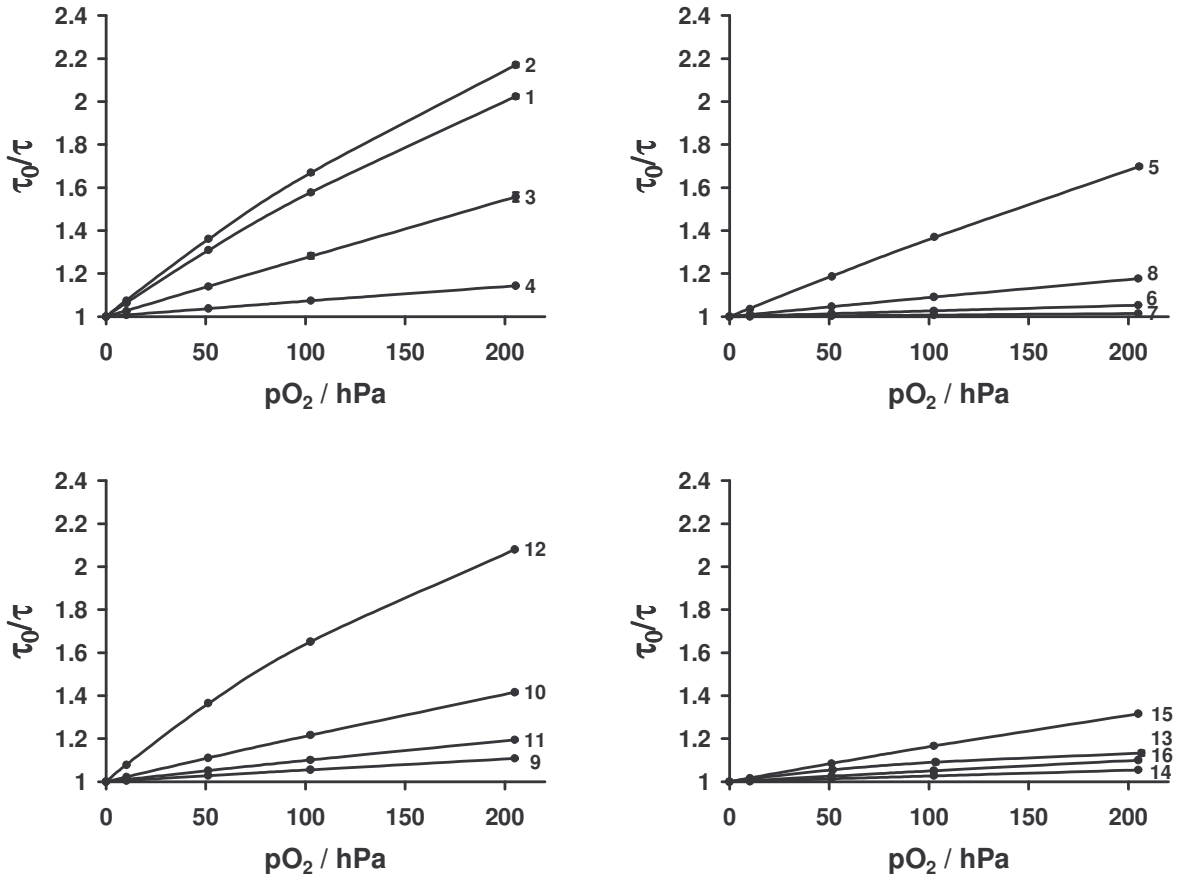

	Polymer	f_1	$Ksv_1 \times 10^3$ / hPa^{-1}	$Ksv_2 \times 10^3$ / hPa^{-1}	χ^2
1	EC46	0.82	7.9	0	4×10^{-6}
2	EC49	0.82	9.2	0	7×10^{-6}
3	PFE-VFP	0.97	2.8	0	9×10^{-6}
4	PSAN	0.73	1.0	0	1×10^{-7}
5	CAc	0.87	4.3	0	1×10^{-5}
6	PVPh	0.53	0.5	0	3×10^{-7}
7	PVMK	1	0.1	0	4×10^{-7}
8	PSu	0.77	1.2	0	7×10^{-8}
9	PVC-iBVE	0.68	0.8	0	3×10^{-7}
10	POMMIE	0.84	2.6	0	8×10^{-7}
11	PC	0.73	1.4	0	7×10^{-8}
12	PTBS	0.75	10.7	0.1	6×10^{-6}
13	PAN	0.20	7.1	0	4×10^{-7}
14	PVC	1	0.3	0	9×10^{-7}
15	PS	0.77	2.2	0	1×10^{-6}
16	PMMA	0.73	0.7	0	2×10^{-6}

Figure 3.6. Calibration plots and data of Ru(dpp) in various non plasticized polymers.

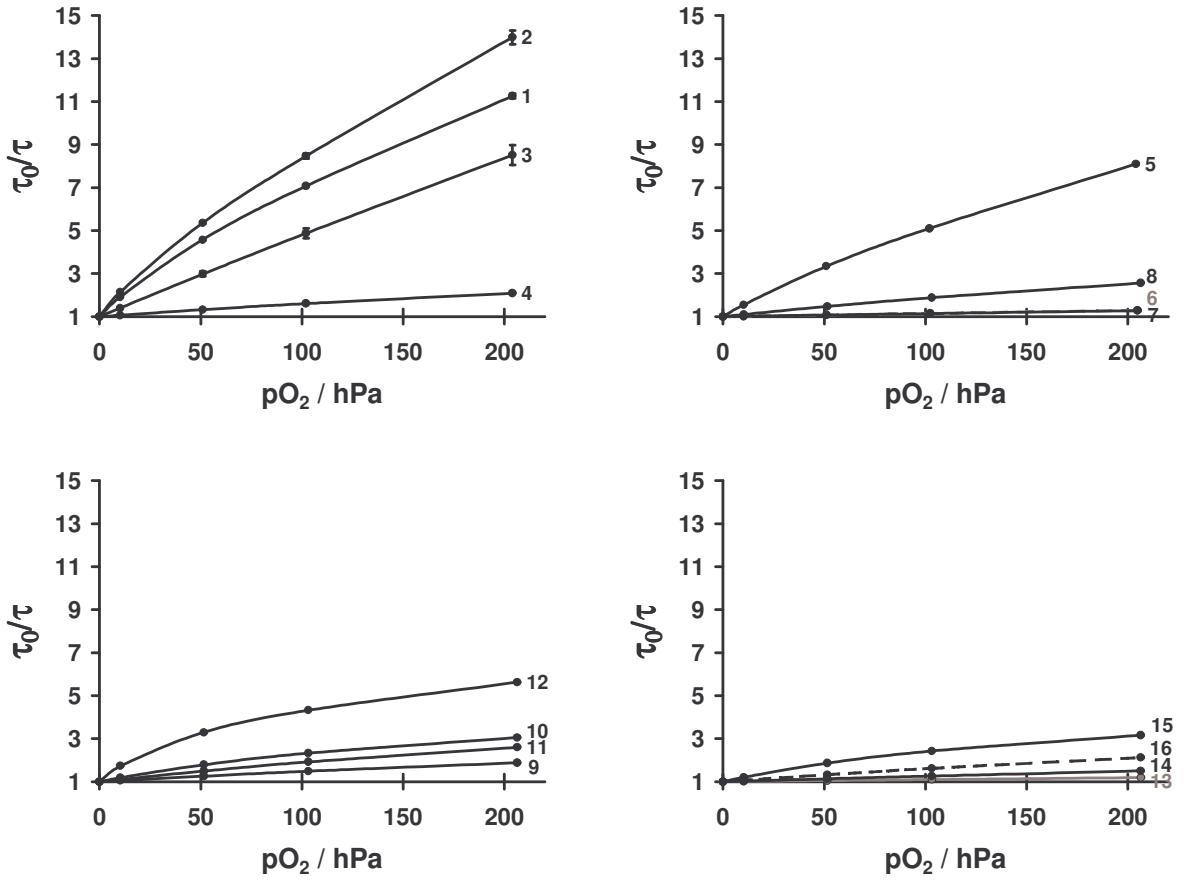

	Polymer	f_1	$Ksv_1 \times 10^3$ / hPa^{-1}	$Ksv_2 \times 10^3$ / hPa^{-1}	χ^2
1	EC46	0.90	107	4.9	1×10^{-4}
2	EC49	0.89	141	8.0	4×10^{-5}
3	PFE-VFP	0.98	40.6	2.6	8×10^{-5}
4	PSAN	0.84	8.1	0	4×10^{-6}
5	CAc	0.89	64.0	4.0	8×10^{-5}
6	PVPh	0.75	2.2	0	6×10^{-7}
7	PVMK	0.78	1.9	0	9×10^{-7}
8	PSu	0.87	11.3	0	1×10^{-5}
9	PVC-iBVE	0.82	6.5	0	1×10^{-6}
10	POMMIE	0.79	24.2	0.5	2×10^{-5}
11	PC	0.86	12.2	0	3×10^{-5}
12	PTBS	0.81	103.2	1.7	3×10^{-4}
13	PAN	0.99	0.9	-	8×10^{-6}
14	PVC	0.82	3.4	0	7×10^{-7}
15	PS	0.78	27.7	0.5	2×10^{-5}
16	PMMA	0.86	7.8	0	3×10^{-6}

Figure 3.7. Calibration plots and data of Pt(PFPP) in various non plasticized polymers.

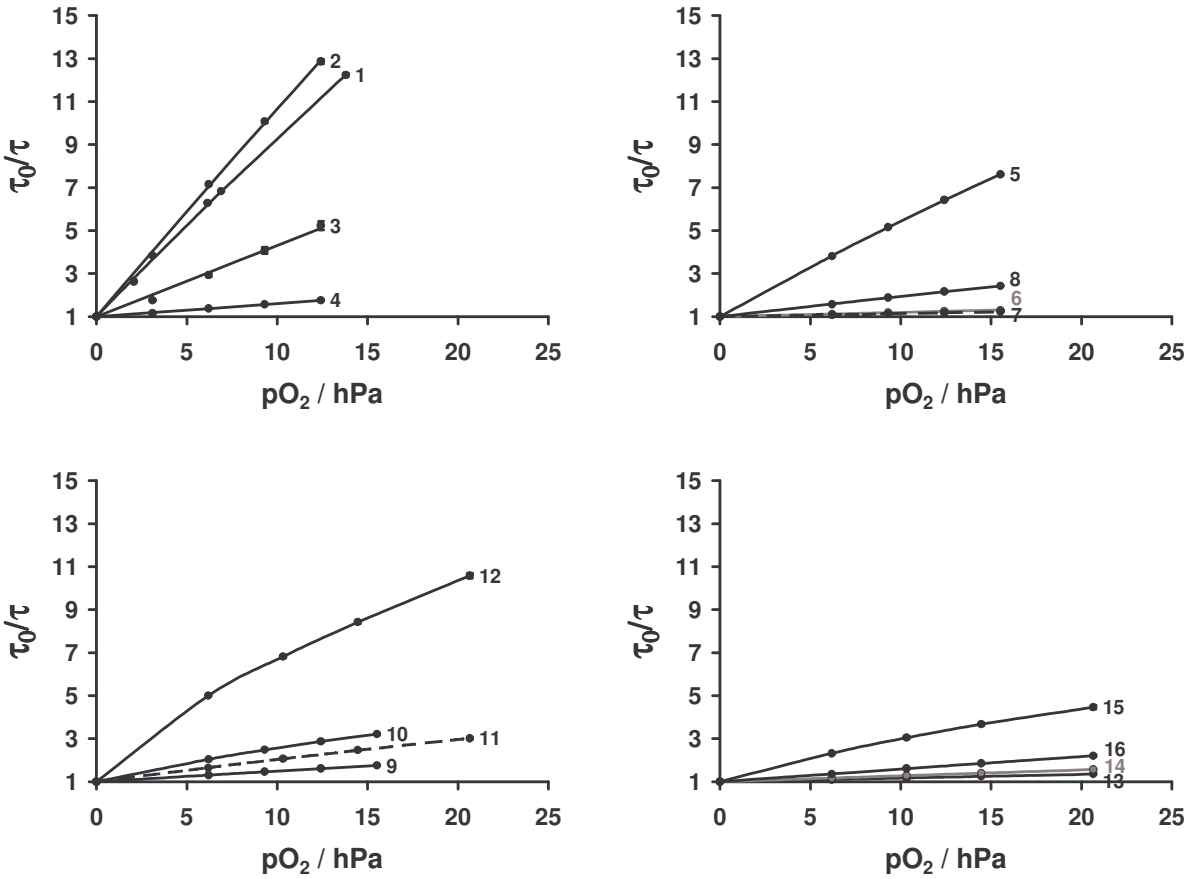

	Polymer	f_1	$Ksv_1 \times 10^3$ / hPa^{-1}	$Ksv_2 \times 10^3$ / hPa^{-1}	χ^2
1	EC46	0.99	878	0	2×10^{-2}
2	EC49	1	992	0	3×10^{-2}
3	PFE-VFP	1	330	0	5×10^{-2}
4	PSAN	1	60.7	0	6×10^{-4}
5	CAc	0.98	485	0	3×10^{-4}
6	PVPh	1	19.4	0	6×10^{-6}
7	PVMK	1	14.2	0	2×10^{-4}
8	PSu	0.97	98.8	0	2×10^{-4}
9	PVC-iBVE	0.95	53.2	0	5×10^{-5}
10	POMMIE	0.90	211	0	1×10^{-4}
11	PC	0.95	114	0	2×10^{-4}
12	PTBS	0.90	1035	37.5	4×10^{-5}
13	PAN	1	17.0	0	3×10^{-4}
14	PVC	1	27.5	0	5×10^{-5}
15	PS	0.92	263	0	1×10^{-5}
16	PMMA	0.99	59.9	0	6×10^{-5}

Figure 3.8. Calibration plots and data of Pd(PFPP) in various non plasticized polymers.

The sensitivity of an oxygen sensor is characterised by the K_{SV} obtained from calibration plots applying the Stern-Volmer equation. Thus, with increasing value of K_{SV} the sensitivity of a sensor material increases. The permeability of a polymer to the target molecule to be detected is a major factor influencing this parameter. The higher the permeability is, the higher is the probability of a collisional deactivation of dye luminescence by oxygen. Figure 3.9. illustrates a correlation of P vs. K_{SV} for Pt(PFPP) encapsulated in EC46, PFE-VFP, PSAN, CAc, PAN, PVC, PS and PMMA. The plot confirms the assumption that K_{SV} will increase with increasing permeability of the polymer, assuming CAc as outlier. Although, no exact mathematical correlation with physical relevance of parameters can be posted with the current data, the trend is significant.

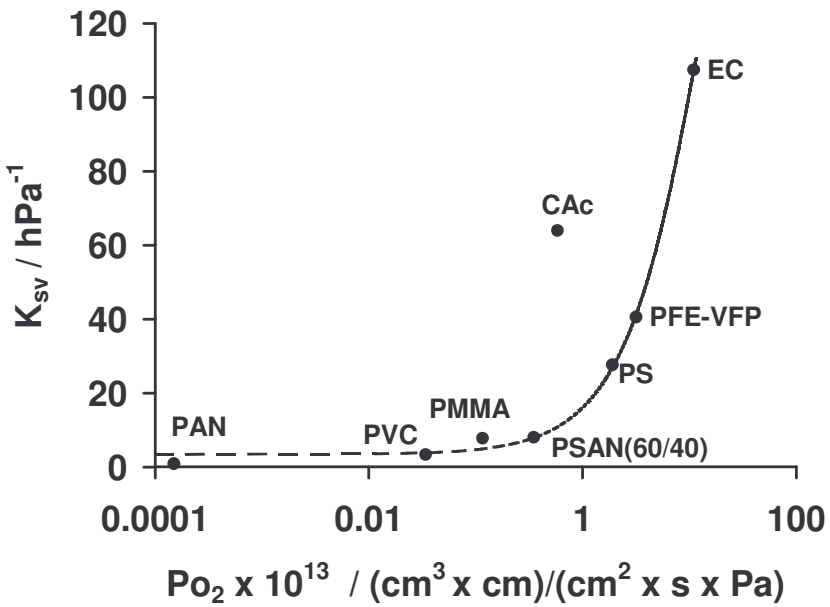

Figure 3.9. Plot of K_{SV} vs. Permeability Po_2 of polymer to oxygen. Permeability data from reference.[29] K_{SV} was taken from initial slope of the fit functions for Pt(PFPP) in the particular polymers. The permeability of PSAN(70/30) was assumed equal to that of PSAN(60/40), and that of PFE-VFP was assumed equal to PTFE. CAc was excluded from trendline calculation.

3.3.3.2. Effect of Plasticizer on the Sensor Properties

As discussed in the former section, the sensitivity of an optical oxygen sensor can generally be described by the Stern-Volmer constant K_{SV}. The greater the value of K_{SV}, the greater is the sensitivity of the thin-film sensor under investigation. Thus, the performance of a sensor material can be tuned by tuning the properties of the composition. This is realised either by exchange of the encapsulation polymer, as described above, or by tuning the permeability properties of the matrix by addition of compatible plasticizers.[25,33,37,38]

The tuning agents TBP, TOP, OBN and NPOE were added to polymer stock solutions creating encapsulation media with fractions of 10, 33 and 50 % (w/w) plasticizer with respect to the amount of polymer in the matrix. Thin film optical sensors prepared with this matrices were calibrated exposing the samples to atmospheres containing oxygen concentrations from 0 to 100 % air saturation (~205 hPa). As predicted the sensitivity of the materials increased on changing the oxygen-sensitive probes from Ru(dphbpy) to Ru(dpp), Pt(PFPP) and Pd(PFPP), respectively – the last being the most sensitive probe. The modified Stern-Volmer equation (see eq. 3.3) was used to describe the relation τ_0/τ versus the oxygen partial pressure. Pt(PFPP) containing sensor materials were highlighted to demonstrate the effect of plasticizer compatibility and concentration on the tuning efficiency of tuning sensor sensitivity.

The particular calibration plots for a selection of polymers are illustrated in figures 3.10 – 3.17. The fit parameters obtained for the respective blends using eq. (3.5) are listed as inserts in the corresponding figures. Screening of blends composed of PVMK or PSu with TOP or OBN in concentrations of 10, 33 and 50 % (w/w) tuning agent did not result in valuable calibration plots. Therefore, these materials were excluded from characterisation. The results obtained for PAN-based sensors indicated a strong enhancement of sensitivity of the material. The significant sensitivity of the non-plasticized PAN film was explained by presence of ambient humidity during drying of the film. The solvent DMF for solubilising the polymer is known to be hygroscopic and thus water vapour is soaked into the wet film causing a poprous structure on drying off the solvent. Consequently, the surface of the film is increased by a manifold and diffusion of oxygen is enhanced. When adding 10 % (w/w) of any plasticizer used to the matrix the sensor materials are almost inert against quenching by oxygen, since the pores can be filled by the agent and diffusion is hindered.

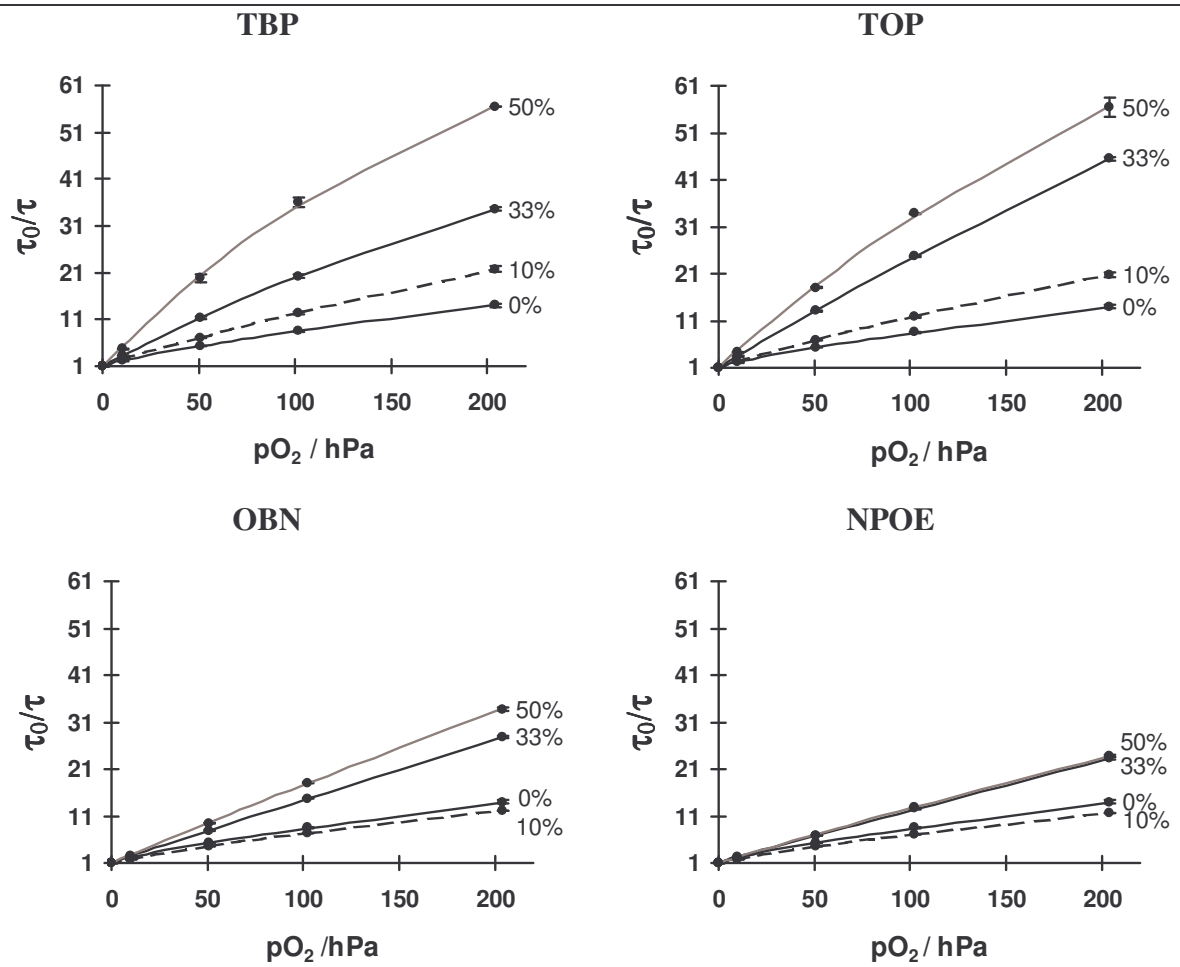

Plasticizer / %(w/w)		f_1	$Ksv_1 \times 10^3$ / hPa^{-1}	$Ksv_2 \times 10^3$ /hPa^{-1}	χ^2
	0	0.89	141	8.0	4×10^{-5}
	10	0.95	156	9.8	1×10^{-4}
TBP	33	0.99	222	0	1×10^{-3}
	50	0.99	441	0	7×10^{-1}
	10	0.96	142	7.6	7×10^{-5}
TOP	33	1	247	0	1×10^{-2}
	50	1	379	0	5×10^{-1}
	10	0.93	91.1	4.9	1×10^{-4}
OBN	33	1	139	0	1×10^{-3}
	50	1	172	0	3×10^{-2}
	10	0.93	88.4	4.2	7×10^{-6}
NPOE	33	1	116	0	2×10^{-3}
	50	1	119	0	8×10^{-3}

Figure 3.10. Calibration plots and data of Pt(PFPP) in EC49 with plasticizers TBP, TOP, OBN and NPOE.

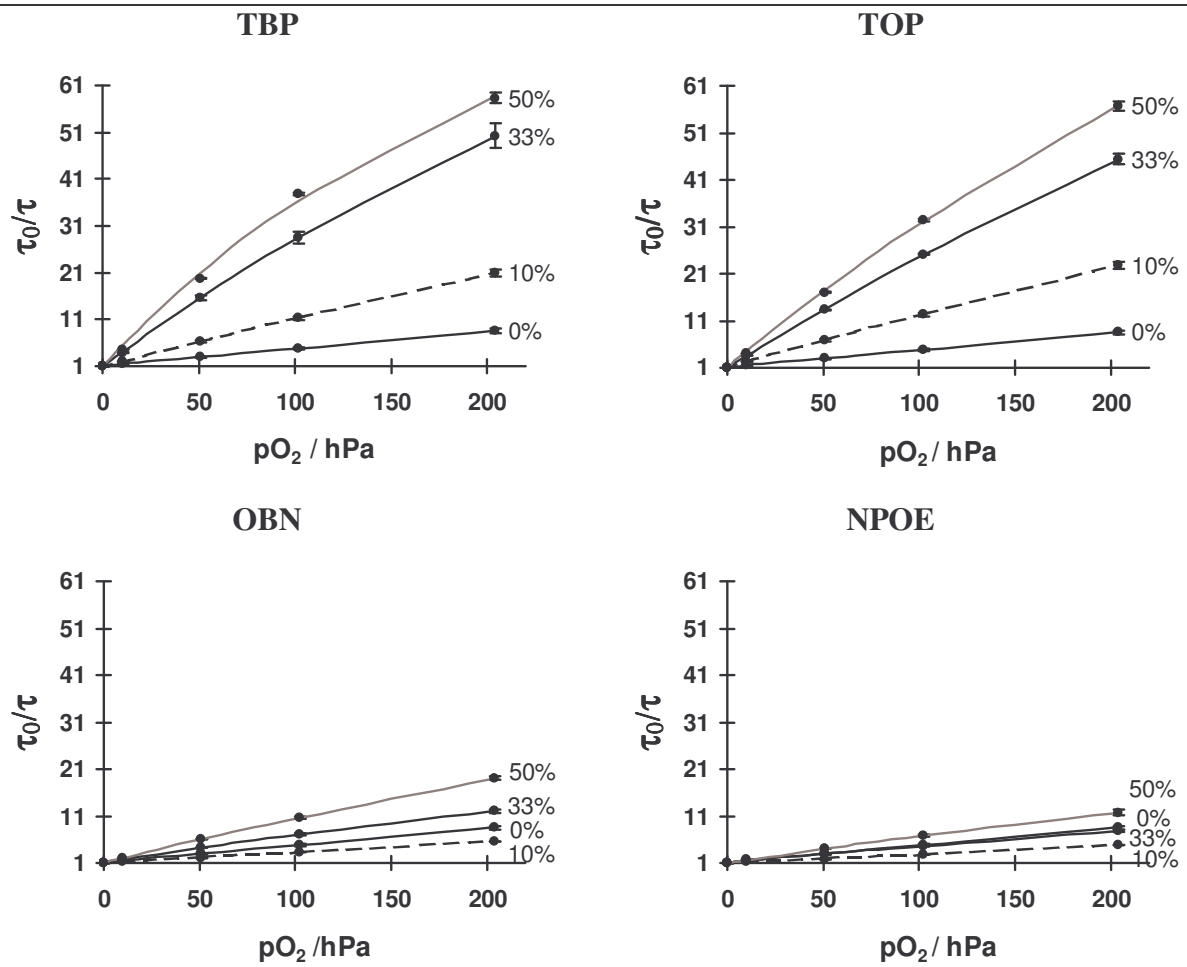

Plasticizer / %(w/w)		f_1	$Ksv_1 \times 10^3$ / hPa^{-1}	$Ksv_2 \times 10^3$ / hPa^{-1}	χ^2
	0	0.98	40.6	2.6	8×10^{-5}
TBP	10	0.99	109	3.7	2×10^{-4}
	33	1	306	0	4×10^{-2}
	50	0.99	452	0	2
TOP	10	0.99	125	5.3	2×10^{-5}
	33	1	256	0	4×10^{-2}
	50	1	344	0	2×10^{-1}
OBN	10	0.74	22.6	22.6	2×10^{-3}
	33	0.89	89.9	9.3	2×10^{-4}
	50	0.99	103	0	1×10^{-4}
NPOE	10	0.73	18.4	18.4	1×10^{-2}
	33	0.60	79.6	16.1	8×10^{-5}
	50	0.98	63.5	0.6	7×10^{-5}

Figure 3.11. Calibration plots and data of Pt(PFPP) in PFE-VFP with various plasticizers TBP, TOP, OBN and NPOE.

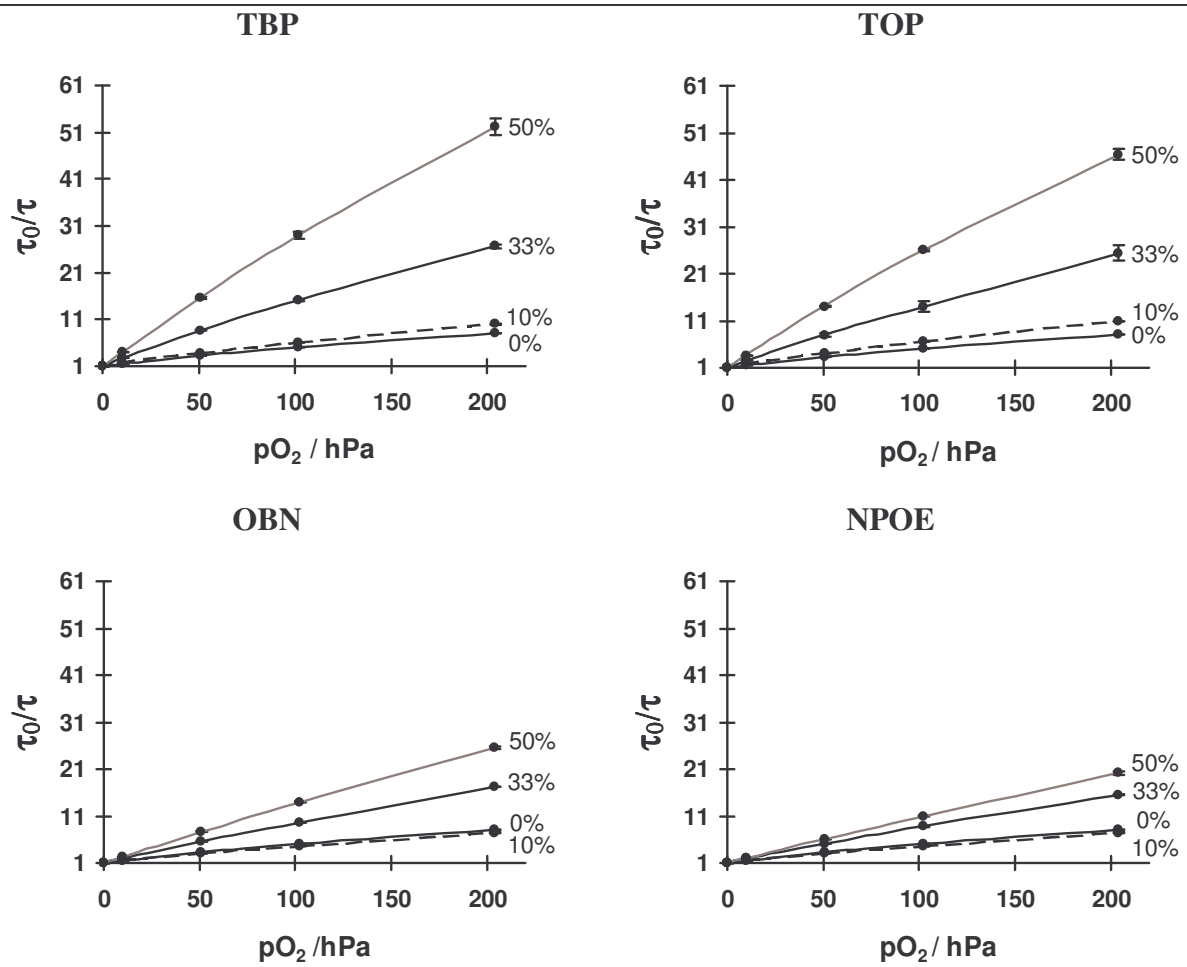

Plasticizer / %(w/w)		f_1	$Ksv_1 \times 10^3$ / hPa^{-1}	$Ksv_2 \times 10^3$ / hPa^{-1}	χ^2
	0	0.89	64.0	4.0	8×10^{-5}
	10	0.91	77.3	4.9	1×10^{-4}
TBP	33	0.98	176	5.3	9×10^{-4}
	50	1	304	0	6×10^{-3}
	10	0.92	81.1	5.4	1×10^{-4}
TOP	33	0.97	163	8.9	8×10^{-5}
	50	1	272	0	2×10^{-2}
	10	0.92	49.3	2.7	9×10^{-5}
OBN	33	0.97	103	5.6	2×10^{-4}
	50	1	136	0	6×10^{-4}
	10	0.91	50.2	3.3	1×10^{-4}
NPOE	33	0.97	93.5	5.2	1×10^{-4}
	50	1	102	0	4×10^{-4}

Figure 3.12. Calibration plots and data of Pt(PFPP) in CAc with plasticizers TBP, TOP, OBN and NPOE.

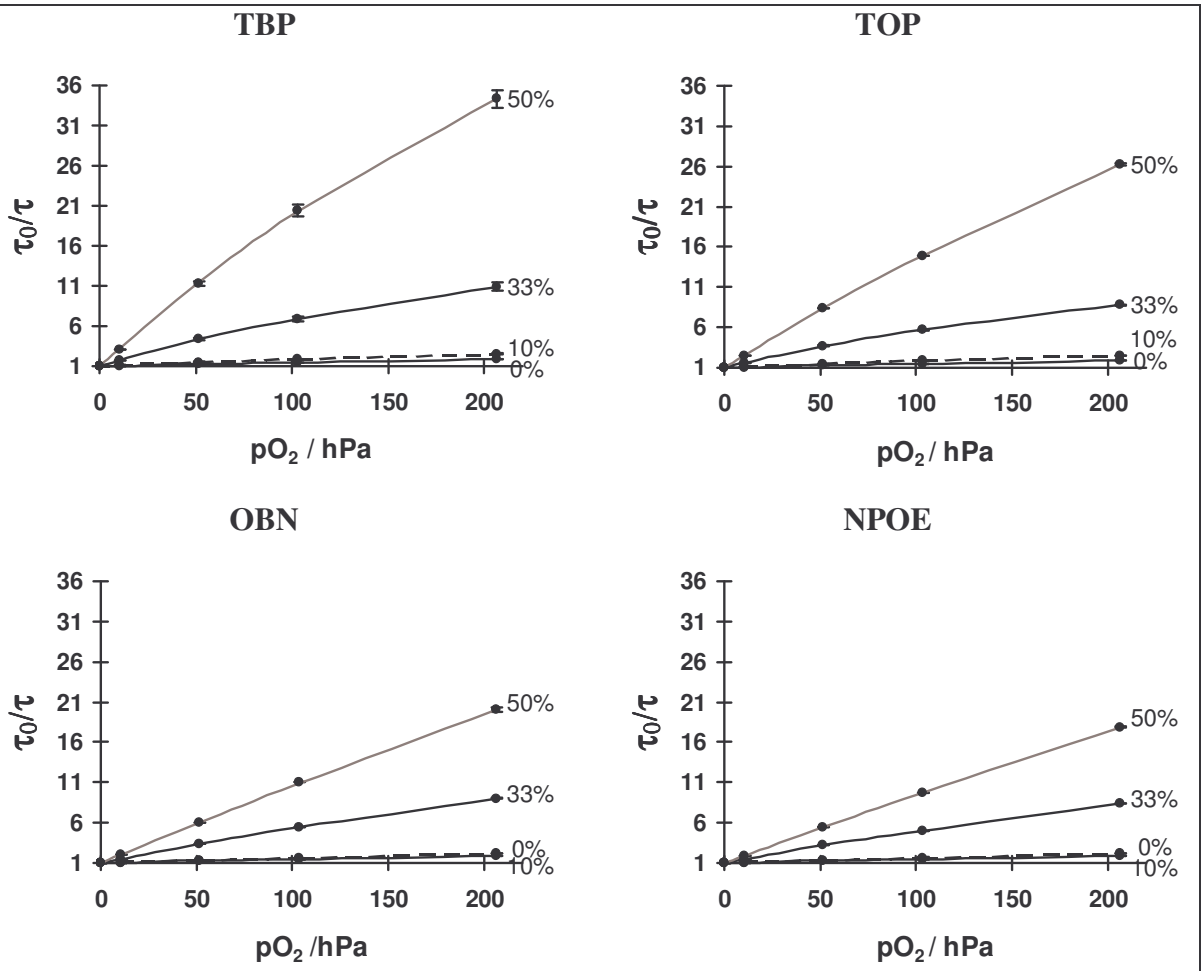

Plasticizer / %(w/w)		f_1	$Ksv_1 \times 10^3$ / hPa^{-1}	$Ksv_2 \times 10^3$ / hPa^{-1}	χ^2
	0	0.82	6.5	0	1×10^{-6}
TBP	10	0.82	13.5	0	9×10^{-6}
	33	0.94	84.8	2.7	3×10^{-5}
	50	0.99	223	0	4×10^{-2}
TOP	10	0.78	14.5	0.3	1×10^{-5}
	33	0.92	71.6	2.3	3×10^{-5}
	50	0.99	153	0.4	4×10^{-4}
OBN	10	0.84	8.7	0	6×10^{-6}
	33	0.96	51.8	2.0	2×10^{-4}
	50	1	101	0	2×10^{-3}
NPOE	10	0.84	8.8	0	9×10^{-6}
	33	0.96	47.5	1.9	1×10^{-4}
	50	1	88.1	0	7×10^{-4}

Figure 3.13. Calibration plots and data of Pt(PFPP) in PVC-iBVE with plasticizers TBP, TOP, OBN and NPOE.

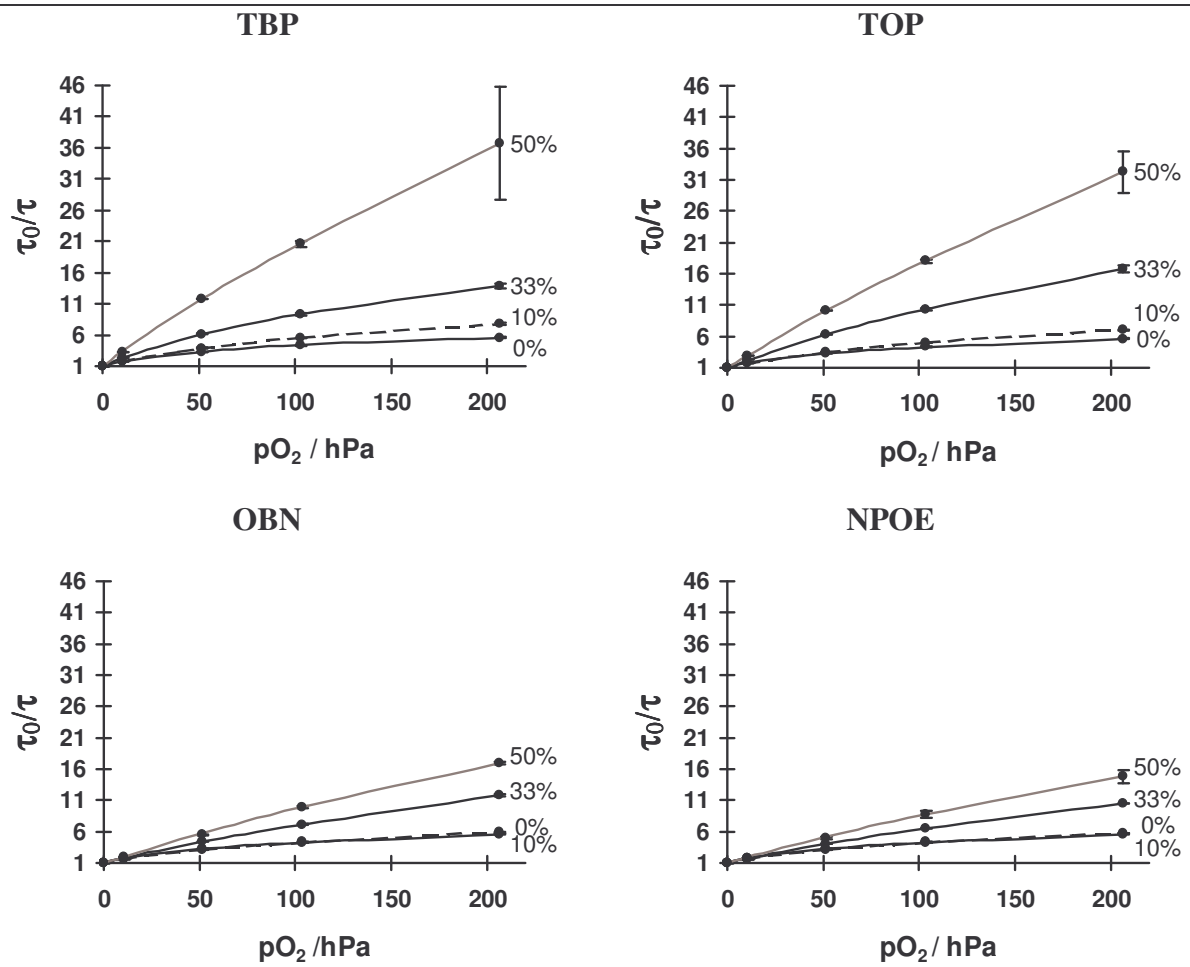

Plasticizer / %(w/w)		f_1	$Ksv_1 \times 10^3$ / hPa^{-1}	$Ksv_2 \times 10^3$ / hPa^{-1}	χ^2
	0	0.81	103	1.7	3×10^{-4}
	10	0.89	92.4	1.6	7×10^{-5}
TBP	33	0.93	160	2.9	1×10^{-4}
	50	0.98	242	4.7	2×10^{-2}
	10	0.88	78.8	1.6	1×10^{-4}
TOP	33	0.96	130	2.4	1×10^{-4}
	50	0.99	194	2.7	9×10^{-3}
	10	0.85	66.3	1.5	2×10^{-6}
OBN	33	0.95	81.3	3.0	1×10^{-3}
	50	0.99	96.8	0	3×10^{-2}
	10	0.85	68.7	1.4	1×10^{-5}
NPOE	33	0.96	71.4	1.2	2×10^{-4}
	50	0.99	86.1	0	2×10^{-2}

Figure 3.14. Calibration plots and data of Pt(PFPP) in PTBS with plasticizers TBP, TOP, OBN and NPOE.

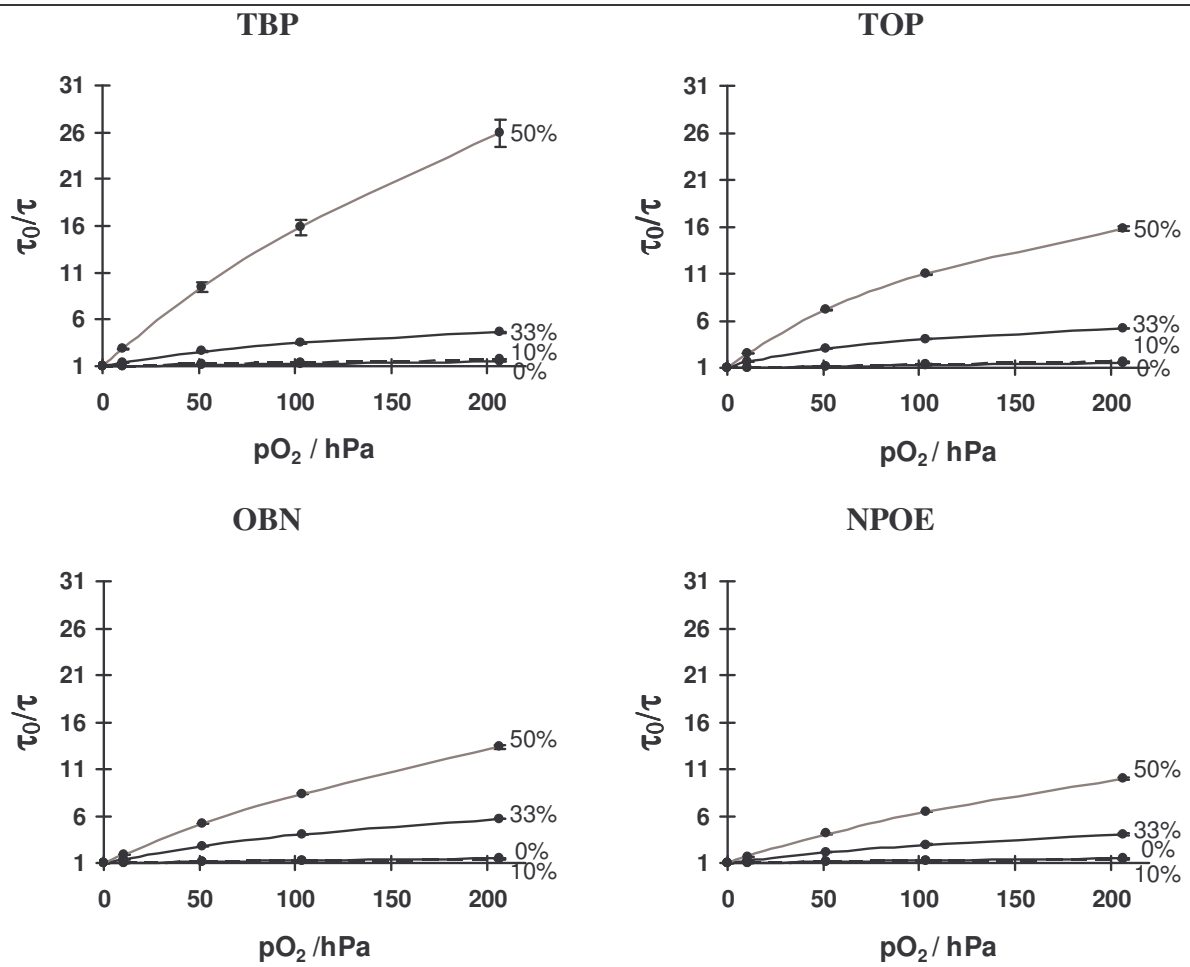

Plasticizer / %(w/w)		f_1	$Ksv_1 \times 10^3$ / hPa^{-1}	$Ksv_2 \times 10^3$ / hPa^{-1}	χ^2
	0	0.82	3.4	0	6×10^{-7}
TBP	10	0.83	4.8	0	1×10^{-5}
	33	0.83	51.8	0.8	4×10^{-5}
	50	0.98	196	1.5	2×10^{-3}
TOP	10	0.66	5.2	0.7	7×10^{-8}
	33	0.84	76.8	0.7	1×10^{-5}
	50	0.96	168	0.7	6×10^{-5}
OBN	10	0.85	2.7	0	1×10^{-6}
	33	0.89	49.7	0.9	1×10^{-4}
	50	0.96	98.0	1.3	4×10^{-4}
NPOE	10	0.81	2.8	0	4×10^{-7}
	33	0.84	33.4	0.6	2×10^{-5}
	50	0.95	75.3	1.2	4×10^{-4}

Figure 3.15. Calibration plots and data of Pt(PFPP) in PVC with plasticizers TBP, TOP, OBN and NPOE.

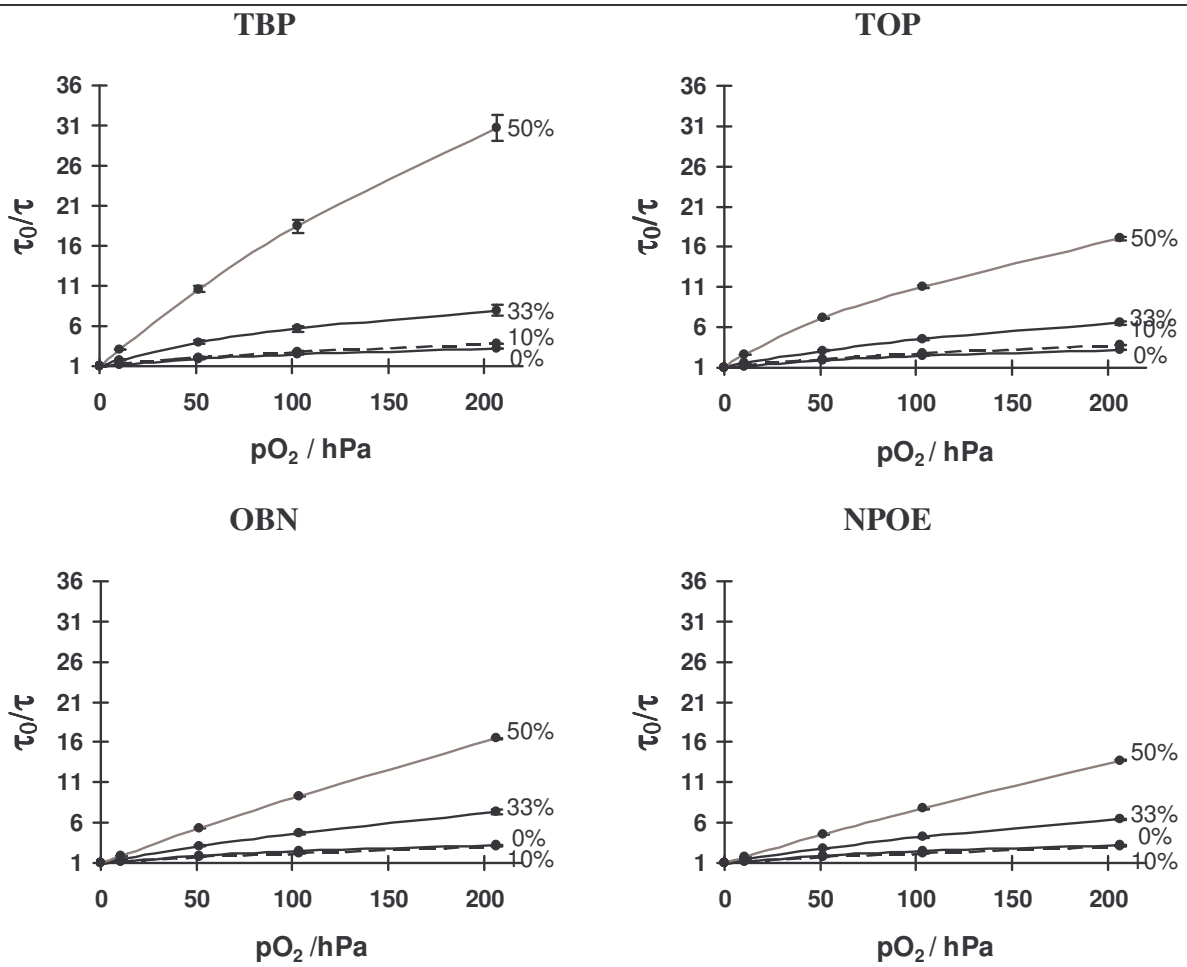

Plasticizer / %(w/w)		f_1	$Ksv_1 \times 10^3$ / hPa^{-1}	$Ksv_2 \times 10^3$ / hPa^{-1}	χ^2
	0	0.78	27.7	0.5	2×10^{-5}
TBP	10	0.83	32.3	0.7	4×10^{-5}
	33	0.89	95.2	1.7	5×10^{-6}
	50	0.99	210	0.3	6×10^{-4}
TOP	10	0.86	26.6	0.4	4×10^{-5}
	33	0.87	64.1	2.3	2×10^{-4}
	50	0.94	185	3.3	2×10^{-3}
OBN	10	0.84	18.0	0.3	2×10^{-5}
	33	0.93	50.8	1.7	8×10^{-5}
	50	0.99	88.1	0.5	5×10^{-4}
NPOE	10	0.83	18.7	0.3	2×10^{-5}
	33	0.91	44.7	1.5	7×10^{-5}
	50	0.98	73.4	2.1	4×10^{-4}

Figure 3.16. Calibration plots and data of Pt(PFPP) in PS with plasticizers TBP, TOP, OBN and NPOE.

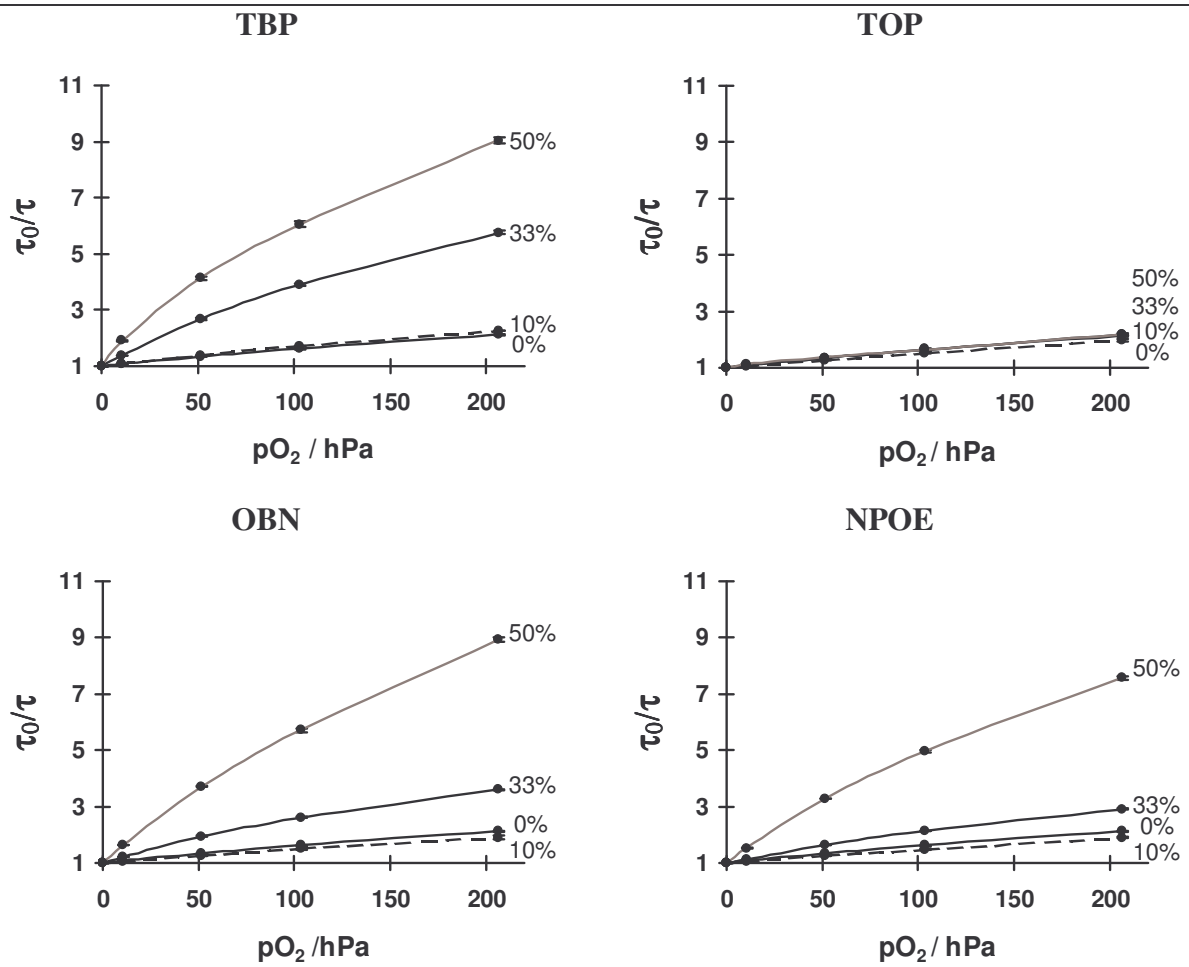

Plasticizer / %(w/w)		f_1	$Ksv_1 \times 10^3$ / hPa^{-1}	$Ksv_2 \times 10^3$ / hPa^{-1}	χ^2
	0	0.86	7.8	0	3×10^{-6}
	10	0.88	8.6	0	1×10^{-5}
TBP	33	0.89	44.3	1.3	9×10^{-5}
	50	0.86	116	4.2	6×10^{-4}
	10	0.87	6.4	0	4×10^{-7}
TOP	33	0.88	7.7	0	5×10^{-6}
	50	0.09	268	4.9	2×10^{-4}
	10	0.85	6.1	0	3×10^{-6}
OBN	33	0.82	26.8	0.8	3×10^{-5}
	50	0.92	71.1	2.7	2×10^{5}
	10	0.87	5.8	0	2×10^{-6}
NPOE	33	0.81	17.3	0.6	2×10^{-5}
	50	0.91	58.8	1.8	2×10^{-5}

Figure 3.17. Calibration plots and data of Pt(PFPP) in PMMA with plasticizers TBP, TOP, OBN and NPOE.

EC46, EC49, CAc, PVC-iBVE, POMMIE and PVC formed transparent films with all plasticizers used. Samples of PFE-VFP or PVPh were transparent with TBP or TOP, yet with 33 and 50 % (w/w) OBN or NPOE, respectively, they became turbid. Formulations with PSu showed phase separation by building droplets with all plasticizers. With exception of POMMIE and PMMA the values for f_1 increased continuously to approx. 0.95 – 1 on rising the plasticizer concentration from 0 to 50 % (w/w) TBP or TOP. This was attended by a steady increase of the fitted Ksv_1, and TBP having a bigger effect than TOP. Whereas the first caused an increase in Ksv_1 compared to non plasticized polymer by factors of 3.6 (EC46), 3.1 (EC49), 11.3 (PFE-VFP), 4.7 (CAc), 32.9 (PVPh), 34.1 (PVC-iBVE), 2.3 (PTBS), 58 (PVC) and 7.6 (PS), TOP caused increase by factors of 3.1, 2.7, 8.5, 4.3, 22.5, 23.4, 1.8, 50 and 6.7, respectively. Overall the sensitivity of the materials rises with increasing plasticizer content. This was attributed to higher mobility of probe and target gas in plasticized polymer matrix, resulting in higher probability of collisional deactivation of probe luminescence. Ksv_1, as marker for the sensitivity, and f_1, a measure of homogeneity of the micro structure, were increased with plasticising the matrix. Similar results were obtained for f_1 with OBN and NPOE in EC46, EC49, CAc, PTBS, PVC and PS. It is remarkable that on changing from pure polymer matrix to media with 10 % (w/w) plasticizer OBN, here, the Ksv_1 was decreased in the respective matrices to factors of 0.67 (0.67 for NPOE), 0.65 (0.63), 0.77 (0.78), 0.64 (0.66), 0.80 (0.84) and 0.65 (0.68) of those obtained for pure polymer. Only with fractions of 33 and 50 % (w/w) plasticizer the initial value of Ksv_1 is exceeded. As a result materials containing 10 % (w/w) were less sensitive than the pure polymer matrices, but films with 33 and 50 % (w/w) OBN or NPOE were more sensitive.

A rough discrimination feature for the comparison of the sensitivity of different materials is the oxygen partial pressure at which the initial luminescence decay time of an oxygen sensor in oxygen-free atmosphere is reduced by 50 %, i.e., $pO_2(\tau_0/\tau = 2)$. This value can be obtained by inserting the fit parameters calculated into equation 3.5 and solving the equation to pO_2. The smaller this value is the more sensitive is the sensor. Additionally, it gives a rough estimation for the dynamic range of the sensor. In table 3.4 the calculated values for selected sensor materials are illustrated. The above mentioned effects of TBP, TOP, OBN and NPOE on the sensitivity of a sensor material could be affirmed.

Table 3.4. Effect of plasticizer on sensitivity to oxygen of a selection of materials containing Pt(PFPP), expressed by $pO_2(\tau_0/\tau = 2)$, i.e., the oxygen partial pressure where the decay time of the probe is reduced to ½ of the initial decay time in oxygen-free atmosphere. The lower the value of pO_2 in this table is, the higher is the sensitivity of the sensor. The plasticizer content is given as units of w/w referring to 1 g support.

Polymer	non plasticized	TBP			TOP			OBN			NPOE		
		10 %	33 %	50 %	10 %	33 %	50 %	10 %	33 %	50 %	10 %	33 %	50 %
EC 49	8.8	7	4.6	2.3	7.6	4.1	2.7	12.5	7.2	5.8	12.9	8.6	8.4
PFE-VFP	25.4	9.3	3.3	2.2	8.2	3.9	2.9	44.2	13.4	9.9	54.5	23.6	16.3
PSAN	183.2	130.4	56.6	16.5	192.4	230.1	281	209.9	47.2	19.8	209.7	69.6	21
CAc	19.3	15.4	5.9	3.3	14.5	6.5	3.7	23.6	10.3	7.4	23.6	11.4	9.9
PVC-iBVE	242.2	114.7	13.4	4.6	119.4	16.5	6.7	170.6	20.9	10	168.9	22.9	11.4
POMMIE	69.9	78	59.4	13.9	88.8	68.5	20.7	130.5	81.9	24.1	134.2	101.4	30.9
PTBS	15.2	13.7	7.2	4.3	16.5	8.3	5.3	20.8	13.6	10.6	20.5	15.3	12
PVC	468.2	308.6	28.7	5.3	357	19.2	6.5	538.7	25.7	11	564.3	43	14.8
PS	62.3	46.1	13.4	4.9	51.8	20.7	6.1	80.2	22.9	11.6	79.3	26.6	14.1
PMMA	178.9	155.3	28.4	11.7	213.7	171.3	170.2	233.2	55.5	16.6	231.4	87.8	20.3

3.4. Conclusion

The design of typical oxygen sensors includes blends of gas permeable polymers as support, lipophilic quenchable luminescent dyes and, probably, agents for fine-tuning permeability of the polymer matrix to oxygen. The selection of components is essential for the specification of the dynamic range and the optical properties of the sensor.

The combinatorial approach to the high-throughput blending and characterisation of optical gas sensors presented in chapter 2 was successfully applied to a study of optical oxygen sensors. The setup for high-throughput automatic blending of polymer, indicator and tuning agent stock solutions enabled the reliable and fast preparation of sensor cocktails. A database was built up for storing composition of each sensor and aligning the characterisation data to unique sample identifiers for subsequent analysis. This extensive electronic data management enabled comparison of sensory properties of materials by applying queries for desired parameters, like filtering of all materials for containing the polymer EC46 and Pt(PFPP) and comparing the sensitivity versus concentration of a certain plasticizer. The measurement setup presented was successfully applied for the high-throughput characterisation of the optical properties of the sensor materials under investigation. Measurement execution and acquisition and storage of luminescence intensities and phase shifts between excitation and emission phases was performed automatically.

The combinatorial approach providing the fast and automatic preparation and characterisation of sensor materials and data basing enabled the built up of an extensive data matrix for characterisation and comparison of various sensor materials. The assumption that the type of polymer has an intensive influence on the sensitivity of an oxygen sensor was affirmed impressively. PTBS was found as promising alternative for PS as encapsulation polymer for Pt(PFPP) or other oxygen-sensitive dyes. The sensitivity of Pt(PFPP) in PTBS expressed by Ksv was 270 % higher than in PS showing similar physical stability of the sensor films. The addition of plasticizers, e.g., TBP or TOP, enabled an enhancement of sensitivity of the materials. Whereas, it was found that OBN and NPOE at concentrations of 10 % (w/w) in the matrix caused a decrease in sensitivity of the oxygen sensors.

In conclusion, the successful application of the combinatorial approach to this study is a proof of principle. The setup developed is feasible for the high-throughput blending of viscous organic polymer solutions with solutions of target oriented sensor chemistry and the high-throughput experimentation for characterisation of the optical properties of the materials

under investigation. Subsequently, this approach will be adapted to the development of more complex sensor systems, i.e., colourimetric carbon dioxide and ammonia sensors.

3.5. References

1 Römpp H., ***Römpp Lexikon Umwelt***, Thieme, Stuttgart (2004).

2 Atkinson M. J., Thomas F. I. M., Larson N., Terrill E., Morita K., and Liu C. C., ***A Micro-Hole Potentiostatic Oxygen Sensor for Oceanic CTDs***, Deep Sea Res. Part I Oceanogr. Res. Pap **42**, 761-771, (1995).

3 Klimant I., Kuehl M., Glud R. N., and Holst G., ***Optical Measurement of Oxygen and Temperature in Microscale: Strategies and Biological Applications***, Sens. Actuators **B38**, 29-37, (1997).

4 Peterson J., I, Fitzgerald R., V, and Buckhold D. K., ***Fiber-Optic Probe for In Vivo Measurement of Oxygen Partial Pressure***, Anal. Chem. **56**, 62-67, (1984).

5 Miller W. W., Yafuso M., Yan C. F., Hui H. K., and Arick S., ***Performance of an In-Vivo, Continuous Blood-Gas Monitor with Disposable Probe***, Clin. Chem **33**, 1538-1542, (1987).

6 Opitz N. and Lübbers D. W., ***Kinetics and Transient Times of Fluorescence Optical Sensors (Optodes) for Blood Gas Analysis (O_2, CO_2, pH)***, Adv. Exp. Med. Biol. **215**, 45-50, (1987).

7 Leiner M. J. P., ***Optical Sensors for In Vitro Blood Gas Analysis***, Sens. Actuators **B29**, 169-173, (1995).

8 Swenson F. J., ***Development and Evaluation of Optical Sensors for the Detection of Bacteria***, Sens. Actuators **B11**, 315-321, (1993).

9 Siggaard-Andersen O., Goethgen I. H., Wimberley P. D., Rasmussen J. P., and Fogh-Andersen N., ***Evaluation of the Gas-STAT Fluorescence Sensors for Continuous Measurement of pH, pCO_2 and pO_2 During Cardiopulmonary Bypass and Hypothermia***, Scand. J. Clin. Lab. Invest. Suppl. **48**, 77-84, (1988).

10 Gehrich J. L., Lübbers D. W., Opitz N., Hansmann D. R., Miller W. W., Tusa J. K., and Yafuso M., ***Optical Fluorescence and its Application to an Intravascular Blood Gas Monitoring System***, IEEE Trans. Biomed. Eng. **33**, 117-132, (1986).

11 Weigl B. H., Holobar A., Trettnak W., Klimant I., Kraus H., O'Leary P., and Wolfbeis O. S., ***Optical Triple Sensor for Measuring pH, Oxygen and Carbon Dioxide***, J. Biotechnol. **32**, 127-138, (1994).

12 Lakowicz J. R., ***Principles of Fluorescence Spectroscopy 2nd Ed.***, Kluwer Academic/Plenum Press, New York (1999).

13 Amao Y., ***Probes and Polymers for Optical Sensing of Oxygen***, Mikrochim. Acta **143**, 1-12, (2003).

14 Liebsch G., Klimant I., Frank B., Holst G., and Wolfbeis O. S., ***Luminescence Lifetime Imaging of Oxygen, pH, and Carbon Dioxide Distribution Using Optical Sensors***, Appl. Spectrosc. **54**, 548-559, (2000).

15 Klimant I. and Wolfbeis O. S., ***Oxygen-Sensitive Luminescent Materials Based on Silicone-Soluble Ruthenium Diimine Complexes***, Anal. Chem. **67**, 3160-3166, (1995).

16 www.porphyrin-systems.de

17 www.vwr.com

18 www.sigmaaldrich.com

19 www.goodfellow.com

20 www.linde.de

21 www.mksinst.com

22 Wolfbeis O. S. and Editor., ***Fiber Optic Chemical Sensors and Biosensors, Vol. 2***, ***Chapter 10***, 19-53, CRC Press, Boca Raton (1991).

23 Douglas P. and Eaton K., ***Response Characteristics of Thin Film Oxygen Sensors, Pt and Pd Octaethylporphyrins in Polymer Films***, Sens. Actuators **B82**, 200-208, (2002).

24 Amao Y., Asai K., and Okura I., ***Oxygen Sensing Based on Lifetime of Photoexcited Triplet State of Platinum Porphyrin-Polystyrene Film Using Time-Resolved Spectroscopy***, Journal of Porphyrins and Phthalocyanines **4**, 292-299, (2000).

25 Mills A. and Lepre A., ***Controlling the Response Characteristics of Luminescent Porphyrin Plastic Film Sensors for Oxygen***, Anal. Chem. **69**, 4653-4659, (1997).

26 Mills A. and Williams F. C., ***Chemical Influences on the Luminescence of Ruthenium Diimine Complexes and its Response to Oxygen***, Thin Solid Films **306**, 163-170, (1997).

27 Draxler S., Lippitsch M. E., Klimant I., Kraus H., and Wolfbeis O. S., ***Effects of Polymer Matrixes on the Time-Resolved Luminescence of a Ruthenium Complex Quenched by Oxygen***, Journal of Physical Chemistry **99**, 3162-3167, (1995).

28 Mills A., ***Effect of Plasticizer Viscosity on the Sensitivity of an [Ru(bpy)$_3^{2+}$(Ph$_4$B$^-$)$_2$]-Based Optical Oxygen Sensor***, Analyst **123**, 1135-1140, (1998).

29 Pauly S., ***Permeability and Diffusion Data***, in ***Polymer Handbook, Fourth Edition***, Brandrup J. and Immergut E. H. (eds.), Wiley-VCH, New York (1998).

30 Hartmann P., Leiner M. J. P., and Lippitsch M. E., ***Response Characteristics of Luminescent Oxygen Sensors***, Sens. Actuators **B29**, 251-257, (1995).

31 Xu W., Schmidt R., Whaley M., Demas J. N., DeGraff B. A., Karikari E. K., and Famer B. A., ***Oxygen Sensors Based on Luminescence Quenching: Interactions of Pyrene with the Polymer Supports***, Anal. Chem. **67**, 3172-3180, (1995).

32 Hartmann P., Leiner M. J. P., and Lippitsch M. E., ***Luminescence Quenching Behavior of an Oxygen Sensor Based on a Ru(II) Complex Dissolved in Polystyrene***, Anal. Chem. **67**, 88-93, (1995).

33 Hartmann P. and Trettnak W., ***Effects of Polymer Matrixes on Calibration Functions of Luminescent Oxygen Sensors Based on Porphyrin Ketone Complexes***, Anal. Chem. **68**, 2615-2620, (1996).

34 Carraway E. R., Demas J. N., and DeGraff B. A., ***Luminescence Quenching Mechanism for Microheterogeneous Systems***, Anal. Chem. **63**, 332-336, (1991).

35 Carraway E. R., Demas J. N., DeGraff B. A., and Bacon J. R., ***Photophysics and Photochemistry of Oxygen Sensors Based on Luminescent Transition-Metal Complexes***, Anal. Chem. **63**, 337-342, (1991).

36 Demas J. N., DeGraff B. A., and Xu W., ***Modeling of Luminescence Quenching-Based Sensors: Comparison of Multisite and Nonlinear Gas Solubility Models***, Anal. Chem. **67**, 1377-1380, (1995).

37 Mills A., ***Effect of Plasticizer Viscosity on the Sensitivity of an [Ru(bpy)$_3^{2+}$(Ph$_4$B$^-$)$_2$]-based Optical Oxygen Sensor***, Analyst **123**, 1135-1140, (1998).

38 Mills A., Lepre A., and Wild L., ***Effect of Plasticizer-Polymer Compatibility on the Response Characteristics of Optical Thin Film CO_2 and O_2 Sensing Films***, Anal. Chim. Acta **362**, 193-202, (1998).

Chapter 4. Combinatorial Approach to the Development of Optical CO_2 Gas Sensors

4.1. Introduction

Carbon dioxide is an odourless, non-inflammable, colourless gas. The maximum allowable concentration (MAC) is 9000 mg / m^3.[1] As a key parameter in biological carbon cycle, it is formed in combustion of carbon containing materials, fermentation and respiration of animals, and assimilated by plants in photosynthesis. It is of tremendous impact to the environment through global warming. Carbon dioxide absorbs infrared radiation and prevents it from re-escaping to space. The retained energy causes an increase of temperature on the surface of the earth. On the other hand CO_2 is drawn from the atmosphere by the oceans, reducing the greenhouse effect by acting as a sink for carbon dioxide. The steady gas exchange between hydrosphere and atmosphere is of major importance to global warming.

Besides the ecological influence of carbon dioxide, it is used for many industrial processes including chemical syntheses or preservation of products in food packaging industry. Thus, quantitative monitoring of carbon dioxide is of high interest in numerous applications, including medical, environmental and industrial analyses.[2-6] Industrial applications include quality control for food packaging by modified atmospheric packing or process control in biotechnological processes.

Among the well established electrochemical determination of carbon dioxide with the so called "Severinghaus"-electrode optical measurement methods are of great interest in research for pCO_2 determination. Optical methods include infra-red spectroscopy detecting directly the characteristic carbon dioxide absorbance.[7] However, this method needs bulky and expensive equipment. Optical sensors for pCO_2 determination offer significant advantages compared to electrodes and infra-red spectroscopy. They are cheaper, easier to manufacture and handle, and they can easily be miniaturised. An attractive approach to optimise optical carbon dioxide sensors was the use of thin plastic film sensors utilising polymer in which a pH-sensitive dye was incorporated along with a phase transfer agent.[8,9] The preparation of sensor cocktails for this type of sensors was improved by direct preparation of a salt-free indicator ion pair.[10] Based on the plastic film technique the carbon dioxide concentration can

be detected via the pCO_2-dependent absorbance change of the indicator dye or the change of fluorescence intensity of a pH-sensitive luminescent dye.[6,11-13]

The development of optical carbon dioxide sensors is of great interest due to the manifold of conceivable applications. Yet, all present carbon dioxide sensors lack of stability. In terms of long-term stability this is due to poisoning of the sensor via irreversible acidification by acidic gases like HCl, SO_2 or NO_2. Additionally, triphenyl methane-based indicators are subject to gas fading, i.e. the irreversible oxidation of the dye by oxidising gases like NO_x. The adaptation of combinatorial methods to the development offers a promising solution for these drawbacks. The speed-up of material development may lead to more stable sensors with equal or better performance than existing ones. The increase of the knowledge base may help finding formulations suitable for future applications of pCO_2 sensors or understand better the principles of component effects. Thus, the combinatorial approach was adapted to the development of absorbance-based optical carbon dioxide sensors to proof the suitability of the method to more complex sensor systems, compared to oxygen sensors.

4.2. Concept

The determination of carbon dioxide with optical sensors utilises pH-sensitive dyes changing colour or fluorescence when the pH of the surrounding medium is changed according to a change of the ambient carbon dioxide level.[8,14-18] Ionic dyes are solubilised in apolar media like organic polymers via ion pairing, e.g. with quaternary ammonium compounds (Q^+). Thereby the two species of the transducer, i.e., protonated and deprotonated dye, exhibit different absorbance maxima. The sensing mechanism is based on this acid-base reaction according to the following equilibria

$$\{Q^+OH^- \cdot xH_2O\} + CO_2 \rightleftharpoons \{Q^+HCO_3^- \cdot xH_2O\} \tag{4.1a}$$

and

$$\begin{aligned}\{Q^+D^- \cdot x\,H_2O\} + \{Q^+HCO_3^- \cdot x\,H_2O\} \rightleftharpoons \\ \{Q^+HCO_3^- \cdot (x-1)H_2O \cdot HD\} + \{Q^+OH^- \cdot x\,H_2O\}\end{aligned} \tag{4.1b}$$

These equilibria can be summarised by

$$\underset{\text{Colour A}}{\{Q^+D^- \cdot x\,H_2O\}} + CO_{2(g)} \overset{\alpha}{\rightleftharpoons} \underset{\text{Colour B}}{\{Q^+HCO_3^- \cdot (x-1)H_2O \cdot HD\}} \tag{4.2}$$

where Q^+ is the quaternary ammonium cation, D^- is the deprotonated dye, HD is the protonated dye and α is the equilibrium constant. From this reaction the following equation can be derived

$$\alpha \cdot pCO_2 = \frac{[\{Q^+HCO_3^- \cdot (x-1)H_2O \cdot HD\}]}{[\{Q^+D^- \cdot xH_2O\}]} \tag{4.3}$$

where $[\{Q^+HCO_3^-\cdot(x\text{-}1)\ H_2O\cdot HD\}]$ and $[\{Q^+D^-\cdot x\ H_2O\}]$ are the equilibrium concentrations of the protonated and the deprotonated dye, respectively, and pCO_2 is the carbon dioxide partial pressure. With $[\{Q^+D^-\cdot x\ H_2O\}]_0$ being the initial concentration applied of the base form of the dye in the film the equation (4.3) is modified with

$$[\{Q^+HCO_3^- \cdot (x-1)H_2O \cdot HD\}] = [\{Q^+D^- \cdot xH_2O\}]_0 - [\{Q^+D^- \cdot xH_2O\}] \tag{4.4}$$

to

$$\alpha \cdot pCO_2 = \frac{[\{Q^+D^- \cdot xH_2O\}]_0 - [\{Q^+D^- \cdot xH_2O\}]}{[\{Q^+D^- \cdot xH_2O\}]} \tag{4.5}$$

or

$$\alpha \cdot pCO_2 = \frac{[\{Q^+D^- \cdot xH_2O\}]_0}{[\{Q^+D^- \cdot xH_2O\}]} - 1 \tag{4.5a}$$

Assuming Lambert-Beer´s Law is obeyed, the absorbance A at λ_{max} of the deprotonated dye is expressed by a linear function $A = \varepsilon \times c \times d$. If the protonated species does not absorb significantly at λ_{max} of the base form, $[\{Q^+D^-\cdot x\ H_2O\}]_0$ and $[\{Q^+D^-\cdot x\ H_2O\}]$ can be substituted by A_0 and A, i.e. the absorbance of the dye anion in absence of carbon dioxide and at ambient concentration of CO_2, respectively. Thus, the equation

$$\frac{A_0}{A} = 1 + \alpha \cdot pCO_2 \tag{4.6}$$

is obtained describing a linear relation between the ratio of A_0/A and the ambient carbon dioxide concentration. The response of optical CO_2 sensors can be calibrated plotting the ratio A_0/A as a function of pCO_2.

4.3. Experimental

4.3.1. Chemicals

4.3.1.1. Polymers

In the study on optical carbon dioxide sensors the polymers listed in Chapter 3, section *3.2.1.3 Polymers* were used as support for the thin-film sensors. Their chemical structures are given

in figure 4.1 for inspection. All polymers were purchased from Aldrich[19] with exception of poly(methyl methacrylate) from Goodfellow.[20] Stock solutions of various concentration were prepared by dissolving the respective polymer in compatible organic solvent for automatic processing with MicroLab® S liquid handling robot. For concentrations of stock solutions processed and solvent see Chapter 3, section *3.2.1.3 Polymers*.

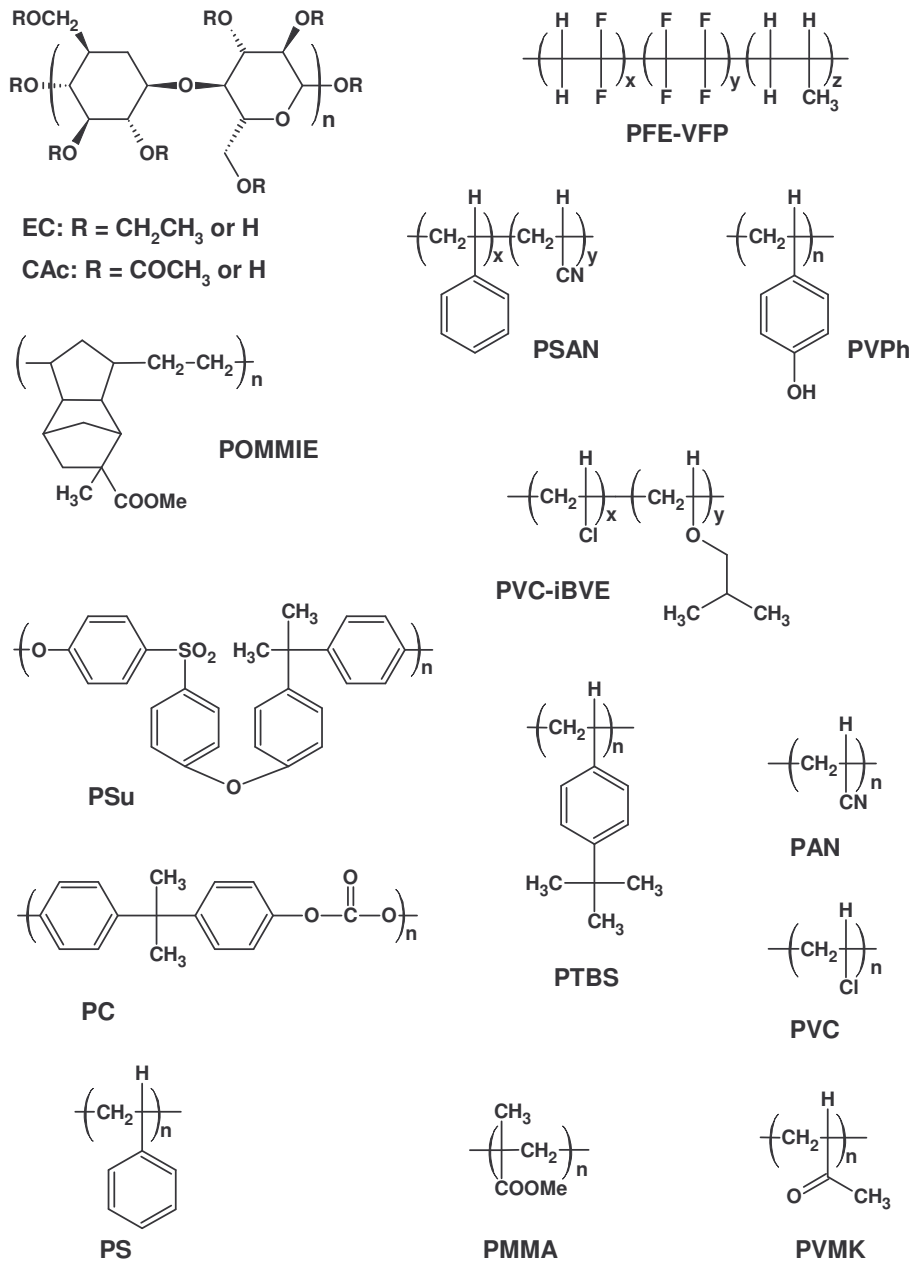

Figure 4.1. Chemical structures of the polymers used in the study on optical carbon dioxide sensors

4.3.1.2. Reagents and Solvents

Silver(I) oxide of pure grade (purum, ≥ 99.0 %) was purchased from Fluka.[19]
Ethanol, methanol, toluene, acetone, chloroform, dichloromethane, dimethylformamide and tetrahydrofurane were purchased from Merck.[21] All solvents were of analytical grade and used without further purification.

4.3.1.3. Quaternary Ammonium Bases and Precursors

In this study quaternary ammonium hydroxides of increasing number of long side chains were applied. The compounds are shown in table 4.1. Tetrabutylammonium hydroxide 30-hydrate (prod.no. 86859, anal. grade: purris, ≥ 99.0 %; TBA−OH) and tetraocylammonium hydroxide (prod.no. 87993, anal. grade: purum, ~ 20 % in methanol; TOA-OH) were purchased from Fluka and used without further purification. Hexadecyl trimethyl ammonium hydroxide (CTA-OH), didodecyl dimethyl ammonium hydroxide (DDDMA-OH) and tridodecyl methyl ammonium hydroxide (TDMA-OH) were prepared from the corresponding halides. CTA-Br (prod.no. 52370, anal. grade: purum, ≥ 96.0 %) DDDMA-Br (prod.no. 36785, anal. grade: purum, ≥ 98.0 %) and TDMA-Cl (prod.no. 91662, anal. grade: purum, ≥ 97.0 %) were purchased from Fluka.

The hydroxides CTA-OH, DDDMA-OH and TDMA-OH were prepared according to a published synthesis[13], as follows: 1.82 g (5 mmol) CTA-Br, 2.31 g (5 mmol) DDDMA-Br and 2.86 g (5 mmol) TDMA-Cl were dissolved in 15 mL methanol each. To each ammonium halide solution 1.16 g (5 mmol) wet silver oxide were added and the suspensions were stirred in closed, dark flasks at + 4 °C over night. Subsequently the solids were filtered and the solutions were evaporated under vacuum. 0.5 M stock solutions were prepared dissolving the solid hydroxides in 10 mL methanol, and processed with the MicroLab S.

Methanolic TOAOH solution was processed as delivered. Hydroxide concentration was evaluated by acid-base titration. TBAOH stock solution (c = 0.5 M) was prepared dissolving 3.9995 g dry hydroxide in 10 mL methanol.

Table 4.1. Chemical structures of quaternary ammonium hydroxides used in the study on optical pCO_2 sensors.

Quaternary ammonium hydroxide	Structure of ammonium compound
tetrabutyl ammonium hydroxide (TBA-OH)	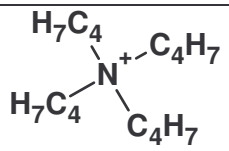
hexadecyltrimethyl ammonium hydroxide (CTA-OH)	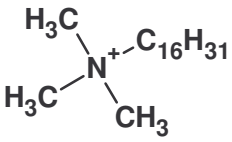
didodecyldimethyl ammonium hydroxide (DDDMA-OH)	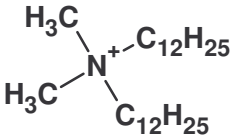
tridodecylmethyl ammonium hydroxide (TDMA-OH)	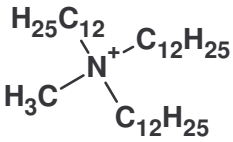
tetraoctyl ammonium hydroxide (TOA-OH)	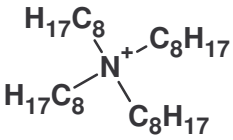

4.3.1.4. Indicator Dyes

The pH indicator dyes listed in table 4.2 were selected for use in polymeric thin film carbon dioxide sensors and tested for their performance in CO_2 determination. All dyes shown in figure 4.2 were processed as stock solutions of the respective TDMA ion pairs in toluene.

The TDMA ion pairs of the indicator dyes were synthesised according to a modified general procedure adapted from synthesis described earlier:[22,23] 500µmol of sodium salt of the respective dye were dissolved in 30 mL water. The pH of the solution was adjusted with 0.1 N hydrochloric acid to form the protonated (acid) form of the dye. An excess amount – according to the molar ratio between dye and TDMA in the ion pair – of a solution of TDMA-Cl in acetone (500 µmol / 15 mL) was added dropwise to the dye solution with a dropping funnel. The mixture was stirred at room temperature over night to allow completion of the ion pairing and evaporation of the acetone. The ion pair was extracted with 30 mL toluene from the aqueous solution and, after evaporation of the organic solvent in a rotary evaporator, dried in a desiccator over sodium hydroxide. The molar ratios of dye and TDMA-Cl in the ion pair, the net molecular weight of ion pairs and elemental analysis data are given in table 4.3.

Table 4.2. List of pH indicators used in screening of carbon dioxide sensors.

Indicator Dye / Acronym		pK_D in H_2O	λ_{max} (D^-) in H_2O	Prod.No.	Supplier
m-cresol purple	MCP	8.3 [24]	580 nm	857890	Aldrich[19]
brilliant yellow	BRY		500 nm	201375	Aldrich
thymol blue	TB	9.2 – 9.7[24]	595 nm	32727	Aldrich
bromophenol blue	BPB	4.1[24]	600 nm	32768	Fluka[19]
bromocresol green	BCG	4.9[24]	615 nm	114367	Aldrich
phenol red	PR	8.0[24]	560 nm	107241	Merck[21]
cresol red	CR	8.5[24]	570 nm	114480	Fluka
alizarin red S	ARS	5.5[25]	560 nm	106279	Merck
orange I	OI	8.3[24]	490 nm	75360	Fluka
xylenol blue	XB	9.5[24]	595 nm	114561	Aldrich
xylenol orange	XO	10.4; 12.3[24]	580 nm	33825	Riedel de Haën[19]
bromocresol purple	BCP	6.4[24]	585 nm	860891	Aldrich

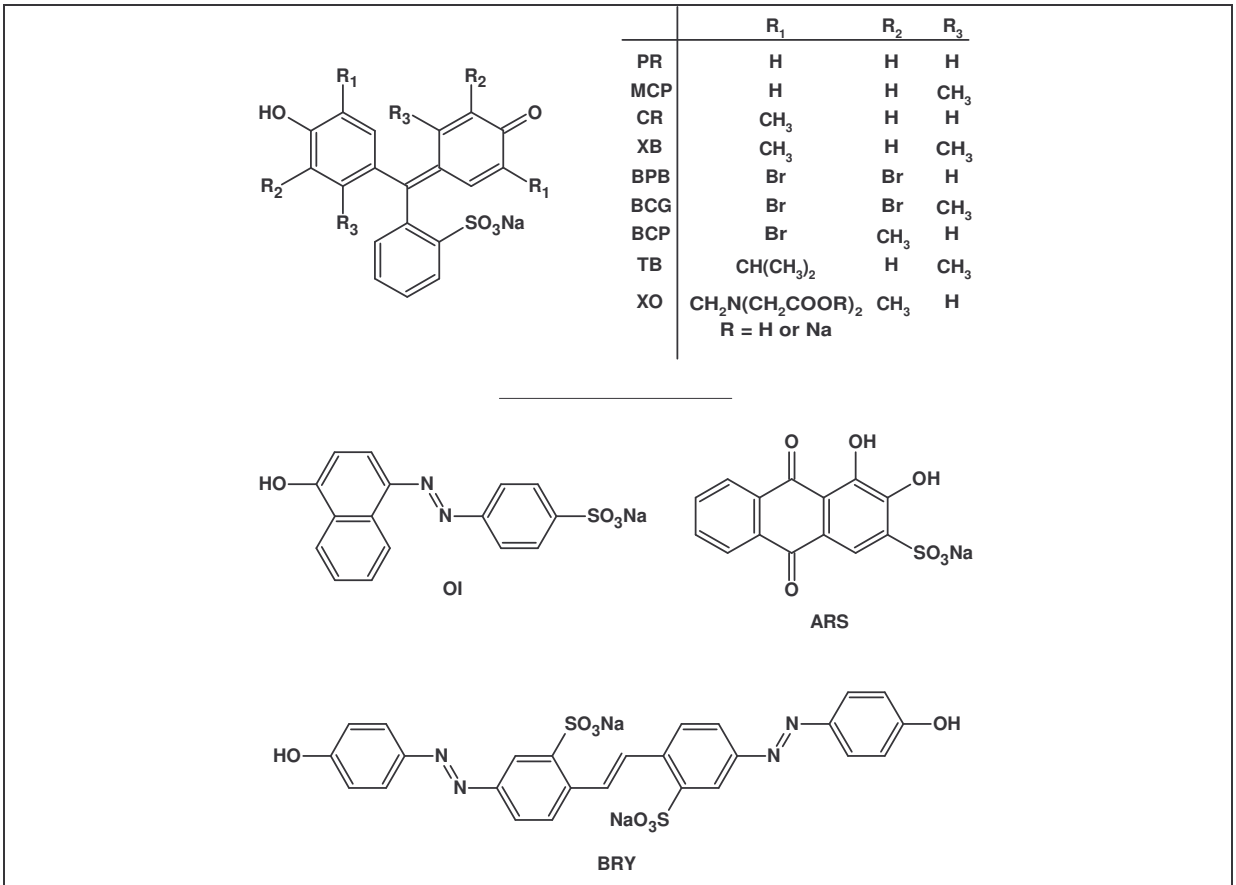

Figure 4.2. Chemical structures of the dyes applied to screening for carbon dioxide sensors.

Table 4.3. Indicator ion pairs applied in the study on optical carbon dioxide sensors.

						Elemental analysis (calc./found)		
Ion Pair	Abbr.	Formula	MW	ratio	yield	C	H	N
m-cresol purple – TDMA	MCP	$C_{58}H_{95}NO_5S$	918.45	1:1	85 %	75.85/74.83	10.43/10.68	1.53/1.80
brilliant yellow – TDMA	BRY	$C_{100}H_{174}N_6O_8S_2$	1652.62	1:2	78 %	72.68/71.42	10.61/10.26	5.09/4.73
thymol blue – TDMA	TB	$C_{64}H_{107}NO_5S$	1002.60	1:1	88 %	76.67/73.01	10.76/10.78	1.40/1.46
bromophenol blue – TDMA	BPB	$C_{56}H_{87}Br_4NO_5S$	1205.98	1:1	85 %	55.77/53.65	7.27/7.26	1.16/1.08
bromocresol green – TDMA	BCG	$C_{58}H_{91}Br_4NO_5S$	1234.03	1:1	78 %	56.45/56.43	7.43/7.68	1.14/1.26
phenol red – TDMA	PR	$C_{56}H_{91}NO_5S$	890.39	1:1	89 %	75.54/73.79	10.30/10.70	1.57/1.59
cresol red – TDMA	CR	$C_{58}H_{95}NO_5S$	918.45	1:1	88 %	75.85/75.24	10.43/10.53	1.53/1.42
alizarin red S – TDMA	ARS	$C_{51}H_{87}NO_7S$	858.31	1:1	85 %	71.37/71.96	10.22/10.78	1.63/1.67
orange I – TDMA	OI	$C_{53}H_{89}N_3O_4S$	864.36	1:1	85 %	73.65/72.51	10.38/11.26	4.86/4.36
xylenol blue – TDMA	XB	$C_{60}H_{99}NO_5S$	946.50	1:1	86 %	76.14/76.11	10.54/10.32	1.48/1.49
xylenol orange – TDMA	XO	$C_{183}H_{348}N_6O_{13}S$	2872.82	1:4	75 %	76.51/75.07	12.21/12.75	2.93/2.50
bromocresol purple – TDMA	BCP	$C_{58}H_{93}Br_2NO_5S$	1076.24	1:1	88 %	64.73	8.71	1.30

4.3.1.5. Gases

Nitrogen (purity 99.999 %), synthetic air (oxygen content 20.9 %) and carbon dioxide test gas with CO_2 contents of 5 % and 20 % in nitrogen were purchased from Linde GmbH, Germany.[26]

4.3.2. Preparation of Sensor Materials

The preparation of optical carbon dioxide sensors was performed using the high-throughput blending method and apparatus described in chapter 2, *2.2.2. Combinatorial Blending* and *2.3.1. Instrumentation for Library Preparation*.

The general composition of a sensor used in the screening process included 20 mg polymer, 500 mmol/kg base and 10 mmol/kg indicator ion pair, referring to 1 kg dry polymer. The desired volumes of the respective component solutions, given in table 4.4, were calculated in an EXCEL sheet supplied with the concentrations of all stock solutions used. The concentration of the TOA-OH stock solution was 0.33 M, stock solutions of CTA-OH, DDDMA-OH and TDMA-OH were 0.5 M. All indicator stock solutions were prepared dissolving 20 mg ion pair in 5 mL toluene. Polymer stock solutions were prepared according to table 3.1 (see chapter 3, section *3.2.1.3. Polymers*).

The desired quantities of each component were dispensed into sample vials with the MicroLab S executing a predefined procedure (see Appendix B). After shaking the vials, 6 - 9 µL of the sensor cocktails were then transferred into the corresponding wells of the etched glass substrates using the liquid handler. The sensors were dried in ambient air over night allowing toluene to evaporate and then placed into the high-throughput characterisation setup.

Table 4.4. Volumes of each component necessary to prepare a carbon dioxide sensor composed of 20 mg polymer, 10 µmol base and 0.2 µmol indicator ion pair (IP), according to the stock solution concentrations given in the Excel sheet with a master recipe.

Polymer	Volume / µL	Base	Volume / µL	IP	Volume / µL
EC46	666	TOA-OH	30.1	MCP	2.3
EC49	667	CTA-OH	20.0	BRY	4.4
PFE-VFP	400	DDDMA-OH	20.0	TB	2.5
PSAN	400	TBA-OH	20.0	BPB	3.0
CAc	394	TDMA-OH	20.0	BCG	3.1
PVPh	400			PR	2.2
PVMK	800			CR	2.3
PSu	399			ARS	2.0
PVC-iBVE	100			OI	2.2
POMMIE	133			XB	2.4
PC	399			XO	6.2
PTBS	100			BCP	2.7
PAN	400				
PVC	799				
PS	200				
PMMA	800				

4.3.3. Characterisation of Optical Carbon Dioxide Sensors

The sensor libraries were characterised using the setup for absorbance measurements described in chapter 2, section *2.3.2. Setup for Library Characterisation*. All absorbance measurements were performed at 20 ± 2°C unless otherwise stated. Substrates loaded with sensor spots were mounted in the optical gas chamber and exposed to test atmospheres with carbon dioxide concentrations of 0, 0.25, 0.5, 1, 3 and 5 % CO_2, respectively. The humidity of the gas flow was controlled with a humidity sensor and adjusted to 50 % r.H. (relative humidity) by blending water saturated and anhydrous gas flows. The PMA 11 multi-channel analyser was used for acquisition of the absorbance spectra of the samples when exposed to the respective test atmosphere. The LabView-based control software synchronised all measurement apparatus and stored the spectra in indexed files according to carbon dioxide concentration in test gas. These data were imported into a purpose-built EXCEL sheet

including VBA macros for evaluation of peak wavelengths and extraction of absorbance values A at λ_{max} of the sensors in the respective test atmospheres. The performance of the sensor materials was evaluated by plotting the ratio A_0/A as a function of pCO_2 according to equation (4.6), where A_0 was the absorbance of the films in absence of carbon dioxide and A was the absorbance when exposed to the respective test atmosphere with defined carbon dioxide concentration.

4.4. Results and Discussion

4.4.1. Choice of Materials

According to the acidic character of carbon dioxide, the indicator dye used has to be applied in the basic form. On exposure to CO_2 the dyes reversibly have to change absorbance due to protonation by carbonic acid produced with traces of water in the film. Suitable indicator dyes include azo dyes, sulfonephthaleins, nitrophenols and phthaleins. The indicators used in screening for carbon dioxide sensors were selected from these types of dyes, exhibiting pK_a values in the range from 5 – 9 in water. Their chemical structure allowed easy lipophilisation via ion pairing and they showed desired significant difference in absorbance spectra between basic and acidic pH. Furthermore, the absorbance maxima of the basic forms of the dyes were around 590 – 630 nm making them compatible to red LED-based devices. Thus, sensor films of these indicators can be mounted into low cost instrumentation being composed of a cheap LED for illumination, the sensor chemistry and a low cost photodiode as detector.

Quaternary ammonium hydroxides were used as lipophilic buffers. The quaternary cation can act as counter ion for solubilisation of anionic indicator molecules and the buffer provides bound water molecules necessary for the creation of carbonic acid from ambient carbon dioxide. The carbonic acid then dissociating to H^+ and bicarbonate (HCO_3^-) causes a decrease of pH in the surrounding medium. This can be observed via the colour change of the indicator dye. Thereby, the bicarbonate is stabilised by the quaternary cation in the film.

The polymer has two major functions. The first is the solubilisation of the sensing chemistry providing chemical and physical compatibility and stability to all components. Secondly, it has to exhibit sufficient permeability to target gas, since the permeability influences the sensitivity and response time of a sensor. For application in aqueous media the polymer acts as barrier for ions from bulk solution causing pH changes in the matrix and thus interfering the sensing mechanism. The polymers selected fulfil most of these requirements.

They have proven permeability to gases in the study on optical oxygen sensors. Their compatibility to carbon dioxide sensors is subject of this chapter.

Plasticizers benefit the permeability properties of polymers and thus introduction of these results in enhancement of sensitivity of optical carbon dioxide sensors. On the other hand they also increase temperature dependence of the sensors. Thus, it is of interest to find polymer / indicator / buffer combinations without using plasticizer to minimise the temperature effect on the response of optical carbon dioxide sensors. Additionally, with rising number of components the complexity of the sensor system increases and it becomes more difficult to search for trends in effects of single components in the overall system. For practical realisation of automated blending the increasing number of possible solvents is a potential cause of system break down, since the selection of solvents is limited by the general solubility of all components in the used solvents.

4.4.2. Library Design

A typical solid state optical carbon dioxide sensor, as described here, consists of a supporting polymer, a lipophilic buffer, a pH-sensitive dye dissolved in this matrix and probably a plasticizer. Thus, leaving the plasticizer out of consideration there are three orders of freedom for development and optimisation of optical pCO_2 sensors, i.e., a) the type of polymer, b) the type of buffer and c) the type of indicator.

The polymers, indicators and buffers used in this study span up a matrix of 960 sensor formulations to be tested. This matrix was divided into sublibraries for practical reasons, namely solubility of the components in organic solvents. In first order the type of polymer was fixed. Secondly, the buffer to be used was selected. These polymer-buffer compositions were blended with the indicators under investigation to form carbon dioxide sensitive materials. Six spots of each formulation were cast on a substrate for statistical analysis of the calibration of the sensor materials. The structure of library discrimination is illustrated in figure 4.3. Thus, the glass substrates were loaded with sample cocktails of identical polymer - buffer composition varying the indicator species. After all indicator dyes were introduced the buffer was changed and again all possible formulations were prepared by the robot. This was repeated until all buffers and indicators were mixed with one type of polymer. The library was completed repeating this procedure for all polymers under investigation.

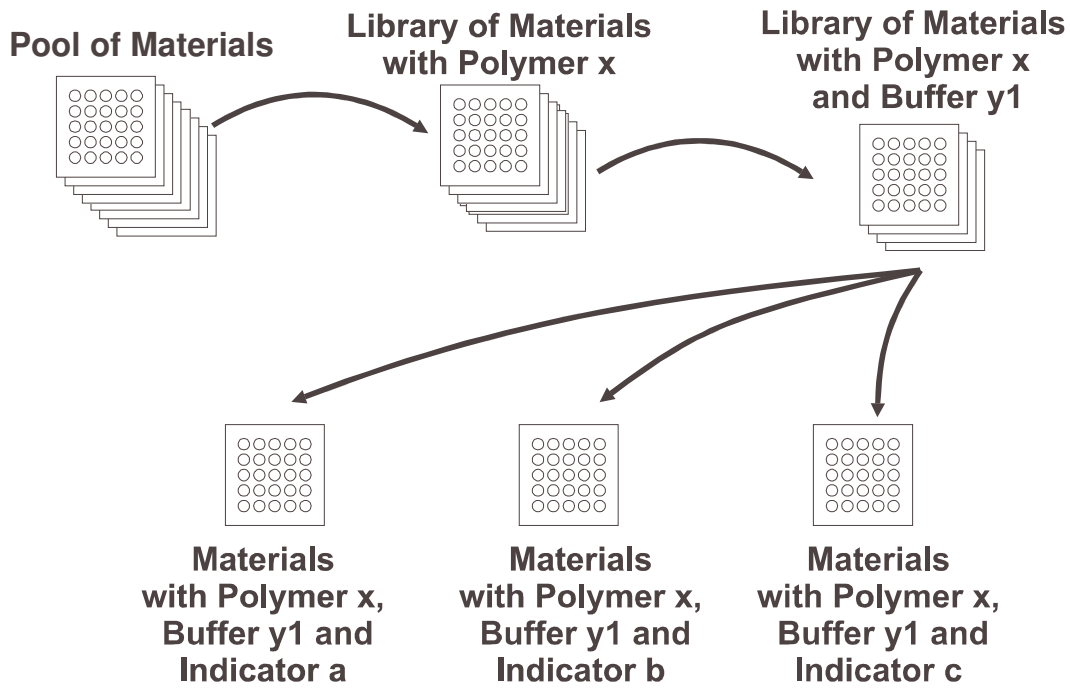

Figure 4.3. Structure of sensor library and separation to sublibraries for discrimination of sensor materials.

4.4.3. Library Management

It is obvious that 960 potential sensor materials can hardly be managed manually. Thus, analogous to the oxygen sensor study a database was necessary for management of preparation and characterisation data of the samples under investigation. The key steps for building up the database are illustrated in figure 4.4.

In contrast to the study described in chapter 3 the data obtained and processed for each sample here was bigger by a factor of ca. 500. Whereas for a luminescence decay time-based oxygen sensor the intensity and the phase shift between excitation and emission of the luminescence signal was stored for each sample exposed to a defined atmosphere (2 data points per spot and atmosphere), here for each sensor spot one absorbance spectrum in the range from 400 to 800 nm with **1024 (!)** data points was obtained per test atmosphere. The acquisition of the absorbance spectra was necessary for preliminary data evaluation, since the absorbance of a chromophore strongly depends on the encapsulating medium (polarity of surrounding medium). For characterisation of the samples the absorbance maxima (λ_{max}) had to be evaluated and then the absorbance values at λ_{max} were extracted according to the ambient atmosphere applied for characterisation. Although, only one absorbance value at λ_{max} per test atmosphere was required for characterisation of the sensor material and stored for calibration the whole spectra had to be processed. Again for this step automation was

necessary. VBA code was developed to speed up import of the raw data into EXCEL spreadsheets, evaluation of maximum wavelength and extraction of absorbance at λ_{max}. The data were checked manually by comparing the generated λ_{max} with absorbance spectra. This could not be automised, since the functions for peak selection could not be optimised that much to distinguish between local maxima and irregular noise. The absorbance maximum of each sample was searched in the range from 500 to 700 nm. If the absorbance values at the border lines of the search interval exceeded the local maximum absorbance around 600 - 630 nm, the latter could not be separated. Thus, the wavelength of maximum absorbance had to be evaluated manually for those materials. The ratios A_0/A were calculated from the absorbance values obtained. These ratios were plotted as function of pCO_2 giving the calibration plots for each sensor material.

The characterisation data were put into the Access® data base built up. The compositions of the samples were allocated to unique identifiers and stored in a preparation table. A second table contained the processed measurement data (ratio A_0/A and corresponding pCO_2) allocated to the corresponding sample indices. This indexing enabled the simultaneous highlighting of preparation and calibration data of each sensor material. The comparison of sensory properties of multiple samples was provided by searching for record sets meeting the respective queries for a certain polymer, buffer or indicator.

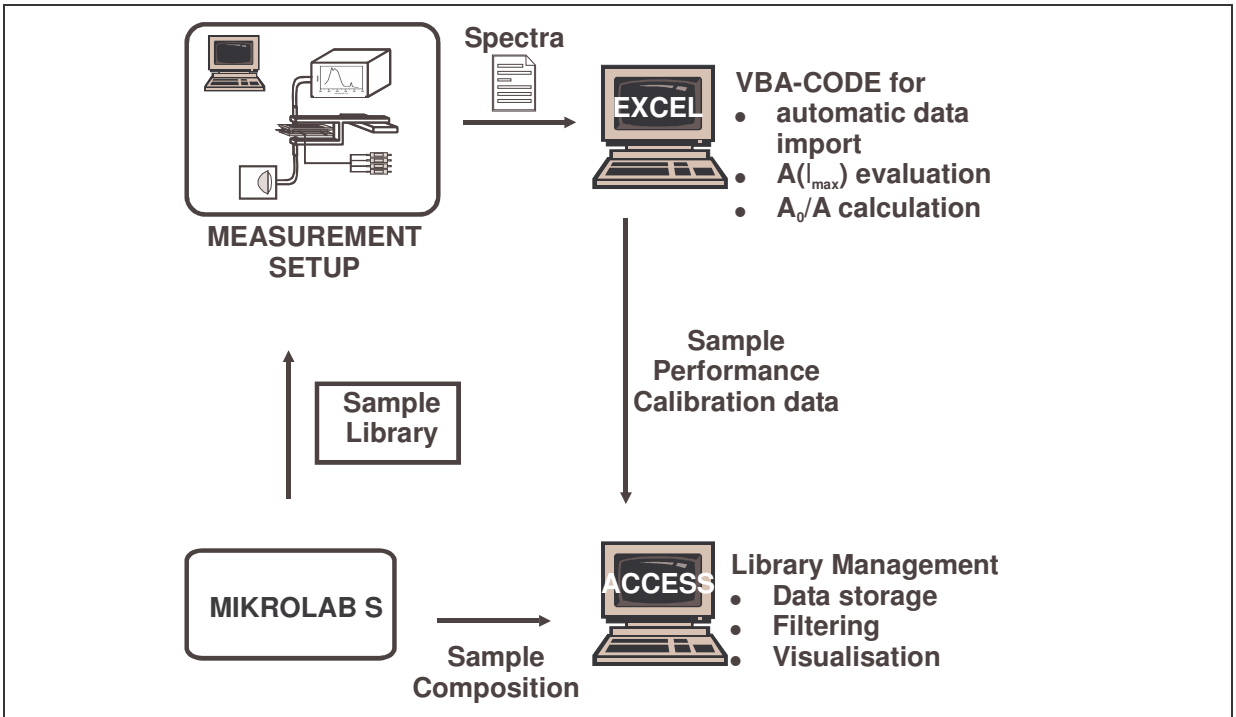

Figure 4.4. Work flow of database build up.

4.4.4. Screening of Sensor Materials

Processibility and Stability of Precursor Solutions for Carbon Dioxide Sensors

Useful carbon dioxide sensors had to exhibit compatibility, physical and chemical stability of the components and response to target gas. Unless otherwise stated polymers used were compatible to sensor chemistry and formed transparent cocktails without precipitation of components from mixed solutions. Thin films usually were transparent.

Upon preparation of cocktails comprising the polymers cellulose acetate and poly(acrylonitrile) it was observed that after addition of buffer the polymer precipitated from solution. The sample cocktails remained turbid even after thorough shaking. Cocktails containing CAc changed from blue colour of the basic form of the dye to yellow due to irreversible acidification. The precipitation of PAN from solution was caused by insufficient miscibility with other solvents than DMF. Thus, these two polymers were judged incompatible with the sensor chemistry of a carbon dioxide sensor. Cellulose acetate was degraded by basic hydrolysis with the lipophilic ammonium base. In accordance to previous information polymers are not viable for carbon dioxide sensors when being degradable by basic hydrolysis.[27]

Cocktail solutions prepared with PMMA dissolved in chloroform were not stable for long term storage. Traces of HCl produced slowly in the solvent caused protonation of the dye anion and neutralisation of the base. Freshly prepared sensor cocktails were cast on the glass substrates and the solvent was evaporated. After 72 hours the dry films still exhibited unchanged blue colour and sensitivity to carbon dioxide. In contrast to the precursor solution, no degradation was observed for the ready to use thin film. Thus, for the preparation of carbon dioxide sensors comprising PMMA as supporting polymer the component stock solutions were prepared freshly and processed immediately to form the dry thin-films. Sensor cocktails prepared alternatively with THF as solvent for the polymer PMMA were stable and did not show observable degradation, but dissolving the polymer takes much longer in THF compared to chloroform.

It is known that commercial PVC contains acidic moieties present in the polymer. Thus, it seemed not viable for use in carbon dioxide sensors.[27] Pre-treatment of crude polymer powder with aqueous sodium hydroxide solution was performed to remove traces of acid from the polymer. Sensor cocktails prepared comprising the pre-treated polymer were stable and did not show protonation of the dye observable by conversion from basic to acidic colour of sensors. This enabled the use of the polymer for preparation of potential carbon dioxide sensors and screening of their sensory properties.

Effect of Component Variation on Sensitivity of Polymer / TOA-OH / Indicator - based Sensors

According to equation (4.6) the sensitivity of a colorimetric carbon dioxide sensor is determined by the slope of the function describing the decrease of absorbance of the base form of an indicator in a sensor as a function of increasing pCO_2. The bigger the gradient α, the bigger is the sensitivity of the sensor. It is obvious that the slope strongly depends - upon other influencing parameters - on the permeability of the polymer to carbon dioxide and on the acid dissociation constant pK_D of the indicator dye.[27-29] Typically, the pK_D of useful dyes is in the range from 5 – 10.

These indicator dyes were dissolved in various matrices comprising an organic polymer and TOA-OH base with concentrations of 10 mmol dye and 500 mmol base per 1 kg polymer. From each sensor cocktail 6 sample spots were placed onto the glass substrate evaluating the reproducibility. The sensor materials prepared were exposed to atmospheres with concentrations of 0, 0.25, 0.5, 1, 3 and 5 % carbon dioxide in nitrogen. The absorbance spectra of the equilibrated samples were recorded and the calculated ratios A_0/A were plotted as functions of pCO_2. The response of the sensor materials were expected to be of linear relation between A_0/A and pCO_2 according to equation (4.6). Thus, with linear regression of the characterisation data it was performed to determine the parameters of the linear functions specifying the response of the samples. The gradient α of the equation was used as a measure for the sensitivity of the sensor materials. The linearity of the calibration plots was characterised by the correlation coefficient R^2, by definition ranging from 0 to 1. For $R^2 = 1$ all experimental data points are identical with the predicted values calculated from the ideal linear regression model. The more R^2 differs from 1, the less is the significance and accuracy of the predicted values.

The results from linear regression of the calibration functions were put into the CO_2 sensor database. This enabled the comparison of the different sensor materials with focus on the change of sensitivity upon changing the material composition. It was found that the sensitivity increased upon exchange of the indicator dye with a transducer having a higher pK_A. This trend was in good agreement with theory and literature.[27-29] The increase of the slope of the calibration functions, and consequently the sensitivity of the sensor materials, is illustrated in figure 4.5. Here, the response of materials is shown comprising the polymer EC46, 500 mmol TOA-OH per 1 kg polymer and 10 mmol pH-sensitive indicator ion pair per 1 kg matrix (including both polymer and base).

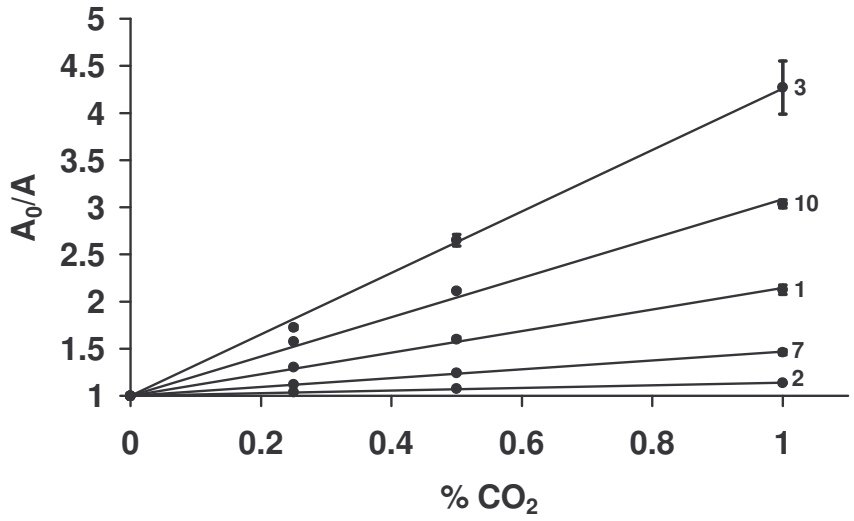

Figure 4.5. Calibration plots of carbon dioxide sensors comprising EC46/TOA-OH and the dyes MCP (1), BRY (2), TB (3), CR (7) and XB (10), respectively.

It can be seen that the sensitivity of the respective sample sensor increased upon changing from phenol red (pK_D = 8.0) to m-cresol purple (8.3), thymol blue (9.2 - 9.7) or p-xylenol blue (9.5). The initial slopes of the calibration curves were calculated to be 114.5 ± 4.9 atm^{-1} (MCP), 14.1 ± 0.4 atm^{-1} (BRY), 325.9 ± 23.3 atm^{-1} (TB), 46.8 ± 2.8 atm^{-1} (CR) and 208.6 ± 3.9 atm^{-1} (XB) in the range from 0 to 1 % CO_2. Yet the higher slope of the thymol blue-based material in comparison to the p-xylenol blue based sensor indicated that not only the acidity of the dye was effecting the sensitivity. Aqueous solutions of these two indicators show same transition interval upon incremental increase of pH of the solution and, thus, pK values of p-xylenol blue and of thymol blue – with variations depending on reference source - were assumed of equal magnitude. This would result in the prediction that both materials show same behaviour. The experimental data showed that besides the acidity of the pH-sensitive dye obviously additionally steric effects are influencing the response characteristics of the sensor materials. Comparing the chemical structures of thymol blue and p-xylenol blue shown in figure 4.6, the higher sensitivity of the first can be attributed to a lower stability of the indicator–TOA ion pair formed in the considered thin film. This was deduced to a greater steric shielding of the phenolate group by the iso-propyl residue in *ortho* position in thymol blue. As a result, the voluminous tetraoctylammonium cation has a bigger distance to the anion and the electrostatic interaction is weaker. Thus, carbon dioxide sensors based on EC46, TOA-OH and TB were more sensitive than the analogue with XB.

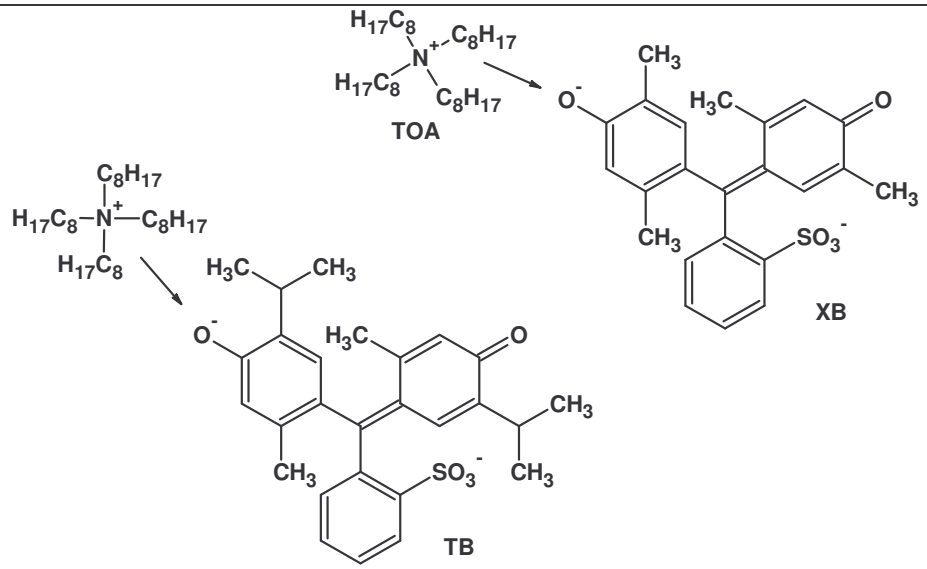

Figure 4.6. Chemical structures of TB and XB showing the steric demand of the side chain in ortho position of the phenolate group.

A second ethyl cellulose polymer EC49 was used in the screening for carbon dioxide sensor materials. Results obtained for this basis matrix confirmed the observations made with EC46. Sensor materials with EC49 expressed higher sensitivity to carbon dioxide compared to the previously described matrix. The initial slopes were calculated to be 390.7 ± 47.2 atm^{-1} (MCP), 65.5 ± 1.5 atm^{-1} (BRY), 976.6 ± 70.2 atm^{-1} (TB), 48.6 ± 1.7 atm^{-1} (PR), 90.6 ± 5.9 atm^{-1} (CR) and 503.0 ± 20.4 atm^{-1} (XB). The relative responses of the particular indicator dyes to each other showed the same order in films utilising EC46 and EC49. This was construed a confirmation that primary effects based on structural differences of thymol blue and p-xylenol blue caused the higher sensitivity of the first in the cellulosic matrices. Although an additional influence of the polymer was not excluded.[8] The higher sensitivity of the sensors in EC49 was deduced from a lower polarity and higher hydrophobicity of the polymer, compared to EC46. Due to the increased ethoxyl content the protonated neutral form of the respective dye, built with increasing carbon dioxide concentration, is stabilized shifting the sensitivity to lower pCO_2. The calibration plots of the materials comprising EC49 with the previously mentioned sensitive chemistry are illustrated in figure 4.7. The slopes obtained from best fits showed an increase of 240 % for MCP, 380 % for TB and 210 % for XB upon exchanging EC46 by EC49 as support.

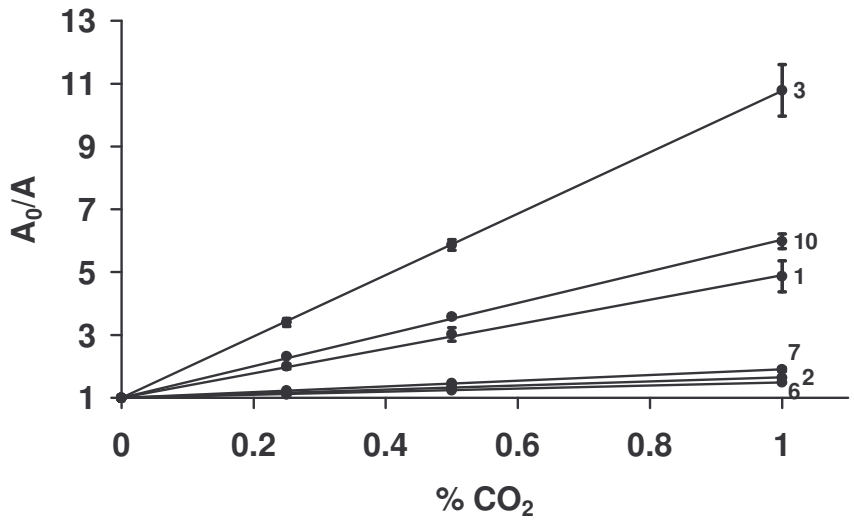

Figure 4.7. Calibration plots of carbon dioxide sensors comprising EC49/TOA-OH and the dyes MCP(1), BRY(2), TB(3), PR(6), CR(7) and XB(10), respectively.

Alternatives for the cellulosic polymers were investigated from the materials included in table 4.1. The responses of sensor materials comprising these non cellulosic polymers were characterised in analogous way to the strategy mentioned above. According to the nature of the calibration function ($A_0/A=1+\alpha\ pCO_2$) the error of α increased with increasing pCO_2. This was due to the growing relative error of decreasing A upon incrementally increasing levels of CO_2. Highly sensitive materials, i.e. sensors with a slope $> 300\ atm^{-1}$ when expressing pCO_2 in atmospheres (1 atm = 100 % CO_2) showed relative standard errors increasing to > 20 % with increasing carbon dioxide concentration to 3 % or 5 %. Thus, the calibration curves of the sensor response of all materials were fitted linear in the range from 0 – 1 % CO_2. The slopes obtained from these fits were put into the database again and sorting with respect to sensor composition was performed.

A table with the gradients of each sensor material was generated and linked to the respective material composition for identification of the "hits" with best performance. The hit-sensors were identified according to the following selection criteria: (a) the slope exceeded the threshold value $50\ atm^{-1}$, (b) the relative standard deviation of the slope was < 20 % and (c) the correlation coefficient of the linear fit was > 0.9. 20 materials under investigation comprising non cellulosic polymers and the base TOA-OH met these demands and offered potential alternatives to the ethyl cellulose-based carbon dioxide sensors. The compositions of these hit sensors are listed in table 4.5 with the respective fit parameters.

PS / TOA-OH / MCP, expressing a slope of $379.1 \pm 52.7\ atm^{-1}$, offered almost equal sensitivity compared to the EC49 analogue. The response of PVC-iBVE and PVC-based

samples was in between of EC46 and EC49. The most sensitive material based on EC49 comprised TOA-OH and thymol blue. It expressed a slope of 976.6 ± 70.2 atm^{-1}. Compared to this formulation highly sensitive alternative materials comprising thymol blue were found on basis of the polymers PVC-iBVE, POMMIE, PTBS, PS and PMMA with slopes of 704 ± 119, 565 ± 70, 1207 ± 208, 503 ± 178 and 690 ± 237 atm^{-1}, respectively. The latter two were excluded from the hit-set due to their slope having an r.s.d > 20 % obtained from screening. Although, this may be a result from varying drying behaviour. The sensor cocktails were placed onto the glass substrate by the MicroLab S® and the solvent was evaporated at room temperature. Variations in cocktail volume dispensed may result in different drying behaviour, and thus, in different film structure and sensitivity due to convection of compounds upon evaporation of the solvent. This could be overcome when preparing a single sensor film by spin coating or with a home-made knife-coating device in order to obtain homogeneous film thickness and drying behaviour. The sensor material based on PTBS expressed the highest slope and, thus, highest sensitivity in this selection. It was estimated suitable for determination of carbon dioxide in the range of up to 1 % CO_2.

Table 4.5. Hit sensors obtained from screening for carbon dioxide sensing materials based on non cellulosic polymers and TOA-OH as basis matrix. Comparison of average slopes α (> 50 atm^{-1}) in the range from 0 to 1 % CO_2, relative standard deviation (r.s.d.(α) < 20 %; n = 6) and correlation coefficients R^2 from best fits.

Polymer-ID	Base-ID	Indicator-ID	α / atm^{-1}	r.s.d.(α) / %	R^2
PSAN	TOA-OH	MCP	182.8	10.4	0.995
PSAN	TOA-OH	TB	386.5	5.1	0.979
PSAN	TOA-OH	XB	221.8	11.8	0.976
PVC-iBVE	TOA-OH	MCP	259.8	4.5	0.996
PVC-iBVE	TOA-OH	TB	703.7	16.9	0.996
PVC-iBVE	TOA-OH	XB	294.8	4.0	0.998
POMMIE	TOA-OH	TB	565.4	12.4	0.997
POMMIE	TOA-OH	CR	58.1	17.2	0.999
PTBS	TOA-OH	BRY	65.3	9.6	1.000
PTBS	TOA-OH	TB	1206.5	17.2	0.991
PTBS	TOA-OH	PR	56.6	7.9	0.999
PTBS	TOA-OH	CR	92.2	5.3	0.999
PTBS	TOA-OH	XB	339.1	13.5	0.952
PVC	TOA-OH	MCP	250.4	5.8	0.974
PVC	TOA-OH	PR	61.6	1.2	0.988
PVC	TOA-OH	CR	156.9	3.9	0.990
PS	TOA-OH	MCP	379.1	13.9	0.994
PMMA	TOA-OH	MCP	283.3	2.3	0.995
PMMA	TOA-OH	PR	63.0	9.6	1.000
PMMA	TOA-OH	CR	121.5	8.3	1.000

Apparently, the polymers PSAN, PVC-iBVE, POMMIE, PTBS, PVC, PS and PMMA were found potential alternatives for use as encapsulation media for the pH-sensitive chemistry. The sensitivity of sensor materials comprising these polymers and TOA-OH was investigated for the different indicator dyes used in this study. TB and XB-based PVC sensors did not result in sensitive films. In this polymer these two dyes were present in the protonated form assuming irreversible acification due to the high pK of the dyes by volatile acids present in the laboratory or due to low pH of the polymer. Exemplary, the calibration plots of sensors composed of the polymers PVC-iBVE, PTBS, PS and PMMA, the base TOA-OH and sensitive dyes are illustrated in figure 4.8.

For all sample polymers most sensitive film were obtained with thymol blue. The sensitivity trend upon exchange of the indicator dye used was similar that obtained for the EC49 matrix when using the polymers PSAN, PVC-iBVE, POMMIE or PMMA. This was attributed to a polar nature of these polymers due to the presence of polar functional groups, i.e., the nitrile residues in PSAN, the chloride residues and oxygen in etheric side chains in PVC-iBVE, and the carboxy methyl ester group in POMMIE and in PMMA.

The polymers PTBS and PS not exhibiting such polar functional groups showed different behaviour. In both polymers thymol blue gave most sensitive sensor films. In contrast to the prior polymers, here sensors comprising MCP were more sensitive than analogues with xylenol blue (see figure 4.8). Comparing the chemical structure of both indicators the phenolate group of the first is more exposed and that one of the latter dye has a methyl residue in ortho position. We suggested that the sensitivity of these type of carbon dioxide sensors strongly depended on the stability of the electrostatic attraction of the counter charges of the ion pair. In polar polymer matrices, additionally, the phenolate anion is more stable than in apolar matrices. Thus, the accessibility of the phenolate for attack by proton was better for MCP than for XB in PTBS and PS when TOA-OH is used as base. In these polymers the protonated form of the dye was judged to be more stable resulting in less stable ion pair. Thus, the recovery of the sensor was suggested to be much slower than the response due to this effect. This was confirmed by investigation of the time dependent response of the materials based on MCP. Compared to the EC49 matrix in PTBS and PS the recovery of MCP sensors were much slower than their response upon exposition to carbon dioxide.

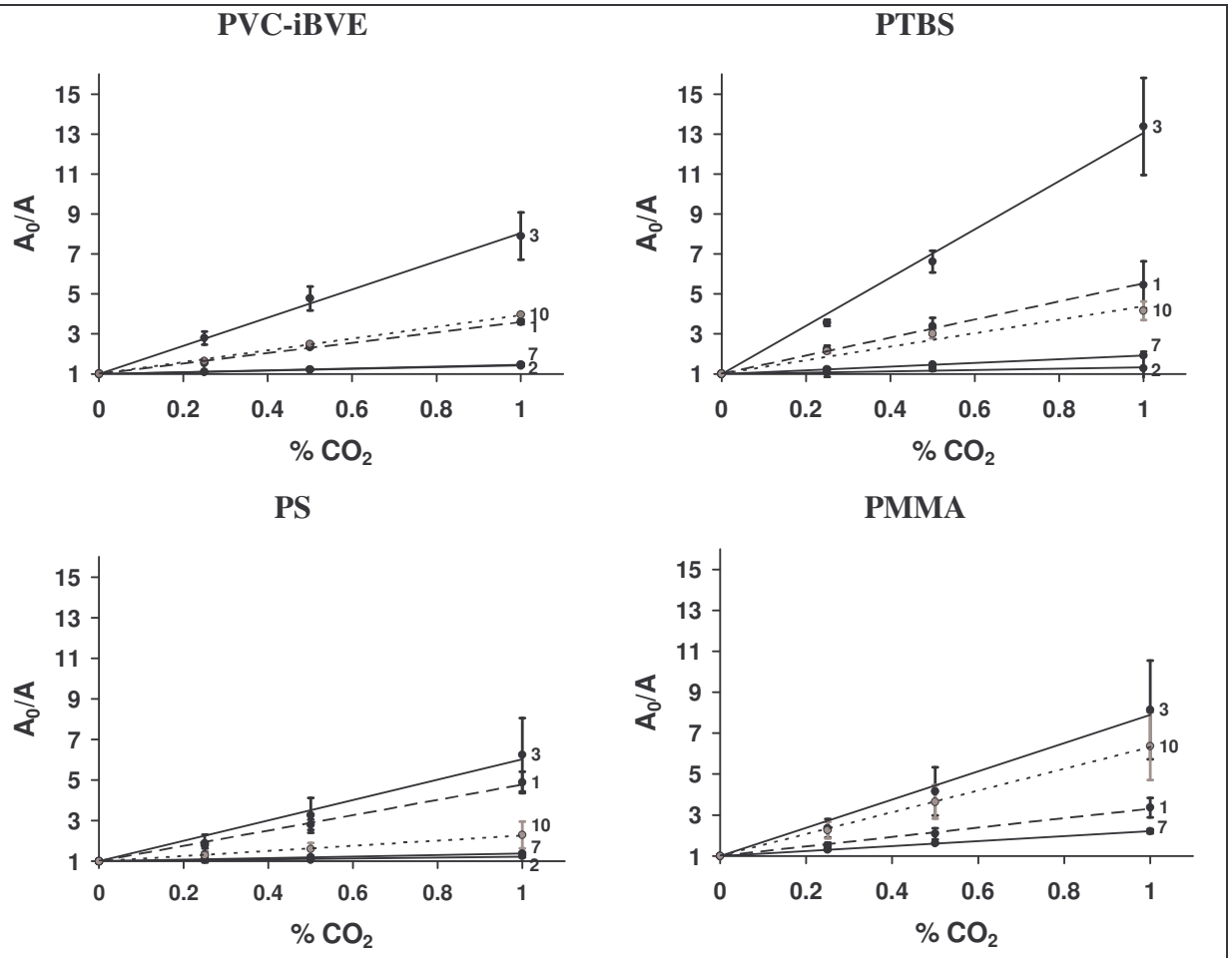

Figure 4.8. Calibration plot of carbon dioxide sensors composed of the polymers PVC-iBVE, PTBS, PS and PMMA utilising TOA-OH and the pH-sensitive dyes MCP (1), BRY (2), TB (3), CR (7) and XB (10).

Effect of Base Variation on the Sensitivity of the Hit Carbon Dioxide Sensors

In the previous section lead sensors were identified to be composed of PSAN, PVC-iBVE, POMMIE, PTBS, PVC, PS, PMMA and - used as standard matrix for many CO_2 sensors in literature - ethyl cellulose. Utilising the indicator dyes MCP, TB and XB highly sensitive sensor materials were obtained. The lipophilic base used was TOA-OH.

These materials were fine-tuned by exchanging the lipophilic base previously used by quaternary ammonium hydroxides with increasing number of long side chains enhancing the lipophilic character of the ammonium cation. The compounds were selected from tetrabutyl ammonium hydroxide (TBA-OH, 4 short chains), cetyltrimethyl ammonium hydroxide (CTA-OH, one long chain), didodecyldimethyl ammonium hydroxide (DDDMA-OH, 2 long chains), tridodecylmethyl ammonium hydroxide (TDMA-OH, 3 long chains) and the previously described tetraoctyl ammonium hydroxide (TOA-OH, 4 long chains). The effect of this modification on the sensitivity of the lead polymer-based materials was investigated via

evaluation of the calibration plots of the dyes MCP, TB and XB in the respective polymers. The figures 4.9 – 4.13 illustrate the sensitivity of the various sensor materials according to the ammonium cation used by visualising the gradients α obtained from best fits in the range from 0 – 1 % CO_2. The respective values and standard deviations of α (n = 6) are summarised in table 4.6 to point up the trends found.

Most sensitive sensors were obtained from CTA-OH in EC46-MCP-based matrices. Almost equal sensitivity was received with both, TBA-OH and TOA-OH. Increasing the number of long side chains in the ammonium cation resulted in increased gradients. This effect may be attributed to the growing steric demand of the particular cation resulting in an increased distance of the counter ions and the lower effective charge density of the voluminous cations. Thus, the stability of the ion pair was lowered with increasing volume of the base and, consequently, the sensitivity increased. Whereas using TB did not result in significant trends for sensitivity upon exchange of the ammonium compound, XB-based EC46 sensors gave similar results with the different agents.

In contrast to the previously described trends, the EC49 matrix did not result in most sensitive materials using CTA-OH with any of the dyes here. MCP sensors showed a decrease of sensitivity upon switching between TBA-OH, CTA-OH, DDDMA-OH and TDMA-OH. Thus, the stability of the ion pair increased with increasing volume of the base. The effect of the steric demand in the – compared to EC46 – less polar medium EC49 was attributed to be overcompensated by the electrostatic attraction of the counter charges in the ion pair. TOA-OH resulted in most sensitive materials based on EC49 - MCP. Sensors utilising TBA-OH were most sensitive when the formulation contained TB or XB. With TB no significant trend was observed upon exchanging CTA-OH by DDDMA-OH or TDMA-OH. The increasing steric demand of the base upon switching from the latter two to TOA-OH, analogous to the EC46 matrix, caused a decrease of the ion pair stability and thus more sensitive sensor materials comprising XB.

In the PSAN matrix TB did not result in sensitive materials with CTA-OH. Highest gradient of the calibration curve were obtained with TOA-OH using this pH-sensitive dye. When the dyes MCP or XB were encapsulated in this polymer the sensitivity increased from TBA-OH and CTA-OH to DDDMA-OH, as well as, from TDMA-OH to TOA-OH. This again could be attributed to the increasing steric demand of the ammonium compounds. Yet the trend is not completely continuous indicating additional influencing parameters from the polymer.

Apparently, MCP and TB encapsulated in POMMIE showed growing sensitivity with using more voluminous quaternary ammonium compounds. This trend was also observed for XB, where the sensitivity increased continuously from TBA-OH, CTA-OH, DDDMA-OH and TDMA-OH to TOA-OH. Steric effects influencing the stability of the ion pair were attributed to be major reason for this due to increasing distance between the counter charges.

In PVC-iBVE MCP and TB showed similar trend of behaviour between the various bases used. Between CTA-OH, DDDMA-OH and TDMA-OH the sensitivity of the respective matrices increased indicating a decreased electrostatic attraction between cation and anion in the ion pair. With TDMA-OH most sensitive materials were obtained for both indicators with respect to the other bases.

Initially the sensitivity of all PTBS and PS sensors described here decreased starting from TBA-OH. This trend turned around for the MCP utilising materials with the use of TDMA-OH in both matrices. The XB-based samples exhibited highest sensitivity with TBA-OH. When TB-PTBS was used only with TOA-OH higher sensitivity was achieved with respect to the other ammonium compounds. In PS the different bases caused an increase of the gradients from CTA-OH to TOA-OH with both TB and XB. The decrease of sensitivity was attributed to an more efficient shielding of the particular charges in the ion pair from attack by protonation of the dye anion with incremental increase of pCO_2. In contrast to that the increase of the lipohilic character of the base caused growing sensitivity due to lower effective charge density of the cation and increased steric demand. The point of inflection of these opposite effects was determined by the overcompensation of the first by the latter.

TBA-OH resulted in highly sensitive materials in the PMMA matrix utilising MCP and XB. The automised preparation system failed in the formulation of TB sensors when TBA-OH or DDDMA-OH were used. For all indicators the sensitivity increased upon increasing the molecular volume of the base. This was attributed to a growing distance between the charges in the ion pair and an decreasing effective charge of the cation weakening the stability of the electrostatic bond.

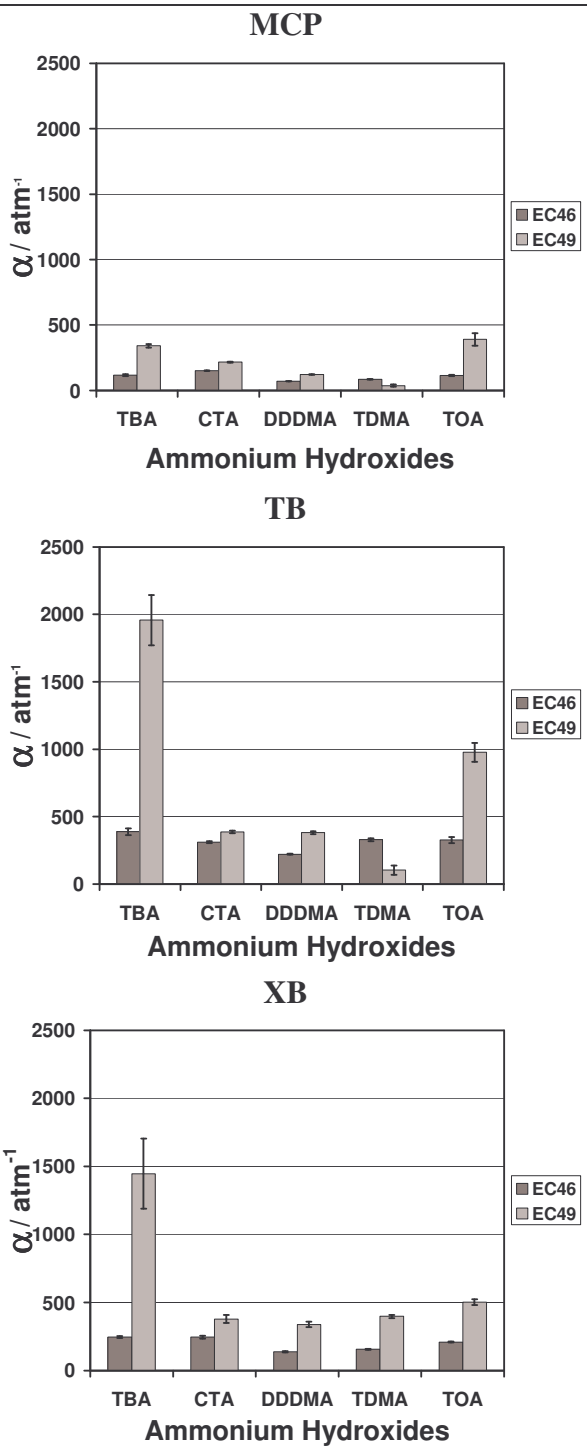

Figure 4.9. Effect of exchanging the base on the sensitivity (gradients α) of the sensor materials based on MCP, TB and XB dissolved in EC46 and EC49, respectively. TBA-OH, CTA-OH, DDDMA-OH, TDMA-OH and TOA-OH were used.

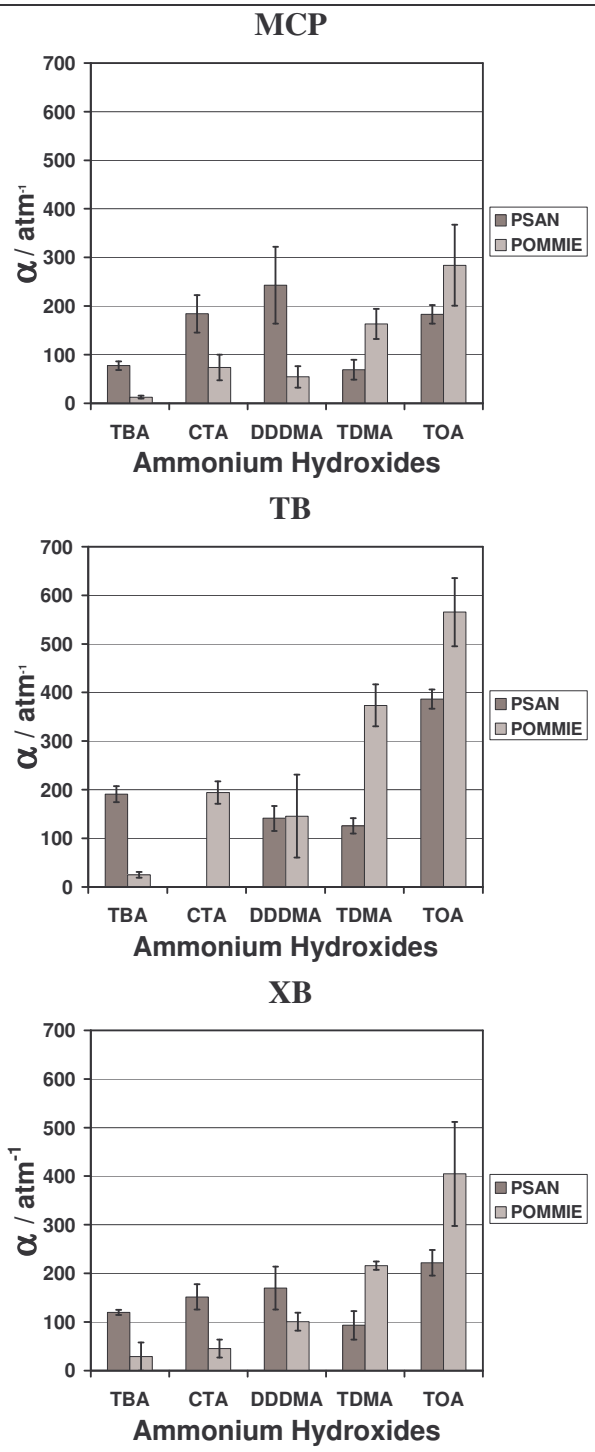

Figure 4.10. Effect of exchanging the base on the sensitivity (gradients α) of the sensor materials based on MCP, TB and XB dissolved in PSAN and POMMIE, respectively. TBA-OH, CTA-OH, DDDMA-OH, TDMA-OH and TOA-OH were used.

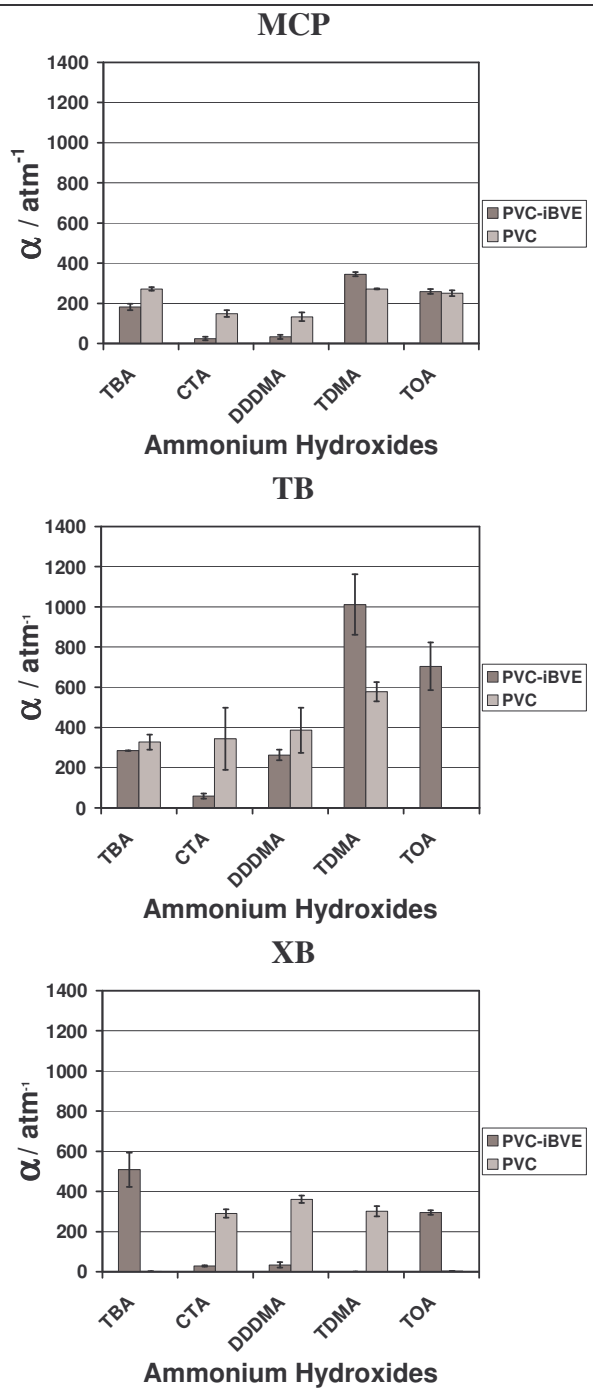

Figure 4.11. Effect of exchanging the base on the sensitivity (gradients α) of the sensor materials based on MCP, TB and XB dissolved in PVC-iBVE and PVC, respectively. TBA-OH, CTA-OH, DDDMA-OH, TDMA-OH and TOA-OH were used.

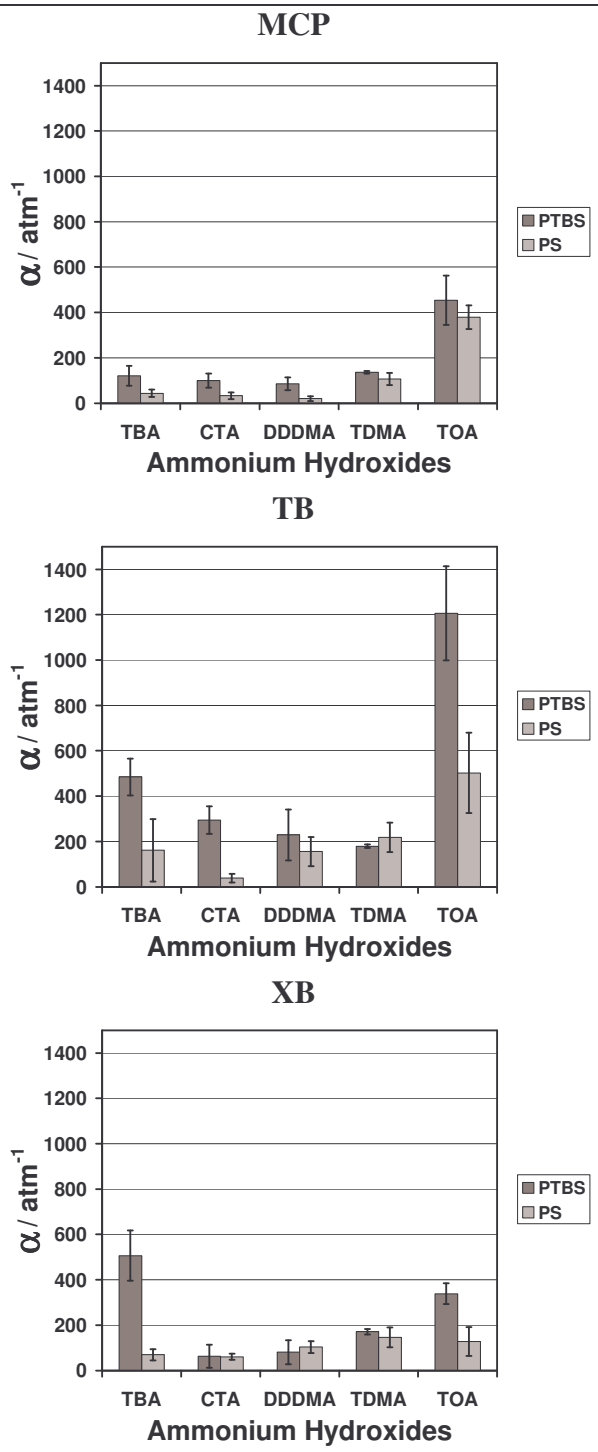

Figure 4.12. Effect of exchanging the base on the sensitivity (gradients α) of the sensor materials based on MCP, TB and XB dissolved in PTBS and PS, respectively. TBA-OH, CTA-OH, DDDMA-OH, TDMA-OH and TOA-OH were used.

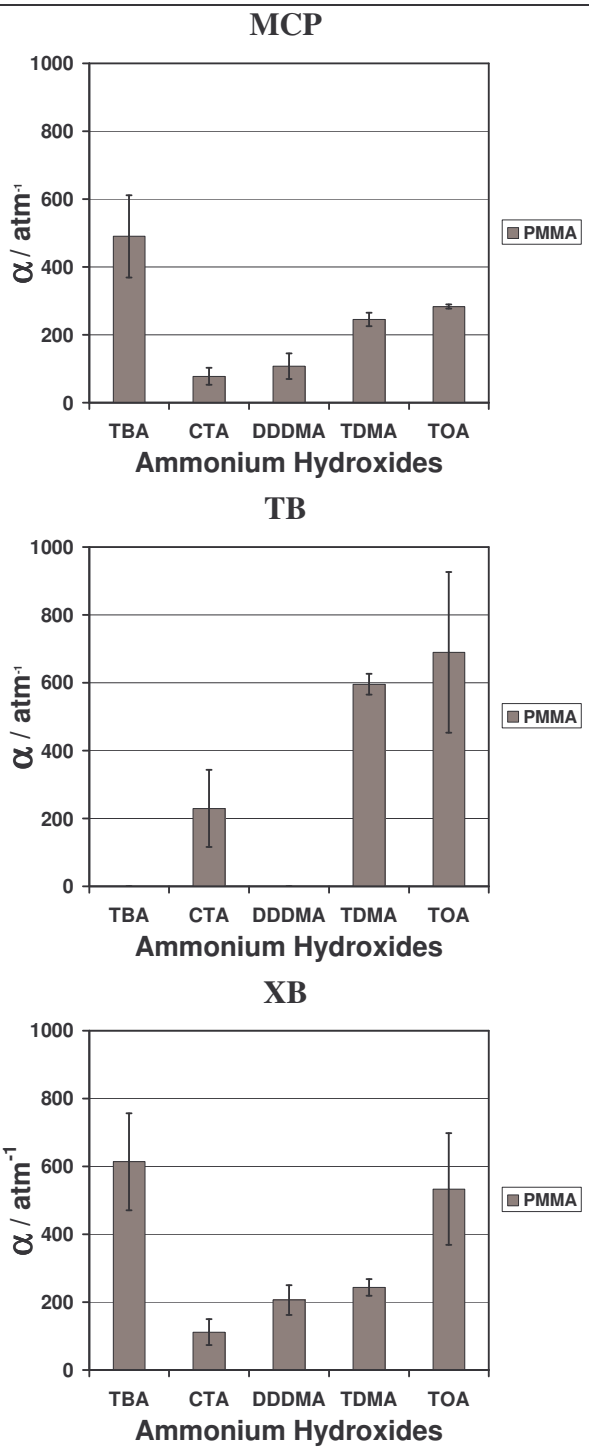

Figure 4.13. Effect of exchanging the base on the sensitivity (gradients α) of the sensor materials based on MCP, TB and XB dissolved in PMMA. TBA-OH, CTA-OH, DDDMA-OH, TDMA-OH and TOA-OH were used.

Table 4.6. Summary of the gradients α obtained from best fits of the calibration plots of the study on the base effect.

		α / atm^{-1}		
		MCP	TB	XB
EC46	TBA-OH	119 ± 7	387 ± 25	246 ± 8
EC46	CTA-OH	151 ± 3	311 ± 7	246 ± 11
EC46	DDDMA-OH	71 ± 1	221 ± 4	137 ± 4
EC46	TDMA-OH	86 ± 2	328 ± 10	155 ± 4
EC46	TOA-OH	115 ± 5	326 ± 23	209 ± 4
EC49	TBA-OH	342 ± 14	1957 ± 185	1447 ± 257
EC49	CTA-OH	217 ± 4	387 ± 9	379 ± 30
EC49	DDDMA-OH	123 ± 3	381 ± 11	339 ± 21
EC49	TDMA-OH	38 ± 9	102 ± 34	398 ± 12
EC49	TOA-OH	391 ± 47	977 ± 70	503 ± 20
PSAN	TBA-OH	77 ± 9	191 ± 17	120 ± 5
PSAN	CTA-OH	184 ± 39	n.d.	151 ± 26
PSAN	DDDMA-OH	243 ± 79	141 ± 26	170 ± 44
PSAN	TDMA-OH	69 ± 20	126 ± 16	93 ± 29
PSAN	TOA-OH	183 ± 19	387 ± 20	222 ± 26
POMMIE	TBA-OH	13 ± 3	25 ± 6	29 ± 29
POMMIE	CTA-OH	74 ± 26	194 ± 23	45 ± 19
POMMIE	DDDMA-OH	54 ± 22	146 ± 85	101 ± 19
POMMIE	TDMA-OH	163 ± 31	373 ± 43	216 ± 9
POMMIE	TOA-OH	284 ± 83	565 ± 70	405 ± 107
PVC-co	TBA-OH	182 ± 16	286 ± 0	508 ± 85
PVC-co	CTA-OH	24 ± 9	59 ± 12	29 ± 3
PVC-co	DDDMA-OH	33 ± 11	263 ± 26	34 ± 14
PVC-co	TDMA-OH	345 ± 10	1012 ± 151	n.d.
PVC-co	TOA-OH	260 ± 12	704 ± 119	295 ± 12
PVC	TBA-OH	272 ± 9	327± 38	n.d.
PVC	CTA-OH	149 ± 17	344 ± 155	290 ± 21
PVC	DDDMA-OH	133 ± 22	386 ± 113	361 ± 18
PVC	TDMA-OH	272 ± 3	578 ± 48	301 ± 25

PVC	TOA-OH	250 ± 15	n.d.	n.d.
PTBS	TBA-OH	121 ± 44	485 ± 81	507 ± 111
PTBS	CTA-OH	100 ± 31	294 ± 61	63 ± 51
PTBS	DDDMA-OH	86 ± 29	229 ± 113	81 ± 54
PTBS	TDMA-OH	136 ± 6	179 ± 8	171 ± 12
PTBS	TOA-OH	454 ± 109	1207 ± 208	339 ± 46
PS	TBA-OH	44 ± 17	161± 137	70 ± 25
PS	CTA-OH	33 ± 15	39 ± 20	60 ± 13
PS	DDDMA-OH	20 ± 11	156 ± 64	103 ± 26
PS	TDMA-OH	107 ± 27	218 ± 64	146 ± 43
PS	TOA-OH	379 ± 53	503± 178	127 ± 64
PMMA	TBA-OH	490 ± 122		614 ± 143
PMMA	CTA-OH	78 ± 25	229 ± 114	112 ± 38
PMMA	DDDMA-OH	108 ± 38		206 ± 44
PMMA	TDMA-OH	245 ± 20	596 ± 31	243 ± 25
PMMA	TOA-OH	283 ± 7	690 ± 237	533 ± 165

4.4.5. Detailed Characterisation of Selected Lead Sensors for Carbon Dioxide

From high-throughput screening of the library for carbon dioxide sensors PSAN, PTBS, PVC, PS and PMMA were found to be promising polymer matrices. They gave best performance when using TOA-OH compared to the other bases investigated. Cocktails of these lead materials with TOA-OH and MCP were prepared according to the previous described procedures (see section 4.3.3.). The response of thin film optical sensors, as used here, is known to be temperature dependent.[8,30] Thus, the performance of the leads sensors was compared to the performance of the formulation EC49 / TOA-OH / MCP with respect to effects of temperature and humidity on the sensitivity of the materials to carbon dioxide.

The PVC-based sensor was destroyed during the determination of temperature dependent response of the samples. The initial absorbance at λ_{max} (605 nm) of the dye anion on exposure to nitrogen at was observed to decrease upon increasing temperature. At a measurement temperature of 50 °C no sensitivity to carbon dioxide was detected. A visual test after measurement confirmed that the sensor film had turned orange. This indicated that the dye was irreversibly acidified. This may be attributed to HCl in the film protonating the indicator anion. Thus, results from this material were discarded from the study.

Effect of Temperature on the Sensitivity of Lead Sensors for Carbon Dioxide

The lead sensor materials were subjected to temperatures between 10 °C and 50 °C in order to evaluate a temperature-dependency of the sensor response. The absorbance spectra of the samples were recorded upon exposure of the films to various concentrations of CO_2 in nitrogen, as described previously (see section 4.4.4.). The respective A_0/A ratios were calculated from the absorbance changes at λ_{max} (605 nm) of the equilibrated sensors exposed to test gas and plotted against the ambient pCO_2 (in %) in the range from 0 – 5 % CO_2. As expected the sensitivity of the film decreased with increasing temperature. The calibration plots of the lead sensors are illustrated in the figures 4.14 – 4.18. Apparently, the calibration plots of EC49, PTBS and PMMA showed linear response of the sensors to carbon dioxide for CO_2 concentrations from 0 to 5 % in nitrogen. PSAN and PS showed negative deviations of the calibration curves for concentrations higher than 1 % CO_2. With respect to the results for pO_2 sensors utilising these polymers (see chapter 3) this effect may be attributed to the structure of the polymer. According to the model discussed domains of different permeability to the target gas may also result in different CO_2 concentrations in the micro environment of the sensor chemistry.[31,32] Consequently, the response signal detected may consist of two or more fractions with particular different gradients α.

Yet, adaptation of the multi-site model was not favourable for the characterisation of this type of sensors and the linear model (eq. 4.6) was used. Due to the nature of the ratio A_0/A the error increased with increasing pCO_2. At high carbon dioxide concentrations A was low compared to A_0. Thus, deviations of the recorded absorbance value caused by signal noise had a significantly increasing relative effect on the ratio with increasing CO_2 concentration.

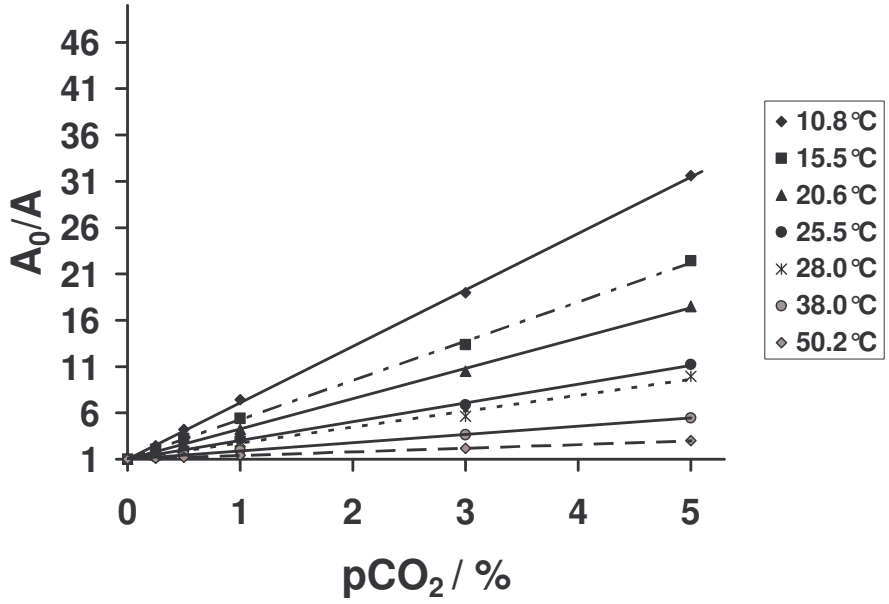

Figure 4.14. Calibration curves of EC49 / TOA-OH / MCP subjected to various measurement temperatures upon exposure to 0, 0.25, 0.5, 1, 3 and 5 % CO_2.

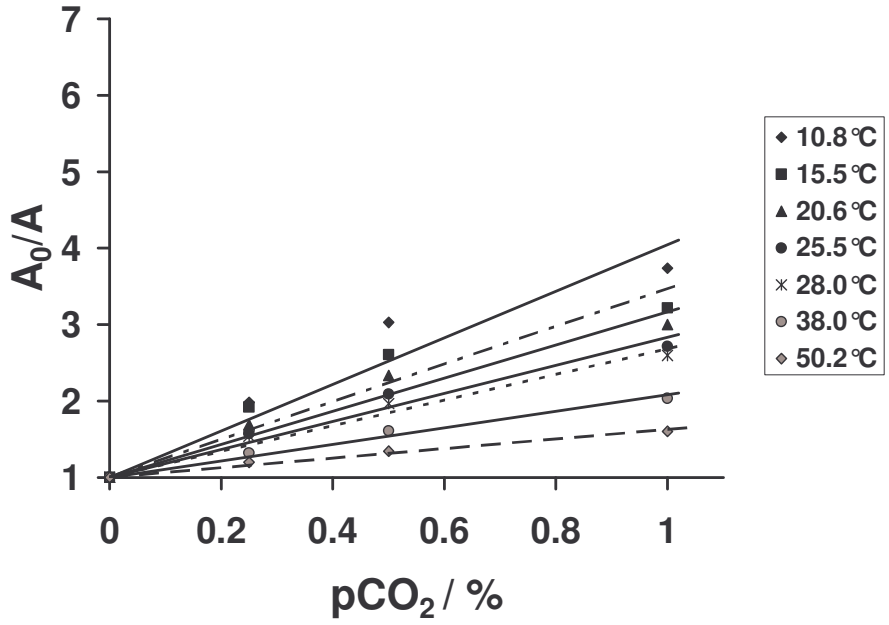

Figure 4.15. Calibration plots of PSAN / TOA-OH / MCP subjected to various measurement temperatures upon exposure to CO_2 The calibration plot is shown for pCO_2 levels of 0, 0.25, 0.5 and 1 % carbon dioxide due to the negative deviation of the plot for concentration > 1 %.

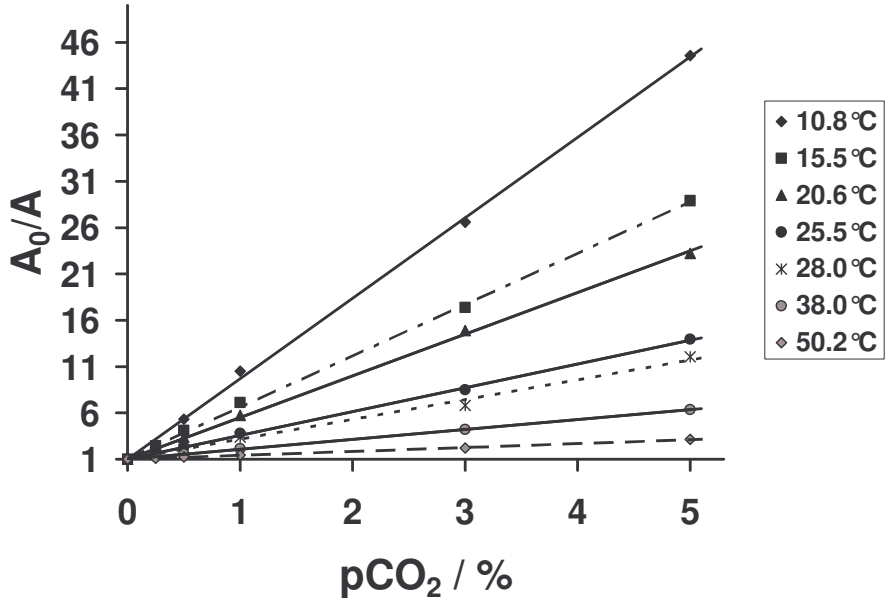

Figure 4.16. Calibration plots of PTBS / TOA-OH / MCP subjected to various measurement temperatures upon exposure to 0, 0.25, 0.5, 1, 3 and 5 % CO_2.

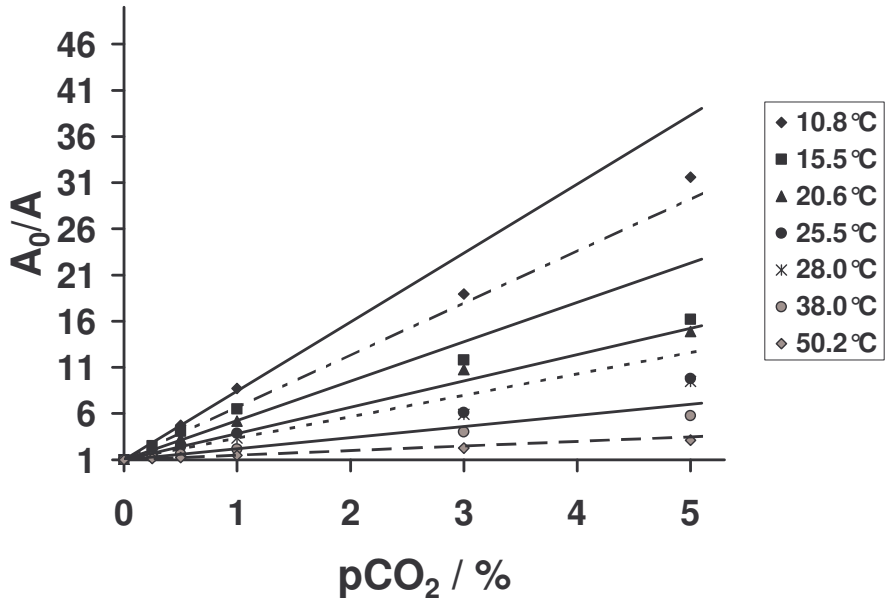

Figure 4.17. Calibration plots of PS / TOA-OH / MCP subjected to various measurement temperatures upon exposure to 0, 0.25, 0.5, 1, 3 and 5 % CO_2.

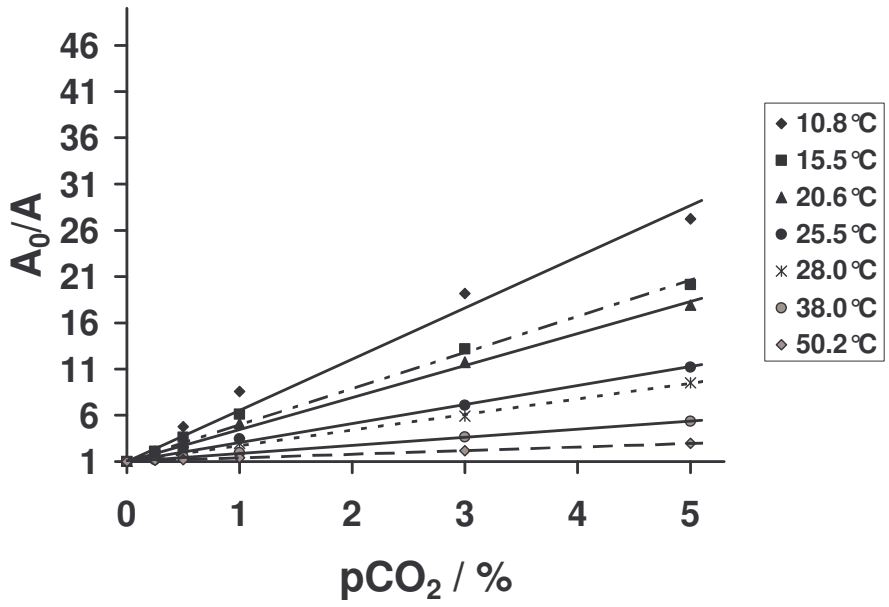

Figure 4.18. Calibration plots of PMMA / TOA-OH / MCP subjected to various measurement temperatures upon exposure to 0, 0.25, 0.5, 1, 3 and 5 % CO_2.

For comparison of the temperature dependent response of PSAN and PS-based sensors with materials utilising the polymers EC49, PTBS and PMMA all calibration plots were fitted in the range from 0 – 1 % CO_2. In this concentration range all curves were almost linear. From the gradients of the fit functions of each sensor material at the ambient temperatures (T) the respective α were obtained. The equilibrium constant of the reaction, given in (4.2), monitored by recording the absorbance changes at λ_{max} of the dye anion was taken to be equal to the gradient of the plots of A_0/A vs. pCO_2 when the carbon dioxide partial pressure was taken as units of atmospheres (1 % CO_2 = 0.01 atm at a barometric pressure of 1 atm). From thermodynamics it is known that the equilibrium constant of an equilibrated system is

$$\Delta G^0 = -RT\ln(\alpha) \tag{4.7}$$

where ΔG^0 is the standard Gibbs free energy change of the equilibrium reaction. According to the Gibbs-Helmholtz equation ΔG^0 is determined as $\Delta G^0 = \Delta H^0 - T\Delta S^0$, where ΔH^0 is the standard free enthalpy change and ΔS^0 is the standard entropy change.[33] This equation was placed into equation (4.7) gives a linear correlation between $\ln(\alpha)$ and T^{-1}:

$$\ln(\alpha) = -\frac{\Delta G^0}{RT} = -\frac{\Delta H^0}{RT} + \frac{\Delta S^0}{R} \tag{4.8}$$

By plotting $\ln(\alpha)$ versus 1/T a linear correlation was found describing the temperature dependency of the respective sensor. From linear regression thermodynamic parameters of the system were determined where $-\Delta H^0/R$ was equal to the gradient of the regression function

and $\Delta S^0/R$ was the axis intercept.[8,17] The particular plots for each sensor are shown in the figures 4.19 and 4.20. The thermodynamic data obtained are listed in table 4.7. The values obtained for the samples are comparable to data found in literature for similar formulations.[8,34]

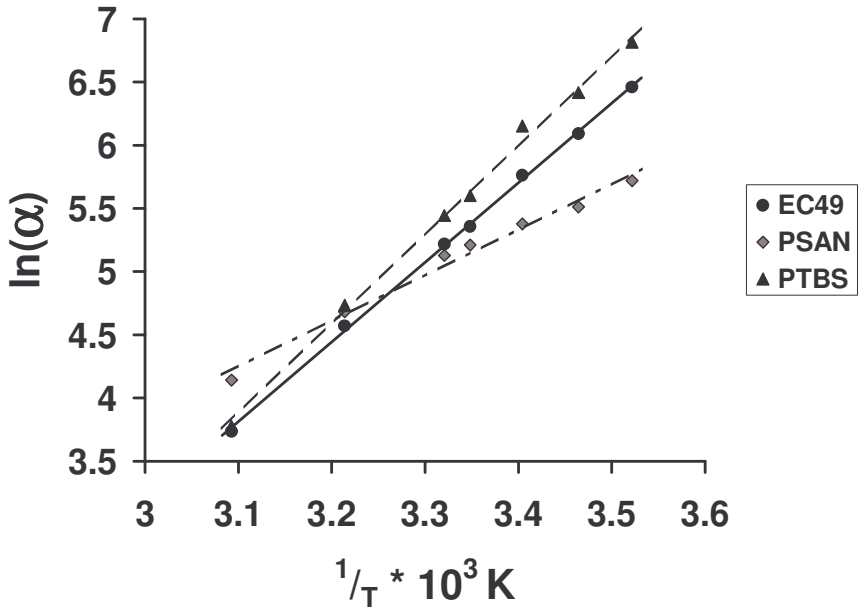

Figure 4.19. Plot of ln(α) vs. T^{-1} of the TOA-OH / MCP sensor when dissolved in EC49, PSAN and PTBS.

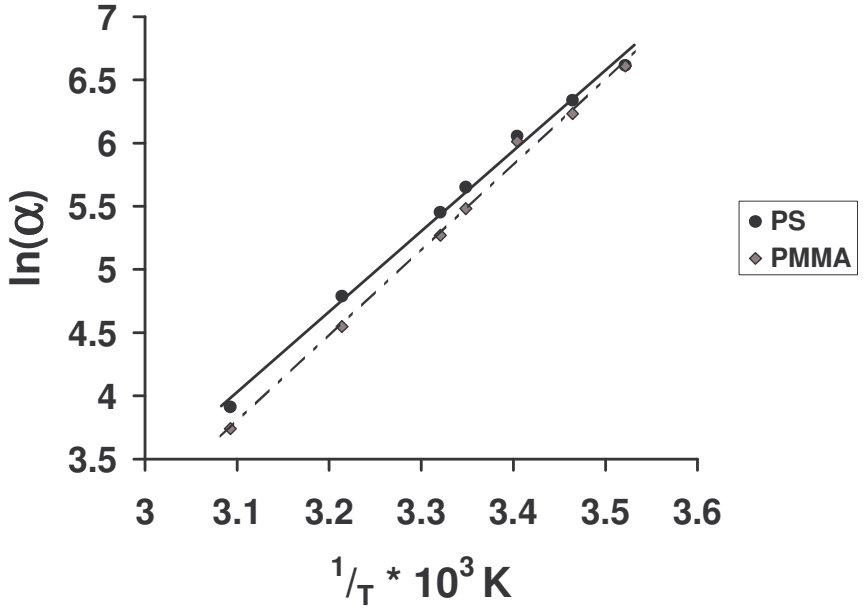

Figure 4.20. Plot of ln(α) vs. T^{-1} of the TOA-OH / MCP sensor when dissolved in PS and PMMA.

Table 4.7. Thermodynamic data for the lead sensors obtained from linear regression on the plots of ln(α) vs. T^{-1} in the figures 4.17 and 4.18.

Sensor Composition	gradient	intercept	$\frac{\Delta H^0}{kJ \cdot mol^{-1}}$	$\frac{\Delta S^0}{J \cdot K^{-1} \cdot mol^{-1}}$
EC49 / TOA-OH / MCP	6300.4 ± 85.5	-15.7 ± 0.3	-52.4 ± 0.7	-130.7 ± 2.4
PSAN / TOA-OH / MCP	3624.3 ± 193.6	-7.0 ± 0.6	-30.1 ± 1.6	-58.1 ± 5.4
PTBS / TOA-OH / MCP	7070.9 ±192.6	-18.0 ± 0.6	-58.8 ± 1.6	-150.0 ± 5.3
PS / TOA-OH / MCP	6359.2 ± 199.0	-15.7 ± 0.7	-52.9 ± 1.7	-130.4 ± 5.5
PMMA / TOA-OH / MCP	6790.5 ± 206.7	-17.3 ± 0.7	56.5 ± 1.7	-143.4 ± 5.7

Effect of Relative Humidity on the Response of the Lead Sensors

The lead sensors from the previous study on the temperature effect were subjected to test atmospheres of 0, 40, 50, 60 and 90 % relative humidity (r.H.). The absorbance changes at λ_{max} (605 nm) were recorded at ambient r.H. the sensors were exposed to. The particular ratios A_0/A were plotted vs. % CO_2 to determine the effect of r.H. on the sensitivity of the sensor materials. Figure 4.21 illustrates the calibration plots obtained upon exposure to various levels of r.H.

At a level of 5 ± 3 % r.H. the sensitivity of the sensor films was significantly lower compared to the response observed for higher levels of relative humidity. This may be deduced to the absence of dissolved water in the film resulting in a hindering of the equilibrium reaction due to the absence of water necessary to build carbonic acid reacting with the base to the bicarbonate. Upon increasing humidity the sensitivity was increased. At levels of 36 ± 3 % r.H. the samples showed highest response to carbon dioxide. Apparently, the gradients of the calibration curves decreased with increasing level of r.H from 36 % - 90 %. Although, compared to the difference between 5 % and 36 % the change from 36 % - 90 % is negligible. The trend is similar for all polymers investigated here.

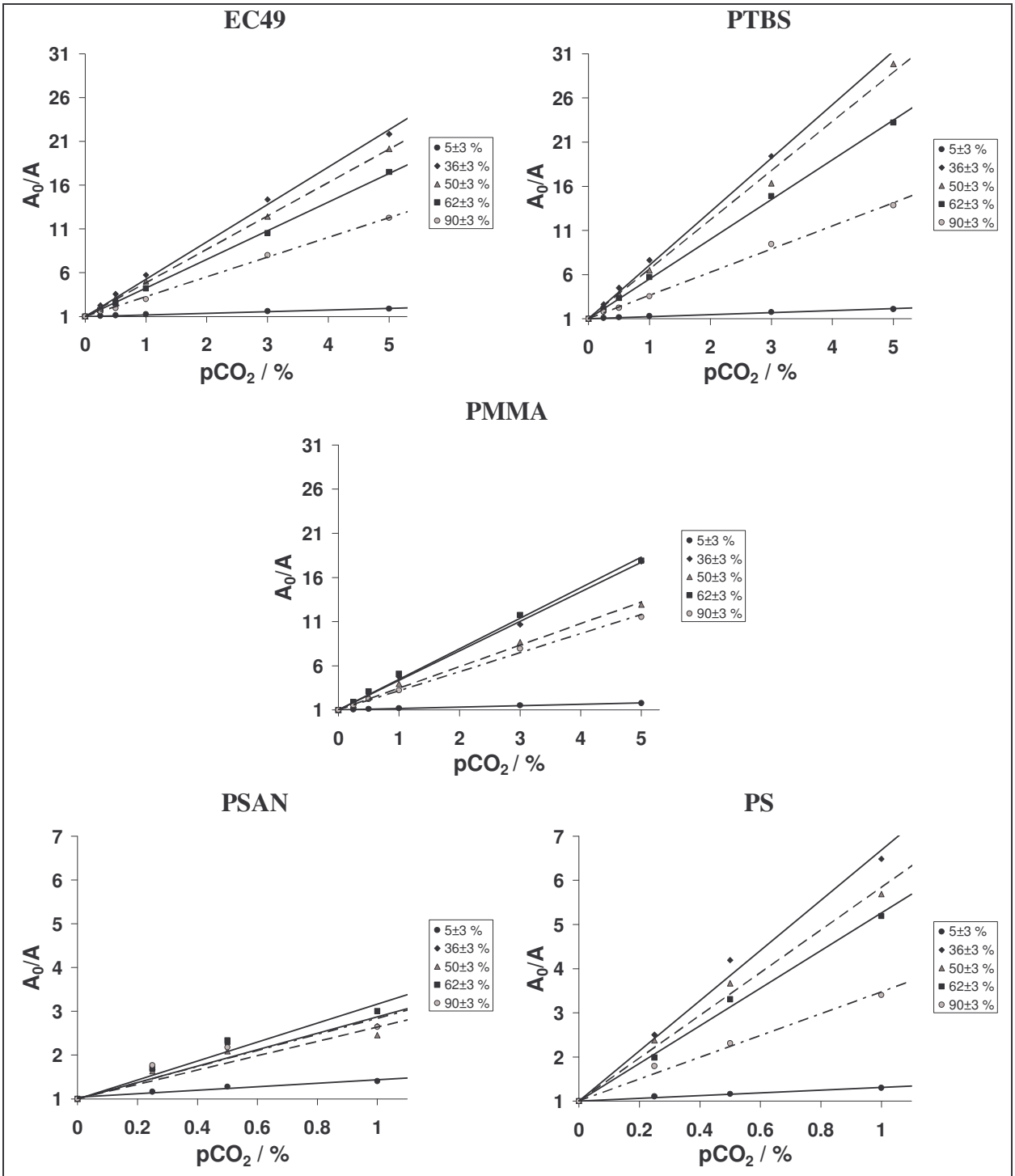

Figure 4.21. Humidity-dependent calibration plots of carbon dioxide sensors based on TOA-OH / MCP when dissolved in EC49, PSAN, PTBS, PS and PMMA. The films were exposed to 0, 0.25, 0.5, 1, 3 and 5 % CO_2 at levels of 5, 36, 50, 62 and 90 % r.H, respectively. The graphs of PSAN and PS show the calibration curves between 0 and 1 % CO_2 due to negative deviations of the plots for concentrations > 1 % carbon dioxide.

4.5. Conclusion

An liquid handling apparatus was successfully adapted to the high-throughput blending of organic stock solutions containing the compounds included in an optical carbon dioxide sensor. Due to the more complex sensor system – compared to oxygen sensors – the compatibility of the different compounds is essential for the successful preparation of thin films. Incompatibility of polymer and quaternary ammonium base resulted in precipitation of polymer from sample solution cocktail and such cocktails could not be processed. If all components were compatible sensor spots were successfully cast onto glass substrates and characterised to their sensitivity to carbon dioxide.

A high-throughput screening apparatus for the evaluation of sensor response via the acquisition of the absorbance spectra was built up and employed in the development of optical carbon dioxide sensors. Due to the high amount of data obtained for each sample highly sophisticated EXCEL® macros were developed for the evaluation of absorbance values at the respective λ_{max}. The calibration data were stored in a purpose-built Access® database including the preparation parameters of the liquid handling system for each sensor material.
Using the high-throughput blending and screening apparatus a library of 960 sensors containing 16 polymers, 5 quaternary ammonium hydroxides and 12 pH-sensitive indicator dyes was created and characterised. In a first approach the polymers and indicator dyes were screened using TOA-OH as agent. The effects of polymer and pK of the dyes were investigated and prospective sensor formulations were found. Useful polymers were identified from EC, PSAN, POMMIE, PTBS, PS, PVC and PMMA. The influence of the polymer on the sensitivity of various useful indicator dyes was investigated.

In the second approach quaternary ammonium hydroxides with increasing number of voluminous side chains were applied to investigate their efficiency of tuning properties of a sensor containing a particular polymer - inidcator combination in the film. The effect of the bases was discussed on the tuning of the lead polymers identified in the first approach. It was found that increasing the number of long chains in the ammonium cation had significantly different influence on the sensitivity of the samples for each of the polymer-indicator combinations investigated. From these results it was concluded that, although the pK of the indicator was the factor determining the sensitivity, the stability of the indicator base ion pair had to be considered, as well. Increasing the stability of the ion pair resulted in less sensitive films. Consequently, lower stability resulted in higher sensitivity of a particular dye. The lipolicic character, the effective charge density and steric factors of the base, as well as the structure of the indicator were attributed to influence the stability of the ion pair. The

molecular volume of the base was deduced to have two oppositional effects. On the one side increasing the volume resulted in growing distance of the opposite charges in the ion pair reducing the electrostatic attraction. On the other side voluminous side chains in non symmetric ammonium compounds would be oriented to the out side of the ion pair acting as lipophilic shield hindering the protonation of the dye.

The sensor materials were shown to respond reversibly to changes of carbon dioxide concentration in the test atmospheres. According to theory, the recovery times were bigger than the response times. The temperature dependency and the dependency on relative humidity of the sensor response of the lead family polymers was investigated. As expected, all films were subject to temperature variation. At 0 % r.H. the sensitivity of the films were very low compared to humid test atmospheres. The calibration curves of the sensors showed highest gradients at 36 % r.H. and the gradients decreased with increasing relative humidity at constant temperature. This was attributed to a lower pCO_2 in humid atmospheres and the structure of the polymer determining the content of water and CO_2 in the membrane.

4.6. References

1 Römpp H., ***Römpp Lexikon Umwelt***, Thieme, Stuttgart (2004).

2 Swenson F. J., ***Development and Evaluation of Optical Sensors for the Detection of Bacteria***, Sens. Actuators **B11**, 315-321, (1993).

3 Leiner M. J. P., ***Optical Sensors for In Vitro Blood Gas Analysis***, Sens. Actuators **B29**, 169-173, (1995).

4 Siggaard-Andersen O., Goethgen I. H., Wimberley P. D., Rasmussen J. P., and Fogh-Andersen N., ***Evaluation of the Gas-STAT Fluorescence Sensors for Continuous Measurement of pH, pCO_2 and pO_2 During Cardiopulmonary Bypass and Hypothermia***, Scand. J. Clin. Lab. Invest. Suppl. **48**, 77-84, (1988).

5 Weigl B. H., Holobar A., Trettnak W., Klimant I., Kraus H., O'Leary P., and Wolfbeis O. S., ***Optical Triple Sensor for Measuring pH, Oxygen and Carbon Dioxide***, J. Biotechnol. **32**, 127-138, (1994).

6 Wolfbeis O. S., Kovacs B., Goswami K., and Klainer S. M., ***Fiber Optic Fluorescence Carbon Dioxide Sensor for Environmental Monitoring***, Mikrochim. Acta **129**, 181-188, (1998).

7 Werle P., Muecke R., D'Amato F., and Lancia T., ***Near-Infrared Trace-Gas Sensors Based on Room-Temperature Diode Lasers***, Appl. Phys. B **B67**, 307-315, (1998).

8 Mills A., Chang Q., and McMurray N., ***Equilibrium Studies on Colorimetric Plastic Film Sensors for Carbon Dioxide***, Anal. Chem. **64**, 1383-1389, (1992).

9 McMurray H. N., ***Novel Thin Optical Film Sensors for the Detection of Carbon Dioxide***, J. Mater. Chem. **2**, 401-406, (1992).

10 Weigl B. H. and Wolfbeis O. S., ***New Hydrophobic Materials for Optical Carbon Dioxide Sensors Based on Ion Pairing***, Anal. Chim. Acta **302**, 249-254, (1995).

11 Mills A. and Chang Q., ***Fluorescence Plastic thin-film Sensors for Carbon Dioxide***, Analyst **118**, 839-843, (1993).

12 Mills A. and Chang Q., ***Colorimetric Polymer Film Sensors for Dissolved Carbon Dioxide***, Sens. Actuators **B21**, 83-89, (1994).

13 McMurray H. N. and Albadran J., ***Colorimetric and Fluorimetric Polymer Membrane Gas-Sensing Materials***, MRS Bulletin **24**, 55-59, (1999).

14 Wolfbeis O. S., Weis L. J., Leiner M. J. P., and Ziegler W. E., ***Fiber-Optic Fluorosensor for Oxygen and Carbon Dioxide***, Anal. Chem. **60**, 2028-2030, (1988).

15 Weigl B. H., Holobar A., Rodriguez N. V., and Wolfbeis O. S., ***Chemically and Mechanically Resistant Carbon Dioxide Optrode Based on a Covalently Immobilised pH Indicator***, Anal. Chim. Acta **282**, 335-343, (1993).

16 Weigl B. H., Holobar A., Rodriguez N. V., and Wolfbeis O. S., ***Robust Carbon Dioxide Optrode Based on a Covalently Immobilised pH Indicator***, Proc. SPIE – Int. Soc. Opt. Eng. **2068**, 2-10, (1994).

17 Mills A. and Monaf L., ***Thin Plastic Film Colorimetric Sensors for Carbon Dioxide: Effect of Plasticizer on Response***, Analyst **121**, 535-540, (1996).

18 Wolfbeis O. S., Klimant I., Werner T., Huber C., Kosch U., Krause C., Neurauter G., and Durkop A., ***Set of Luminescence Decay Time Based Chemical Sensors for Clinical Applications***, Sens. Actuators **B51**, 17-24, (1998).

19 www.sigmaaldrich.com

20 www.goodfellow.com

21 www.vwr.com

22 Werner T., Klimant I., and Wolfbeis O. S., ***Ammonia-Sensitive Polymer Matrix Employing Immobilised Indicator Ion Pairs***, Analyst **120**, 1627-1631, (1995).

23 Mohr G. J., Werner T., Oehme I., Preininger C., Klimant I., Kovacs B., and Wolfbeis O. S., ***Novel Optical Sensor Materials Based on Solubilisation of Polar Dyes in Apolar Polymers***, Adv. Mater. **9**, 1108-1113, (1997).

24 Bishop E., ***Indicators***, Pergamon Press, New York (1972).

25 Zittel H. E. and Florence T. M., ***Voltammetric and Spectrophotometric Study of the Zirconium-Alizarine Red S Complex***, Anal. Chem. **39**, 320-326, (1967).

26 www.linde.de

27 Mills A., Lepre A., and Wild L., ***Effect of Plasticizer-Polymer Compatibility on the Response Characteristics of Optical Thin Film CO_2 and O_2 Sensing Films***, Anal. Chim. Acta **362**, 193-202, (1998).

28 Mills A. and Lepre A., ***Controlling the Response Characteristics of Luminescent Porphyrin Plastic Film Sensors for Oxygen***, Anal. Chem. **69**, 4653-4659, (1997).

29 Mills A. and Chang Q., ***Tuning Colorimetric and Fluorometric Gas Sensors for Carbon Dioxide***, Anal. Chim. Acta **285**, 113-123, (1994).

30 Mills A. and Lepre A., ***Development of Novel Thermochromic Plastic Films for Optical Temperature Sensing***, Analyst **124**, 685-689, (1999).

31 Carraway E. R., Demas J. N., and DeGraff B. A., ***Luminescence Quenching Mechanism for Microheterogeneous Systems***, Anal. Chem. **63**, 332-336, (1991).

32 Demas J. N., DeGraff B. A., and Xu W., ***Modeling of Luminescence Quenching-Based Sensors: Comparison of Multisite and Nonlinear Gas Solubility Models***, Anal. Chem. **67**, 1377-1380, (1995).

33 Wedler G., ***Lehrbuch der Physikalischen Chemie 4^{th} Ed.***, Wiley-VCH, Weinheim (1997).

34 Neurauter G., Klimant I., and Wolfbeis O. S., ***Microsecond Lifetime-Based Optical Carbon Dioxide Sensor Using Luminescence Resonance Energy Transfer***, Anal. Chim. Acta **382**, 67-75, (1999).

Chapter 5. Combinatorial Approach to the Development of Optical Sensors for Gaseous Ammonia

5.1. Introduction

Ammonia is a colourless and irritant gas of pungent, penetrative odour, and it is highly toxic.[1] The MAC value for a daily exposure over 8 hours is 35 mg / m^3 corresponding to 50 ppm (v/v). NH_3 is used as source material in many industrial processes including synthesis of urea, nitric acid, artificial fibers, fertilizers and many other products. Furthermore, it can be utilised as refrigerant. On the other hand, ammonia is one of the pollutants causing the green house effect and one of the main irritants to human. In water, it is known to be toxic to organisms, especially for fish the lethal concentration is LC_{50}(Fish) = 0.77 – 7 mg / L, and according to the *European Council Directive 78/659/EWG Appendix I* a guide level of 25 µg / L should not be exceeded.[1-3] Thus, continuous online monitoring of ammonia concentration is of interest for industrial, clinical and environmental analysis including, among other applications, leakage detection for process control, analysis of drinking and surface waters, or control of water quality for fish farming.

Optical sensors offer several advantages when compared to susceptible, bulky and expensive electrodes for ammonia analysis. They are cheap, easier to produce, can easily be miniaturised, and they are more robust. Several optical methods for the determination of ammonia in gas phase and dissolved have been described using optical sensors. One type of sensors is based on the determination of the change of pH inside the sensor matrix utilising the pH-dependent response of a pH indicator or an energy transfer sensor.[2-11] The materials described here are also based on this sensor principle monitoring the pH variation. Another type of ammonia sensors utilises ammonium ion-selective ionophores and H^+-selective chromoionophores.[12-14] Yet, principally, these types of sensors also utilise acid – base reactions. The type of ammonium ion-selective ionophore is mainly tuning selectivity of the sensor for ammonia.

The combinatorial approach will be applied in this study to speed-up the testing of possible polymer supports and pH-sensitive indicators for the development of optical ammonia gas sensors. The effect of tuning agents on the performance of particular materials will be investigated.

5.2. Theory

Due to the alkaline character of ammonia it can be determined with optical sensors - colorimetric or fluorimetric - utilising pH-sensitive dyes. The change of their particular optical properties with changing pH of the surrounding microenvironment when subjected to varying levels of apparent ammonia is detected as sensing signal. The sensing mechanism is based on the following acid – base equilibrium reaction between gaseous ammonia and the weak indicator acid:

$$HD + NH_3(g) \overset{\alpha'}{\rightleftharpoons} NH_4^+D^- \qquad (5.1)$$

Acid Colour Alkaline Colour

where HD and D^- are the acidic and alkaline forms of the indicator dye, respectively. This can be illustrated with the reaction scheme shown in figure 5.1.

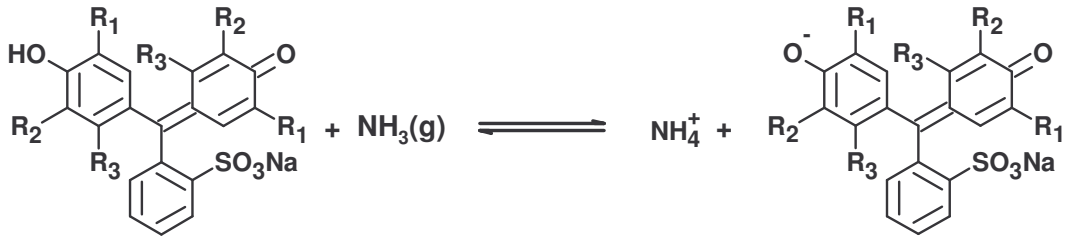

Acid Colour A **Alkaline Colour B**

Figure 5.1. Reaction scheme of absorbance-based ammonia sensors.

It is obvious that the sensitivity of such a sensor will increase with increasing acidity (K_A) of the indicator dye. α' is the overall equilibrium constant of the sensing equilibrium covering the acid – base reaction and the solvation of gaseous ammonia in the film. It can be calculated from the equation

$$\alpha' = \frac{[NH_4^+D^-]}{[HD]\times[NH_3]} \qquad (5.2)$$

where the bracket bordered symbols denote the equilibrium concentrations of the particular components. The concentration of ammonia in the matrix is directly linked to its partial pressure pNH_3 in the test atmosphere. Thus, equation (5.2) can be transformed to

$$\alpha \times pNH_3 = \frac{[NH_4^+D^-]}{[HD]} = R \qquad (5.3)$$

Apparently, the ammonia concentration can be described by the ratio R between deprotonated and protonated dye. This ratio can be determined with spectroscopic techniques. In case here, absorbance spectroscopy is used, since the absorbance of the coloured species is directly linked to its concentration. Under the stipulation that the Lambert-Beer Law is obeyed and absorbance measurements are performed at a wavelength where only the alkaline form of the dye absorbs, R can be calculated by the equation:[7]

$$R = \frac{[NH_4^+D^-]}{[HD]} = \frac{[NH_4^+D^-]}{[HD]_0 - [NH_4^+D^-]} = \frac{\{Abs(NH_4^+D^-) - Abs(NH_4^+D^-)_0\}}{\{Abs(NH_4^+D^-)_\infty - Abs(NH_4^+D^-)\}} \qquad (5.4)$$

where $Abs(NH_4^+D^-)_0$ is the absorbance of the film in absence of ammonia, $Abs(NH_4^+D^-)$ is its absorbance at an apparent level of ammonia given in units of atmospheres, and $Abs(NH_4^+D^-)_\infty$ is the absorbance of the film when the all indicator is converted to the alkaline form. Thus, a plot of R against the pNH_3 can be used for characterisation of sensor response. This calibration scheme was applied for all triphenyl methane dyes in the approach described here.

Instead of the neutral form the dye can also be applied cation able to deprotonate. This is the case for some acridine-based indicators. The reaction scheme is illustrated in figure 5.2 for inspection.

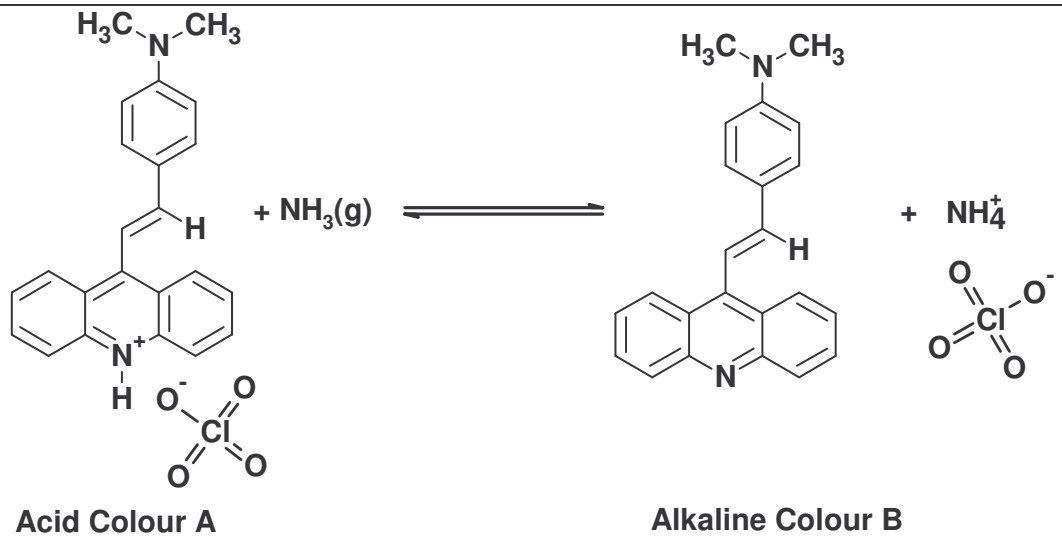

Figure 5.2. Reaction scheme for acridinium-based ammonia sensors.

These types of pH-sensitive indicators exhibit long wavelength absorbance bands due to the delocalisation of the positive charge in the aromatic system. The deprotonation by ammonia causes a decrease of these absorbance bands and an increase of the short wavelength absorbance of the base form of the dye.

Alternatively to the pure acid – base equilibria mentioned above, it is also possible that the change of optical properties is a result of a reaction following the deprotonation subsequently. In the case of the xanthene dyes like rhodamine B - or analogues - the deprotonation of the carboxy group in the phenol ring can be succeeded by a lactonisation according to the following scheme (figure 5.3):[2,15]

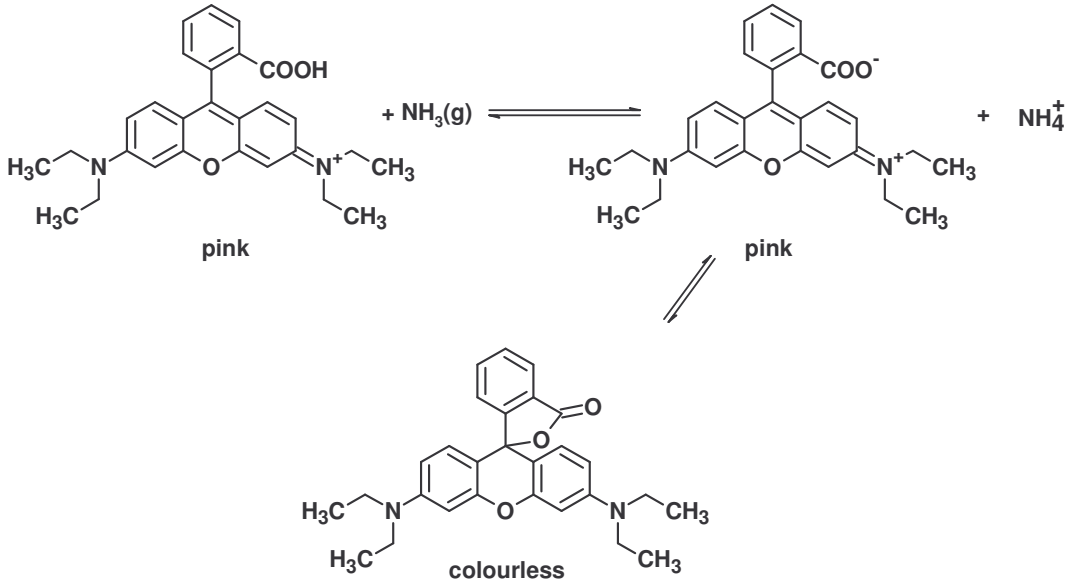

Figure 5.3. Reaction scheme of pNH_3 sensors based on lactonisation of the indicator.

This subsequent equilibrium reaction is solvent dependent. Thus, in apolar aprotic media like organic polymers the lactone form is preferred after deprotonation and all zwitter-ions formed via the acid-base reaction of rhodamine B with ammonia were assumed to react to the colourless lactone form. The response of sensor materials based on rhodamines thus show a decrease of absorbance of the acidic form detected with increasing levels of apparent ammonia in the test atmosphere.

In both cases (schemes in fig. 5.2 and 5.3), the concentration of ammonia can be described by the ratio between concentration of alkaline species (neutral form or lactone, respectively) and acid concentration:

$$\alpha \times pNH_3 = \frac{[L]}{[HD^+]} = \frac{[HD^+]_0 - [HD^+]}{[HD^+]} = \frac{\{Abs(HD^+)_0 - Abs(HD^+)\}}{\{Abs(HD^+) - Abs(HD^+)_\infty\}} \qquad (5.5)$$

where $[HD^+]_0$ is the initial concentration of rhodamine, [L] and $[HD^+]$ are the equilibrium concentrations of lactone and acid. $Abs(HD^+)_0$ and $Abs(HD^+)$ are the absorbance of the film in absence and at apparent levels of ammonia, respectively. $Abs(HD^+)_\infty$ is the absorbance of the film when all rhodamine is deprotonated and converted to lactone. Since the lactone does

not absorb at λ_{max} of the acidic form this value trends to zero and may be neglected simplifying equation (5.5) to

$$\alpha \times pNH_3 = \frac{Abs(HD^+)_0 - Abs(HD^+)}{Abs(HD^+)} = \frac{A_0}{A} - 1 \qquad (5.6)$$

According to that, the response of this type of sensors can be characterised plotting the ratio A_0/A between the absorbance of the film in absence of ammonia and at apparent ammonia levels versus the ammonia concentration applied.

5.3. Materials and Methods

5.3.1. Chemicals

5.3.1.1. Reagents and Solvents

9-Methyl acridine (anal. grade 99+ %) was supplied from ACROS (Belgium).[16] 4,4-dimethylamino benzaldehyde, 4,4-dimethylamino cinnamaldehyde, sodium perchlorate and 1N hydrochloric acid were from Merck (Darmstadt).[17] TDMA-Cl was from Fluka.[18] Toluene, ethanol, chloroform and THF were from Merck.

5.3.1.2. Polymers

The polymers used in high-throughput screening were the same as in the studies on optical oxygen or carbon dioxide sensors (see chapter 3, *section 3.2.1.3. Polymers*). Their chemical structure is shown in figure 5.4 for inspection. All polymers used in high-throughput screening were purchased from Aldrich[18] with exception of poly(methyl methacrylate) being from Goodfellow.[19] Stock solutions of these batches were prepared dissolving the appropriate amount in a suitable organic solvent. The concentrations of the polymer solutions The concentrations of the stock solutions were adjusted to grant proccessibility with the MicroLab® S liquid handling robot.

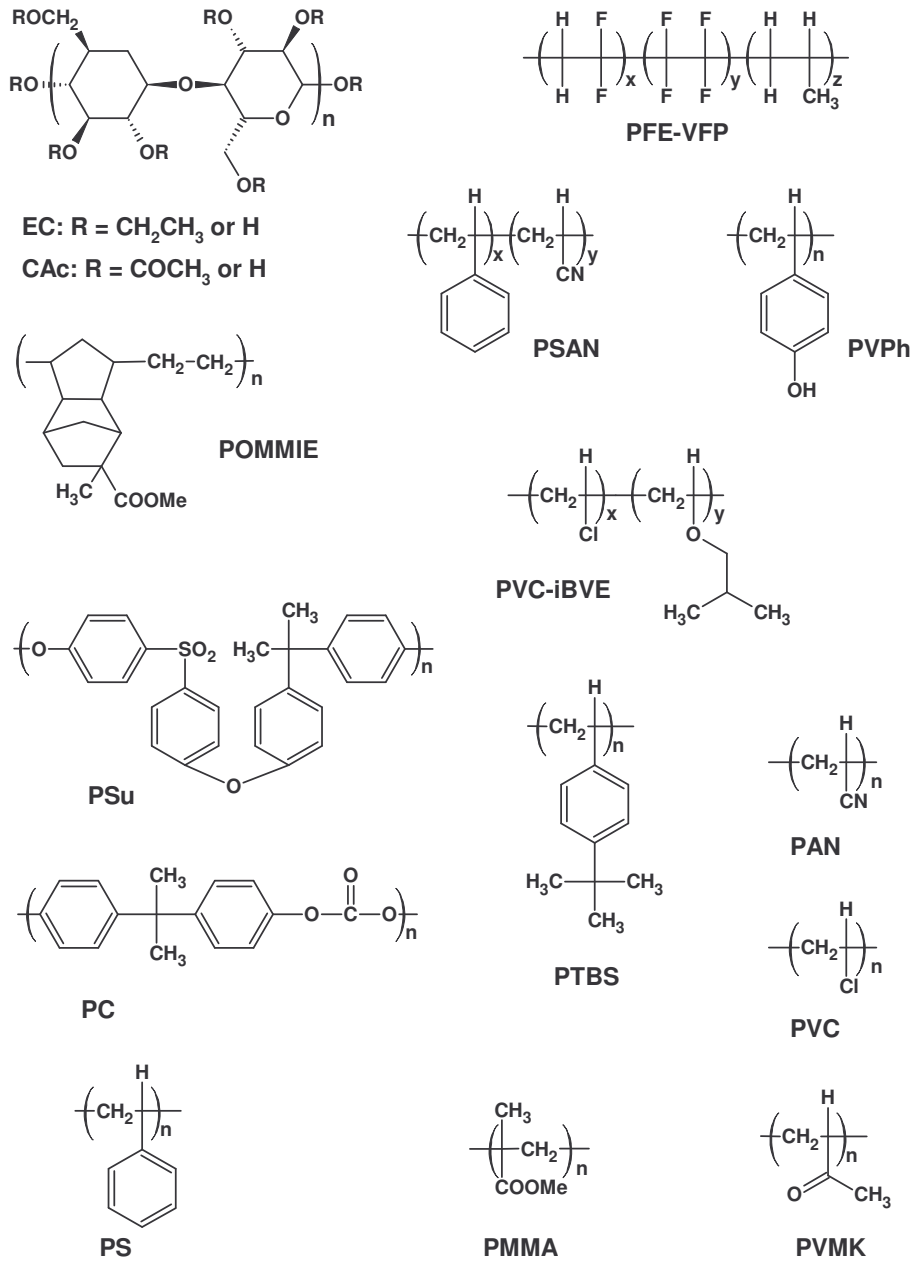

Figure 5.4. Chemical structures of the polymers used in the screening of optical ammonia gas sensors.

5.3.1.3. Tuning Agents - Plasticizers and Ionophores

The plasticizers tributyl phoshate (**TBP,** prod. no. 90820), tris(2-ethylhexyl)phosphate (**TOP,** prod. no. 93301), 2-(octyloxy)bezonitrile (**OBN,** prod. no 75069) and 2-nitrophenyl octyl ether (**NPOE,** prod. no. 73732) were used to plasticize the above mentioned polymers. All plasticizers were purchased from Fluka. Stock solutions processed with MicroLab® S were made dissolving 2.5 g plasticizer in 10 mL THF. 4´,4´´(5´´)-Di-tert-butyldibenzo-18-crown-6 (prod. no. 34682) shown in figure 5.5 was purchased from Fluka.

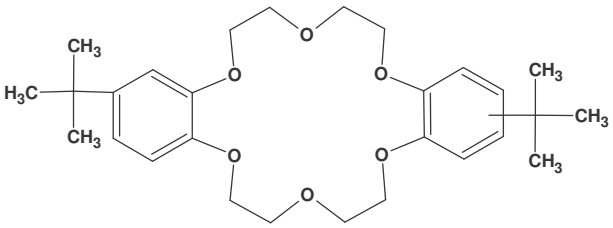

Figure 5.5. Chemical structure of the crown ether 4´,4´´(5´´)-di-tert-butyldibenzo-18-crown-6

5.3.1.4. Indicators used in Screening

The indicators included in table 5.2 were employed in high-throughput screening for optical ammonia gas sensors. Chemical structures of the xanthene dyes ad the phthalocyanine are shown in figure 5.6. TDMA ion pairs of the triphenyl methane dyes were prepared according to *chapter 3, section 4.3.2. Preparation of Indicator Ion Pairs*. The preparation procedures of rhodamine B perchlorate and 9-(4-dialkylaminostyryl) acridiidium perchlorates are described in section 5.3.2.

Table 5.2. Data on Indicator dyes applied in high-throughput screening and observation wavelength λ_{max}.

Indicators		pK_D (OH) in H_2O	λ_{max} (obs) in H_2O	Prod.No.	Supplier
A Triphenyl methane dyes					
m-cresol purple	MCP	8.3 [20]	580 nm[a]	857890	Aldrich[18]
thymol blue	TB	9.2 – 9.7[20]	595 nm[a]	32727	Aldrich
bromophenol blue	BPB	4.1[20]	600 nm[a]	32768	Fluka[18]
bromocresol green	BCG	4.9[20]	615 nm[a]	114367	Aldrich
phenol red	PR	8.0[20]	560 nm[a]	107241	Merck[17]
cresol red	CR	8.5[20]	570 nm[a]	114480	Fluka
alizarin red S	ARS	5.5[21]	560 nm[a]	106279	Merck
xylenol blue	XB	9.5[20]	595 nm[a]	114561	Aldrich
xylenol orange	XO	10.4[20]	580 nm[a]	33825	Riedel de Haën[18]
bromocresol purple	BCP	6.4[20]	585 nm[a]	860891	Aldrich
tetrabromophenol blue	TBPB	3.5	610 nm[a]	236047	Aldrich
chrome azurol S	CAS	~ 11	600 nm	102477	Merck
B Azo dyes					
brilliant yellow	BRY	~ 7	500 nm[a]	201375	Aldrich

orange I	OI	8.3[20]	490 nm[a]	75360	Fluka
C Xanthene dyes					
rhodamine B	RB	-	560 nm[b]	107599	Merck
rhodamine 6G	R6G	-	530 nm[b]	252433	Aldrich
eosin B	EOB	6.5	520 nm[b]	861006	Aldrich
erythrosin B	ERB		540 nm[b]	200964	Aldrich
D Phthalocyanine					
octabutoxy phthalocyanine	OBPC	-	~ 700 nm[b]	383805	Aldrich
E Acridinium dyes					
9-(4,4-dimethylamino styryl) acridine	DMASA	4.9[c]	618 nm[c]	Prep.; *section 5.3.2.2.*	
9-(4,4-dimethylamino cinnamyl) acridine	DMACA	4.6[c]	640 nm[c]	Prep.; *section 5.3.2.3.*	

[a] dye anion; [b] acid form of dye; [c] from reference[22], pK_a in ethanol

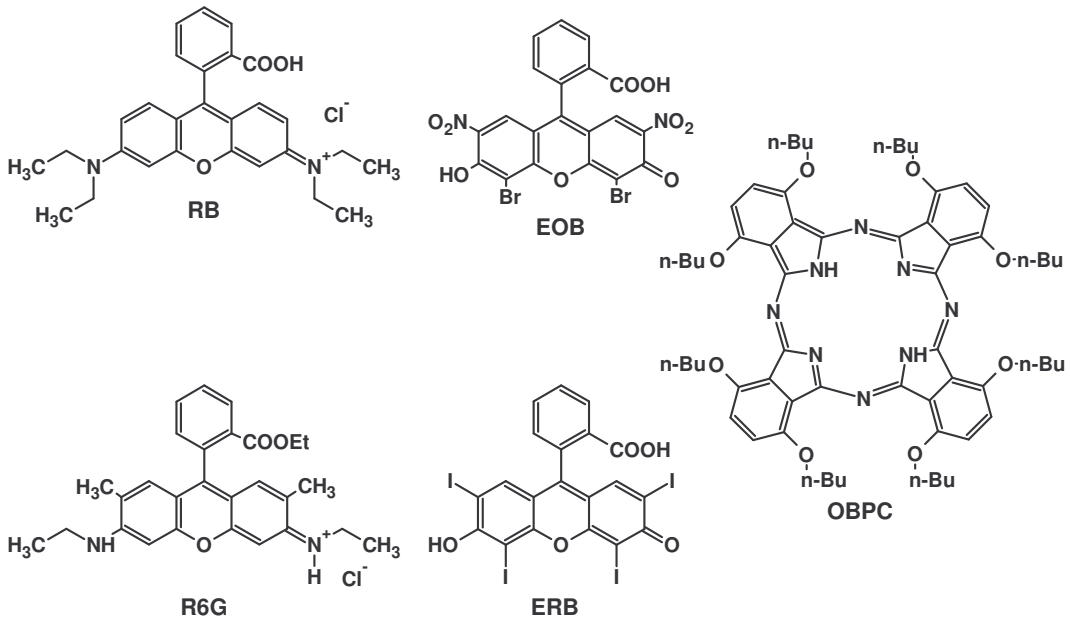

Figure 5.6. Chemical structures of the xanthene dyes and the phthalocyanine tested. For the structures of the triphenyl methane dyes see *chapter 4, section 4.3.1.4. Indicators*.

5.3.1.5. Test Gases

Nitrogen (purity 99.999 %) and ammonia (100 ppm in synthetic air) were purchased from Linde.[23] Test atmospheres were prepared by blending nitrogen with appropriate amounts of ammonia test gas.

5.3.2. Preparation of Indicator Perchlorates

5.3.2.1. Preparation of Rhodamine B Perchlorate

Rhodamine B perchlorate was prepared according to a protocol described earlier.[2] 0.5 g (1.6 mmol) rhodamine B were dissolved in 60 mL water. 0.15 g sodium perchlorate were dissolved in 10mL water and added to the stirred dye solution. After 30 min, the red precipitate was filtered with suction, washed 3 times with 2 mL portions of water and dried over night at 60 °C. Elemental analysis (calc./found) for $C_{28}H_{31}ClN_2O_7$ (MW 543.01 g / mol): C 61.93 / 62.27; H 5.75 / 5.57; N 5.16 / 5.17.

5.3.2.2. Preparation of 9-(4,4-Dimethylaminostyryl) Acridinium Perchlorate (DMASA)

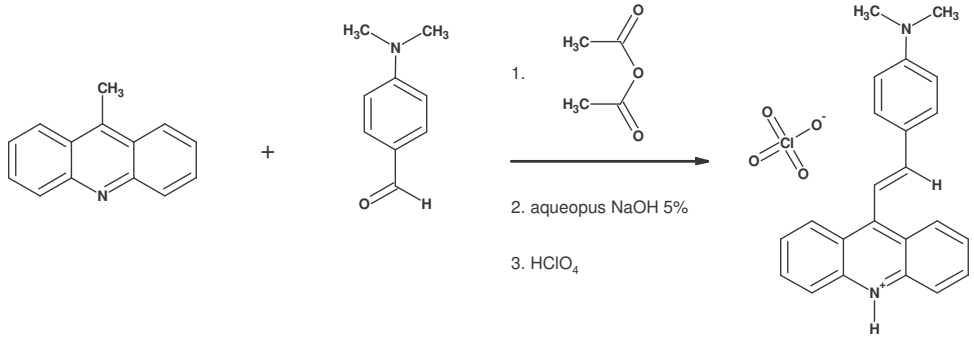

The sysnthesis of 9-(4,4-dimethylaminostryl) acridine was prepared according to a protocol described earlier.[22] 0,483 g (2.5 mmol) 9-methylacridine and 0,373 g (2.5 mmol) 4,4-dimethylamino benzaldehyde were refluxed in 7 mL acetic anhydride at 145 °C. After 4 h, the intensive red coloured solution was cooled to room temperature and 25 mL aqueous sodium hydroxide (5 % w/w) were added. The brown precipitate formed is filtered and washed with water to neutrality. The crude product was recrystallised from 25 ml ethanol (yield: 0.529 g, 65 % orange powder). Elemental analysis (calc./found) of $C_{23}H_{20}N_2$ (MW 324.42 g / mol):

C 85.15 / 84.96; H 6.21 / 5.81; N 8.63 / 8.65.

0.2 g (0.62 mmol) 9-(4,4-dimethylamino styryl) acridine were dissolved in 20 mL water and 500 µL 1 N HCl. 0.1 g (0.8 mmol) sodium perchlorate were added to the stirred solution. After 30 min, the dark blue precipitate was filtered, washed with water and dried at 60 °C.

5.3.2.3. Preparation of 9-(4,4-Dimethylaminocinnamyl) Acridinium Perchlorate (DMACA)

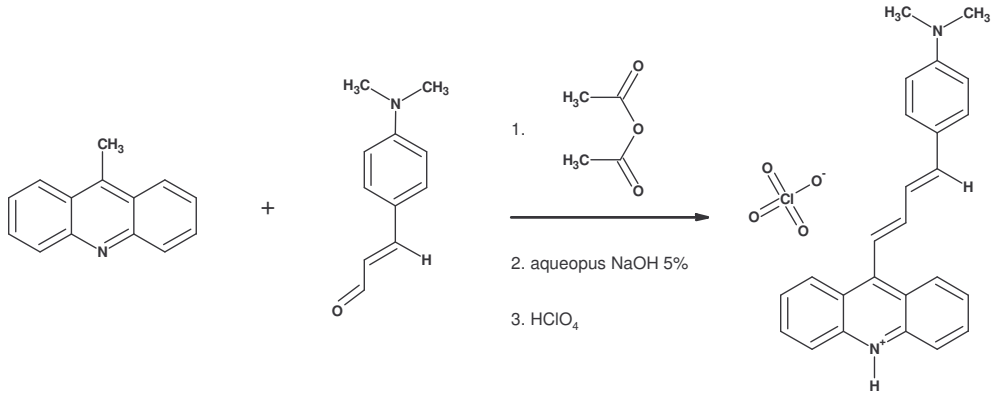

9-(4,4-dimethylaminocinnamyl) acridine was prepared analogous to the prior compound. 0,483 g 9-methylacridin und 0.438 g 4,4-dimethylamino cinnamaldehyde were refluxed in 7 mL acetic anhydride at 145 °C. After 4 h, the red solution was cooled to room temperature and 25 mL aqueous sodium hydroxide (5 % w/w) were added. The bronze precipitate was filtered and washed with water. 9-(4,4-dimethylaminocinnamyl) acridine was recrystallised from 20 mL ethanol (yield: 0.359 g, 41 % orange needles). Elemental analysis (calc./found) of $C_{25}H_{22}N_2$ (MW 350.46 g / mol):

C 85.68 / 85.57; H 6.33 / 6.07; N 7.99 / 7.99.

To a stirred solution of 0.2 g (0.57 mmol) acridinium compound in 20 mL water and 500 µL 1 N HCl 0.1 g (0.8 mmol) sodium perchlorate were added. After 30 min, the blue-green product was filtered with suction, washed with water and dried at 60 °C.

5.3.3. Preparation of Sensor Materials

Stock solutions of the compounds were prepared and placed to pre-defined positions on the working area of the MicroLab S® liquid handling device described in chapter 2, section *2.3.1. Instrumentation for Library Preparation*. The concentration of each solution was stored in an EXCEL®-sheet supplying the sampler software. Sensor cocktails were prepared by automatic execution of the purpose-built blending procedure (see Appendix C).

Plasticizer-free sample cocktails were generally composed of 500 µL polymer stock solution. The concentration of dye in the plastic film was set to 20 mmol per 1 kg dry matrix. The respective volumes of indicator stock solutions necessary to create this composition were calculated in the blending procedure - according to the amount of matrix dissolved in 500 µL polymer solution - and dispensed to the sample vials.

The contents of plasticizer, when used, were varied between 10, 33, 50 and 66 % (w/w) of polymer matrix. The volumes necessary to create the plasticized matrices were calculated

in the blending procedure and dispensed to the sample vials. Thereby, the amount of pure polymer added to a sample vial was reduced whilst the amount of pure plasticizer was increased in order to obtain equal amount (mass) of plasticized matrix (m(polymer) + m(plasticizer) = const.) for each polymer - plasticizer mixture. The concentration of dye in the plasticized film again was set to 20 mmol per 1 kg dry matrix. The volumes of the particular indicator stock solutions added were equal to those for the plasticizer-free cocktails.

10 µL of each sample cocktail were transferred to glass substrates with the MicroLab® S liquid dispenser and the solvents were evaporated. Before characterisation the dry films of the hit sensors were conditioned storing them for 30 min in a desiccator over concentrated hydrochloric acid. Subsequently, excess acid was evaporated placing the substrates in a nitrogen flow over night.

In the first screening the matrix consisted of all possible combinations of indicator with polymer. This involved the blending of 22 indicators with 15 polymers resulting in 330 sensor materials. After evaluation of the performance of the materials potential the indicators BPB, BCG, rhodamine B and 9-(4,4-dimethyl aminostyryl)acridinium perchlorate were selected for hit sensors. Additionally, suitable polymers were identified to be EC, PFE-VFP, CAc, PVC-iBVE, POMMIE, PTBS, PVC, PS and PMMA. In the second step, sensor materials composed of these hit components were prepared and tested (36 materials). Third, a selection of suitable compositions was fine-tuned via the introduction of plasticizers TBP, TOP, OBN and NPOE in concentrations of 0, 10, 33, 50 and 66 % w/w.

5.3.4. Characterisation of Optical Ammonia Gas Sensors

The ammonia gas sensors were characterised using the high-throughput screening setup for absorbance measurements described in chapter 2, section *2.3.2. Setup for Library Characterisation*. The absorbance spectra were recorded upon exposure of the samples to test gas with varying ammonia gas concentrations. All absorbance measurements were performed automatically at 20 ± 2 °C and 50 ± 5 % r.H. unless otherwise stated. The raw data were imported by purpose-built VBA-macros into EXCEL® worksheets for evaluation the absorbance values of the sensor films exposed to the particular test gases. The performance of the sensor materials was evaluated via the calibration curves plotting the respective sensor signal as a function of ammonia concentration.

Depending on the screening procedures the ammonia content in the test atmospheres was varied between 0, 10, 25, 50 and 100 ppm by blending nitrogen with ammonia test gas

(100 ppm and 200 ppm v/v in nitrogen, respectively). Constant relative humidity of 50 % r.H. was obtained mixing humidified nitrogen carrier flow with anhydrous nitrogen or test gas, respectively. Atmospheres of approx. 50 % (v/v) ammonia in nitrogen were prepared flushing 50 mL / min dry nitrogen through a concentrated aqueous ammonia solution (25 % w/w).
Time-dependent measurements were performed with the high-throughput setup in semi-automatic mode. Single spots, measurement wavelengths and constant flow rates of varying ammonia content were selected manually. Data acquisition and flow rate control were performed by software.

5.4. Results and Discussion

5.4.1. Choice of Materials

Indicator dyes were selected according to their pH-sensitive protolytic properties. They all exhibit acidic functional groups able to dissociate protons. The deprotonation and possible following reactions result in a change of optical properties between protonated and deprotonated species. Triphenyl methane dyes were applied in their acidic form. Upon exposure to ammonia the phenolic proton was dissociated and the base form of the dye was formed. Thus, with increasing ammonia concentration the absorbance of this species ($\lambda_{max} \approx 590 – 630$ nm) was increased. The growing absorbance value was detected as function of pNH_3. In the case of 9-(4,4-dimethylamino styryl) acridinium dyes the deprotonation caused a decrease of the absorbance maximum around 630 nm. Xanthene-based rhodamine dyes display good photostability and advantageous absorbance properties with $\lambda_{max} \sim 560 – 580$ nm in the screened polymers. Their ability to form colourless lactones when a carboxy group at the phenyl ring is deprotonated rendered them promising for ammonia gas determination. Rhodamine B was found to be suitable for sensing ammonia in solution and thus it was assumed applicable in this study.[2] Rhodamine 6G, in contrast, did not show any detectable sensitivity to ammonia, since it cannot form a lactone. The carboxy group is esterfied.

Polymers were chosen according to their processibility with the automated liquid handling robot used for preparation of the sensor cocktails. Thus, main criteria for the selection were solubility in organic solvents and aprotic character. The polarity of the materials also was taken into consideration, since it influences the stability of the charged and uncharged molecules in the film, e.g. the ammonium cation or dye species formed in the sensor reaction. Thus, the sensitivity and reversibility may be affected. Plasticizers were

chosen according to their compatibility to the polymers used in high-throughput screening. They were selected from aprotic species not interfering the pH-sensitive response of the indicator dyes.

The crown ether was selected due to its good solubility in organic solvents and the polymer matrix. Further criteria were commercial availability and cheap price compared to other ammonium ionophores like nonactin or valinomycin.

5.4.2. Screening for Sensor Materials

For a first screening sensor cocktails composed of the possible polymer-indicator combinations were prepared with the MicroLab® S and transferred to glass substrates. The absorbance spectra were recorded upon exposure of the sample spots to test gas with ammonia concentrations of 0, 50 and 100 ppm for 5 min each. Subsequently, they were exposed to nitrogen for 15 min for evaluation of reversibility of the response. The sensor matrix included 315 different binary mixtures prepared by dissolving each dye from table 5.2 in any polymer illustrated in figure 5.4. Hits were selected manually by evaluation of the absorbance spectra of all tested formulations (compare database structure in Appendix F). Acceptance criteria were significant changes of absorbance with increasing ammonia concentration and – at least partial – reversibility of the sensor response. From the first screening the indicator dyes bromophenol blue, bromocresol green, rhodamine B and 9-(4,4-dimethylaminostyryl) acridinium perchlorate dissolved in various polymers were identified suitable, since they showed sensitivity to 50 ppm ammonia. Useful polymers were from EC, PFE-VFP, CAc, PVC-iBVE, POMMIE, PTBS, PVC, PS and PMMA. Combinations of these materials were subjected to further testing in a second screening.

Sensor materials composed of the hit components were prepared and their optical properties were characterised upon exposure of the samples to 0, 10, 25 and 50 ppm NH_3 in a second, more detailed, screening procedure. The materials were subjected to each test atmosphere for 20 min. Subsequently, they were recovered for 30 min in a nitrogen atmosphere. The matrix of sensor materials built up by mixing each of the four hit indicators with each hit polymer is illustrated in table 5.4 giving also an overview of the performance of the materials.

Table 5.4. Matrix of sensor materials composed of components showing sensitivity to ammonia gas.

		Indicator dye			
		BPB	BCG	$RBClO_4$	DMASA
Polymer	EC49	✓	✓	✓	✓, **very poor**
	PFE-VFP	✓	✓	✓	✓, **very poor**
	CAc	✓	×	×	×
	PVC-iBVE	✓	✓	×	✓, **very poor**
	POMMIE	×	✓	×	×
	PTBS	✓	✓	×	✓, **very poor**
	PVC	✓	✓	×	✓, **very poor**
	PS	✓	✓	×	×
	PMMA	✓	✓	×	✓, **poor**

✓ **sensor shows response to ammonia;** × **no significant response to ammonia.**

In figure 5.7 the absorbance changes of bromophenol blue in EC, PFE-VFP, CAc, PVC-iBVE, PTBS, PVC, PS and PMMA are shown exemplary. It can be seen that the absorbance of the samples increased with increasing ammonia concentration due to the acid-base reaction between the dye and the target gas. Obviously, the sensor materials did not recover completely within the set time period with exception of the polymers EC and PTBS. This may be attributed to a lower permeability of the polymers to ammonia and a stabilisation of the ammonium cation, formed during the acid-base reaction, in the polymer via the formation of an ion pair with the dye anion. The maximum change (A_∞) was observed exposing the sensor materials to a concentrated ammonia atmosphere. The sensitivity of each sample containing bromophenol blue or bromocresol green was evaluated calculating the R values ($R = (A-A_0)/(A_\infty-A)$) as a function of ammonia concentration.

The absorbance of rhodamine B and 9-(4,4-dimethylaminostyryl) acridinium perchlorate decreased with increasing ammonia concentration. In terms of rhodamine B this was explained by the lactonisation of the dye upon deprotonation of the carboxy group. This is displayed in figure 5.8. The poor performance of the sensor materials can be explained by the insufficient activation of the dye during membrane preparation and too low permeability of the non-plasticized matrices. Due to the apolar environment around the dye rhodamine B partially was present in the lactone form. The absorbance values at λ_{max} (570 nm in EC49) being lower than expected affirm this suggestion. According to a lower sensitivity of the

lactonisation reaction – compared to the acid-base reaction of BPB – these materials showed poor performance in the matrices investigated.

Upon dissociation of the acridinium dye the delocalisation of electrons was reduced in the molecule resulting in an observable decrease of the absorbance at 630 nm. The absorbance of the samples containing DMASA in the various polymers was lower than 0.1 causing high signal noise. This rendered the non-plasticized polymer matrices incompatible for characterisation. Thus, these samples were discarded since the materials also showed very poor recovery.

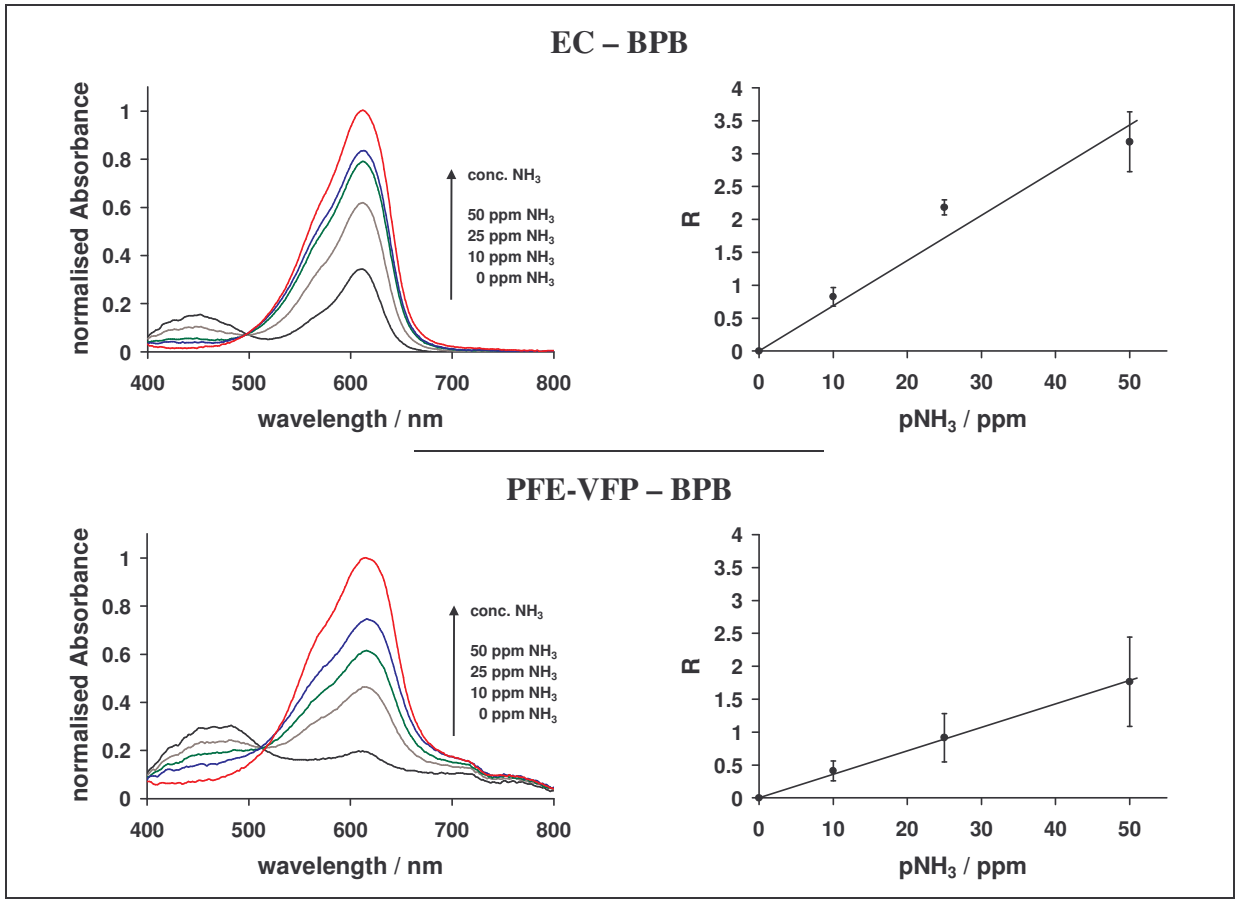

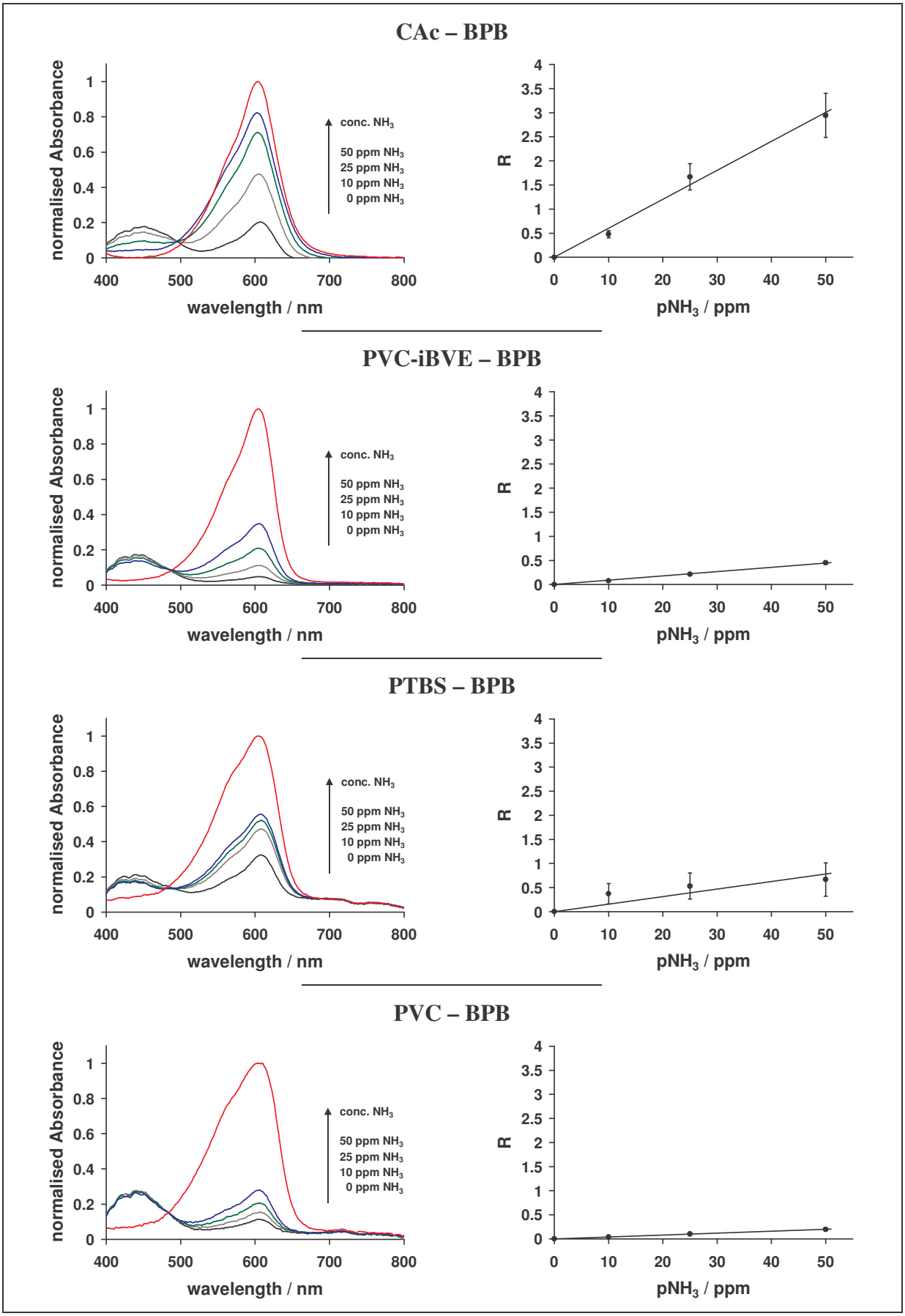
CAc – BPB
normalised Absorbance
wavelength / nm
conc. NH3
50 ppm NH3
25 ppm NH3
10 ppm NH3
0 ppm NH3
R
pNH3 / ppm
PVC-iBVE – BPB
normalised Absorbance
wavelength / nm
conc. NH3
50 ppm NH3
25 ppm NH3
10 ppm NH3
0 ppm NH3
R
pNH3 / ppm
PTBS – BPB
normalised Absorbance
wavelength / nm
conc. NH3
50 ppm NH3
25 ppm NH3
10 ppm NH3
0 ppm NH3
R
pNH3 / ppm
PVC – BPB
normalised Absorbance
wavelength / nm
conc. NH3
50 ppm NH3
25 ppm NH3
10 ppm NH3
0 ppm NH3
R
pNH3 / ppm

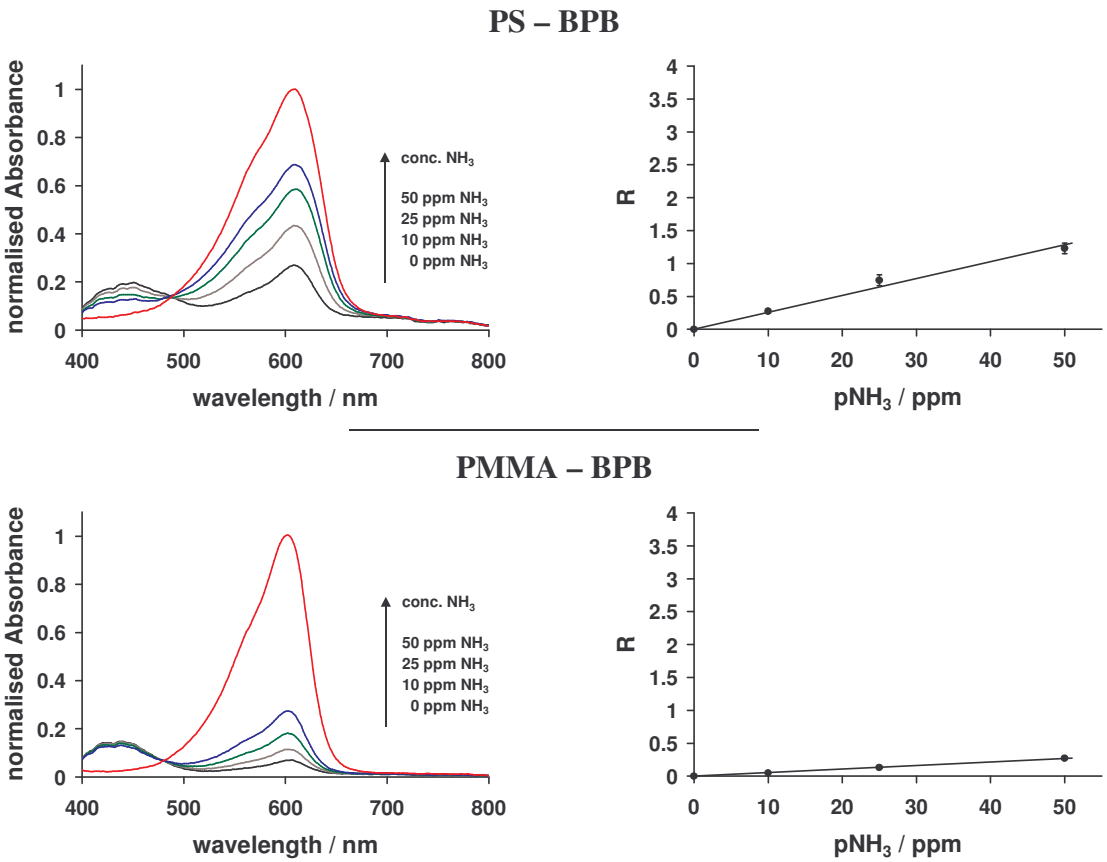

Figure 5.7. Absorbance Spectra and calibration curves of bromophenol blue in EC, PFE-VFP, CAc, PVC-iBVE, PTBS, PVC, PS and PMMA upon exposure to 0 ppm, 10 ppm, 25 ppm and 50 ppm NH_3 (from bottom to top). The red line represents the absorbance spectra in concentrated ammonia atmosphere.

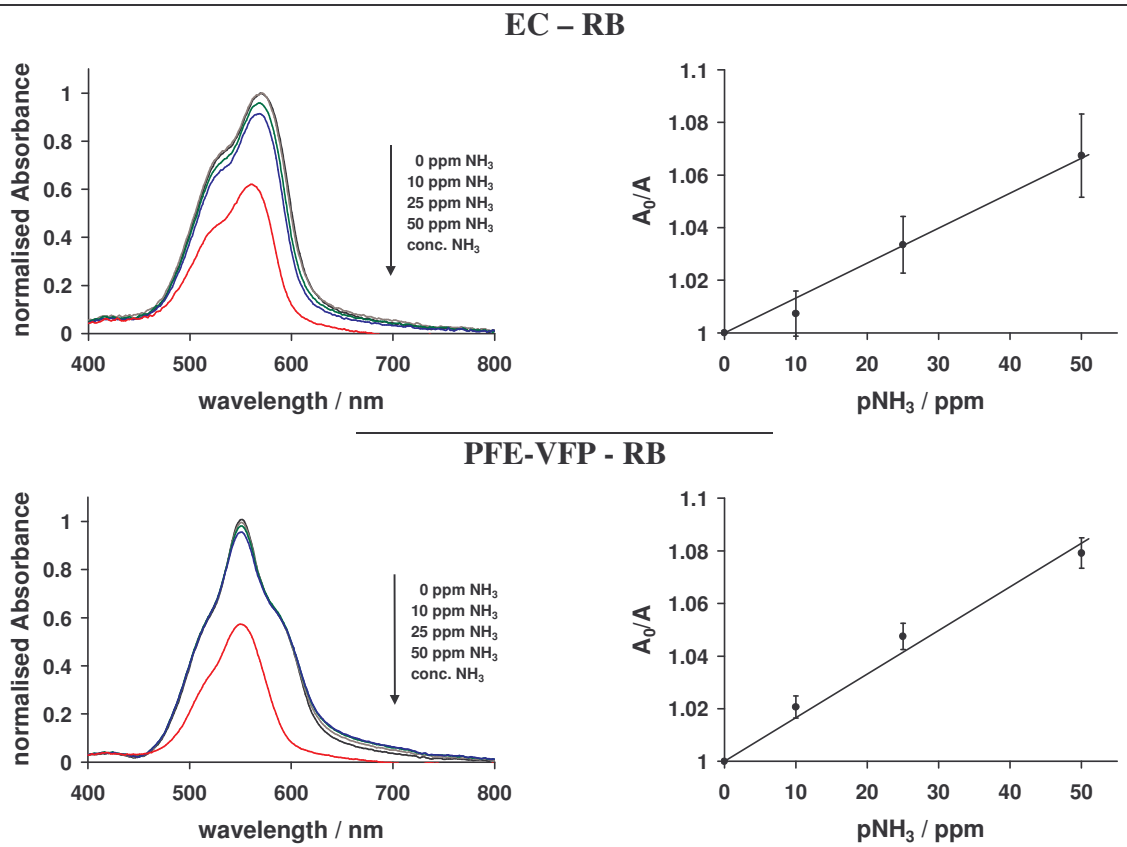

Figure 5.8. Absorbance Spectra and calibration plots of rhodamine B in EC and PFE-VFP exposed to 0 ppm, 10 ppm, 25 ppm and 50 ppm NH_3. The red line represents the absorbance in concentrated ammonia atmosphere.

As a result, the second screening showed that in non-plasticized polymer matrices the triphenyl methane dyes BPB and BCG showed best performance in various polymers. At 50 ppm ammonia the materials based on ethyl cellulose showed R values of 3.2 and 1.4, respectively. At this concentration 80 % of BPB and 70 % of BCG were converted to the particular alkaline form of the dye (50 % conversion $\Leftrightarrow$ R = 1). The response of rhodamine B was limited to ethyl cellulose and PFE-copolymer showing a ratio A_0/A at 50 ppm of 1.07 and 1.09, respectively. This corresponded particularly to 7 % and 8 % lactonisation (50 % lactonisation $\Leftrightarrow$ $A_0/A = 2$). Thus, the prior two indicators were considered valuable for further investigation due to their better performance.

5.4.3. Tuning Performance of Ammonia Sensors

5.4.3.1. Effect of Plasticizer

The polymers ethyl cellulose, PTBS, PVC and polystyrene were selected from the above described screening. According to prior results with oxygen sensors, it was suggested that sensor materials composed of these lead matrices containing either BPB or BCG can be tuned via employment of various plasticizers. Thus, the softeners TBP, TOP, OBN and NPOE were applied to the polymer matrices in concentrations of 0, 10, 33 and 50 % (w/w). The slopes of the linear best fits of the calibration curves of the non-plasticized matrices are shown in table 5.5.

Table 5.5. Slopes from best fits of the calibration curves of non-plasticized ammonia sensors.

	Slope of linear fit: $\alpha \times 10^3$ / ppm^{-1}	
	BPB	BCG
EC49	68.8 ± 7.5	27.1 ± 1.8
PTBS	13.7 ± 1.6	8.5 ± 0.4
PVC	3.9 ± 0.6	1.1 ± 0.2
PS	25.7 ± 1.9	17.7 ± 0.1

On this basis the tuning efficiency can be determined. The calibration plots of each plasticized sample were evaluated and the gradients of the fit functions describing the sensitivity of the sensor materials were calculated. In figure 5.9 the effect of the various softeners on the matrices containing BPB can be seen. The relative changes of the slopes were obtained from calculating the ratio of the gradient of a particular plasticized material and the non-plasticized matrix. Obviously, with TBP the sensitivity of the EC sensors was improved continuously with increasing softener concentration. When OBN or NPOE were used, highest sensitivity was achieved at a plasticizer concentration of 33 % (w/w). Higher softener content leads to a decrease of the gradients of the calibration plots. In the PTBS and PS matrices TBP and TOP caused a decrease of sensitivity. Although the same effect was seen for OBN and NPOE in PS, the sensitivity of the PTBS matrix was almost unaffected by increasing plasticizer content. The gradients of the PVC sensors increased continuously with increasing concentration of any plasticizer used. The trends observed for the BCG-based sensors can be seen in figure 5.10. EC49–BCP–based sensors showed an increase of the gradient by ~ 20 % upon increasing the TBP content from 0 to 50 % (w/w) of the matrix. The sensitivity of PVC–BCP-based materials was optimised with all plasticizers used. The gradients increased approx.

by factors of 16, 7, 17 and 15, when TBP, TOP, OBN and NPOE were applied at levels of 50 % (w/w) to the polymer matrices. All other sensor formulations showed decrease of sensitivity upon increasing plasticizer content.

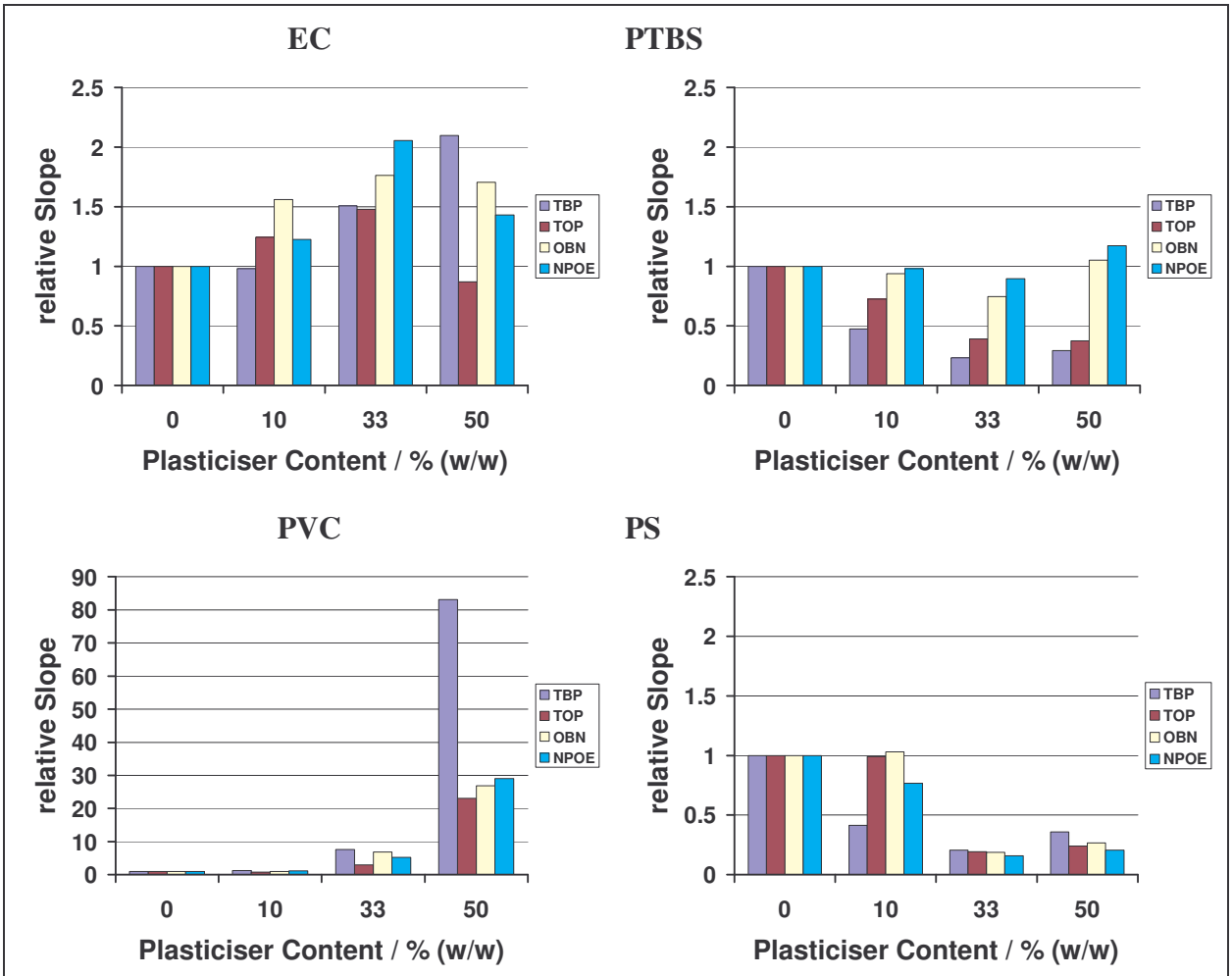

Figure 5.9. Effect of softeners on the sensitivity of ammonia gas sensors based on BPB in EC49 (A), PTBS (B), PVC (C) and PS (D). Relative slopes were obtained from the ratios of the gradients of the particular plasticized materials and the non-plasticized matrix.

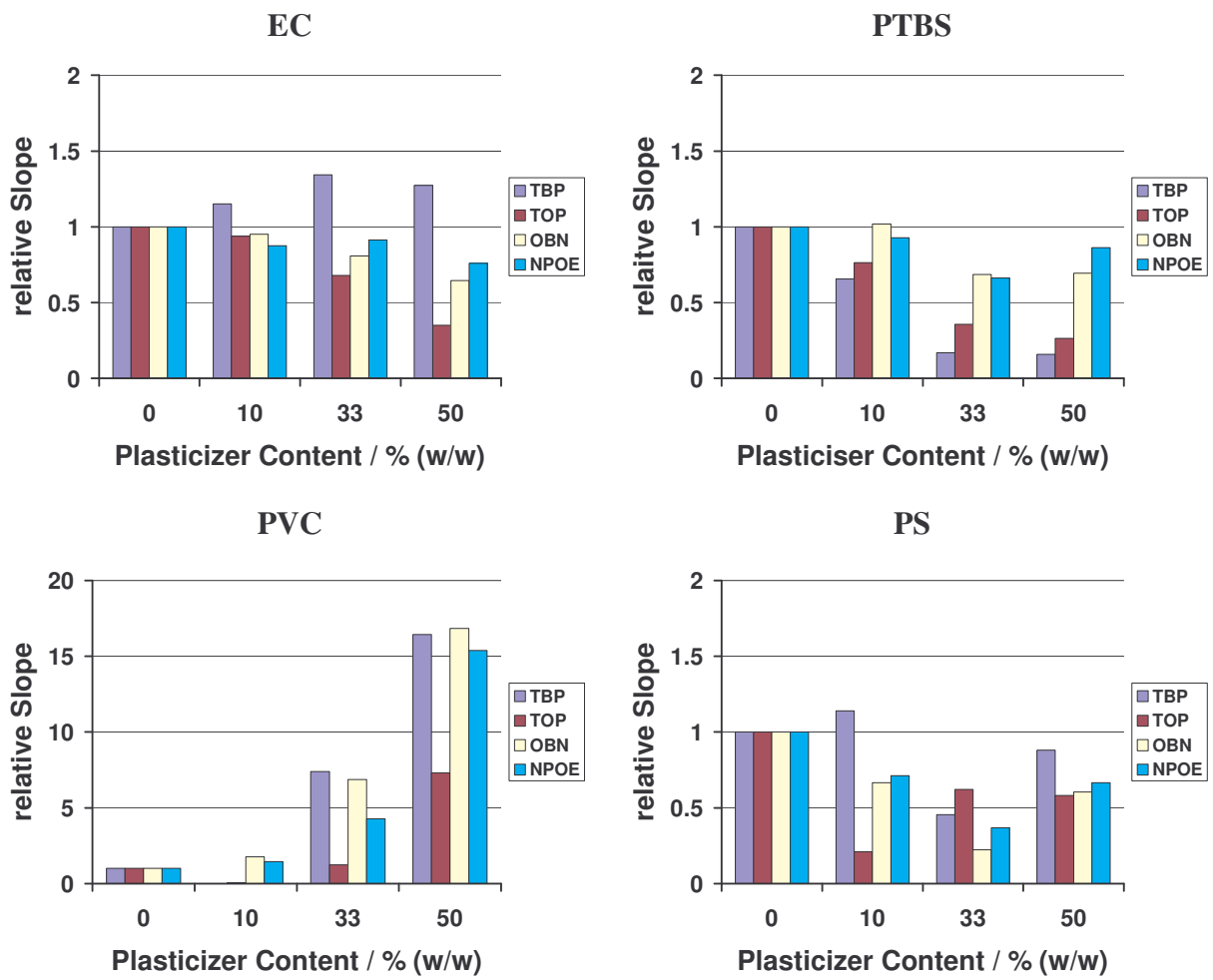

Figure 5.10. Effect of softeners on the sensitivity of ammonia gas sensors based on BCG in EC49 (A), PTBS (B), PVC (C) and PS (D). Relative slopes were obtained from the ratios of the gradients of the particular plasticized materials and the non-plasticized matrix.

The use of plasticizers was deemed necessary to obtain acceptably fast response. Although, the plasticizers did not coercively increase sensitivity of for example polystyrene-based sensors, they enhanced performance due to decrease of response time. The permeability P of a gas into a polymer is linked to the diffusion coefficient D and the solubility S of a gas in a particular polymer. Thus, increasing the plasticizer content in a polymer matrix usually leads to an increase of the diffusion coefficient of the gas into a particular polymer. As a result the response time of the sensor material is affected and the response is more rapid than that of a non-plasticized matrix. Though, the resulting matrix may offer lower permeability than the non-plasticized due to over compensation of this effect by a reduced solubility of the target gas in the softened matrix. Thus, the observed decrease of sensitivity can be attributed to a decrease of solubility of the target gas with increasing plasticizer content. Yet, the sensitivity of PVC was increased dramatically upon plastification. Plasticized PVC and ethyl cellulose showed almost equal sensitivity. This was attributed to an increase of permeability of non-

plasticized PVC to ammonia to a level similar to that of ethyl cellulose (see chapter 1, *section 1.2.2. Composition of Polymer-Based Optical Chemical Gas Sensors*, table 1.1).

Although, the rhodamine B sensor showed only poor response in non-plasticized ethyl cellulose - and may be therefore discarded – the performance of this matrix was successfully tuned applying NPOE at a level of 50 % (w/w).The respective absorbance spectrum is illustrated in figure 5.11. Apparently, in absence of ammonia the zwitter-ionic form of the dye is stabilised better in plasticized ethyl cellulose than in pure polymer as can be seen by comparing the shape of the absorbance spectra shown in figure 5.8 and figure 5.11. Thus, the dynamic range of the absorbance change is increased. Upon application of NPOE at a level of 50 % (w/w) the ratio A_0/A at an ammonia level of 50 ppm in test gas increased to 1.25. This corresponds to a decrease of absorbance of 7 % in pure polymer and 20 % in plasticized ethyl cellulose.

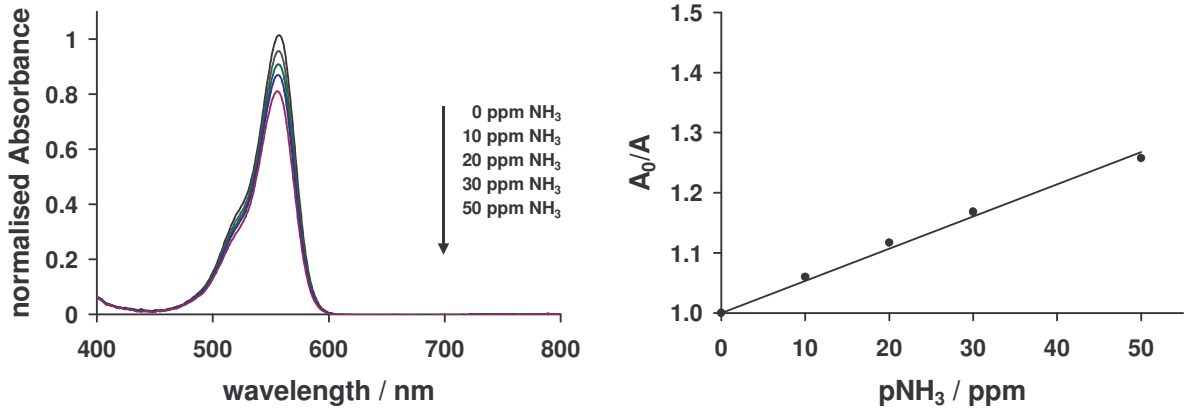

Figure 5.11. Absorbance Spectra and calibration plot of rhodamine B perchlorate (20 mmol/kg) in an ethyl cellulose matrix containing 50 % (w/w) NPOE upon exposure ammonia levels of 0, 10, 20, 30 and 50 ppm at 25 °C.

5.4.3.2. Effect of Crown Ether

The sensitivity of sensor materials composed of ethyl cellulose and BCG was found not to be tuned via the addition of plasticizers. Thus, in order to increase the ammonia concentration in the sensor film an alternative approach was necessary. In agreement with literature neutral ionophores used for ion-exchange in optical ammonium sensors were judged promising agents.[12,13,24] 4´,4´´(5´´)-di-tert-butyldibenzo-18-crown-6 was added to a sensor formulation, based on EC and BCG (20 mmol/kg) containing 66 % (w/w) NPOE, at levels of 10, 15, 20

and 50 mmol / kg matrix. The absorbance spectra of the samples were recorded at ammonia levels of 0, 10, 25 and 50 ppm. The maximum absorbance change was obtained exposing the samples to a concentrated ammonia atmosphere created via flushing nitrogen through 25 % aqueous ammonia solution. The response of the sensor materials containing 0, 10, 20 and 50 mmol/kg crown ether, respectively, are illustrated in figure 5.12.

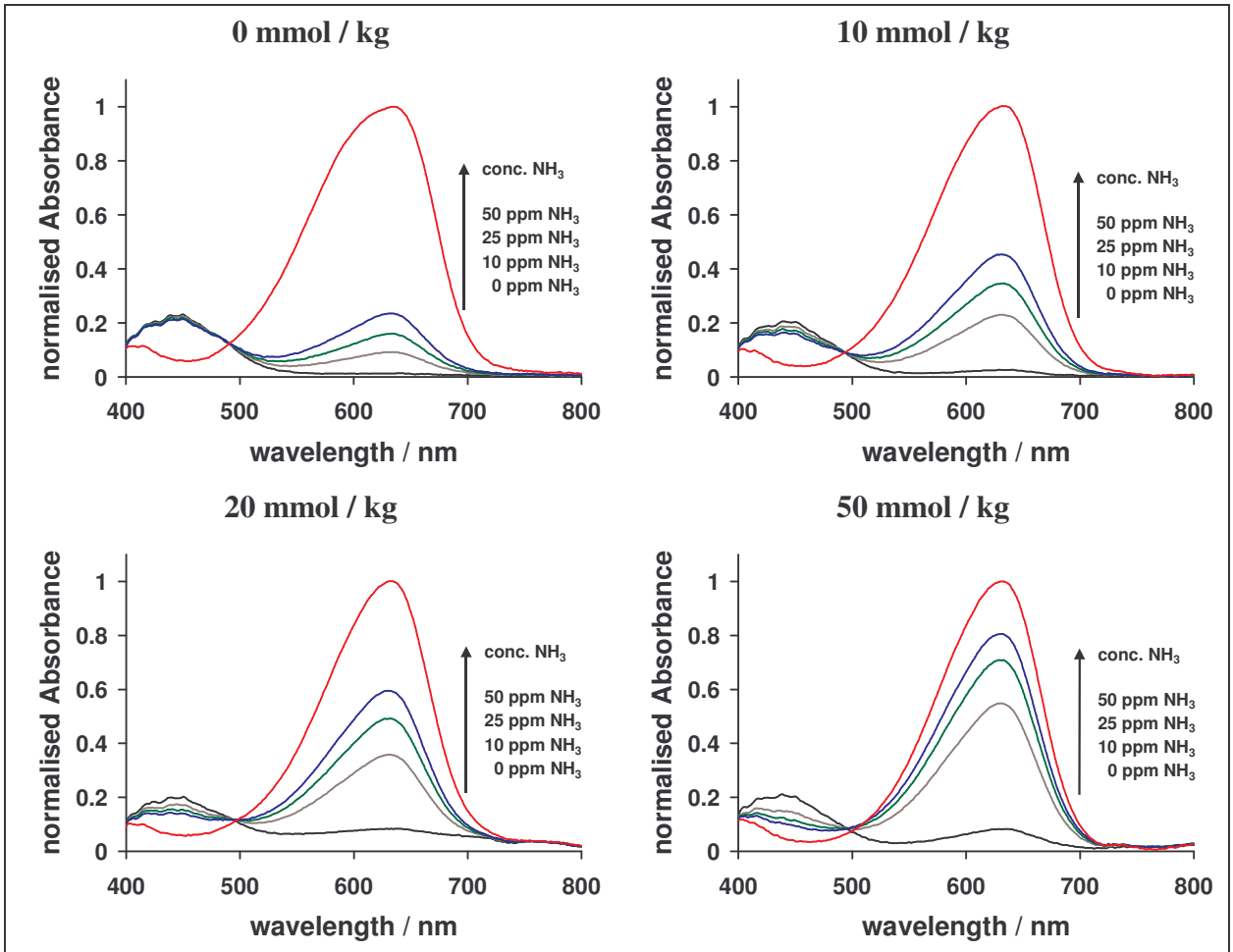

Figure 5.12. Absorbance spectra of BCG–EC-based ammonia sensors exposed to 0, 10, 25 and 50 ppm ammonia. Maximum absorbance (red line) was obtained in a concentrated ammonia atmosphere. The concentration of crown ether in the matrix was varied between 0 and 50 mmol/kg.

As it can be seen from the absorbance spectra the sensitivity of the samples to ammonia increased with increasing content of crown ether in the matrix. Thus, addition of this tuning agent was effective for enhancing the performance of the sensor materials. The sensitivity of a sample containing 50 mmol / kg agent showed an increase by a factor of ~ 10 compared to that of the matrix without tuning agent. This is also pointed up in figure 5.13 showing the slopes of the linear best fits of the calibration curves as function of concentration of additive.

Apparently, the plot shows an almost linear relation between the gradients and content of crown ether. The increase of sensitivity was attributed to an enhanced concentration of ammonia in the film via the complexation of the ammonium cation by the crown ether. Second, the NH_4^+ ion was stabilised in the matrix through the complex formation visualised in figure 5.14. Additionally, this equilibrium reaction can be considered a sink for free ammonium in the film forcing the sensing reaction equilibrium to the product side. This was supported by the slow recovery of the sensors (> 45 min) when the ammonia level in the test atmosphere was reduced from 100 ppm to 0 ppm.

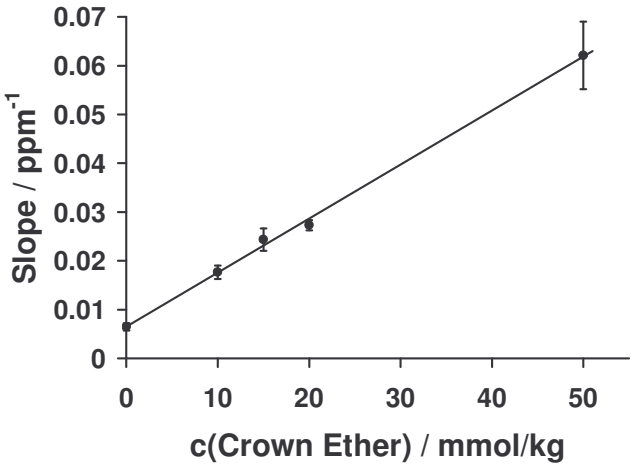

Figure 5.13. Slopes of the linear best fits of sensor materials containing 0, 10, 15, 20 and 50 mmol crown ether per 1 kg matrix. (n=6)

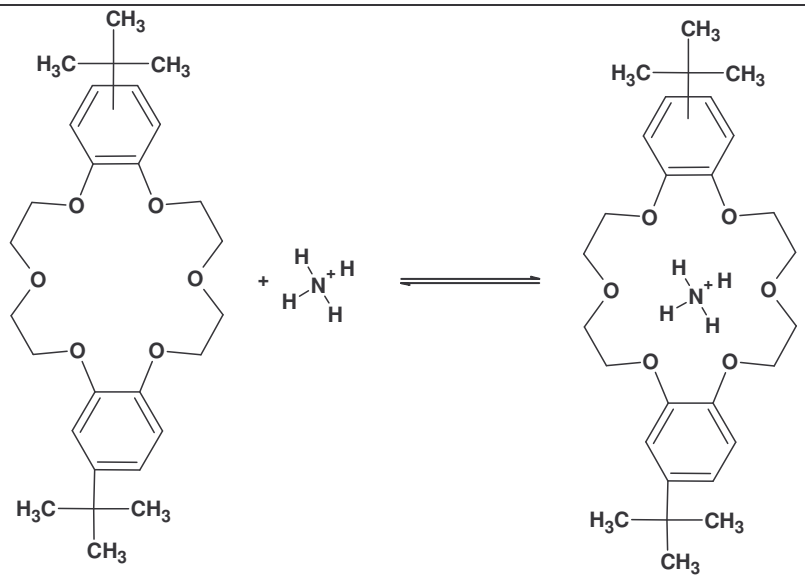

Figure 5.14. Complexation of ammonium ion by crown ether stabilising the cation in apolar matrix.

The crown ether increases the sensitivity of the BCG sensor. Due to the identical reaction principle for all triphenyl methane dye-based ammonia sensors it can be assumed that this tuning effect will also appear with other dyes than BCG. Consequently, a sensor composed of the polymer EC, a plasticizer NPOE and BPB should show an equal increase of sensitivity.

Additionally, the crown ether can enhance selectivity of the sensor for ammonia compared to other basic gases like the homologues methyl amine or ethyl amine. The structure of the crown ether perfectly fits the size of the ammonium cation for complexation. Other amines do not fit into the ring of the crown ether and cannot establish comparable interactions.

On the other hand, time-dependent measurements showed that the response (↑) and recovery times (↓) decreased with increasing concentration of crown ether on changing between ammonia levels of 50 and 100 ppm. The times t_{90} where 90 % of the signal change were obtained are listed in table 5.7. Obviously, although the response was faster with increasing crown ether concentration, the ratio between response and recovery time decreased in the same order. This was reasonable taking into consideration that the ammonium cation formed in the acid-base reaction was complexed in a second, parallel, equilibrium reaction.

A possible reason for the decrease of response times is a reduction of the activation energy of the sensing reaction with increasing crown ether content in the film. The agent may be considered a catalyst for the acid-base reaction between ammonia dissolved in the film and the indicator dye.

Table 5.7. Response and recovery times of EC-BCG-based sensor materials with varying crown ether content on changing the ammonia level in the test atmosphere between 50 ppm to 100 ppm.

Content of crown ether	$t_{90\uparrow}$ / s 50 ppm → 100 ppm	$t_{90\downarrow}$ /s 100 ppm → 50 ppm
0 mmol/kg	274 ± 14	349 ± 29
10 mmol/kg	167 ± 12	270 ± 14
50 mmol/kg	67 ± 8	163 ± 9

5.4.4. Temperature-dependent Response of Lead Sensors

The response of these sensor materials was likely to be temperature-sensitive. First, the solubility of ammonia in the film and, second, the equilibrium constant of the sensing reaction

were likely to decrease with increasing measurement temperature. Thus, optimised sensor materials were selected from the formulations investigated through the screening and optimisation process. The materials given in table 5.8 were suggested as lead sensors. Although, rhodamine B perchlorate did not show sufficient sensitivity in pure ethyl cellulose, the observed optimisation of the sensor via application of NPOE at a level of 50 % (w/w) rendered this material worth to be tested in this study.

Table 5.8. Composition of the sensor materials investigated for their temperature sensitivity.

	Matrix composition		
	Polymer	Plasticizer	Indicator per kg matrix
M1	ethyl cellulose 33 % (w/w)	NPOE 66 % (w/w)	20 mmol BPB
M2	ethyl cellulose 33 % (w/w)	NPOE 66 % (w/w)	20 mmol BCG
M3	PVC 33 % (w/w)	NPOE 66 % (w/w)	20 mmol BPB
M4	PVC 33 % (w/w)	NPOE 66 % (w/w)	20 mmol BCG
M5	ethyl cellulose 50 % (w/w)	NPOE 50 % (w/w)	20 mmol $RBClO_4$

The samples were subjected to temperatures between 15 and 45 °C. Their absorbance was recorded for exposure to test atmospheres containing 0, 10, 20, 30, 40 and 50 ppm ammonia in nitrogen. The calibration plots of M1 - M5 at the prevalent temperatures are shown in figure 5.15. The response of the sensors can be described well by linear fit functions within the concentration range investigated. The temperature sensitivity of the sensor materials can be quantified plotting ln(α) vs. 1/T, where α is the gradient of the linear fit function of each sensor (when pNH_3 is given in units of atmospheres, 1 ppm = 10^{-6} atm) and T is the particular temperature at which the sample was measured. The resulting plots give good straight lines as can be seen in figure 5.16. The gradient of each line gives $-\Delta H^0/R$ and the intercept is equal to $\Delta S^0/R$ when the ammonia concentration is given in units of atmospheres for the calculation of α (see chapter 4, *section 4.4.5.1. Effect of Temperature on the Sensitivity of Lead Sensors for Carbon Dioxide*). The values of ΔH^0 and ΔS^0 obtained from analysis of figure 5.16 are given in table 5.9. As it can be seen both are negative and, thus, associated with an overall exothermic reaction and loss of entropy. The data obtained is comparable and close to reported values for similar sensor types.[7] Compared to values obtained for carbon dioxide sensors (see chapter 4, section *4.4.5.1. Effect of Temperature on the Sensitivity of Lead Sensors for Carbon Dioxide*) the particular ΔH^0, here, are higher related to a bigger temperature sensitivity of the sensing reaction

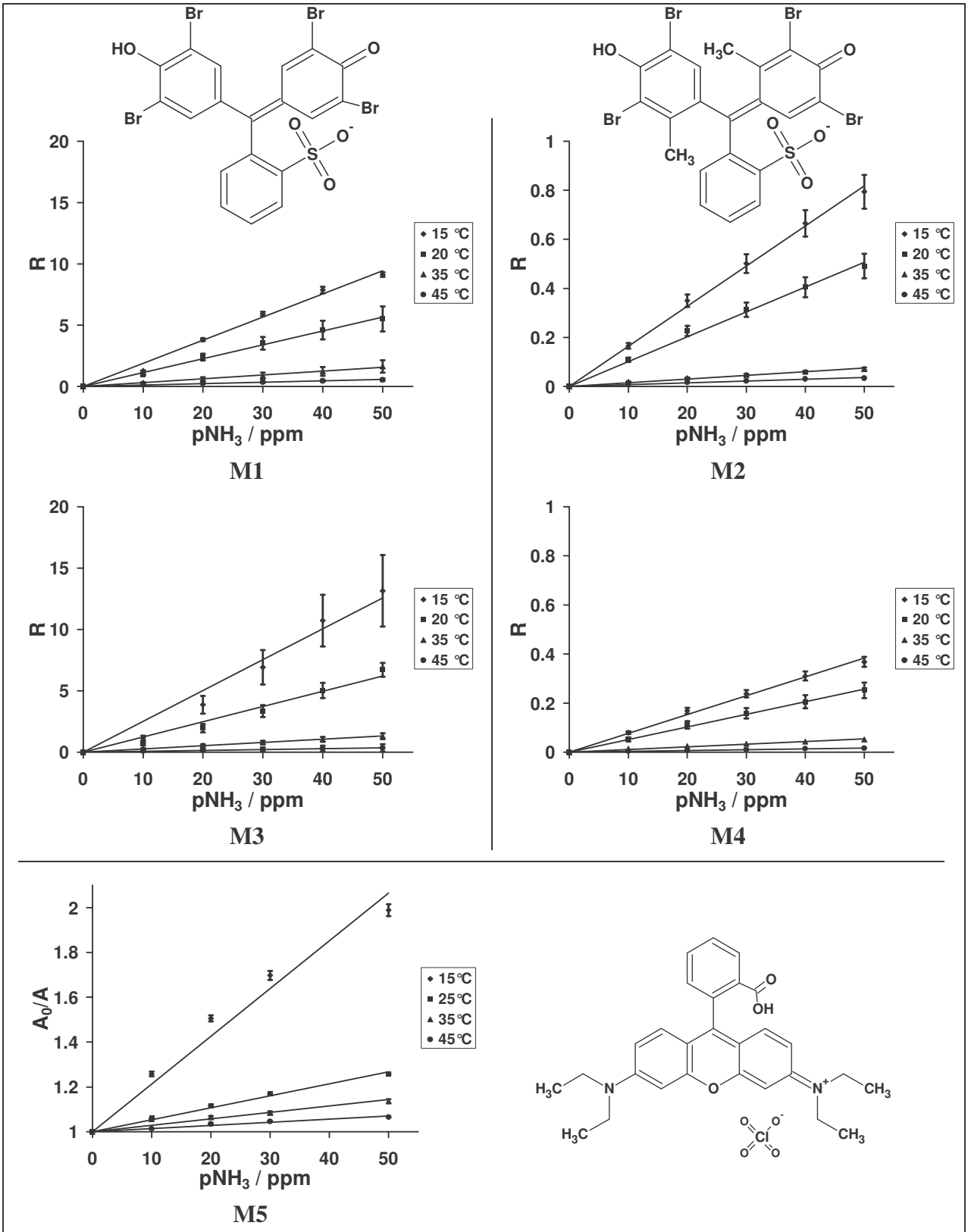

Figure 5.15. Temperature-dependent calibration plots of sensor films M1 – M5.

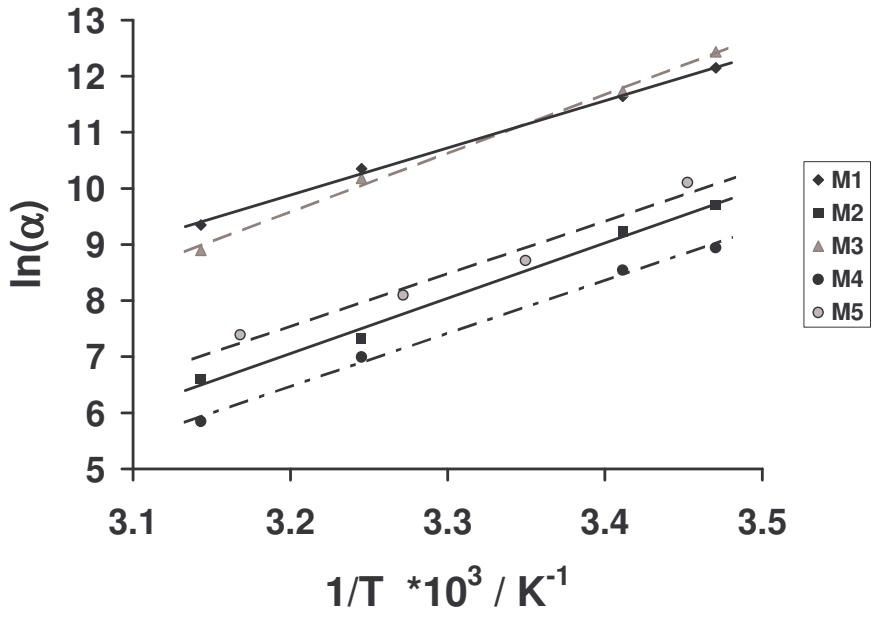

Figure 5.16. Temperature sensitivity of the sensor films M1 – M5 illustrated by plotting ln(α) versus the temperature they were subjected for calibration.

Table 5.9. Thermodynamic data for the sensor films M1 – M5 obtained from analysis of figure 5.15 applying the function $\ln(\alpha) = m \times (1/T) + b$ for linear regression.

	m	b	ΔH^0 / kJ × mol^{-1}	ΔS^0 / J × mol^{-1} × K^{-1}
M1	8412.2 ± 296.6	-17.0 ± 1.0	69.9 ± 2.5	-141.6 ± 8.2
M2	9851.1 ± 626.7	-24.5 ± 2.1	81.9 ± 5.2	-203.4 ± 17.3
M3	10522.5 ± 452.7	-24.1 ± 1.5	87.5 ± 3.8	-200.4 ± 12.5
M4	9496.9 ± 471.5	-23.9 ± 1.6	79.0 ± 3.9	-198.9 ± 13.0
M5	9418.1 ± 1196.9	-22.6 ± 4.0	78.3 ± 10.0	-187.9 ± 33.0

5.4.5. Effect of Relative Humidity on the Response of Lead Sensors to NH_3

Figure 5.17 shows the calibration plots of M1 – M5 subjected to test atmospheres of varying ammonia concentration at levels between 0 and 50 % relative humidity (r.H.). M1 – M4 were exposed to 0, 10, 20, 30, 40 and 50 ppm ammonia in nitrogen at 0, 10, 30 and 50 % r.H. M5 was subjected to 0, 20, 40, 60 and 100 ppm NH_3 test gas at levels of 0, 25 and 50 % r.H.

Apparently, the response of all films is affected significantly between 0 and 50 % r.H. However, the difference between 0 and 10 % r.H. was negligible for the sensors M1 - M4. Sensors M1 and M3 (indicator BPB) showed a decrease of the gradients of the calibration plots with increasing the level of relative humidity from 0 to 50 %. In contrast to that, the

slopes for M2 and M4 increased with increasing level of relative humidity. Variation between 30 and 50 % r.H. resulted in increasing sensitivity for both ethyl cellulose-based films and for the PVC-based film containing BCG. Yet, the humidity effect on the response of M4 was negligible compared to M1 and M2.

M5 also shows significant sensitivity of the response to variation of the level of relative humidity. The gradients of the calibration plots increased with varying relative humidity between 0 and 50 % r.H. Additionally, the calibration curve for a level of 50 % r.H. showed significant deviation from linearity that cannot be explained simply by a variation of the effective ammonia concentration.

The decrease of sensitivity may be explained by a reduction of the apparent ammonia concentration in agreement with reported findings.[13] On the other hand, increasing levels of relative humidity from 0 to 50 % r.H. had opposite effects on BPB and BCG-based materials. It also had to be taken into consideration that with increasing humidity from 30 to 50 % r.H for M1, M2 and M4, and 25 to 50 % r.H. for M5, resulted in an increase of sensitivity. This was illustrated by the increasing gradients of the particular calibration plots. Thus, a possible explanation for this finding may additionally be the formation of ammonium hydroxide in the sensing film via the uptake of water in the film reacting with the ammonia gas. As a result, the microenvironment of the indicator dye would show enhanced “aqueous” or hydrophilic character easing the acid – base reaction between ammonia and the indicator dye. This could be tracked by an increase of sensitivity like it is shown for M2, M4 and M5 in figure 5.17. In summary, the sensor M4 showed lowest interference when varying the apparent level of humidity around 50 % r.H.

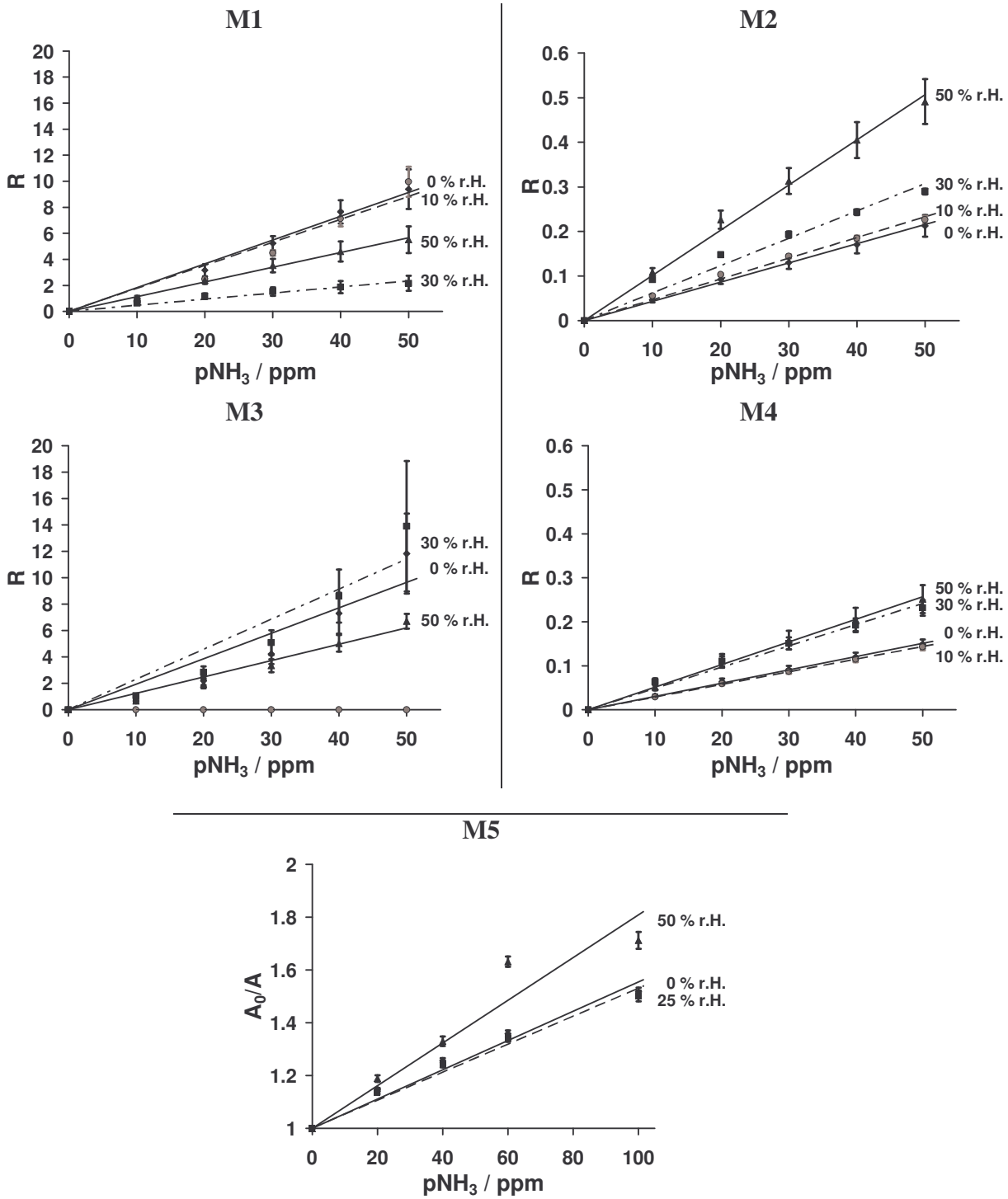

Figure 5.17. Response of sensors M1 – M5 to ammonia gas when subjected to humidity levels between 0 and 50 % r.H.

5.5. Conclusion

Sensor films were prepared by automatic blending of component stock solutions necessary for the creation of optical ammonia gas sensors and transfer of the sample cocktails to supporting glass substrates. Characterisation procedures were developed providing the comparability of sensor performance. The automated characterisation setup was successfully applied for the data acquisition.

Using these tools for high-throughput blending and screening ammonia-sensitive materials could be identified from a pool of 360 polymer – indicator combinations. The application of plasticizers was found to be essential for providing acceptably fast response of the materials. However, the sensors were slower than carbon dioxide or oxygen sensors in the same matrix. Thus, the effect of plasticizer type and concentration on the sensitivity of the plasticized sensor materials was investigated for the hit sensors spreading up a matrix of 128 samples tested. Optimised, stable and reproducible, formulations for sensor films were found from these. Ethyl cellulose and PVC were most suitable polymers when plasticized with NPOE. The TDMA ion pairs of bromophenol blue and bromocresol green, and rhodamine B perchlorate were best indicator dyes. Application of BPB resulted in most sensitive materials.

The temperature-dependent response of the lead sensors was evaluated in the range between 15 and 25 °C. As expected, all materials were sensitive to temperature and the gradients α of the particular calibration plots decreased with increasing temperature. Thus, the sensitivity of the samples to ammonia decreased in the same order. Analysis of the plots of $\ln(\alpha)$ versus 1/T delivered thermodynamic data, i.e. ΔH^0 and ΔS^0, for the sensor films. The values obtained were comparable to those reported in literature.

The response of lead sensor films subjected to test gas with ammonia concentrations between 0 and 50 ppm was evaluated at humidity levels between 0 and 50 % r.H. Opposite trends were found for the sensitivity of the materials between dry gas and 50 % r.H., respectively, depending on the dye (BPB or BCG) used in the particular polymer matrix. Increasing the humidity of the test gas from an apparent level of 25 or 30 % r.H. to 50 % r.H. resulted in an increase of sensitivity for all samples investigated.

5.6. References

1 Römpp H., ***Römpp Lexikon Umwelt***, Thieme, Stuttgart (2004).

2 Preininger C., Mohr G. J., Klimant I., and Wolfbeis O. S., ***Ammonia Fluorosensors Based on Reversible Lactonisation of Polymer-Entrapped Rhodamine Dyes, and the Effects of Plasticizers***, Anal. Chim. Acta **334**, 113-123, (1996).

3 Werner T., Klimant I., and Wolfbeis O. S., ***Ammonia-Sensitive Polymer Matrix Employing Immobilised Indicator Ion Pairs***, Analyst **120**, 1627-1631, (1995).

4 Wolfbeis O. S. and Posch H. E., ***Fiber-Optic Fluorescing Sensor for Ammonia***, Anal. Chim. Acta **185**, 321-327, (1986).

5 Werner T., Klimant I., and Wolfbeis O. S., ***Optical Sensor for Ammonia Based on the Inner Filter Effect of Fluorescence***, J. Fluorescence **4**, 41-44, (1994).

6 Brandenburg A., Edelhaeuser R., Werner T., He H., and Wolfbeis O. S., ***Ammonia Detection via Integrated Optical Evanescent Wave Sensors***, Mikrochim. Acta **121**, 95-105, (1995).

7 Mills A., Wild L., and Chang Q., ***Plastic Colorimetric Film Sensors for Gaseous Ammonia***, Mikrochim. Acta **121**, 225-236, (1995).

8 Trinkel M., Trettnak W., Reininger F., Benes R., O'Leary P., and Wolfbeis O. S., ***Optochemical Sensor for Ammonia Based on a Lipophilised pH Indicator in a Hydrophobic Matrix***, International Journal of Environmental Analytical Chemistry **67**, 237-251, (1997).

9 Mohr G. J., Werner T., Oehme I., Preininger C., Klimant I., Kovacs B., and Wolfbeis O. S., ***Novel Optical Sensor Materials Based on Solubilisation of Polar Dyes in Apolar Polymers***, Adv. Mater. **9**, 1108-1113, (1997).

10 Lobnik A. and Wolfbeis O. S., ***Sol-Gel Based Optical Sensor for Dissolved Ammonia***, Sens. Actuators **B51**, 203-207, (1998).

11 Gruenke U. and Buerger H., ***Ammonia Sensor Based on Optochemistry***, GIT Labor-Fachzeitschrift **43**, 112,114-112,116, (1999).

12 Ozawa S., Hauser P. C., Seiler K., Tan S. S. S., Morf W. E., and Simon W., ***Ammonia-Gas-Selective Optical Sensors Based on Neutral Ionophores***, Anal. Chem. **63**, 640-644, (1991).

13 West S. J., Ozawa S., Seiler K., Tan S. S. S., and Simon W., ***Selective Ionophore-Based Optical Sensors for Ammonia Measurement in Air***, Anal. Chem. **64**, 533-540, (1992).

14 Grady T., Butler T., Maccraith B. D., Diamond D., and Mckervey M. A., ***Optical Sensor for Gaseous Ammonia with Tuneable Sensitivity***, Analyst **122**, 803-806, (1997).

15 Preininger C. and Mohr G. J., ***Fluorosensors for Ammonia Using Rhodamines Immobilised in Plasticized Poly(vinyl chloride) and in Sol-Gel; A Comparative Study***, Anal. Chim. Acta **342**, 207-213, (1997).

16 www.acros.be

17 www.vwr.com

18 www.sigmaaldrich.com

19 www.goodfellow.com

20 Bishop E., ***Indicators***, Pergamon Press, New York (1972).

21 Zittel H. E. and Florence T. M., ***Voltammetric and Spectrophotometric Study of the Zirconium-Alizarine Red S Complex***, Anal. Chem. **39**, 320-326, (1967).

22 Lindauer H., Czerney P., and Grummt U. W., ***9-(4-Dialkylaminostyryl)Acridines - A New Class of Acidochromic Dyes***, J. Prakt. Chem. **336**, 521-524, (1994).

23 www.linde.de

24 Li H. and Wolfbeis O. S., ***Determination of Urease Activity by Flow-Injection Analysis Using an Ammonium-Selective Optrode as the Detector***, Anal. Chim. Acta **276**, 115-119, (1993).

6. Summary

This thesis describes a combinatorial approach to the development of optical gas sensors. Tools for the automated high-throughput blending of component stock solutions for the preparation of sensor cocktails are presented including instrumentation and strategies for target oriented preparation protocols. A modular, automated characterisation setup is presented providing a tool for fast calibration of multiple samples under identical experimental conditions. The feasibility of the approach is validated, and the approach is applied in studies on the development of optical sensors for oxygen, carbon dioxide and ammonia.

Chapter 1 gives a short introduction concerning the development of combinatorial chemistry and its potential in materials science. In succession, optical chemical sensing for determination of important gases is introduced followed by the prospective impact of the combinatorial approach to sensor development.

In Chapter 2, the concept of the combinatorial approach to development of optical gas sensors is presented. In general, the approach is divided in three units: (a) Library preparation, (b) library characterisation and (c) library evolution, all interlinked via database supported data management. Instrumentation for the high-throughput blending of organic solutions of sensor components and for the automated characterisation of multiple sensor spots are presented. The performance of the single modules are validated and it is shown that the modular setup enables an easy exchange of detection units. Maximum concentrations of polymer stock solutions processible with the liquid dispenser are evaluated, thus providing a stable blending process.

In Chapter 3, the tools developed are applied to a study on optical oxygen sensors. Oxygen-quenchable indicator dyes are dissolved in organic polymers which are cast as thin films on solid supports. The sensitivities of the resulting thin polymer films are evaluate and the performance of the characterisation setup is validated. Also, the effect of plasticizers on the sensitivity of the polymer supported probes is investigated. It was found that increasing the concentration of plasticizer in the polymer film resulted in an increase of sensitivity of the probes to oxygen quenching.

Chapter 4 describes the combinatorial approach for the development of colorimetric carbon dioxide sensors. The automatic liquid dispensing system was adapted to the combinatorial blending of polymer, phase-transfer agent and indicator stock solutions. Purpose-built blending procedures were developed for the process control. The automated

characterisation setup was modified to provide high speed characterisation of multiple sensor spots via absorbance spectroscopy. Preparation and characterisation data were implemented in a purpose-built Access® database providing tools for the evaluation of the performance of particular sensor formulations and the comparison of their performance with respect to composition. The sensitivity of the materials subjected to carbon dioxide atmospheres of CO_2-levels between 0 and 5% was investigated for the variation of sensor composition. Non cellulosic polymers were found as promising alternatives to the well established EC-based carbon dioxide sensors. The effect of the structure of the lipophilic base (phase-transfer agent) was investigated for quaternary ammonium compounds of increasing number of long aliphatic residues. It was found that the structure of the base significantly influences the performance of a sensor material containing particular indicator dye. Although the pK of the dye was the main factor determining the sensitivity of materials with same polymer support, the structure of the base had to be considered as well. The sensor materials developed were shown to respond reversibly to changes of carbon dioxide concentration in the test atmosphere. Additionally, the materials were shown to be subject to changes in temperature and relative humidity.

In Chapter 5, the combinatorial approach is applied to the development of optical ammonia gas sensors. pH-sensitive indicator dyes were incorporated in polymer support and screened for their sensitivity to gaseous ammonia at levels of 50 % r.H. Analytical equations were developed and applied for the characterisation of the performance of lead sensor materials. These were tuned via the introduction of varying levels of plasticizers. Good results were obtained for materials based on ethyl cellulose and PVC, both plasticized with NPOE. Suitable indicator dyes were identified from bromophenol blue and bromocresol green, applied as TDMA ion pairs, and rhodamine B perchlorate. The sensitivity of a bromocresol green sensor was tuned via the application of the neutral ionophore 4´,4´´(5´´)-di-*tert*.-butyl dibenzo-18-crown-6. This was attributed to enhancement of stability of the ammonium ion due to complexation. Assuming an equal effect of the crown ether on a bromophenol blue sensor, highly sensitive materials may be obtained suitable for the determination of dissolved ammonia at levels of interest in environmental analysis. Besides the increase of sensitivity, the crown ether is expected to increase selectivity of the sensor for ammonia compared to other amines in agreement with similar results reported for other ammonia selective ionophores.. The sensitivity of the sensor materials was shown to be dependent on temperature and on changes of relative humidity in the test atmosphere containing ammonia gas in concentrations between 0 and 50 ppm.

In conclusion, the combinatorial approach has been introduced successfully to the development of optical gas sensors. The modular design allows the easy modification of the measurement setup according to the method applied. With the tools developed either absorbance-based or luminescence quenching-based sensing schemes can be applied. The approach has shown to be a valuable tool for the development of optical gas sensors and for the increase of knowledge base on the performance of particular sensor types. It may facilitate future research. Yet, the system needs further optimisation in terms of high-throughput for preparation and characterisation. Future work will also involve built-up of data management, data reduction and evaluation tools. In summary, the combinatorial or high-throughput approach may have highest potential when combined with rational design used in conventional sensor development.

7. Zusammenfassung

Diese Arbeit beschreibt einen kombinatorischen Ansatz für die Entwicklung von optischen Gassensoren. Es werden Werkzeuge für die automatisierte Herstellung von Sensor Cocktails vorgestellt. Mischungen von Stammlösungen von Sensorzutaten werden im Hochdurchsatz hergestellt. Instrumentierung und Ansätze für zielgerichtete Herstellungsvorschriften werden hierzu einbezogen. Ein modular aufgebauter automatischer Messstand, ein Werkzeug das die schnelle Charakterisierung vom vielen Proben unter identischen Versuchsbedingungen sicherstellt, wird vorgestellt. Die Eignung des Ansatzes wird validiert. Dieser wird auf die Entwicklung von optischen Sensoren für Sauerstoff, Kohlendioxid und Ammoniak angewandt.

Das Kapitel 1 gibt eine kurze Einführung in die Entwicklung der kombinatorischen Chemie und ihr Potential in den Materialwissenschaften. Im Anschluss werden Sensorprinzipien für die optische Bestimmung relevanter Gase vorgestellt, gefolgt von dem potentiellen Einfluss eines kombinatorischen Ansatzes für die Sensorentwicklung.

In Kapitel 2 wird das Konzept des kombinatorischen Ansatzes für die Entwicklung optischer Gassensoren vorgestellt. Generell kann der Ansatz in drei Einheiten gegliedert werden: (a) Die Herstellung von Sensorbibliotheken, (b) die Charakterisierung und (c) die Optimierung der Bibliotheken. Alle Teile sind durch datenbankgestütze Datenverwaltung miteinender verbunden. Geräte für die Hochdurchsatzmischung organischer Lösungen von Sensorzutaten und für die automatisierte Charakterisierung von vielen Sensorproben weren vorgestellt. Die Leistung der einzelnen Komponenten wird validiert und es wird gezeigt, dass der modulare Aufbau einen einfachen Austausch der Detektoreinheit ermöglicht. Die maximale Konzentration von Polymerlösungen, die mit dem Pipettierroboter verarbeitet werden kann, wird ermittelt um eine störungsfreie Prozessführung zu gewährleisten.

Die entwickelten Werkzeuge werden im Kapitel 3 in einer Studie über optische Sauerstoffsensoren angewendet. Durch Sauerstoff löschbare Farbstoffe werden in organischen Polymeren gelöst. Diese werden als dünne Filme auf feste Substrate aufgebracht. Die Sauerstoffempfindlichkeit der gebildeten Polymerfilme wird bestimmt und die Leistungsfähigkeit des Messaufbaus nachgewiesen. Außerdem wird der Einfluss von Weichmachern auf die Empfindlichkeit der polymerbasierenden Proben untersucht. Es kann gezeigt werden, dass eine Erhöhung der Weichmacherkonzentration im Polymerfilm erwartungsgemäß, zu einer Erhöhung der Sensitivität gegenüber der Lumineszenzlöschung durch Sauerstoff führt.

Das vierte Kapitel beschreibt den kombinatorischen Ansatz in der Entwicklung von kolorimetrischen Kohlendioxidsensoren. Das automatische Flüssigkeitspipetiersystem wurde für die kombinatorische Mischung organischer Stammlösungen von Polymeren, Phasentransferreagenzien und Indikatoren angepasst. Selbstentwickelte Mischprozeduren wurden erarbeitet um die Herstellungsprozesse zu kontrollieren. Der automatische Messplatz wurde verändert um die schnelle absorptionsspektroskopische Charakterisierung vieler Sensorproben zu gewährleisten. Informationen aus der Herstellung und Kalibrierdaten wurden in eine selbstentwickelte Access®-Datenbank eingetragen. Diese stellt Werkzeuge für die Ermittlung der Leistungsfähigkeit einzelner Sensorformulierungen und für den Vergleich der Sensoreigenschaften verschiedener Sensorenzusammensetzungen untereinander bereit. Die Empfindlichkeit der Materialien variabler Zusammensetzung gegenüber Kohlendioxid wurde durch Begasung mit Testatmosphären mit einem CO_2-Gehalt zwischen 0 und 5 % (v/v) ermittelt. Nicht auf Cellulose basierende Polymere wurden als Alternativen für etablierte, auf Ethylcellulose basierende, CO_2-Sensoren gefunden. Der Einfluss der Basenstruktur wurde für lipophile quaternäre Ammoniumverbindungen mit steigender Anzahl langkettiger aliphatischer Seitenketten untersucht. Es wurde gezeigt, dass die Struktur der Base die Empfindlichkeit eines Sensors mit einem bestimmten Indikator beeinflusst. Obwohl hauptsächlich der pK-Wert des Farbstoffs die Empfindlichkeit von Materialien gleicher Polymerbasis bestimmt, musste die Struktur der Base mit bedacht werden. Die entwickelten Sensormaterialien reagierten reversibel auf Veräderungen der Kohlendioxidkonzentration in den Testgasen Zusätzlich wurde die Temperatur- und Feuchtenabhängigkeit der Materialien ermittelt.

Im Kapitel 5 wird der kombinatorische Ansatz auf die Entwicklung von optischen Ammoniakgassensoren angewendet. pH-empfindliche Farbstoffe wurden dazu in Polymeren gelöst und die Empfindlichkeit der Sensoren gegenüber Ammoniak bei kostanter Luftfeuchtigkeit von 50 r.H. bestimmt Analytische Gleichungen wurden erarbeitet und angewendet um die Leistung von Leitsensoren zu charakterisieren. Diese Materialien wurden durch die Einführung von Weichmachern optimiert. Gute Ergebnisse wurden mit Materialien erzielt die auf mit 50% NPOE weichgemachter Ethylcellulose und PVC basierten. Geeignete Indikatoren waren die TDMA-Ionenpaare von Bromphenolblau und Bromkresolgrün sowie Rhodamin B – Perchlorat. Die Empfindlichkeit einen Bromkresolgrünsensors wurde mit dem neutralen Ionophor 4´,4´´(5´´)-di-*tert*.-butyl dibenzo-18-Krone-6 optimiert. Die gesteigerte Empfindlichkeit wurde auf die Stabilisierung des bei der Sensorrektion gebildeten Ammoniumkations durch die Komplexierung mit dem Kronenether zurückgeführt. Nimmt

man einen equivalenten des Kronenethers auf einen auf Bromphenolblau basierenden Sensor an, dann können hoch sensitive Materialien erhalten werden die geeignet sind die Konzentration von gelösten Ammoniak im biologisch relevanten Bereich von Umweltanalysen zu bestimmen. Neben der Erhöhung der Sensitivität ist, in Übereinstimmung mit Literaturzitaten über andere Ionophore, auch eine Erhöhung der Selektivität durch den Kronenether gegenüber anderen Aminen zu erwarten. Es wurde gezeigt, dass die Empfindlichkeit der Ammoniaksensoren im Messbereich von 0 bis50 ppm temperatur- und feuchteabhängig ist.

Schlussfolgernd kann die Übertragung des kombinatorische Ansatz auf die Entwicklung von optischen Gassensoren als erfolgreich betrachtet werden. Der modulare Aufbau des Systems erlaubt die einfache Modifizierung des Messplatzes je nach angewandter Messmethode. Mit den entwickelten Werkzeugen können entweder auf Absorptionsspektroskopie oder auf Lumineszenzlöschung basierende Prinzipien angewendet werden. Das System hat sich als wertvolles Mittel für die Entwicklung von optischen Gassensoren und die Erweiterung der Informationsbasis über die Leistung einzelner Sensormaterialien erwiesen. Es kann die zukünftige Forschung beschleunigen. Allerdings ist eine weitere Optimierung des Probendurchsatzes bei der Herstellung und bei der Charakterisierung der Sensormaterialien notwendig. Zukünftige Arbeiten müssen außerdem die Entwicklung von Datenverwaltungs-, Datenreduzierungs- und Charakterisierungswerkzeugen beinhalten. Zusammenfassend besitzt der kombinatorische oder Hochdurchsatzansatz das größte Potential wenn er mit rationaler Versuchsplanung, wie sie in konventionellen Methoden zum Einsatz kommt, kombiniert wird.

8. Curiculum Vitae

Name:	Apostolidis	
Vorname:	Athanasios	
Geburtsdatum:	14.06.1974	
Geburtsort:	Vilsbiburg	
Nationalität	Griechisch	
Schulbildung:	1980 – 1984	Grundschule Pfeffenhausen
	1984 – 1985	Gymnasium Mainburg
	1985 – 1993	Joseph-von-Fraunhofer Gymnasium Cham
Schulabschluss:	7/1993	Abitur
Wehrdienst:	9/1996 – 11/1996	Grundausbildung 523. Infanterieregiment Mavrodendri, Griechenland
Studium	11/1993 – 6/1998	Chemie (Diplom) Universität Regensburg
	6/1998	Diplomprüfung
	10/1998 – 7/1999	Diplomarbeit am Institut für Analytische Chemie, Chemo- und Biosensorik, Universität Regensburg
		Thema: *Multi-Channel Optical Protein Detector for Continuous Annular Chromatography*
Studienabschluss:	7/1999	Diplom Chemiker
Promotion:	4/2000 – 6/2004	Doktorarbeit am Institut für Analytische Chemie, Chemo- und Biosensorik, Universität Regensburg
		Thema: Combinatorial Approach for Development of Optical Gas Sensors - Concept and Application of High-Throughput Experimentation
Zusatzqualifikationen	8/1999 – 12/2000	Freiberuflicher Mitarbeiter bei der Presens GmbH, Regensburg
		Entwicklung von Beschichtungstechnologien and Produktion von faseroptischen Mikrosensoren
	1/2001 – 11/2001	Entwicklung von Antihaftbeschichtungen für die Mühlbauer AG, Roding
Sprachen:		Griechisch (Muttersprache)
		Deutsch (sehr gut)
		Englisch (sehr gut)
Hobbies und Interessen:		Radfahren, Lesen, Schwimmen, Tauchen

9. List of Presentations and Publications

Diploma Thesis

Multi-Channel Optical Protein Detector for Continuous Annular Chromatography, Institute of Analytical Chemistry Chemo- and Biosensors, University of Regensburg (1999)

Papers

1. Apostolidis Athanasios; Lehmann Hartmut; Schwotzer Gunter; Willsch Reinhardt; Prior Albert; Wolfgang Jürgen; Klimant Ingo; Wolfbeis Otto S., ***Fiber Optic Multi-Channel Protein Detector for Use in Preparative Continuous Annular Chromatography***, J. Chromatogr. A, **967**, 183-189, (2002).

2. Athanasios Apostolidis, Ingo Klimant, Damian Andrzejewski, and Otto S. Wolfbeis; ***A Combinatorial Approach for Development of Materials for Optical Sensing of Gases***; J. Comb. Chem., **6**, 325-331, (2004).

Posterpresentations

4/2000	***A Simple Method for Multi-Channel Protein Detection in Continuous Annular Chromatography***, *Europt(r)ode V*, Lyon, France
7/2001	***Combinatorial Synthesis and Automated Characterisation of Optical Gas Sensor Materials****, Symposium of the European Society for Combinatorial Sciences – Eurocombi I*, Budapest, Hungary
4/2002	***High-Throughput Synthesis and Characterisation of Optical Gas Sensor Materials by Combinatorial Chemistry***, *Eurot(r)ode VI*, Manchester, UK

10. Abbreviations, Acronyms and Symbols

α	equilibrium constant of acid-base equilibrium
A	absorbance
atm	atmosphere(s) 1atm = 760 Torr = 1013.25 hPa
CC	combinatorial chemistry
dphbpy	4,4´-diphenyl-2,2´-bipyridyl
dpp	4,7-diphenyl-1,10-phenanthroline
f_{mod}	modulation frequency
h	hour(s)
HTS	high-throughput screening
I	light intensity
IR	infrared
K_{SV}	Stern-Volmer constant
λ	wavelength
λ_{em}	wavelength of emission maximum
λ_{ex}	wavelength of excitation
λ_{max}	wavelength of absorbance maximum
LED	light emitting diode
µm	micrometer
µL	microliter
µs	microsecond(s)
M	1 mol / L
MAC	maximum allowable concentration for 8 hour exposure per day
min	minute(s)
nm	nanometer
P	permeability
pCO_2	carbon dioxide partial pressure
pK_D	acid dissociation constant
PMT	photo multiplier tube
pNH_3	ammonia partial pressure
pO_2	oxygen partial pressure
ppm	parts per million

Pt(PFPP)	5,10,15,20-tetrakis-(2,3,4,5,6-pentafluorophenyl)-porphyrin-Pt(II)
Pd(PFPP)	5,10,15,20-tetrakis-(2,3,4,5,6-pentafluorophenyl)-porphyrin-Pd(II)
r.H.	relative humidity
Ru(dphbpy)	ruthenium(II)-tris-4,4´-diphenyl-2,2´-bipyridyl
Ru(dpp)	ruthenium(II)-tris-4,7-diphenyl-1,10-phenanthroline
θ	phase shift or phase angle of modulated light
τ	luminescence lifetime (decay time)
T	absolute temperature in Kelvin
t	time
t_{90}	time to reach 90 % of equilibrium signal
THF	tetrahydrofurane
TMS	trimethylsilylpropanesulfonate
UV	ultraviolet
vis	visible
v/v	volume per volume

Appendix

A Source Code of MicroLab® S Procedure for the Preparation Oxygen Sensor Cocktails

```
1
2                              Program for the Production of Oxygen Sensor Library Cocktails
3   Initialise single needle arm
4   Initialise dispenser 1
5
6
7
8                        Opening of the EXCEL-Sheet which contains the volumes to be mixed
9   Open Excel : C:\WINDOWS\Desktop\EXCEL-SHEETS MikroLabS\Sensorkomposition Oxygen1.xls
10
11
12  ____________________________________________________________________________________
13  Input Preparation Parameters
14
15  User message Max. Number of Combinations Poly x Ind x WM = 64
16     Input value for N_polymers in range 0 to  32 Default is 0
17     Input value for N_indicators in range 0 to  32 Default is 0
18     Input value for N_WM in range 0 to  32 Default is 0
19     Input value for N_CWM in range 0 to  10 Default is 0
20     Input value for polpos in range 1 to  20 Default is 1
21     Input value for indstart1 in range 1 to  16 Default is 1
22     Input value for wmpos in range 1 to  10 Default is 1
23
24
25  Input plasticizer Concentrations incl. 0 %
26
27   Loop N_CWM
28      i=_sysloop[1]
29      Input value for CWM[i] in range 0 to  70 Default is 0
30   End of loop
31
32  ____________________________________________________________________________________
33  ADD POLYMER
34  Set new position in Polymer to polpos for single needle arm
35  Loop N_indicators
36    Loop N_polymers
37       x=_sysloop[2]+5+polpos
38       z=_sysloop[2]+polpos-1
39       Set new position in Polymer to z for single needle arm
40       Read from Excel : Oxy
41       Loop N_WM
42          Loop N_CWM
43             i=_sysloop[4]
44             v_pol[i]=Pol*(100-CWM[i])/100
45             Aspirate 10 + v_pol[i] ul from Polymer with syringe  1 , speed  50 seconds per stroke
46             Dispense  v_pol[i] ul to  Proben with syringe  1 , speed  20 seconds per stroke
47             Write to Excel : $z
48             Write to Excel : $v_pol[i]
49             Wash needle with syringe  1, 5 mm above bottom in Waschen, 0 ul 1 times, lift 20 mm
50          End of loop
51       End of loop
52       Wash needle with syringe  1, 5 mm above bottom in Waschen, 500 ul 2 times, lift 20 mm
53    End of loop
```

```
End of loop

_____________________________________________________________________________
ADD PLASTICIZER

b=0
d=0
start=1
Loop N_WM
    Target Position of Plasticizer on Mixing Rack
    Set new position in Indikator to wmpos for single needle arm
    y=_sysloop[1]+5+wmpos
    wm_num=_sysloop[1]+wmpos-1
    Read from Excel : Oxy
    Loop N_CWM
      k=_sysloop[2]
      v_plasti=plasti*CWM[k]
      b=b+1
       Loop N_indicators
          Loop N_polymers
            d=d+1
             offset=N_WM*N_CWM
             position=start+(d-1)*offset+(b-1)
             Set new position in Indikator to wm_num for single needle arm
             Set new position in Proben to position for single needle arm
             If v_plasti = 0 jump to Endif
               Aspirate 5 + v_plasti ul from Indikator with syringe  2 , speed 15 seconds per stroke
               Dispense  v_plasti ul to  Proben with syringe  2 , speed  10 seconds per stroke
               Wash needle with syringe  2, 5 mm above bottom in Waschen, 100 ul 1 times, lift 20 mm
             Endif
             Write to Excel : $wm_num
             Write to Excel : $CWM[k]
             Write to Excel : $v_plasti
          End of loop
      End of loop
      d=0
    End of loop
End of loop

_____________________________________________________________________________
ADD INDICATOR

instart=indstart1+16
Set new position in Indikator to instart for single needle arm
Set new position in Proben to 1 for single needle arm

Loop N_indicators
  n_ind=_sysloop[1]+indstart1-1
  z_ind=indstart1+5+_sysloop[1]
  Read from Excel : Oxy
     Loop N_polymers
       Loop N_WM
          Loop N_CWM
             Aspirate 5 + v_ind ul from Indikator with syringe  2 , speed  20 seconds per stroke
             Dispense  v_ind ul to  Proben with syringe  2 , speed  20 seconds per stroke
             Write to Excel : $n_ind
             Write to Excel : $v_ind
          End of loop
          Wash needle with syringe  2, 5 mm above bottom in Waschen, 100 ul 2 times, lift 20 mm
       End of loop
       Washtime  2 s
     End of loop
     Set new position in Indikator to old position plus 1 for single needle arm
```

```
End of loop

Close Excel

Wash needle with syringe  1, 5 mm above bottom in Waschen, 2500 ul 2 times, lift 20 mm
Washtime  10 s
Initialise single needle arm

End of method
```

B Source Code of MicroLab® S Procedure for the Preparation Carbon Dioxide Sensor Cocktails

```

Program for the Preparation of Carbon Dioxide Sensor Cocktails

 Initialise System
        Initialise single needle arm
        Dispenser initialisieren 1

Open Excel : C:\Eigene Dateien\ARBEIT\Synthese\Hamilton-tabellen\Excel
Tabellen\Sensorkomposition P-B-FS1.xls

_____________________________________________________________________________

        Input of Preparation Paramters for Library Production of Polymer-Indicator-Buffer

User message Maximum Number of Tripel (P-B-FS) = 64 !!

   Maximum Number of Different Compositions on Substrate is 9 !

   Number of Polymers on Substrate (Max.12)
                                          Input value for POL in range 0 to  12 Default is 1
   Number of Buffers on Substrate (Max.12)
                                          Input value for BAS in range 0 to  12 Default is 1
   Number of Indicator Ion pairs on Substrate (Max.12)
                                          Input value for FS in range 0 to  12 Default is 1

    Start-ID of Polymer:
                                    Input value for STARTPOL in range 0 to  19 Default is 1
    Start-ID of Buffer:
                                    Input value for STARTBAS in range 0 to  19 Default is 1
    START-ID of Indicator:
                                    Input value for STARTFS in range 0 to  19 Default is 1


              Number of Cocktails: POL*BAS*FS
N_POL=BAS*FS
N_BAS=POL*FS
N_FS=POL*BAS

        N_POL = Number of Cocktails with same Polymer
        N_BAS = Number Cocktails with same Buffer
          N_FS = Number Cocktails with same Indicator

_____________________________________________________________________________

1. ADD POLYMER
```

```
45
46        START=STARTPOL+10
47        Set new position in Polymer to STARTPOL for single needle arm
48           Loop POL
49              Read from Excel : Hamilton
50                 Loop N_POL
51                    Aspirate 5 + V_POL ul from Polymer with syringe  1 , speed  60 seconds per stroke
52                    Dispense  V_POL ul to  Proben with syringe  1 , speed  45 seconds per stroke
53                    Wash needle with syringe  1, 2 mm above bottom in Waschen, 1500 ul 1 times, lift 10 mm
54                    End of loop
55           Set new position in Polymer to old position plus 1 for single needle arm
56
57                                  Wash Needle
58             Wash needle with syringe  1, 2 mm above bottom in Waschen, 1000 ul 2 times, lift 10 mm
59           End of loop
60
61  ____________________________________________________________________________________________
62          Target position of buffer on mixing rack:
63          Pos = LOOP(FS) + (LOOP(POL)-1)*BAS*FS + (LOOP(BAS)-1)*FS
64
65  2. ADD BUFFER
66
67        START=STARTBAS+10
68        Set new position in Indikator to STARTBAS for single needle arm
69        Loop BAS
70           Read from Excel : Hamilton
71           Set new position in Proben to 1 for single needle arm
72              Loop POL
73                    Loop FS
74                         If V_BAS > 95 jump to Endif
75                            Aspirate 5 + V_BAS ul from Indikator with syringe  2 , speed  12 seconds per stroke
76                             POSITION=_sysloop[3]+(_sysloop[2]-1)*BAS*FS+(_sysloop[1]-1)*FS
77                             Set new position in Proben to POSITION for single needle arm
78                             Dispense  V_BAS ul to  Proben with syringe  2 , speed  10 seconds per stroke
79                             Wash needle with syringe  2, 2 mm above bottom in Waschen, 100 ul 2 times, lift
                                10 mm
80                          Endif
81                         If V_BAS <= 95 jump to Endif
82                            Aspirate 5 + V_BAS ul from Indikator with syringe  1 , speed  12 seconds per stroke
83                            POSITION=_sysloop[3]+(_sysloop[2]-1)*BAS*FS+(_sysloop[1]-1)*FS
84                            Set new position in Proben to POSITION for single needle arm
85                            Dispense  V_BAS ul to  Proben with syringe  1 , speed  10 seconds per stroke
86                            Wash needle with syringe 1, 2 mm above bottom in Waschen, 200 ul 2 times, lift 10
                              mm
87                          Endif
88                    End of loop
89
90                              Wash Needle
91                    Wash needle with syringe  1, 2 mm above bottom in Waschen, 1000 ul 2 times, lift 10 mm
92              End of loop
93              Set new position in Indikator to old position plus 1 for single needle arm
94           End of loop
95
96  ____________________________________________________________________________________________
97
98     Position of Vial for addition of indicator:
99     POS=LOOP(FS)+(LOOP(POL)-1)*BAS*FS+(LOOP(BAS)-1)*FS
100
101
102 3. ADD INDICATOR
103
104   START=STARTFS+10
```

```
105   START2=STARTFS+16
106    Set new position in Indikator to START2 for single needle arm
107     Loop FS
108         Read from Excel : Hamilton
109         Set new position in Proben to 1 for single needle arm
110          Loop POL
111              Loop BAS
112                If V_FS > 95 jump to Endif
113                     Aspirate 5 + V_FS ul from Indikator with syringe  2 , speed  10 seconds per stroke
114                     POSITION=_sysloop[1]+(_sysloop[2]-1)*BAS*FS+(_sysloop[3]-1)*FS
115                     Set new position in Proben to POSITION for single needle arm
116                     Dispense V_FS ul to Proben with syringe 2 , speed 500 steps per second
117                     Wash needle with syringe  2, 2 mm above bottom in Waschen, 100 ul 2 times, lift 10 mm
118                Endif
119                If V_FS <= 95 jump to Endif
120                      Aspirate 5 + V_FS ul from Indikator with syringe  1 , speed  10 seconds per stroke
121                      POSITION=_sysloop[1]+(_sysloop[2]-1)*BAS*FS+(_sysloop[3]-1)*FS
122                      Set new position in Proben to POSITION for single needle arm
123                      Dispense V_FS ul to Proben with syringe  1 , speed  500 steps per second
124                     Wash needle with syringe  1, 2 mm above bottom in Waschen, 200 ul 2 times, lift 10 mm
125                Endif
126              End of loop
127
128               Wash Needle
129              Wash needle with syringe  1, 2 mm above bottom in Waschen, 200 ul 2 times, lift 20 mm
130          End of loop
131          Set new position in Indikator to old position plus 1 for single needle arm
132    End of loop
133
134
135  End of method
```

C Source Code of MicroLab® S Procedure for the Preparation Ammonia Sensor Cocktails

```
1     Program for Preparation of Ammonia Sensors
2           Initialise System
3               Initialise single needle arm
4               Dispenser initialisieren 1
5               Washtime  2 s
6              Open Excel : C:\Eigene Dateien\Bosch\NH3-P-WM-FS1.xls
7     ____________________________________________________________________________________
8
9         Input Paramter for Preparation of Ammonia Sensor Library of Type: Polymer-Plasticizer-Indicator
10
11    User message Max. Numer of Triples  = 64 !!
12
13    Number of Polymers on Substrate (Max.12)
14                    Input value for POL in range 0 to  12 Default is 1
15    Number of Plasticizers on Substrate (Max.12)
16                    Input value for WM in range 0 to  32 Default is 1
17    Number of Plasticizer Concentrations (incl. 0%)
18                    Input value for N_CWM in range 0 to  9 Default is 0
19           Input of Plasticizer Concentrations in Library
20                    Loop N_CWM
21                      i=_sysloop[1]
22                      Input value for CWM[i] in range 0 to  66 Default is 0
23                    End of loop
```

```
Number of Indicators on Substrate (Max.12)
                Input value for FS in range 0 to  32 Default is 1

Start-ID of Polymer:
                Input value for STARTPOL in range 0 to  19 Default is 1
Start-ID of Plasticizer:
                Input value for STARTWM in range 0 to  19 Default is 1
Start-ID of Indicator:
                Input value for STARTFS in range 0 to  32 Default is 1

        Number of Cocktails: POL*WM*FS*N_CWM
_____________________________________________________________________________

1. Provide 10 µL conc. HCl in THF 1% (v/v)

z=POL*WM*FS*N_CWM
THF=z*10+20
  If z < 9 jump to Endif
    Aspirate 10 + THF ul from THF_HCl with syringe  1 , speed  10 seconds per stroke
      Loop z
        Dispense  10 ul to  Proben with syringe  1 , speed  5 seconds per stroke
      End of loop
    Wash needle with syringe  1, 5 mm above bottom in Waschen, 300 ul 4 times, lift 20 mm
  Endif

  If z >= 9 jump to Endif
    Aspirate 10 + THF ul from THF_HCl with syringe  2 , speed  10 seconds per stroke
      Loop z
        Dispense  10 ul to  Proben with syringe  2 , speed  5 seconds per stroke
      End of loop
    Wash needle with syringe  2, 5 mm above bottom in Waschen, 100 ul 5 times, lift 20 mm
  Endif
_____________________________________________________________________________

2. ADD POLYMER

        ZEILEPOLSTART=STARTPOL+7
Set new position in Proben to 1 for single needle arm
Loop FS
   Loop POL
p_pos=_sysloop[2]+STARTPOL-1
   Set new position in Poly to p_pos for single needle arm
    Read from Excel : Mischung
      Loop WM
          Loop N_CWM
            i=_sysloop[4]
            v_p=V_POL*(100-CWM[i])/100
            Aspirate 5 + v_p ul from Poly with syringe  1 , speed  50 seconds per stroke
            Dispense  v_p ul to  Proben with syringe  1 , speed  30 seconds per stroke
            Wash needle with syringe  1, 2 mm above bottom in Waschen, 1500 ul 1 times, lift 10 mm
          End of loop
      End of loop
   End of loop
End of loop
Set new position in Poly to old position plus 1 for single needle arm

Wash Needle
Wash needle with syringe  1, 2 mm above bottom in Waschen, 1000 ul 2 times, lift 10 mm
Washtime  10 s

_____________________________________________________________________________
```

```
86   3. ADD PLASTICIZER
87
88   Loop FS
89       Loop POL
90           Loop WM
91               Loop N_CWM
92                   i=_sysloop[4]
93                   "    wm_pos = Position im Weichmacherrack für Ansaugen von Weichmacher
94                   wm_pos=(_sysloop[3]-1)+STARTWM
95                   Set new position in Weichmacher to wm_pos for single needle arm
96                   z_wm=_sysloop[3]+7
97                   z_pol=_sysloop[2]+7
98                   Read from Excel : Mischung
99                   Read from Excel : Mischung
100                  v_wm=CWM[i]*m_p*v0_wm
101                  "     pos_wm = Position im Probenrack für Zugabe von WM
102                  a=(_sysloop[1]-1)*N_CWM*WM*POL
103                  b=(_sysloop[2]-1)*N_CWM*WM
104                  c=(_sysloop[3]-1)*N_CWM
105                  d=a+b+c
106                  pos_wm=_sysloop[4]+d
107                  Set new position in Proben to pos_wm for single needle arm
108                  If v_wm = 0 jump to Endif
109                      Aspirate 10 + v_wm ul from Weichmacher with syringe  2 , speed  5 seconds per stroke
110                      Dispense  v_wm ul to  Proben with syringe  2 , speed  5 seconds per stroke
111                      Wash needle with syringe  2, 5 mm above bottom in Waschen, 0 ul 1 times, lift 20 mm
112                  Endif
113              End of loop
114              Wash needle with syringe  1, 5 mm above bottom in Waschen, 500 ul 2 times, lift 20 mm
115              Washtime  5 s
116          End of loop
117      End of loop
118  End of loop
119
120  ____________________________________________________________________________________________
121
122  4. ADD INDICATOR
123
124  Set new position in Farbstoff to STARTFS for single needle arm
125  Set new position in Proben to 1 for single needle arm
126    Loop FS
127      ZEILEFS=STARTFS+7+(_sysloop[1]-1)
128      Read from Excel : Mischung
129          Loop POL
130              Lesen der Masse des aktuellen Polymers m_POL in Zeile P_aktuell
131              P_aktuell=ZEILEPOLSTART+(_sysloop[2]-1)
132              Read from Excel : Mischung
133              Loop WM
134                Loop N_CWM
135                  V_FS=V0_FS*m_POL
136                  If V_FS > 95 jump to Endif
137                      Aspirate 5 + V_FS ul from Farbstoff with syringe  2 , speed  10 seconds per stroke
138                      Dispense  V_FS ul to  Proben with syringe  2 , speed  500 steps per second
139                      Wash needle with syringe  2, 2 mm above bottom in Waschen, 100 ul 2 times, lift 1
140                  Endif
141                  If V_FS <= 95 jump to Endif
142                      Aspirate 5 + V_FS ul from Farbstoff with syringe  1 , speed  10 seconds per stroke
143                      Dispense  V_FS ul to  Proben with syringe  1 , speed  500 steps per second
144                      Wash needle with syringe  1, 2 mm above bottom in Waschen, 200 ul 2 times, lift 1
145                  Endif
146              End of loop
147                Washtime  3 s
```

```
148             End of loop
149           End of loop
150           Set new position in Farbstoff to old position plus 1 for single needle arm
151       End of loop
152       ____________________________________________________________________________
153   End of method
```

D Database for the Preparation and Characterisation of Optical pO_2 Sensors

The database is built up by (1) tables defining the particular components and (2) tables containing the preparation and characterisation data linked to the tables from (1).

The number of sensors is defined by the possible combinations of the particular components. In the study on oxygen sensors all possible polymer-indicator-plasticizer combinations were prepared varying the plasticizer content between 0, 10, 33 and 50 % (w/w):

Matrix Size: 4 (indicators) × 4 (plasticizers) × 4 (No. of plasticizer conc.) × 16 (polymers)

= 1024 Sensors (incl. 256 duplicates)

Table Identifying the Indicator dye used:

Ind-ID	FS-Name
1	$Ru(II)(dpbpy)_3$
2	$Ru(II)(dpp)_3$
3	Pt(II)-meso tetra(pentafluorophenyl)porphyrin
4	Pd(II)-meso tetra(pentafluorophenyl)porphyrin

Table Identifying the Supporting Polymer:

Polymer-ID	Polymer-Name
1	EC 46
2	EC 49
3	Poly (tetrafluoro-ethylene-co-vinylidenefluorid-co-propylene)
4	Poly (styrene-co-acrylonitril)
5	Celluloseacetat
6	Poly (4-vinyl phenol)
7	Poly (vinyl methyl keton)
8	Polysulfone
9	Poly (vinylchlorid-co-isobutyl vinyl ether)
10	Poly {[(octahydro-5-methoxy carbonyl)-5-methyl-4,7-methano-1H-indene-1,3-diyl]-1,2-ethanediyl}
11	Poly (Bisphenol) A carbonate
12	Poly (4-tert-butylstyrene)
13	Polyacrylonitril
14	Polyvinylchlorid
15	Polystyrol

Polymer-ID	Polymer-Name
16	Poly (methylmethacrylat)

Table Identifying the Plasticizer (Pl) used:

Pl-ID	Pl-Name	Pl-Abbrev.
1	Tributylphosphate	TBP
2	Tris(2-ethylhexyl)phosphat	TOP
3	2-(Octyloxy)benzonitril	OBN
4	Nitrophenyl octyl ether	NPOE

Table containing Sensor Composition for a Selection of Materials

Sensor-ID	Polymer-ID	Pl-ID Sensor	% Pl	Ind-ID	Plate
1	1	1	0	1	Oxy1
2	1	1	10	1	Oxy1
3	1	1	33	1	Oxy1
4	1	1	50	1	Oxy1
5	1	2	0	1	Oxy1
6	1	2	10	1	Oxy1
7	1	2	33	1	Oxy1
8	1	2	50	1	Oxy1
9	1	3	0	1	Oxy1
10	1	3	10	1	Oxy1
11	1	3	33	1	Oxy1
12	1	3	50	1	Oxy1
13	1	4	0	1	Oxy1
14	1	4	10	1	Oxy1
15	1	4	33	1	Oxy1
16	1	4	50	1	Oxy1
17	2	1	0	1	Oxy2
18	2	1	10	1	Oxy2
19	2	1	33	1	Oxy2
20	2	1	50	1	Oxy2
21	2	2	0	1	Oxy2
22	2	2	10	1	Oxy2
23	2	2	33	1	Oxy2
24	2	2	50	1	Oxy2
25	2	3	0	1	Oxy2
26	2	3	10	1	Oxy2
27	2	3	33	1	Oxy2
28	2	3	50	1	Oxy2
29	2	4	0	1	Oxy2
30	2	4	10	1	Oxy2
31	2	4	33	1	Oxy2
32	2	4	50	1	Oxy2

Sensor-ID	Polymer-ID	Pl-ID Sensor	% Pl	Ind-ID	Plate
33	3	1	0	1	Oxy3
34	3	1	10	1	Oxy3
35	3	1	33	1	Oxy3

Table with Measurement Data indexed by the Sensor-ID from table with Preparation Data for a Selection of Sensors

Sensor-ID	O_2-Concentration / hPa	τ_0/τ Spot 1	Spot 2	Spot 3	Average	s.d.
8	0	1	1	1	1	0
8	10.25	1.027178	1.024393	1.026621	1.026064	0.001203
8	51.25	1.138449	1.134538	1.132474	1.135154	0.002477
8	102.5	1.265772	1.258304	1.2589	1.260992	0.003388
8	205	1.511554	1.500588	1.499608	1.503916	0.005415
9	0		1	1	1	0
9	10.25		1.017411	1.017406	1.017408	0.000002
9	51.25		1.083681	1.081336	1.082509	0.001172
9	102.5		1.15522	1.154733	1.154976	0.000243
9	205		1.290527	1.294224	1.292375	0.001848
10	0	1	1	1	1	0
10	10.25	1.009843	1.010556	1.010914	1.010438	0.000445
10	51.25	1.061778	1.061831	1.058873	1.060827	0.001381
10	102.5	1.12029	1.119233	1.119705	1.119742	0.000432
10	205	1.234391	1.232542	1.233198	1.233377	0.000765
11	0	1	1	1	1	0
11	10.25	1.022147	1.017443	1.020308	1.019966	0.001935
11	51.25	1.094501	1.092836	1.092353	1.09323	0.00092
11	102.5	1.184047	1.185541	1.179692	1.183093	0.002481
11	205	1.359357	1.35401	1.354417	1.355928	0.00243
12	0	1	1	1	1	0
12	10.25	1.025051	1.023582	1.023911	1.024181	0.000629
12	51.25	1.131464	1.128566	1.12913	1.12972	0.001254
12	102.5	1.261819	1.263351	1.253949	1.259706	0.004118
12	205	1.512819	1.511737	1.496604	1.507053	0.007402
13	0	1	1	1	1	0
13	10.25	1.018836	1.015612	1.01348	1.015976	0.002201
13	51.25	1.077077	1.080557	1.079499	1.079044	0.001456
13	102.5	1.155488	1.155545	1.157457	1.156163	0.000915
13	205	1.287254	1.293195	1.300139	1.293529	0.005265

E Database for the Preparation and Characterisation of Optical pCO_2 Sensors

In the study on optical pCO_2 sensors the same polymers were used as in the study on pO_2 sensors. The definition of polymer-ID is identical to the above table. The number of sensors is defined by the possible combinations of the particular components. In this study all possible polymer-indicator-buffer combinations were prepared with the general composition of:

x mg polymer 500 mmol buffer per 1 kg polymer 20 mmol indicator per 1 kg polymer

Matrix Size: 12 (indicators) × 4 (buffers) × 16 (polymers)

= 768 Sensors

Table Identifying the Indicator used:

Ind-ID	Indicator-Name	Abbrev.
1	m-cresolpurple	MCP
2	brilliant yellow	BRY
3	thymol blue	TB
4	bromophenol blue	BPB
5	bromocresol green	BCG
6	phenol red	PR
7	cresol red	CR
8	alizarin red S	ARS
9	orange I	OI
10	xylenol blue	XB
11	xylenol orange	XO
12	bromocresol purple	BCP

Table Identifying the buffer used:

Base-ID	Base-Name
1	TOA-OH
2	TOA-HPO_4
12	CTA-OH
13	DDDMA-OH
14	TBA-OH
15	TDMA-OH

Table Identifying the Material Composition for a Selection of Sensors

Sensor-ID	Polymer-ID	Base-ID	Indicator-ID	Plate
63	2	1	3	plt034
70	2	1	10	plt035
75	2	12	3	plt011
82	2	12	10	plt020
87	2	13	3	plt011
94	2	13	10	plt021
99	2	14	3	plt030
106	2	14	10	plt031
111	2	15	3	plt040
118	2	15	10	plt041
663	12	1	3	plt072
670	12	1	10	plt073
675	12	12	3	plt074
682	12	12	10	plt075
687	12	13	3	plt076
694	12	13	10	plt077
699	12	14	3	plt078
706	12	14	10	plt079
711	12	15	3	plt080
718	12	15	10	plt081
903	16	1	3	plt103
910	16	1	10	plt104
915	16	12	3	plt105
922	16	12	10	plt106
927	16	13	3	plt107
934	16	13	10	plt108
939	16	14	3	plt109
946	16	14	10	plt110
951	16	15	3	plt111
958	16	15	10	plt112

Table with Measurement Data Indexed by the Sensor-ID from Table with Preparation Data Illustrated for a Selection of Sensors

Sensor-ID	pCO_2 / %	A_0/A							
		Spot 1	Spot 2	Spot 3	Spot 4	Spot 5	Spot 6	Average	s.d.
682	0	1	1	1	1	1	1	1	0
682	0.25	1.04	1.03	1.16	1.03	1.26	1.06	1.10	0.08
682	0.5	1.08	1.07	1.55	1.08	1.70	1.22	1.28	0.24
682	1	1.13	1.16	2.38	1.22	2.30	1.70	1.65	0.52
682	3	1.27	1.65	4.12	2.61	3.77	3.21	2.77	1.04
682	5	1.59	3.33	5.28	6.09	4.56	4.28	4.19	1.43
903	0	1	1	1	1	1	1	1	0
903	0.25	2.37	2.05	2.67	1.57	3.00	2.43	2.35	0.45
903	0.5	4.33	3.24	4.77	2.36	6.11	4.11	4.15	1.17
903	1	9.05	6.00	8.89	4.54	12.14	8.168	8.13	2.4
903	3	29.55	20.73	24.11	16.19	35.91	26.17	25.44	6.27
903	5	55.83	39.02	47.17	26.81	103.25	51.05	53.85	23.9

F Database with Sensor used in Screening for Optical pNH_3 Sensors

The database contains the data on composition of the materials prepared in the initial screening for optical pNH_3-sensors. For evaluation of sensitivity of each material the absorbance spectra were imported and the sensors showing sensitivity to ammonia were marked.

Screening Matrix 1: 21 (indicators) × 16 (polymers) = **336 Sensor Materials**

Table Identifying the Indicator used in Screening

Ind-ID-Screening	Ind-Name	Abbrev.
1	m-cresol purple – TDMA	MCP
2	brilliant yellow – TDMA	BRY
3	thymol blue – TDMA	TB
4	bromophenol blue – TDMA	BPB
5	bromocresol green – TDMA	BCG
6	phenol red – TDMA	PR
7	cresol red – TDMA	CR
8	alizarin red S – TDMA	ARS
9	Orange I – TDMA	OI
10	xylenol blue – TDMA	XB
11	xylenol orange – TDMA	XO
12	bromocresol purple – TDMA	BCP
13	Rhodamin 6 G	R6G
15	tetrabromophenol blue – TDMA	TBPB
16	chrome azurol S	CAS
17	octabutoxyphthalocyanin	OBPC
21	eosin B	EOB
22	erythrosin B	ERB
23	rhodamin B	RB
24	9-(4,4-dimethylamino styryl) acridine	DMASA
25	9-(4,4-dimethylamino cinnamyl) acridine	DMACA

Table linking the Composition of a Sensor Material to Screening Performance for a Selection of Materials

Sensor-ID	Polymer	Ind-Screening	Screening positive
NH3-27	EC49	BRY	No
NH3-31	EC49	PR	No
NH3-49	EC49	DMASA	No
NH3-74	PTFE	DMASA	Yes
NH3-76	PSAN	MCP	No
NH3-77	PSAN	BRY	No
NH3-81	PSAN	PR	No
NH3-99	PSAN	DMASA	Yes
NH3-124	CAc	DMASA	Yes
NH3-126	PVPh	MCP	No
NH3-149	PVPh	DMASA	Yes
NH3-151	PVMK	MCP	No
NH3-199	PSu	DMASA	Yes
NH3-201	PVC-iBVE	MCP	No
NH3-231	POMMIE	PR	Yes
NH3-249	POMMIE	DMASA	Yes

Sensor-ID	Polymer	Ind-Screening	Screening positive
NH3-256	PC	PR	No
NH3-274	PC	DMASA	Yes
NH3-299	PtbS	DMASA	Yes
NH3-349	PVC	DMASA	Yes
NH3-351	PS	MCP	No
NH3-374	PS	DMASA	Yes
NH3-377	PMMA	BRY	No
NH3-399	PMMA	DMASA	Yes